Spin in fractional quantum Hall systems

Karel Výborný

Abstract

The present numerical study concerns fractional quantum Hall systems at filling factors $\nu = \frac{2}{3}$ and $\frac{2}{5}$. By means of the exact diagonalization of systems with few electrons in a rectangle with periodic boundary conditions we investigate the many–body ground states and low–lying excited states. Homogeneous systems as well as systems with some special forms of inhomogeneities are considered. Particular emphasis is put on the spin degree of freedom and on possible analogies to Ising ferromagnets.

The core of the work is set up into four Chapters: experimental results and especially those hinting at ferromagnetism at $\nu = \frac{2}{3}, \frac{2}{5}$ are reviewed and a wider theoretical introduction is given. In another two Chapters, first the homogeneous systems are examined and then the capability of the $\nu = \frac{2}{3}$ systems to form spin structures under the influence of magnetic inhomogeneities is investigated.

For homogeneous systems we first examine the inner structure of the well–established spin polarized and spin singlet incompressible ground states. Based on this study, we propose a new interpretation of the singlet ground state at filling $\frac{2}{3}$. Links to composite fermion theories are mentioned and among them especially those which may seem counterintuitive at the first look. Further, a half–polarized state is found which could become the absolute ground state at $\nu = \frac{2}{3}$ in a narrow range of electron density. We investigate this state and find it in some respects similar to the singlet and polarized ground states, yet the nature of this half–polarized state is not completely explained.

In the next Chapter, the crossover between the polarized and the singlet ground states is studied under the influence of magnetic inhomogeneities which should support formation of domains with different spin polarization. We find that if the domains should indeed form, the energy gap over the crossing ground states has to close. It is proposed that this scenario can still be compatible with the observation of a plateau in the polarization near the transition. A candidate for a state containing domains is presented.

Contents

1 What to study at $\nu = \frac{2}{3}$ in the new millennium?

Correlated systems in the world of quantum mechanics: this is the target area of this thesis. By the first two words, I would like to refer to many–body systems where single–particle models, and also the effective single–particle ones, fail to describe the reality. In classical physics, let us say in astronomy, many–body problems have long been studied. Consider just the problem of three gravitating bodies, for example the Sun, Saturn and Uranus. The full problem cannot be solved analytically, are there some options? Neglecting interactions between the last two, we have two independent *one–particle problems*, Sun–Uranus and Sun–Saturn which can easily be solved. Can we do better? Yes, we can take the Sun–Saturn subsystem and calculate motion of Uranus on this background. And more: with this improved trajectory of Uranus, we can calculate a correction to the motion of Saturn and continue the iteration process. These *effective one–particle problems*, the latter one being *selfconsistent* if the iteration converges, will likely not be analytically soluble, but still they are much simpler than the full three–body problem.

The atom of helium, or a nucleus with two orbiting electrons, is almost the same problem projected to the context of quantum mechanics. Again, omission of interelectronic interaction gives an easily soluble *one–particle model* where Hartree–Fock approximation is an example of an *effective one–particle model*. The best variational Hartree–Fock wavefunction for the ground state is (Sect. 8.4.3. in [74]; see comment [1])

$$\psi_{var}(\boldsymbol{r}_1, \boldsymbol{r}_2) = \exp\left[-Z^*(|\boldsymbol{r}_1| + |\boldsymbol{r}_2|)\right](|\uparrow\downarrow\rangle - |\downarrow\uparrow\rangle), \text{ with } Z^* = 2 - \frac{5}{16} \qquad (1.1)$$

and even though it gives a fairly good estimate for the ground state energy, it obviously fails to describe the fact that the two electrons try to avoid each other. Indeed: fixing $\boldsymbol{r}_1$ and $|\boldsymbol{r}_2|$, we would expect that $|\psi_{var}|^2$ becomes maximal, if the angle φ between $\boldsymbol{r}_1$ and $\boldsymbol{r}_2$ is 180°; instead the Hartree–Fock ψ_{var} in Eq. 1.1 is completely independent on the angle φ. In other words, the two electrons are *uncorrelated* [1]. In order to describe correlations between the two electrons here, we must go beyond the Hartree–Fock approximation.

Similar to superconductivity, the *fractional quantum Hall effect* (Sect. 2.1) is a unique field, where correlations between electrons give rise to macroscopically well observable ground states which we would not expect on the level of a Hartree–Fock approximation. Correlations are introduced by interelectronic interaction and, contrary to atomic physics, the quantization of single–electron energy levels is a consequence of the strong magnetic field (Landau levels). The latter phenomenon leads to another unusual feature of the fractional

quantum Hall systems: Since the Landau levels are highly (macroscopically) degenerate, so are the many–electron states in a non–interacting system; particularly for filling factors below one, where it is useful to be restricted to the lowest Landau level, *all* many–electron states have the same energy. Now, the effect of interelectronic interactions cannot be investigated by perturbation theory, as there is no single ground state to start with or, in other words, there is no small parameter in which we could expand the perturbation series: since energy spacing between the many–body states is zero, the interaction is never a small perturbation, regardless of how weak it is. This fact renders the fractional quantum Hall systems unique from the theoretical point of view and makes completely novel types of quantum–mechanical ground states possible: the best known of these are the incompressible quantum liquids.

Quantum Hall ferromagnetism was one of companions of the *integer* quantum Hall effect (Subsect. 3.6). The observed long–range spin order can be explained by exchange energy gain in the ferromagnetic state and hence Hartree–Fock models are basically sufficient to describe the ongoing physics. However, at the end of the previous millennium, new experimental publications appeared: phenomena reminiscent of ferromagnetism have also been observed in the *fractional* quantum Hall regime, being most pronounced at filling factors $\frac{2}{3}$ and $\frac{2}{5}$. In this situation, Hartree–Fock approximation is no longer acceptable: the spin–ordered states are highly correlated. This area is not very well explored. Instead of a lattice of spins which are all pointing in the same direction, here, we are dealing with itinerant electrons which are either in a fully polarized or in a spin singlet state (Subsect. 2.2). Although both states are incompressible, their structure is quite different.

How far can we extend the analogy between an Ising spin–lattice ferromagnet and fractional quantum Hall systems where two ground states with different spin order compete with each other? This was the leading question of this thesis at the outset of the new millennium. There are several fundamental differences between these two systems: the latter one is itinerant and the liquid–like ground state is stable only owing to correlations while, in a spin–lattice, the electrons are spatially fixed and the ferromagnetism occurs also in classical systems. By observing e.g. hysteresis in magnetotransport, experimentators provided a lot of evidence that the two phenomena are indeed very closely related (Subsect. 2.3), but on the other hand, observations without analogy to usual Ising systems were also reported (Subsect. 2.4). Good, so what is going on in those fractional quantum Hall systems? This is the quest for a theoretician.

The objective of the present work was therefore to study the possible ground states and low–lying excited states at filling factors $\nu = \frac{2}{3}$ and $\frac{2}{5}$ with special attention to their spin structure. The exact diagonalization of few–electron systems in a rectangular geometry with periodic boundary conditions was chosen as a method for this investigation. Earlier, this method provided the fundamental support for composite fermion models and this claim remains in effect until today. Most importantly, the exact diagonalization is capable of predicting new ground states of Coulomb–interacting systems without any *a priori* knowledge about their nature. Apart from the homogeneous systems I also investigated spin structures which can form in the low lying states when an inhomogeneity — a magnetic

or a non–magnetic one — is present in the system.

As indicated above, Chapter 2 summarizes the key experiments which motivated this work. On the other hand, as the reader may infer from the initial part of this introduction, the principal challenge of the study is that we deal with many–body systems. A wide theoretical introduction to the field of fractional quantum Hall systems is therefore necessary and it is given in Chapter 3. After the basic tools for our study are presented, I also briefly recall other approaches and put special emphasis on composite fermion theories (Sec. 3.4).

The majority of the original results of this thesis are contained in the following two Chapters. Homogeneous systems at filling factors $\frac{2}{3}$ and $\frac{2}{5}$ are addressed in Chapter 4. I discuss the structure of the incompressible ferromagnetic states, the singlet and fully polarized ones and investigate a half–polarized state which may be the absolute ground state in a narrow range of external parameters. Since formation of domains of different spin polarization is common in conventional ferromagnets, in Chapter 5 I investigate systems at filling factor $\frac{2}{3}$ on their tendency to split into domains when the singlet and polarized incompressible states have the same energy. The probing tool are magnetic inhomogeneities.

At the end of the beginning, I would like to wish the reader to enjoy reading this thesis. If you are a new–comer to the field of fractional quantum Hall systems, may this work help you to discover how beautiful and original the playgrounds in the lowest Landau level are. And if you are a senior researcher in this field, I hope, this work still brings something you have not known before.

2 Experimental findings and discussion

2.1 Quantum Hall Effect: classical, integer and fractional

The volume of literature on Quantum Hall Effects is vast and an attempt to summarize it here would be preposterous. Rather, I will only try to sketch the *link* between the original Nobel–honoured experiments and objects of my study within this thesis. For a more detailed introduction I suggest the books of Yoshioka [102] or Chakraborty and Pietiläinen [17].

With the term *classical Hall effect* we refer to the fact that a magnetic field (B) along z acting on an electric current (I) along x creates an electric bias (U_{xy}) along y. This voltage drop compensates the Lorentz force which the magnetic field exhibits on charge carriers and hence the *transversal (Hall) resistance* $R_{xy} = U_{xy}/I$ is proportional to B [1]. Since the Lorentz force has been compensated by U_{xy}, the longitudinal resistance R_{xx} should be independent on magnetic field.

The quantum Hall effects are manifested by deviations from the $R_{xy} \propto B$ law, which occur in *two–dimensional* samples of high–mobility (and at low temperatures): around certain values of B/n_e remarkably flat plateaus occur, just as if someone cut horizontal stairs $R_{xy} = h/e^2(1/\nu)$ into the (constantly inclined) slope $R_{xy} \propto B$, Fig. 2.1. Klaus von Klitzing was the first to observe such plateaus[2] and he noticed that they occur at integer values of ν up to very high accuracy [51]. Another finding was that whenever a plateau in R_{xy} occurs, the longitudinal resistance R_{xx} drops to zero; this is an extreme form of Shubnikov–de Haas magnetoresistance oscillations.

Already at the very beginning, the origin of the plateaus was correctly recognised. It is the quantization of motion of a free electron in two dimensions in a perpendicular magnetic field: density of states (of *noninteracting* electrons) consists of the delta peaks[3] at $E_n = \hbar\omega(n + \frac{1}{2})$, $n = 0, 1, \ldots$ and each peak can accommodate eB/h states per unit area and per one spin orientation (up or down). Now, imagine some fixed B. Depending on electron density n_e (i.e. number of occupied states per unit area which can be varied by chemical potential, ergo gate voltage, for instance), two different situations in the ground state can occur: the highest Landau level, where some states are occupied, is (a) completely full or (b) is not completely full. In the latter case, we could say the Fermi level lies in the

[1] Resistivity ϱ_{xy} is equal to $B/n_e e$, n_e and e being the carrier density and charge.

[2] The original experimental device was a silicon MOSFET. In fact, von Klitzing measured R_{xy} as a function of n_e rather than that of B, but this is not essential.

[3] If we neglect impurities in the system, see below.

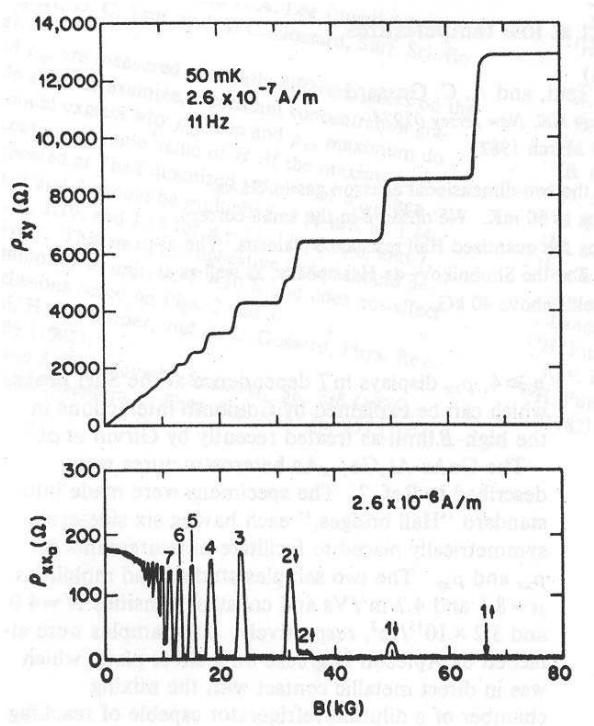

Figure 2.1: Integer quantum Hall effect (from Paalanen *et al.* [76]).

'band', or in other words, there are many excitations of low (zero, in ideal case[3]) energy and the system behaves like a metal; these excitations account just to rearranging electrons in the highest occupied Landau level. Completely different is the case (b): any, even the lowest excitation, must involve promotion of an electron to a higher Landau level and will thus cost at least $\hbar\omega$ in energy.

In this last case, the system is incompressible[4], insulating, or we could say, the Fermi level lies in the gap. A way to reformulate the definition of case (a) and (b) is to introduce the filling factor $\nu = n_e/(eB/h)$ which gives the number of occupied Landau levels. Hereafter (b) means integer value of ν and that is why the effect is called *integer* quantum Hall effect. It takes a long way to explain why these incompressible and compressible states lead to plateaus $R_{xy} = (h/e^2)(1/nu)$ of finite width and as it is not an objective of this thesis to study this interrelationship[5] I take the liberty of referring the interested reader to review and references in Yoshioka's book [102]. Here, I only wish to stress that plateaus in transversal and minima in (or vanishing of) longitudinal resistance herald an incompressible (gapped) many–body ground state.

[4]Infinitesimal excitations (like local increase of electron density, i.e. compression) cost finite energy.
[5]At this place, presence of disorder in the system is essential.

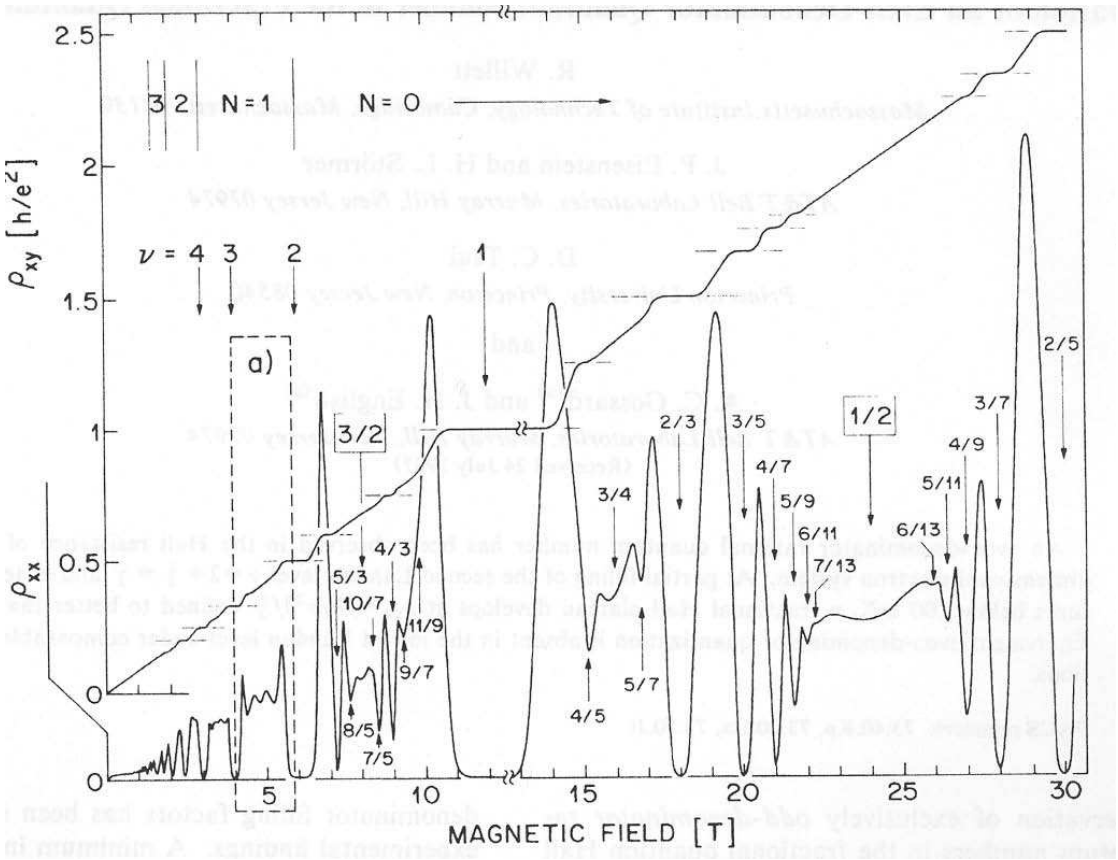

Figure 2.2: Fractional quantum Hall effect (from Willett *et al.* [97]). Filling factor $\nu = \frac{1}{3}$ where the features in the magnetoresistance are strongest, is out of range of this plot.

2.1.1 Many–body physics

Not a long time after the integer quantum Hall effect was discovered, plateaus of $R_{xy} = (h/e^2)(1/\nu)$ were found also for non–integer values of ν. Since the ground state should be gapless within the picture of noninteracting electrons, Tsui, Stormer and Gossard [96] concluded that an incompressible state can occur here only due to interelectronic interactions.

Since 1982 experiments revealed many incompressible ground states at non–integer filling factor, Fig. 2.2. All of them have ν in the form of a fraction p/q with small integers p and q, the denominator being odd in almost all cases. Figure 2.2 shows that the most apparent fractions from the interval $0 < \nu\frac{1}{2}$ belong to the sequence $\nu = p/(2p+1)$.

A fact worth of emphasis is, that no *fractional quantum Hall state* can be explained in the picture of noninteracting electrons. Rather than to consider the scheme of density of states with delta peaks being filled by electrons (which is basically a single electron model) we should therefore focus on a single Landau level (the highest occupied one) and study what many–particle states form therein owing to the electron–electron interaction.

2.2 Ground states with different spin

Soon after Halperin suggested incompressible FQH states which were not fully spin polarized [41], exact diagonalization results indicated that such states can be sometimes energetically more favourable than the fully polarized ones provided Zeeman energy E_Z is small [108],[18].

There are two criteria for the smallness of E_Z: it can be compared either to the cyclotron energy $\hbar\omega$ or to the Coulomb energy $E_C = e^2/(\varepsilon\ell_0)$. In vacuum, it holds $\hbar\omega = \mu_B g B = E_Z$, but this is different in GaAs: small effective mass (rendering ω larger than in vacuum) and smaller effective g–factor yield $E_Z \ll \hbar\omega$. This fact makes the existence of *integer* quantum Hall ferromagnets possible [48].

The latter condition, $E_Z < E_C$, necessary for spin being free in the *fractional* quantum Hall regime (say for filling factors $\nu < 1$), is more restrictive. Its fulfilment can be manipulated on (at least) three ways.

1. *Lower magnetic fields (low electron density).* Because of different scaling of the two quantities with B ($E_Z \propto B$, $E_C \propto \sqrt{B}$), $E_Z < E_C$ is met in the limit $B \to 0$. Experimental drawbacks of this method are, that (a) the absolute value of E_C becomes quite low and thus lower temperatures and higher electron mobilities are required and (b) the electron density must be relatively low and/or the magnetic field relatively high in order to achieve low fractional filling factors $\nu < 1$.

2. *Tilted field.* The Coulomb and cyclotron energies are determined by the z–component of B, just as the motion of electrons is confined to the plane perpendicular to z–axis. Electron spins are not affected by this confinement, hence the Zeeman energy is proportional to the total magnetic field B. By tilting the sample, we can therefore change the ratio between B_z and B and thus between E_C and E_Z. However, since $B \geq B_z$ in any case, we can only make the Zeeman energy effectively larger than Coulomb energy and not smaller.

3. *Pressure dependent g–factor.* By applying hydrostatic pressure to a GaAs sample, we can decrease the effective g–factor. Eventually, it is possible to achieve $E_Z \propto g \approx 0$ or even to change the sign of g but such experiments are very difficult[6].

Tilted field

To my knowledge, first experiments which gave a strong support for non–fully spin polarized FQH ground states, were those of Clark *et al.* [20] and Eisenstein *et al.* [26]. They were both related to states at filling factors $1 < \nu < 2$ (e.g. $\frac{8}{5}$, $\frac{4}{3}$) which are *particle–hole*

[6] Vanishing g factor requires a pressure of about 18 kbar which must be achieved at liquid helium temperature.

conjugates[7] to $\frac{2}{5}$ and $\frac{2}{3}$. Therefore, the electron density ('$\frac{8}{5}$') is not too low (as to make experiments difficult) but low is the density of holes ('$\frac{2}{5} = 2 - \frac{8}{5}$') which are the relevant current carriers. In other words, these experiments get an effective $\frac{2}{5}$ system at much lower magnetic field, namely at field corresponding to $\nu = \frac{8}{5}$ (recall $\nu \propto 1/B$) and the lower the magnetic field, the better for $E_Z(\propto B) \ll E_C(\propto \sqrt{B})$.

Therefore, for the cited experiments, Zeeman energy was indeed small and the observed FQH states were spin–singlets (which are preferred for $E_Z = 0$ at the named filling factors). The actual observation then was that effectively increasing the Zeeman energy (by tilting the magnetic field while keeping B_z constant) a transition to the fully spin polarized state occurs. This conclusion was possible to draw from the reentrant behaviour of longitudinal resistance R_{xx} at $\nu = \frac{8}{5}$: it had a pronounced minimum for zero tilt angle (perpendicular field) which disappeared for at large enough tilt and reappeared for yet higher tilt angles, Fig. 2.3(a).

The primary disadvantage of investigations at filling factor $\frac{8}{5}$ instead of $\frac{2}{5}$ is that the particle–hole conjugation must be granted. This is true only if Landau level mixing is negligible and this in turn requires $E_C \ll \hbar\omega$ which means high magnetic fields.

Landé g–factor modified by hydrostatic pressure

It seems to me that Morawicz *et al.* [67] who were the first to observe the fractional quantum Hall effect under hydrostatic pressure did not recognise that they actually saw the transition to the singlet ground state at filling $\frac{4}{3} = 2 - \frac{2}{3}$. At normal pressure, the corresponding minimum in $R_{xx}(B)$ was absent (just as it should be right at the transition) and it appears with increasing pressure when the Zeeman energy decreases (along with g) preferring thus the singlet state over the polarized one. Although authors of [67] do not discuss the effect of varying g–factor in their experiments, they give a good account of other quantities related to the FQHE which change under hydrostatic pressure (effective mass, dielectric constant, disorder strength).

Later experiments by Kang *et al.* [50] demonstrated clearly the spin transition directly at filling $\nu = \frac{2}{5}$, Fig. 2.3(b). Leadley *et al.* [61] brought the method up to perfection: they achieved pressures high enough to make the g–factor vanish and presented detailed data of transport gaps at $\nu = \frac{2}{5}, \frac{2}{3}$ and $\frac{1}{3}$ as a function of g. Most interestingly, they were also able to make some claims about the existence of skyrmions at filling factor $\frac{1}{3}$. These are the 'composite–fermion–analogy' of skyrmions at filling factor $\nu = 1$.

[7] In presence of spin degree of freedom (and neglecting Landau level mixing), filling factors ν and $2 - \nu$ are particle–hole conjugate. These holes are meant not in the sense of host material bandstructure but rather in the sense of Landau levels: an almost full Landau level has several empty states which we call here holes.

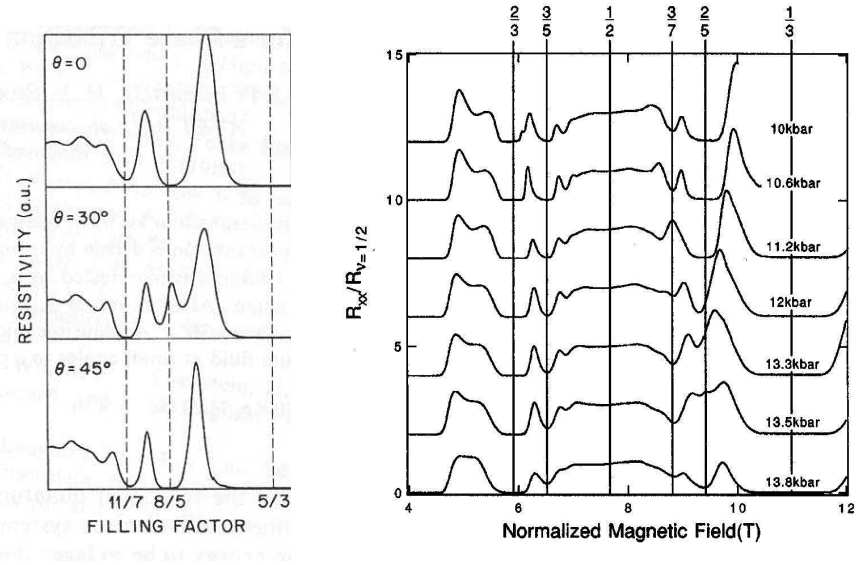

(a) Tilted field

(b) Modified g.

Figure 2.3: Spin transition of the incompressible ground state at filling factors $\frac{8}{5}$ and $\frac{2}{5}$ which are particle–hole conjugates in the limit of no Landau level mixing ($\hbar\omega$ much larger than Zeeman and Coulomb energy). Figures taken from Eisenstein *et al.* ([26], Fig. 2.) and Kang *et al.* ([50], Fig.1).

Spin transitions achieved by varying the electron density

It was not unusual to perform experiments at different electron densities since the very early times of the FQHE and for instance Fig. 3 in [20] shows how presence or absence of a minimum in R_{xx} at $\nu = \frac{4}{3}$ depends on the electron density (or equivalently[8] on B at which it is $\nu = \frac{4}{3}$). The following methods allow to access different electron densities:

- *Strength of doping.* Tsui and Gossard showed in the early times of the IQHE that silicon MOSFET structure used by von Klitzing can be replaced by a GaAs/ GaAlAs heterostructures where Si–donors are spatially separated from the 2D electron gas confined to the triangular potential well at the GaAs/GaAlAs surface [95] [9]. Concentration of the Si–donors determines then the density of electrons in the 2DEG. Obviously, this method allows for one value of electron density per one sample grown.

[8]Eq. 3.6: $\nu = n_e/(eB/h)$ or $n_e = B \cdot (e\nu/h)$. If we choose to study some particular filling factor, say $\nu = \frac{4}{3}$, then the lower the electron density n_e, the lower is the magnetic field B at which we reach this filling factor.

[9]Since the ionized donors are one of major sources of impurity scattering, the concept of separating them from the 2DEG was the crucial step to achieve high mobility samples.

- *Illumination.* By illuminating GaAs/GaAlAs heterostructures the carrier density can be increased. For this purpose, red light–emitting diodes are mounted to samples (e.g. [55]).
- A *gate* is in principle a 'metallic' plate parallel to and separated (by an insulating layer) from the 2D electron gas. Just as in an usual capacitor, voltage applied to the gate V_g controls (is proportional to, in the simples picture) the density of electrons in the 2DEG. Since V_g can be varied continuously it allows to sweep through a whole range of electron densities. This technique is most convenient to study spin transitions induced by varying the ratio of Zeeman and Coulomb energy (or $B \propto n_e$ at fixed ν) but it is technologically nontrivial to prepare gated structures with high mobility. Examples of gated 2D systems are Si–MOSFETs as used by von Klitzing [51], single GaAs/GaAlAs heterostructures (triangular wells) [42] and wide quantum wells with two gates (back and front) [57].

Using a continuous variation of the electron density many results were obtained in the field of phase transitions especially at filling factors $\nu = \frac{2}{3}$ and $\frac{2}{5}$. This will be the topic of the following Section.

Concluding remarks

Experiments described so far demonstrate the existence of FQH ground states with different spins only indirectly. Direct measurements of the spin–polarization of the 2D electron gas were performed later by Kukushkin, see Sec. 2.4. A more detailed review of experimental and theoretical results regarding spin of FQH states was given by Chakraborty [16] (in 2000).

2.3 Phenomena at fractional filling factors reminiscent of ferromagnetism

In the previous Section I sketched how the existence of fractional incompressible ground states with different spin polarization was demonstrated experimentally. In 1998, experimental articles appeared, which indicated that a transition between a spin polarized and spin singlet ground state may be accompanied with unexpected phenomena reminiscent of ferromagnetism. These were works of Kronmüller *et al.* [55] from MPI Stuttgart and Cho *et al.* [19] from the University of Chicago and Santa Barbara.

Kronmüller *et al.* measured the longitudinal resistance (R_{xx}) of a high mobility narrow quantum well[10] during a sweep through magnetic field. A deep minimum is expected

[10]This is a GaAlAs/GaAs/GaAlAs heterostructure. Since the conducting layer of GaAsis only 15 nm wide, electron states are quantized in the growth direction. Moreover, they are energetically far apart due to such a strong confinement. Only the lowest subband (state in the growth direction) is occupied and mixing to higher subbands can be neglected. The system is nearly perfectly two–dimensional.

to occur at filling $\nu = \frac{2}{3}$ (i.e. at corresponding $B = n_e h/(\nu e)$, Eq. 3.6) indicating an incompressible ground state, singlet ($n_e \ll n_c$) or fully polarized ($n_e \gg n_c$). The minimum should vanish for $n_e \approx n_c$, i.e. just at the transition between the two types of ground states[11]. Instead, a sharp peak was observed in R_{xx} around $\nu = \frac{2}{3}$. The peak exceeded typical values of R_{xx} around $\nu = \frac{2}{3}$ often by more than 100% and it was therefore baptised *huge longitudinal magnetoresistance* (HLM), Fig. 2.4.

The most obvious property of the peak was that it occurred only for slow sweeps, it completely disappeared when the magnetic field was changed fast during the measurement of R_{xx}. When the magnetic field was set so that R_{xx} reached just the peak value, the resistance increased in time and saturated on time scales of 10 s. The saturation time was different for different samples, it was longer in Hall bars with larger area (inset in Fig. 2.4). Also, hysteresis of R_{xx} was observed: $R_{xx}(B)$ was different when the magnetic field was swept up or swept down (Fig. 3 in [55]).

Since charge carriers are excited into the quantum well by illuminating the sample, the electron (carrier) density is in practice restricted to one single value (when light is on). Luckily enough, the particular value of n_e in samples of Kronmüller was approximately just the one corresponding to the transition between spin polarized and spin singlet state at filling factor $\frac{2}{3}$. However, the authors of the article [55] verified that the HLR peak disappears in tilted magnetic field where we move off the transition as Zeeman energy becomes larger than Coulomb energy (compared to the case when magnetic field is perpendicular, see Sec. 2.2).

While the longitudinal resistance changed dramatically under the conditions described above, slight changes were also visible in the Hall resistance: hysteresis and shift of the plateau value by about 1% [54]. Similar but less pronounced phenomena were found at filling factor $\nu = \frac{3}{5}$.

Cho *et al.* [19] reported hysteretic phenomena at filling factor $\nu = \frac{2}{5}, \frac{3}{7}, \frac{4}{7}$ and $\frac{4}{9}$, Fig. 2.5(a). This group mastered the technique of varying the effective g–factor by hydrostatic pressure (see Sec. 2.2) which allowed them to show that hysteresis occurs only if the singlet and polarized ground states (of $\nu = \frac{2}{5}$) have similar energy (Fig. 2 in [19]). In later studies [27], the temporal evolution of R_{xx} was studied and a logarithmic behaviour *without saturation* was found[12] In this article, a wide comparison with other types of magnetic materials was also presented.

These findings were published about simultaneously with first experiments on quantum Hall Ising ferromagnetism at integer filling factors [48]. This occurs when two Landau levels (capable of accommodating in total $2eB/h$ states) cross and they are to be occupied by only eB/h states (counted per unit area of 2DEG). Denote states in one of these Landau levels by pseudospin up and states in the other one by pseudospin down. Due to interelectronic interaction (basically exchange energy), the ground state is either *all* electrons with pseudospin up or *all* electrons with pseudospin down, just as in a spin lattice

[11] Cf. with previous Section: low n_e means low B (at which we reach $\nu = \frac{2}{3}$) whereas Zeeman energy will be smaller than Coulomb energy. $B = n_e h/(\frac{2}{3}e)$

[12] Saturation rate $r = \mathrm{d}R_{xx}/\mathrm{d}\log t$ was shown to diverge at low temperatures as $1/T^{\alpha}$ with $\alpha \approx 1.3$.

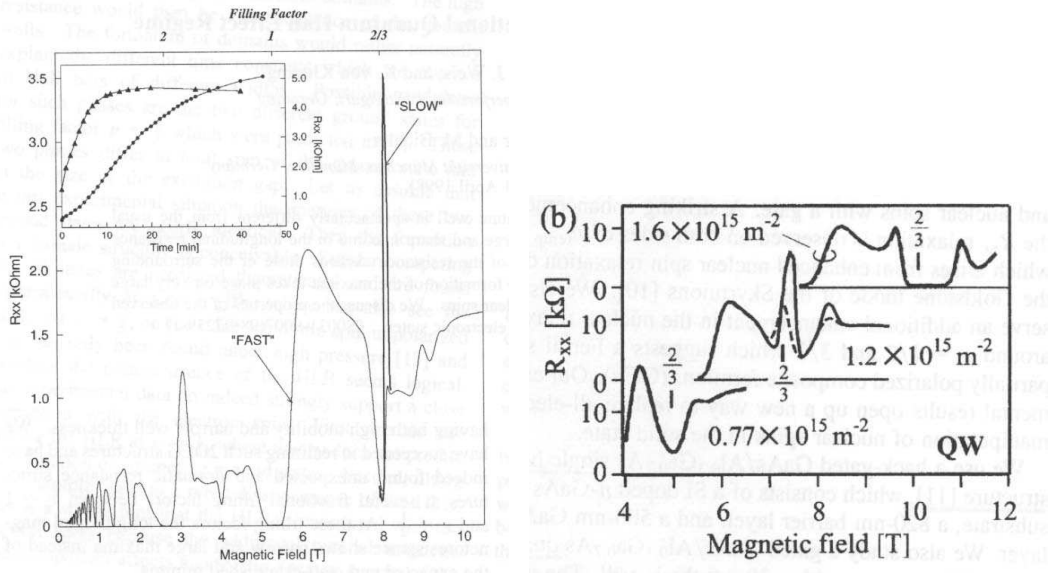

(a) HLR peak was observed only for slow sweeps through magnetic fields.

(b) The effect appears only at the critical electron density where polarized and singlet ground states have the same energy.

Figure 2.4: Huge longitudinal (magneto)resistance (HLR) at filling factor $\nu = \frac{2}{3}$. From Kronmüller *et al.* [55] and Hashimoto *et al.* [42].

with Ising type anisotropy[13]. The system thus exhibits a long–range order in pseudospin, however, its fundamental distinction from spin lattices is, that it is an *itinerant ferromagnet*. Other types than just Ising ferromagnetism is also possible in integer quantum Hall systems. A fundamental classification was given by Jungwirth and MacDonnald [46].

Taking into account the analogy between electronic systems at filling factor $\frac{2}{3}$ or $\frac{2}{5}$ and composite fermion systems at filling factors ± 2, it was suggested [19] that experiments of Kronmüller and Cho demonstrate quantum Hall ferromagnetism of composite fermions.

2.3.1 Further studies

Long relaxation rates of R_{xx} observed by Kronmüller [55] suggested that nuclear spins are somehow involved in the whole business. This link was proven by NMR measurements [53], [23]: the peak resistance of the HLR effect responded sensitively when the sample was irradiated at frequency corresponding to transitions between different spin states of the host material nuclei (gallium or arsenic), Fig. 7 in Ref. [23]. Apart from the implications

[13] $H = \Sigma_{ij} J S_i S_j + \sum_i S_i^2$. This model requires that (in the ground state) nearest neighbours have parallel spin and each spin is either up or down (not e.g. pointing along x).

for this particular experiment, this opens up a new way how to measure nuclear magnetic resonance resistively (rather than by registering how much of the RF signal was absorbed). It is noteworthy, that the nuclear resonance peak (measured in R_{xx}) was *fourfold* split. This is quite unexpected since the nuclei (^{75}As) have spin $I = 3/2$ which allows for *three* different transition frequencies between the four states $I_z = \pm\frac{3}{2}, \pm\frac{1}{2}$. Coupling between electron and nuclear spin in quantum Hall systems had already been known before (Dobers *et al.* [24]) but these works were pioneering in the context of fractional fillings.

Voltage–current characteristics of magnetoresistance around filling factor $\frac{2}{3}$ were also a subject of a thorough study by Kraus *et al.* [52]. Barkhausen jumps (long known from magnetism [14]) in the temporal evolution of R_{xx} at $\nu = \frac{2}{3}$ were found by Smet *et al.* [91] bringing thus another evidence of ferromagnetism, Fig. 2.5(b). Support for the existence of domains (singlet and polarized) was provided also by surface acoustic wave experiments by Dunford *et al.* [25]. Suggestions and demonstrations how to control nuclear spin polarization by manipulating the electron system were presented by Hashimoto *et al.* [42]. Since nuclear spins are one of hot candidates for qubits, such studies were cordially welcome by journals even of the Nature class (Smet *et al.* [90]).

Kraus *et al.* [52] proposed that there are two different operating modes of a $\frac{2}{3}$ system at the (singlet to polarized) transition: the authors of Ref. [52] call them quantum Hall ferromagnetism and huge longitudinal resistance. At low excitation currents, the feature observed in R_{xx} (at $\nu = \frac{2}{3}$ and transition between the two ground states) is small, Fig. 2.6(a), and resistively detected nuclear magnetic resonance of arsenic shows threefold splitting as expected for $I = 3/2$ nuclei [91]. At higher currents, the peak in R_{xx} is big (or, with original words, 'huge') and the NMR signal is fourfold split [53]. Assuming domains of polarized and singlet states in both regimes, the small R_{xx} peak in the former regime is due to scattering of electrons *along* domain wall loops, as it was suggested under conditions of integer QHE systems by Jungwirth and MacDonald [47]. The magnitude of the peak in R_{xx} in the latter regime was explained by scattering of electrons *between* domains whereas the nuclear spin polarization changes (flip–flop scattering) contributing thereby to the disorder potential[14] Nevertheless, convincing evidence for this model was not presented yet.

2.4 Half–polarized states at filling factor $\frac{2}{3}$

The story about filling factor $\frac{2}{3}$ is not complete if we mention only ferromagnetic–like phenomena.

Kukushkin *et al.* [56] employed an optical technique to measure the polarization of the 2D electronic system in a gated single heterostructure. Thus, these experiments allowed to study electron polarization at fixed filling factor and variable electron density (or, equivalently, fixed filling factor and variable magnetic field). At filling factor $\frac{2}{3}$ these experiments

[14] Authors of Ref. [52] speculate that more and more smaller and smaller domains arise in the electronic system in such situation. This would lead to a larger resistance.

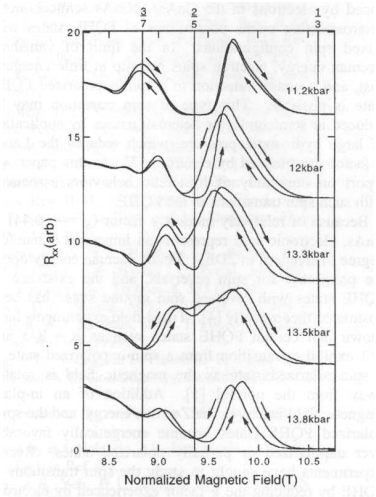

(a) Hysteresis at filling $\frac{2}{5}$ disappears when energies of the singlet and the polarized ground states become too much different (top curve).

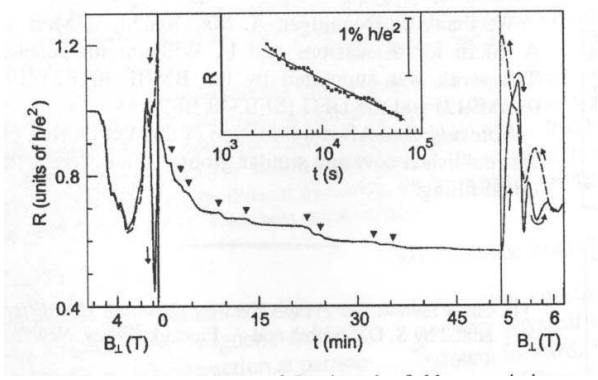

(b) Barkhausen jumps during saturation in time of R_{xx} at its HLR peak value.

Figure 2.5: More evidence for ferromagnetism at filling factors $\frac{2}{3}$ and $\frac{2}{5}$. From Cho *et al.* [19] and Smet *et al.* [91].

confirmed that for low densities (or low Zeeman energy, see Sec. 2.2) the polarization is zero while it is one for high electron densities, Fig. 2.7, just as we expect for spin singlet and fully polarized ground states. However, around the transition between these two a clear plateau at value one half was observed. Similar structures (plateaus in polarization at non–extremal values) were observed also at other filling factors.

Later experiments by Freytag *et al.* suggested that when Zeeman energy is decreased, the fully polarized ground state at $\nu = \frac{2}{3}$ goes into a stable ground state with spin polarization approximately 0.75 or 0.8. However, these experiments could not reach Zeeman energies low enough for the unpolarized (singlet) ground state to take over. The structure studied was a multiple GaAs/GaAlAsquantum well, i.e. many quantum wells ($d = 30$ or 25 nm wide) separated by barriers (250 or 185 nm wide GaAlAslayer) wide enough so that the wells can be considered independent. As a probing tool for the electronic polarization the Knight shift of the NMR signal from gallium nuclei was used[15].

[15]Knight shift is proportional to the polarization of the electron system.

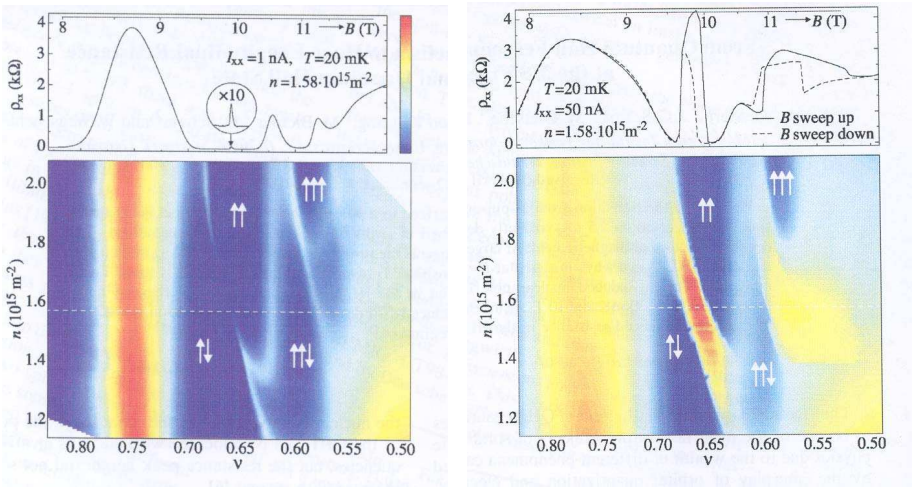

(a) QHF (b) HLR

Figure 2.6: Singlet to spin-polarized transition at filling factor $\frac{2}{3}$: Quantum Hall Ferromagnetism (QHF) at low excitation currents (1 nm) and Huge Longitudinal Resistance (HLR) at high currents (50 nm). Plots show the longitudinal resistance R_{xx} as a function of filling factor ν and electron density n. From Kraus *et al.* [52].

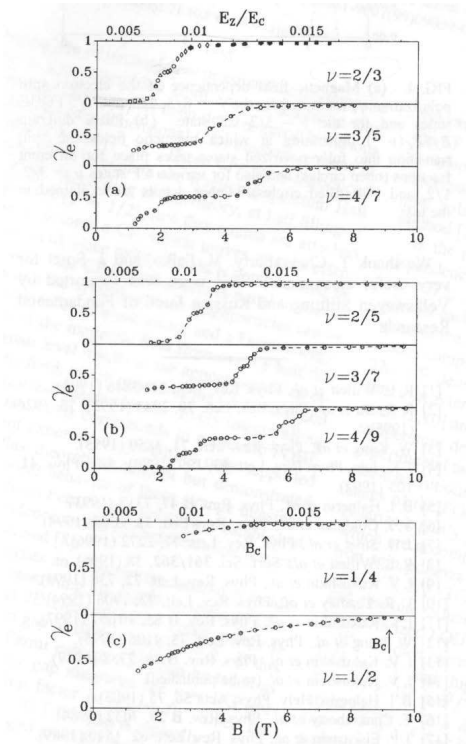

(a) Optical experiments: plateau at polarization one half for $\nu = \frac{2}{3}$.

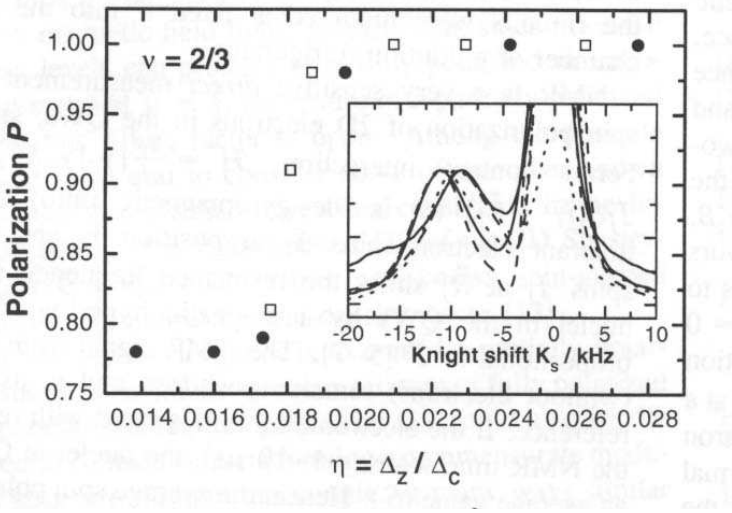

(b) Measurements of the Knight shift: polarization settles at a value between 0.75 and 0.8.

Figure 2.7: Filling factor $\frac{2}{3}$: stable intermediate states with polarization other than zero (singlet state) or one (spin polarized state). From Kukushkin [56] and Freytag [29].

3 Theoretical basics

3.1 One electron in magnetic field

Purpose of this section is to review the textbook problem of one electron confined to a plane subject to a perpendicular magnetic field. A quantum mechanical answer, the macroscopically degenerate Landau levels will be recalled as well as different bases of these Hamiltonian eigenspaces. Various choices of the vector potential gauge will lead us naturally to explicit formulae for wavefunctions which will be useful later when studying many particle systems in a magnetic field. Also, symmetries of the Hamiltonian will be mentioned, especially the magnetic translations which supersede ordinary spatial translations when magnetic field is present.

3.1.1 Magnetic field in quantum mechanics

A painless introduction according to Murthy and Shankar [72].

Everybody (up to a set of measure zero) knows what a classical charged particle moving at velocity v in a plane does if it is subject to a homogeneous magnetic field B. Due to the centripetal Lorentz force, it moves on a circular cyclotron orbit with radius r_c and angular frequency ω:

$$\omega = \frac{|e|B}{m}\,, \qquad r_c = \frac{v}{\omega}$$

Here e is the charge and m the mass of the particle.

Obviously, its energy does not depend on the center of the cyclotron orbit but rather on the position and velocity relative to it. Hereafter, the former coordinate will be called *guiding centre*, R, the latter coordinate will be referred to as *cyclotron coordinate*, $\boldsymbol{\eta}$.

We now want to transfer this concept to quantum mechanics. The cyclotron coordinate will lead to Landau level quantization, the guiding centre coordinate will provide us with the degeneracy of the Landau levels. The Hamiltonian written in terms of p_x, p_y, x, y is

$$H_0 = \frac{1}{2m}(\mathsf{p} + e\mathsf{A})^2 = \frac{1}{2m}\boldsymbol{\Pi}^2\,, \tag{3.1}$$

where the vector potential A defines a homogeneous magnetic field in z–direction, $\mathsf{B} = B\widehat{\mathsf{z}_0} = \nabla \times \mathsf{A}$. Since A is a function of x, y, the *canonical momentum* p fails to be a good quantum number ($[H, \mathsf{p}] \neq 0$) and the *kinetic momentum* $\boldsymbol{\Pi} = [H_0, \mathsf{r}] = m\mathsf{v}$ takes its place.

Now, we perform a coordinate transformation. The cyclotron coordinate is uniquely determined by $\boldsymbol{\eta} \perp \boldsymbol{v}$, i.e. $\boldsymbol{\eta} \propto \widehat{z_0} \times \boldsymbol{\Pi}$ and $|\boldsymbol{\eta}| = r_c$, and the guiding centre by $\boldsymbol{r} = \boldsymbol{R} + \boldsymbol{\eta}$ (see Fig. 3.1).

$$\boldsymbol{\eta} = \frac{\ell_0^2}{\hbar} \widehat{z_0} \times \boldsymbol{\Pi}, \qquad \boldsymbol{R} = \boldsymbol{r} - \boldsymbol{\eta}\,.$$

$$\eta_x = -\frac{\ell_0^2}{\hbar}(p_y + eA_y) \qquad R_x = x + \frac{\ell_0^2}{\hbar}(p_y + eA_y) \tag{3.2}$$

$$\eta_y = \frac{\ell_0^2}{\hbar}(p_x + eA_x) \qquad R_y = y - \frac{\ell_0^2}{\hbar}(p_x + eA_x) \tag{3.3}$$

A convenient length scale, the magnetic length $\ell_0 = \sqrt{\hbar/|e|B}$ has been introduced. These new variables constitute the *same* algebra as p_x, x, p_y, y

$$[\eta_x, \eta_y] = -i\ell_0^2\,, \quad [R_x, R_y] = i\ell_0^2\,, \quad [\eta_j, R_l] = 0\,,\ j, l \in \{x, y\}\,, \tag{3.4}$$

except for that ℓ_0^2 replaced $\hbar$ in $[x, p_x] = i\hbar$. It is worth of a notice that even though $\boldsymbol{\eta}$ and $\boldsymbol{R}$ depend on the gauge, these commutation relations do not. They only depend on magnetic field via $\ell_0^2 \propto 1/B$.

The Hamiltonian reexpressed in these new variables $(\eta_x, \eta_y, R_x, R_y)$ reads

$$H_0 = \frac{\hbar^2}{2m\ell_0^4}\boldsymbol{\eta}^{\,2} = \frac{\hbar^2}{2m\ell_0^4}(\eta_x^2 + \eta_y^2)\,, \qquad \text{and} \qquad [H_0, \boldsymbol{R}] = 0\,. \tag{3.5}$$

It might seem puzzling that coordinates η_x and η_y do not commute. Consider however the cyclotron motion (Fig. 3.1): both η_x and η_y fluctuate within range $[-r_c, r_c]$. If we tried to suppress the fluctuation ($r_c = 0$), we would have to stop the particle completely. A sharp value of position and velocity is however prohibited by the uncertainty principle.

The problem described by Eq. 3.5 is equivalent to the one–dimensional harmonic oscillator, '$p_x^2 + x^2$', owing to the fact that commutators $[x, p_x]$ and $[\eta_x, \eta_y]$ are the same up to a numerical factor. Except for the energy scaling, the spectrum of H_0 in Eq. 3.5 is therefore the same as of the harmonic oscillator

$$E_n = (n + \tfrac{1}{2})\hbar\omega\,.$$

On the other hand, $[H_0, \boldsymbol{R}] = 0$ shows that there is a cyclic coordinate and moreover H_0 is independent of it. This coordinate distinguishes states which belong to the same energy level. Owing to $[R_x, R_y] = i\ell_0^2$ and thus $\Delta R_x \Delta R_y = 2\pi\ell_0^2$, each state occupies thus an area of $2\pi\ell_0^2$ in the $[R_x, R_y]$ space and thus there are $L^2/(2\pi\ell_0^2)$ states in each energy level E_n in a system of area L^2.

The energy levels we have just seen are the *Landau levels*. Their degeneracy, $L^2/(2\pi\ell_0^2)$ states of equal energy E_n in a system of area L^2, is indeed macroscopic: for $B = 1$ T

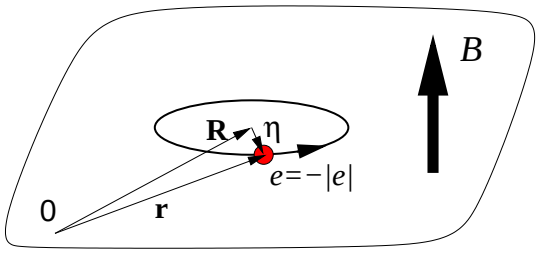

Figure 3.1: Negatively charged particle in a plane: cyclotron coordinate $\boldsymbol{\eta}$ and guiding centre $\boldsymbol{R}$.

there are 0.24×10^{11} states in a system of area 1 cm^2. We should bear in mind that the degeneracy changes proportionally to magnetic field B.

A system of N_e *non-interacting* particles (areal density $N = N_e/L^2$) is essentially described by the Hamiltonian H_0 and in the ground state. Landau levels are simply filled up to the Fermi level. It is therefore handy to define the *filling factor*

$$\nu = \frac{N_e}{L^2/(2\pi\ell_0^2)} = \frac{N}{eB/h} = \frac{N_e}{(BL^2)/(h/e)} = \frac{N_e}{\Phi/\Phi_0} = \frac{N_e}{N_m}\,. \tag{3.6}$$

This number denotes both (a) the number of occupied Landau levels (which can be non-integer if the last Landau level is only partly occupied) and (b) the reciprocal value of the number N_m of magnetic flux quanta Φ_0 passing through the 2D system per particle.

Integer quantum Hall effect occurs just when ν equals an integer. In that case any excitation, even infinitesimal, must promote at least one electron to a higher Landau level and costs therefore a finite energy $\geq \hbar\omega$ rendering the ground state *incompressible*[1]. See Sec. 2.1 for more details.

3.1.2 Wavefunctions and different gauges of magnetic field

So far, we did not choose any particular form of the vector potential. If we want to get explicit expressions for wavefunctions in some particular Landau level, we will have to solve some differential equations. Therein, the vector potential $\boldsymbol{A}$ will appear, and even though not necessary, it is very handy to choose some particular gauge and to make all terms in those differential equations explicit. As the Landau levels are degenerate there are many different bases which span the same space (a particular Landau level). As a matter of fact, the wavefunctions we are going to obtain will reflect the symmetry of the vector potential. We should therefore choose the gauge appropriate to the desired symmetry of the wavefunctions.

In this subsection we will recall gauge invariant formulae for calculating eigenfunctions of H_0 (given by Eq. 3.1). Explicit forms of the wavefunctions in *circular (symmetric) gauge* and *Landau gauge* will be derived in the next subsection.

[1] In a compressible medium, infinitesimal compression must cost infinitesimal energy.

Wavefunctions from gauge invariant formulae

According to Eq. 3.5 there are four operators relevant for the problem of a charged particle in 2D subject to a perpendicular magnetic field: η_x, η_y, R_x and R_y. The former two are responsible for Landau levels (energies of a harmonic oscillator), the latter two for the degeneracy. Regarding the commutation relations, $[\eta_x, \eta_y] = -i\ell_0^2$ and $[R_x, R_y] = i\ell_0^2$ (and $[\eta_{x,y}, R_{x,y}] = 0$), we could reformulate the problem as an abstract two–dimensional harmonic oscillator with one direction 'suppressed' by a vanishing excitation energy

$$H_0 = \frac{\hbar^2}{2m\ell_0^4}(\eta_x^2 + \eta_y^2) + 0 \cdot (R_x^2 + R_y^2)\,.$$

In order to get formulae for eigenstates, we introduce ladder (or creation and annihilation) operators a, b, $[a, a^\dagger] = [b, b^\dagger] = 1$, $[a^{(\dagger)}, b^{(\dagger)}] = 0$

$$\begin{aligned} H_0 &= \hbar\omega(a^\dagger a + \frac{1}{2}) + 0 \cdot (b^\dagger b + \frac{1}{2})\,, \\ & a = (\eta_x - i\eta_y)/(\ell_0\sqrt{2})\,, \qquad b = (R_x + iR_y)/(\ell_0\sqrt{2})\,. \end{aligned} \tag{3.7}$$

Normalized eigenstates to this Hamiltonian are

$$|n, m\rangle = \frac{(a^\dagger)^n}{\sqrt{n!}}\frac{(b^\dagger)^m}{\sqrt{m!}}|0, 0\rangle\,, \tag{3.8}$$

and the ground state is defined by

$$a|0, 0\rangle = 0\,, \qquad b|0, 0\rangle = 0\,. \tag{3.9}$$

The energy of such states, $H_0|n, m\rangle = (n + \frac{1}{2})|n, m\rangle$, is given solely by n while m is the quantum number which distinguishes the degenerate states within one Landau level.

One way to obtain an explicit form of eigenfunctions to H_0 (in the real space representation) is the following: (a) choose one particular gauge of the vector potential A, (b) evaluate the ladder operators (first Eq. 3.2 and $p_i = (\hbar/i)\partial_i$, then Eq. 3.7), (c) get the ground state by solving the differential equation 3.9 and finally (d) obtain an arbitrary state by applying the creation operators, Eq. 3.8.

3.1.3 Angular momentum, symmetric gauge

According to Chakraborty and Pietiläinen [17].

A plane with perpendicular homogeneous magnetic field is obviously rotationally invariant. Therefore we expect the Hamiltonian H_0 (Eq. 3.1) to conform with this symmetry. Let us choose the *symmetric gauge* $\mathsf{A} = \frac{1}{2}B(y, -x, 0)$ and transform H_0 into (dimensionless) polar coordinates according to $x/\ell_0 = r\cos\varphi$, $y/\ell_0 = r\sin\varphi$.

$$H_0 = \frac{1}{2}\hbar\omega\left(-\Big[\underbrace{\frac{\partial^2}{\partial r^2} + \frac{1}{r}\frac{\partial}{\partial r} + \frac{1}{r^2}\frac{\partial^2}{\partial\varphi^2}}_{\Delta} + \frac{1}{4}r^2\Big] - \underbrace{\frac{1}{i\hbar}\frac{\partial}{\partial\varphi}}_{L_z/\hbar}\right) \tag{3.10}$$

This may be called a 'Fock–Darwin form[2]' of H_0 as it is a good starting point to describe 2D quantum dots defined by parabolic confinement in the xy plane (confinement potential simply adds to the $\frac{1}{4}r^2$ term in Eq. 3.10 and the problem remains analytically soluble).

The Hamiltonian H_0 is a sum of two terms: a 2D harmonic oscillator with energy levels $\hbar\omega(i+\frac{1}{2})$, $i = 0, 1, \ldots$ and an angular momentum term contributing by energy[3] $-\hbar\omega m$, $m = 0, 1, \ldots, i$.

$$H_0 = \hbar\omega(a_x^\dagger a_x + a_y^\dagger a_y) - \hbar\omega(L_z/\hbar)\,.$$

The lowest Landau level ($E = \frac{1}{2}\hbar\omega$) consists of states $(i,m) = (0,0)$, $(1,1)$, $(2,2), \ldots$ the first Landau level ($E = \frac{3}{2}\hbar\omega$) of $(1,0)$, $(2,1)$, $(3,2)\ldots$ etc. (see also Fig. 3.3). Obviously

$$E = \hbar\omega\left(\frac{1}{2}i - \frac{1}{2}m + \frac{1}{2}\right) = \hbar\omega\left(n + \frac{1}{2}\right)\,, \qquad \text{where } n = i - m$$

is the Landau level index and each Landau level is infinitely degenerate[4].

Normalized wavefunctions of state (i,m) are simultaneously eigenfunctions of a 2D harmonic oscillator (i-th level) and angular momentum $m\hbar$. Using $n = i - m$ instead of i,

$$\psi_{n,m}(r,\varphi) = \left[\frac{n!}{2\pi 2^m (n+|m|)!}\right]^{1/2} \exp(-im\varphi)\exp(-r^2/4) r^{|m|} L_n^{|m|}(r^2/2)\,, \tag{3.11}$$

$$n = 0, 1, 2, \ldots : \text{ Landau level index}$$
$$m = 0, 1, 2, \ldots : \text{ angular momentum}$$

is expressed in terms of the associated Laguerre polynomials ([35], p. 1037)

$$L_n^m(x) = \frac{1}{n!} e^x x^{-m} \frac{\mathrm{d}^n}{\mathrm{d}x^n}(e^{-x} x^{n+m})\,. \tag{3.12}$$

Complex coordinates

Since we investigate particles moving in a 2D plane and wavefunctions have complex values, it is often helpful to describe the position of a particle by a complex number $z = x + iy$ rather than by a two–component vector. Let us briefly introduce this concept.

The transformation rules are the following

$$z = (x + iy) \qquad \partial_z = \frac{1}{2}(\partial_x - i\partial_y)$$
$$\bar{z} = (x - iy) \qquad \partial_{\bar{z}} = \frac{1}{2}(\partial_x + i\partial_y)\,,$$

[2]Derived by Fock and Darwin in 1928 and 1930, see Refs. in [17], App. A. $[H_0, L_z] = 0$ is obvious in this form.

[3]Note that (i) H_0 is nonnegative rendering $|m| \le i$ inevitably and (ii) each level i is $(i+1)$–fold degenerate as it should be for a 2D oscillator.

[4]If we constrain the system to a finite area of diameter R and allow only states which fulfill $\langle r\rangle < R$, we would recover the known degeneracy. We would have counted $\pi R^2/(2\pi\ell_0^2)$ states in each Landau level n.

and this form grants (apart from others)

$$\partial_z z = \partial_{\bar{z}} \bar{z} = 1\,, \qquad \partial_{\bar{z}} z = \partial_z \bar{z} = 0\,, \qquad \bar{\partial}_z = \partial_{\bar{z}}\,.$$

Setting just for this Subsection $\ell_0 = 1$, the Hamiltonian, Eq. 3.10, takes the form

$$H_0/(\tfrac{1}{2}\hbar\omega) = -\frac{1}{4}(\partial_z \partial_{\bar{z}} + z\bar{z}) + \frac{1}{2} i(z\partial_z - \bar{z}\partial_{\bar{z}})\,,$$

and the eigenfunctions, Eq. 3.11, up to a normalization, are given by

$$\psi_{n,m}(z) = \exp(\tfrac{1}{4} z\bar{z}) \partial_z^n \partial_{\bar{z}}^{m+n} \exp(-\tfrac{1}{2} z\bar{z})\,. \tag{3.13}$$

In particular,

- the lowest Landau level ($n = 0$) is spanned by functions

$$\psi_m(z) = z^m \exp(-\frac{1}{4} z\bar{z}) \tag{3.14}$$

  which can be easily cross–checked with formula 3.11 and the fact $L_0^m(x) = x^m$. Except for the exponential factor, an arbitrary state in the lowest Landau level is an *analytic (holomorph) function*, i.e. it is a power series in variable z and does not contain $\bar{z}$.

- an arbitrary state in the n–th Landau level is a polynomial of n–th degree in the (antianalytic) variable $\bar{z}$.

3.1.4 Magnetic translations, Landau gauge

A plane with perpendicular homogeneous magnetic field is obviously also translationally invariant. Spatial translations applied to the Hamiltonian leave the magnetic field unchanged but may alter the gauge. Operators which conserve also the gauge (and which therefore commute with H_0) are the *magnetic translations* (Zak [106],[107]).

The basic idea of magnetic translations is quite transparent. Consider the Landau gauge: the vector potential $\mathsf{A} = (0, Bx, 0)$ is obviously invariant to translations $y \to y + \Delta y$ (here, ordinary translations and magnetic translations coincide). However, (an ordinary) translation $x \to x + \Delta x$ causes $\mathsf{A} \to \mathsf{A}' = \mathsf{A} + (0, B\Delta x, 0)$. The additional constant vector field has to be accounted for by magnetic translations.

Let us interrupt this discussion at this point and let us write the Hamiltonian H_0 (Eq. 3.1) in Landau gauge

$$H_0 = \frac{1}{2}\hbar\omega \left[-\frac{\partial^2}{\partial x'^2} + \left(-i\frac{\partial}{\partial y'} + x' \right)^2 \right], \qquad (x', y') = (x/\ell_0, y/\ell_0)\,. \tag{3.15}$$

Using a separation ansatz we readily arrive at a one–dimensional harmonic oscillator problem

$$\psi(x', y') = \exp(ik'_y y')\chi(x')\,, \qquad \frac{1}{2}\hbar\omega \left[-\frac{\mathrm{d}^2\chi(x')}{\mathrm{d}x'^2} + (k'_y + x')^2 \chi(x') \right] = E\chi(x')\,.$$

In this effective 1D problem the spectrum does not depend on k'_y which can be an arbitrary real number. Wavefunctions $\chi(x')$ are also k'_y–independent up to a shift by $-k'_y$ (note that $x' = x/\ell_0$ and $k'_y = k_y\ell_0$). Summarized:

$$\begin{aligned} E &= \hbar\omega\left(n+\frac{1}{2}\right) \\ \psi_{n,k'_y}(x',y') &= \exp(-ik'_y y')\exp[-(x'+k'_y)^2/2]h_n(x'+k'_y)\,, \end{aligned} \tag{3.16}$$

$$\begin{aligned} n &= 0,1,2,\ldots: \text{ Landau level index} \\ k'_y &\in [-\infty;\infty]: \text{ momentum along } y \end{aligned}$$

Here $h_n(\tau)$ are (unnormalized) Hermite polynomials defined by

$$h_n(\tau) = (-1)^n \exp(\tau^2)\frac{\mathrm{d}^n}{\mathrm{d}\tau^n}\exp(-\tau^2)\,.$$

Since $h_0(\tau) = 1$, states in the lowest Landau level ($n = 0$) are

$$\psi_{0,k'_y}(x',y') = \exp(-ik'_y y')\exp[-(x'+k'_y)^2/2]\,. \tag{3.17}$$

The infinite degeneracy of each Landau level (there is an infinite number of values for k'_y) is only due to the infinite size of the system considered here. If we were restricted to an area of L^2, values of k'_y would become quantized and we would have counted just $L^2/(2\pi\ell_0^2)$ states (see Subsec. 3.5.1).

Magnetic translations

Let us now find the operator $T(\boldsymbol{u})$ which corresponds to the translational symmetry of a charged particle in a plane with perpendicular homogeneous magnetic field. We will start with ordinary translations $t(\boldsymbol{u}) = \exp(i\boldsymbol{u}\cdot\boldsymbol{p}/\hbar)$ and will demand that the operator commutes with H_0.

The nth Landau level is spanned by wavefunctions ψ_{n,k'_y} (Eq. 3.16) where k'_y runs through all real numbers. By translating this state by $\boldsymbol{u} = (u_x, u_y)$ we expect to get another state lying in the same Landau level[5].

$$\begin{aligned} \boldsymbol{u} = u_x\hat{\boldsymbol{x}}_0 = (u_x,0)\,: &\qquad t(\boldsymbol{u})\psi_{n,k'_y} = \exp(-ik'_y y')\exp[-(x'+k'_y-u_x)^2/2]h_n(x'+k'_y-u_x)\,, \\ \boldsymbol{u} = u_y\hat{\boldsymbol{y}}_0 = (0,u_y)\,: &\qquad t(\boldsymbol{u})\psi_{n,k'_y} = \exp(-ik'_y(y'-u_y))\exp[-(x'+k'_y)^2/2]h_n(x'+k'_y)\,. \end{aligned}$$

In the latter case, $t(u_y\hat{\boldsymbol{y}}_0)\psi_{n,k'_y} = \exp(ik'_y u_y)\psi_{n,k'_y}$, the function remained in the n-th Landau level and acquired only an unessential (constant) phase.

[5] Also from the purely mathematical point of view: this condition is equivalent to that the translation operator commutes with H_0.

The former case is more troublesome: $t(u_x\hat{x}_0)\psi_{n,k'_y} = \exp(iu_x y')\psi_{n,k'_y-u_x}$ is no longer a function in the n-th Landau level (since the phase factor is not constant). We can even show that this function has projections to *all* Landau levels[6] However, there is an easy help. The operator

$$T(u_x\hat{x}_0) = \exp(-iu_x y')t(u_x\hat{x}_0)$$

does not change the modulus of the wavefunction — and thus preserves the effect of translating a localized particle embodied into $t(u_x\hat{x}_0)$ — and it fulfills $T(u_x\hat{x}_0)\psi_{n,k'_y} = \psi_{n,k'_y-u_x}$, i.e. it keeps the state in the same Landau level (it preserves the energy of the state).

A definition of *magnetic translations*, for Landau gauge $\mathsf{A} = (0, Bx, 0)$, is thus at hand:

$$\mathsf{u} = (u'_1, u'_2) : \qquad T(\mathsf{u}) = \exp(-iu'_x y')t(\mathsf{u})\,. \tag{3.18}$$

Up to a constant phase factor, this is a special case of a result valid for any gauge [38] (in dimensionful coordinates)

$$T(\mathsf{u}) = \exp\left(\frac{i}{\hbar}\mathsf{u}\cdot\mathsf{p} - \frac{i}{\ell_0^2}\mathsf{u}\cdot\mathsf{A}/B - \frac{i}{\ell_0^2}\widehat{\mathsf{z}}\cdot\mathsf{u}\times\mathsf{r}\right)\,.$$

To verify that $[T(\mathsf{u}), H_0] = 0$, it is the easiest to show that the generator $\mathsf{u}\cdot\mathsf{p} + (\hbar/\ell_0^2)(\mathsf{u}\cdot\mathsf{A}/B + \widehat{\mathsf{z}}\cdot\mathsf{u}\times\mathsf{x})$ commutes with H_0. Now that we have translation operators commuting with the Hamiltonian we can construct simultaneous eigenstates to H_0 and T. When calculating eigenstates of H_0, this allows us to be restricted to one particular subspace of T. Or, if we already have eigenstates of H_0 we can try to classify them by their T–eigenvalues. If we find an eigenvalue of $\exp(i\mathsf{k}\cdot\mathsf{u})$ for translation $T(\mathsf{u})$, we can identify the state as a wave of wavevector k. This concept will be very useful for many body states (Subsect. 3.5.1).

In contrast to ordinary translations, the magnetic translations do not always commute with each other. Instead they obey the algebra

$$T(\mathsf{u}_1)T(\mathsf{u}_2) = \exp\left(\frac{i}{2\ell_0^2}\widehat{\mathsf{z}}\cdot\mathsf{u}_1\times\mathsf{u}_2\right)T(\mathsf{u}_1+\mathsf{u}_2)$$

rather than simply $t(\mathsf{u}_1)t(\mathsf{u}_2) = t(\mathsf{u}_1+\mathsf{u}_2)$. This relation of magnetic translations implies the Aharonov–Bohm effect: moving a particle along a closed path gives the wavefunction an extra phase of $2A/2\ell_0^2 = 2\pi AB/(h/e) = 2\pi\Phi/\Phi_0$. Quantization of magnetic flux $\Phi = AB$ into flux quanta Φ_0 follows then from single–valuedness of the wavefunction, i.e. the Aharonov–Bohm phase must be an integer multiple of 2π (see Subsec. 3.5.1).

[6] $\langle t(u_x\hat{x}_0)\psi_{n,k'_y}||\psi_{\tilde{n},\tilde{k}'_y}\rangle = \delta_{k'_y,\tilde{k}'_y}c_{n,\tilde{n}}$ where $c_{n,\tilde{n}}$ are the integrals according to x'. These are overlaps of two functions (gaussian times Hermite polynomial) *centered at different positions*, k'_y and $k'_y - u_x$ wherefore the orthogonality relations between different Hermite polynomials are void. $c_{n,\tilde{n}}$ are thus nonzero (and can be expressed in terms of associated Laguerre polynomials).

Complex coordinates

Eigenfunctions to H_0 in the form given by Eq. 3.16 can also be reformulated in terms of variables $z = x + iy$ and $\bar{z}$. A noteworthy fact (analogous to Eq. 3.14 and comments thereafter) is that any state in the lowest Landau level can be expressed as

$$\psi(z) = \exp(-\frac{1}{2}y^2) f(z)\,,$$

where $f(z)$ is an analytic function of z, free of poles in the complex plane.

3.2 What to do when Coulomb interaction comes into play

The quantum mechanical solution of one electron — or many non-interacting electrons in a plane subject to a perpendicular magnetic field is at the root of the integer quantum Hall effect. The basic fact is that for integer filling factors, *any* even arbitrarily small excitation costs at least the energy $\hbar\omega$. This gap renders the ground state incompressible (see comment at the very end of Subsect. 3.1.1). The fractional quantum Hall effect cannot be explained in this picture: for instance at filling factor $\nu = \frac{1}{3}$, a non-interacting system has a many–fold degenerate ground state, or, excitations cost zero energy, the ground state should be compressible. Today it is well established that the effect is due to electron–electron interactions which select among those states one special ground state and separate it by a gap from the excitations.

This section summarizes some basic analytic results about spin–polarized incompressible ground states at some special fractional fillings in the range $0 < \nu < 1$. Several basic types of excitations will be mentioned and finally, incompressible states with less than full spin polarization will be introduced.

3.2.1 Filling factor below one: restriction to the lowest Landau level

The Hamiltonian of the many–electron system consists now of two terms: the kinetic energy (leading to Landau level quantization) and the electron–electron interaction. Until it is explicitely written, we will consider spinless (or fully spin polarized[7]) electrons.

$$H = \sum_{i=1}^{N_e} \frac{\boldsymbol{p}_i^2}{2m} + \frac{e^2}{4\pi\varepsilon}\frac{1}{2}\sum_{i\neq j}\frac{1}{|\boldsymbol{r}_i - \boldsymbol{r}_j|} \tag{3.19}$$

Consider some particular filling factor, $\nu = \frac{1}{3}$ for example, and let us vary the magnetic field[8]. The kinetic energy will change in proportion with $\hbar\omega \propto B$. The interaction energy

[7] For example due to strong Zeeman splitting.

[8] Since $\nu = n/(2\pi\ell_0^2) = n/(eB/\hbar)$, this implies changing the electron density simultaneously.

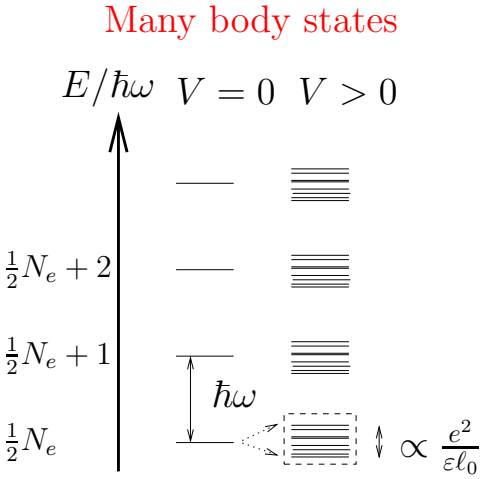

Figure 3.2: Interaction between electrons lifts the huge degeneracy between the many–body states in the lowest Landau level (even when neglecting mixing to higher Landau levels, which is reasonable for $\hbar\omega \gg e^2/\varepsilon\ell_0$). In a real system, the degeneracy is infinite just as the 'whole 2D plane' is infinite. Instead, we consider a square with periodic boundary conditions instead. For example, at filling factor $\nu = \frac{1}{3}$, if there are N_e electrons in the square, Eq. 3.6 implies that there are $N_m = 3N_e$ one electron states available. Without interaction, there are thus $\binom{3N_e}{N_e} \approx (27/4)^{N_e}$ degenerate N_e–electron states (of energy $\frac{1}{2}N_e\hbar\omega$) in the lowest Landau level.

on the other hand scales with $1/a \propto \sqrt{B}$. That is because the typical electron–electron distance a changes as $\sqrt{1/n} = \sqrt{1/(\nu eB/\hbar)} \propto 1/\sqrt{B}$.

In the high field limit we can therefore expect that the Coulomb interaction is a small perturbation[9] which lifts the degeneracy of Landau levels (Fig. 3.2).

A semiquantitative condition for this is

$$\frac{e^2}{4\pi\varepsilon a} \ll \hbar\omega\,, \text{ where}$$

$$a \approx \frac{1}{\sqrt{n}} = \frac{\sqrt{2\pi}\ell_0}{\sqrt{\nu}}\,, \qquad \ell_0^2 = \frac{\hbar}{|eB|}\,, \qquad \omega = \frac{|eB|}{m}$$

Under realistic experimental conditions, this can be fulfilled[10] and it is thus reasonable to start with the assumption that (in strong magnetic fields) all electrons occupy the lowest Landau level. In this approach, kinetic energy is quenched (all electrons have the same kinetic energy, $\frac{1}{2}\hbar\omega$), or in other words, the first term in Eq. 3.19 is merely a constant $N_e\frac{1}{2}\hbar\omega$ which may be omitted.

3.2.2 Laughlin wavefunction

The following n-electron trial wavefunction for the ground state at filling factor $\nu = \frac{1}{3}$ earned R. B. Laughlin the Nobel Prize in 1998 (complex coordinates, see Subsect. 3.1.3)

$$\Psi_L(z_1,\ldots,z_n) = \exp\left(-(|z_1|^2+\ldots+|z_n|^2)/4\ell_0^2\right) \underbrace{\prod\nolimits_{i<j}(z_i-z_j)^3}_{(*)}\,, \qquad (*) = \textstyle\sum_k c_k z_1^{m_{1,k}} z_2^{m_{2,k}} \ldots z_n^{m_{n,k}} \tag{3.20}$$

Let us briefly mention the facts which make this suggestion plausible. [59]

[9] I stress that it is 'small' in respect to the cyclotron energy. It is however large compared to single–particle–level spacing within one Landau level (which is zero in ideal case).

[10] At least with $\approx$ instead of $\ll$.

(i) The state should lie completely in the lowest Landau level. Thus, up to the exponentials, the wavefunction must be a polynomial in each variable z_i and it may not contain any $\bar{z}_i$ (see Eq. 3.14 and following comments).

(ii) Regarding rotational symmetry of the Hamiltonian, the state must be an eigenstate to total angular momentum $M\hbar$. Expanding the product in Eq. 3.20 as indicated, this means that each summand (regardless of k) must have the same sum of exponents, $M = \sum_{i=1}^{n} m_{i,k}$ (note m in Eq. 3.14 is the angular momentum). [60]

(iii) The wavefunction should have the Jastrow form $\Pi_{i<j} g(z_i - z_j)$ (up to the exponential), i.e. watching one pair of electrons, it depends only on their mutual distance, and this dependence is the same for any pair[11].

These points determine the form of Ψ_L in Eq. 3.20 up to the exponent at factors $z_i - z_j$.

(iv) The wavefunction should describe a state of filling factor $\nu = \frac{1}{3}$. This sets the exponent to the value $1/\nu = 3$ as it will be explained shortly (Subsection 3.2.3).

It is striking that none of these arguments involves the particular form of the interelectronic interaction $V(r)$. In this sense it is indeed a matter of luck that Ψ_L describes almost precisely[12] the state of Coulomb–interacting electrons at filling factor $\nu = \frac{1}{3}$. Central reason for this success is a combination of the following three points

(α) single–electron states have large overlaps at filling factor $\frac{1}{3}$ which makes them feel $V(r)$ at very short distances

(β) Coulomb repulsion is very strong at short distances

(γ) electrons in a state described by the Laughlin wavefunction avoid being close to each other, since $|\Psi_L|^2 \propto r^6$ as $r = |z_i - z_j| \to 0$. Therefore the energy of the state Ψ_L is quite low.

It is not hard to see how delicate the success of Ψ_L is. The Laughlin wavefunction can also be used to describe states at filling $\nu = \frac{1}{m}$ with $m = 5, 7, \ldots$. However, for fillings $\nu < \frac{1}{7}$, a hexagonal Wigner crystal has lower energy than the corresponding Laughlin wavefunction [62]. Under these conditions, the effective electron density is much lower[13] and the long–range part of the Coulomb interaction becomes more important than the short–range part (thus point (α) is violated and point (γ) is no longer needed).

[11] It is essential for this ansatz that the interaction is the strongest if two electrons are close to each other. See Subsection 3.3.4 and [102] p. 66 for details.

[12] Numerical tests of Ψ_L are described in Section 3.5.

[13] One electron in the lowest Landau level occupies an area of $2\pi\ell_0^2$ (Subsection 3.1.1), imagine it as a blot of perimeter $\sim \ell_0$. At filling factor $1/m$, there are $n = 2\pi\ell_0^2/m$ electrons (per unit area). Obviously, with growing m (while keeping ℓ_0 constant), the number of electrons decreases and so does their overlap (since size of blots stays the same).

Another example are higher Landau levels. An analogue to Ψ_L can be constructed if, e.g. two Landau levels are full (and taken as an inert background), and the last Landau level has filling of $\frac{1}{3}$. Such states are however typically compressible because the Coulomb interaction is not as strong at short distances in higher Landau levels as in the lowest Landau level (see Fig. 3.5 and explanation in the text about pseudopotentials which effectively describe the interaction if particles are confined to a particular Landau level).

Some other possible physical pictures of ground states at fractional fillings will be mentioned in Subsection 3.2.6.

How to interpret the Laughlin wavefunction

What kind of state does the many–body wavefunction Ψ_L describe? A usual way how to answer this question is to calculate density or density–density correlation functions and we will follow this line in Chapter 4. Laughlin, however, suggested another tricky approach based on a statistical interpretation of quantum mechanical wavefunctions[14] :

$$|\Psi_m|^2 = \exp\left(-\beta E_m(z_1,\ldots,z_n)\right), \qquad E_m(z_1,\ldots,z_n) = -m^2\sum_{j<k}\ln|z_j-z_k| + m\sum_j |z_j|^2/4\ell_0^2 .$$

Assuming that the electrons *are* in the state described by Ψ_m, we may ask what the most likely configurations to be measured will be (imagine making a snapshot of the system, i.e. measuring the position of all electrons simultaneously). The last equation shows that the probability for a particular configuration $z_1,\ldots,z_n$ (in the Laughlin state) is the same as probability of such a configuration in a classical plasma of particles interacting by a repulsive logarithmic interaction[15].

In more detail: a one–component 2D plasma (OCP) with a neutralising homogeneous background (density ϱ) has energy

$$E = -e^2\sum_{j<k}\ln|z_j - z_k| + \frac{1}{2}\pi\varrho e^2\sum_j |z_j|^2 . \tag{3.21}$$

Thus, by comparison, the Laughlin wavefunction corresponds to a classical plasma of particles of charge $e = m$ and an attractive background of density $\varrho = 1/(2\pi\ell_0^2 m)$.

This analogy is very powerful. Even intuitively, we can say that particles will try to spread out uniformly in order to compensate the background charge in every point. Previously known facts about OCP in 2D teach us that Laughlin states are *liquid–like* up to $m \approx 70$ (and crystalline for larger m; however, Laughlin states are no longer ground states of the

[14] Ψ_m is the Laughlin wavefunction Ψ_L with power of three replaced by power of m. Provided m is odd, this wavefunction describes a fermionic state at filling factor $\nu = 1/m$; see (iv) in discussion after Eq. 3.20.

[15] We speak of the plasma as of a classical one since the probability has just been presented as the Boltzmann distribution at one particular temperature which has been set to $2/m$ (follows from $\beta = 1/k_B T$). See also comment [2].

quantum mechanical problem for such high values of m, see above). Techniques known from plasma problems (on basis of Monte–Carlo) allow for a numerical estimation of the energy of Ψ_L up to high precision[16]. Values of some other observables like density–density correlation functions can be evaluated in a similar manner [62], for a review see Sec. 5.4 in [17].

3.2.3 Vortices and zeroes

These two words are of extraordinary importance to the fractional quantum Hall effect, so let us explain them first. A formula tells sometimes more than a thousand words:

$$\begin{array}{cc} \text{zero} & \text{vortex} \\ f_z(z) = z - z_0 & f_v(z) = \arg(z - z_0) = \dfrac{z - z_0}{|z - z_0|}\,. \end{array}$$

Zero and vortex may appear as a feature of a function of a complex variable. Although they are bound to one particular point (z_0), they have an impact on global properties of the function. In particular, going once around the point z_0, the phase of the function changes by 2π [17], irrespective of the path:

$$\oint \mathrm{d}t \frac{\mathrm{d}\arg f\big(z(t)\big)}{\mathrm{d}t} = 2\pi \times \#\text{ of zeroes/vortices enclosed by the curve } z(t)\,, \qquad (3.22)$$

where $z(t)$ is a closed curve which does not intersect itself (to prevent going more than once around a zero).

Zeroes have the nice property of analyticity[18] , vortices not; note also, that vortices are ill-defined for $z = z_0$.

A physicist's view of the vortex/zero counting formula 3.22 is based on the Aharonov–Bohm effect. Imagine the 2D plane pierced by a solenoid carrying magnetic flux Φ. Even though there is no magnetic field outside the solenoid, (the wavefunction of) a particle (charge e) going once around it gathers a phase of $\Phi/(h/e)$. Equation 3.22 (or the requirement of uniqueness of the wavefunction) is then just an expression of the quantization of the magnetic flux, $\Phi = n(h/e) = n\Phi_0$, $n = 0, \pm 1, \ldots$. In agreement with this, it can be shown that passing one magnetic flux quantum at $z = z_0$ adiabatically through the system introduces one new zero into the wavefunction [59].

As far as the phase is considered, a vortex has the same effect as a zero. However, $|f_v(z)| \equiv 1$ and thus adding it to some particular wavefunction does not influence the particle density. On the other hand, not only is a vortex a non–analytic function (analyticity was needed

[16] However, the basic idea here is still the usual goal of Monte Carlo: to evaluate a many–dimensional integral numerically. For example $\langle \Psi_L | H | \Psi_L \rangle$.

[17] A zero counting procedure is based on this observation: consider a holomorph function $f(z)$ free of singularities in region R. The integral $\oint \mathrm{d}z (\mathrm{d}/\mathrm{d}z) \ln f(z)$ around the boundary of R is equal to $2\pi i$–times the number of zeroes of $f(z)$ in the region R.

[18] Or holomorphy: they are continuous and functions of only z, not of z^*.

to stay in the lowest Landau level; see comments after Eq. 3.20), it is not even continuous at $z = z_0$ which is a basic requirement for a quantum mechanical wavefunction. It may be thus regarded only in the framework of some approximation.

It is then *suggestive* to think of the zeroes or vortices of some particular wavefunction as of magnetic flux quanta. Consider the Laughlin wavefunction $\Psi_L(z_1, \ldots, z_n)$ and fix all particles but one, say z_1. We know that Ψ_L describes n electrons confined to a disc of area $A = n/\varrho$ (see Eq. 3.21). Let us therefore fix particles $z_2, \ldots, z_n$ somewhere inside the disc and let us go with z_1 once around. Function $f(z) = \Psi_L(z, z_2, \ldots, z_n)$ is a polynomial of degree $3(n-1)$ (except for the exponential factor which is however nonzero everywhere), it has $3(n-1)$ zeroes within the disc and we thus arrive at the conclusion that the particle z_1 sees $3(n-1)$ flux quanta. Including another three zeroes which come from the center-of-mass part of the wavefunction not included in Eq. 3.20, the total bilance is $3n$ flux quanta and n particles or filling factor $\frac{1}{3}$ (Eq. 3.6).

Note that the zeroes of the Laughlin wavefunction are bound to electrons: factor $(z_i - z_j)^3$ in Eq. 3.20 means that the i–th electron sees a triple zero at the position of the j-th electron. This observation is the starting point of the concept of composite fermions (Sect. 3.4).

3.2.4 Particle–hole symmetry

Particle–hole symmetry provides a mapping between systems at fillings ν and $1-\nu$ (spinless electrons) or ν and $2-\nu$ (spinful electrons). The mapping is exact provided Landau level mixing is absent. An illustrative example: for fully polarized electrons[19] spectra of a $\nu = \frac{1}{3}$ and $\frac{2}{3}$ systems are identical (up to a constant) and the corresponding wavefunctions are related by a (actually simple) transformation.

Think of the lowest Landau level as of a 1D chain; Landau gauge is particularly illustrative for this, one–electron states (Eq. 3.17) are localized along x. The basic idea of the particle–hole symmetry is that two electrons at positions i and j feel the same repulsive force as two holes at the same positions, i.e. the whole 1D chain is full and only at i and j electrons are missing.

Let us put it into mathematical terms. Let $a_j^\dagger$ be a creation operator of a single–electron state with momentum $k_y = 2\pi j/b$, being therefore localised in x–direction around $X_j = k_y \ell_0^2$ (Eq. 3.17). Assuming j can take values[20] $0, \ldots, m-1$, particle–hole conjugated n-body states are

$$a_{j_1}^\dagger \ldots a_{j_n}^\dagger |0\rangle \text{ (particles)} \quad \longleftrightarrow \quad a_{j_1} \ldots a_{j_n} |1\rangle \text{ (holes)}, \tag{3.23}$$

where $|0\rangle$ is an empty Landau level (vacuum) while $|1\rangle \equiv a_0^\dagger \ldots a_{m-1}^\dagger |0\rangle$ is a completely filled Landau level.

[19] Meaning: only the lowest Landau level with spin up is considered, lowest Landau level spin down and all higher Landau levels as far in energy that they can be neglected.

[20] This is the case for periodic boundary conditions.

A straightforward calculation shows that matrices of a translationally invariant two–body operator[21] $\hat{A}$ are the same (up to a multiple of identity matrix and complex conjugation) in an arbitrary n–particle basis and its conjugated $(m-n)$–hole basis. The only approximation we must perform is to neglect Landau level mixing.

Result of the calculation is the following. The diagonal terms of an operator A in the particle basis and in the hole basis fulfil

$$\langle 1|a^\dagger_{j_1}\dots a^\dagger_{j_n}\ A\ a_{j_n}\dots a_{j_1}|1\rangle = \frac{m-2n}{m}\langle 1|\ A\ |1\rangle + \langle 0|a_{j_1}\dots a_{j_n}\ A\ a^\dagger_{j_n}\dots a^\dagger_{j_1}|0\rangle \qquad (3.24)$$

and the off-diagonal terms remain the same up to the complex conjugation.

Two special cases are worth of special attention:

- *Energy.* Spectra of (fully polarized) systems at $\nu = n/m$ and $\nu = (m-n)/m$ are the same up to a shift

  $$E^i_\nu = E^i_{1-\nu} + E_f\,(m-2n)/m\,, \qquad (3.25)$$

  where E_f is the energy of a completely filled (lowest) Landau level. This result does not depend on the form of the interaction $V(r)$. A nice demonstration of formula 3.25 is shown in Fig. 4.39(b).

  Note that conjugated states (Eq. 3.23) may have different values of J (sum of j_i modulo m, Eq. 3.49). For instance: for $m = 4$, consider a three–electron state $|j_1 j_2 j_3\rangle = |013\rangle$ and its particle–hole conjugate $|j_1\rangle = |2\rangle$; the former has $J = 0$ while the latter has $J = 2$. [22].

  Thus, extending the example above, when comparing spectra of $\nu = \frac{3}{4}$ and $\nu = \frac{1}{4}$ systems in subspaces with fixed J, we must look not at the same J's but at $J = 0$ for $\nu = \frac{3}{4}$ and at $J = 2$ for $\nu = \frac{1}{4}$.

- *Density–density correlation functions.* For $g_\Psi(\mathbf{r}) = \langle \sum_{i<j} \delta(\mathbf{r} - \mathbf{r}_i + \mathbf{r}_j)\rangle_\Psi$ we get

  $$g_\Psi(\mathbf{r}) = \frac{m-2n}{m}\big(1 - \exp(-r^2/2\ell_0^2)\big) + g_{\Psi'}(\mathbf{r})\,, \qquad (3.26)$$

  where Ψ and Ψ' are arbitrary particle–hole conjugated states[23]. Note that $g_{\Psi'}$ refers to *electrons* in the 'hole' state. Correlations between holes in Ψ' are the same as those between electrons in Ψ.

  Note, that here $g(\mathbf{r})$ is *not* defined in the normalized form $\delta(\mathbf{r} - \mathbf{r}_i + \mathbf{r}_j)/(n(n-1))$. Also note, that $g(\mathbf{r})$ of a full Landau level may depend on system ('finite–size') parameters: e.g. in a rectangle with periodic boundary conditions, it depends on aspect ratio.

[21] The calculation has been done for the Coulomb operator and the density–density correlation operator. Translational invariance is however the only substantial assumption.

[22] Of course, the 'particle J' (we sum the j_i's of the occupied one–particle states) of the one state is the same as the 'hole J' (we sum j_i's of the empty one–particle states) of the other.

[23] A general n–body state can be written as an expansion in slater determinants of the form shown in Eq. 3.23. The conjugation is then meant to act on all terms individually.

Let us mention that densities of particle–hole conjugated states are related by $n_\Psi(\boldsymbol{r}) = m - n_{\Psi'}(\boldsymbol{r})$, exactly as we expect from the picture of a 'hole' as a 'missing particle'. From this point, the plus sign in Eq. 3.26 might look puzzling. At the second glance, however, '$g_\Psi = n \cdot n$' and therefore '$g_{\Psi'} = (1-n)\cdot(1-n) = 1 - 2n + g_\Psi$'.

3.2.5 More about Laughlin wavefunction: low energy excitations

Laughlin wavefunction Ψ_L (Eq. 3.20) has a beautiful form, yet its energy or correlation function must be evaluated numerically[24] . Despite this, related to Ψ_L, many nontrivial phenomena with clear physical interpretation can be named. Here, we will discuss two particular types of low–energy excitations from the Laughlin state: charge– and spin–density waves.

The Laughlin state has a homogeneous density and making the density non–uniform is quite expensive[25]. It is however possible to construct a superposition of charge–density waves with different phase offsets (all with the same weight) but with the same wavevector $\boldsymbol{Q}$. Such a state can be generated using

$$\Psi_L(z_1,\ldots,z_n) \quad \overset{\text{make CDW}}{\longrightarrow} \quad \sum_{j=1}^{n} \exp(i\boldsymbol{Q}\cdot\boldsymbol{r}_j)\Psi_L(z_1,\ldots,z_n)\,. \tag{3.27}$$

Its density is still uniform and the CDW is seen first in density–density correlations[26] . Energy, or better the dispersion $E(\boldsymbol{Q})$, of such states can be evaluated within single mode approximation and the first ones to accomplish this were Girvin, MacDonald and Platzman [32] (see also Girvin's lectures [31]). Exact diagonalization results then demonstrate that CDWs are indeed among the lowest excitations and thus the single mode approximation is plausible [37] (see also Subsec. 4.1.3). Moreover, excluding spin flip, CDW excitations with $Q\ell_0 \approx 1.4$ where $E(\boldsymbol{Q})$ achieves its minimum (called the magnetoroton minimum), are the lowest excitations at all and determine thus the size of the gap at filling factor $\nu = \frac{1}{3}$.

In multicomponent systems, e.g. when electrons can be spin up or spin down, it is also possible to generate spin–charge density waves by

$$\Psi_L(z_1,\ldots,z_n) \quad \overset{\text{make SCDW}}{\longrightarrow} \quad \sum_{j=1}^{n} \exp(i\boldsymbol{Q}\cdot\boldsymbol{r}_j)S_j^+\Psi_L(z_1,\ldots,z_n)\,, \tag{3.28}$$

[24] Closed formula for the energy was derived by Takano and Isihara [92] but for practical purposes, it must be evaluated by computer. Very exact (and quite simple) expressions for energy and $g(r)$ based on this formula are presented for example by Goerbig [33] (Introductory section about FQHE, formulae 1.12 and 1.13). See also Xia [100].

[25] The currency is one Joule.

[26] By fixing one particle and looking for the density of the other particles (as we do when we evaluate density–density correlation function), we effectively choose just one of the waves out of the superposition. Then we, of course, see a modulated density.

as it was suggested by Rasolt and MacDonald [78]. These states are gapless *Goldstone modes* [34] (in the limit $Q \to 0$), provided the Zeeman splitting vanishes [3]. For nonzero Zeeman splitting $g\mu_B B$ they are simply shifted by $g\mu_B B$ upwards and the ground state remains gapped. A detailed study on how the SDW excitations depend on the form of the electron–electron interaction was published by MacDonald and Palacios [64].

3.2.6 Other fractions and spin

The principal fractions $\nu = 1/m$ along with $\nu = 1 - 1/m$ seem to be well described by Laughlin wavefunctions (except for very small ν where Wigner crystal is more favourable). These are however not all fractions which have been observed in the interval $0 < \nu < 1$. Most other fractions (but not all) are members of the sequences $\nu = p/(2ps \pm 1)$ with p and s integer and they all have odd denominators. It also turned out, that not all fractional quantum Hall states are fully spin polarized and moreover, for one value of filling factor, ground states with different spin polarization are possible, depending on the ration between Zeeman and Coulomb energy (Sec. 5.1 and Sec. 2.2).

In this Subsection I will mention one particular proposal for the ground state wavefunction at fillings which are not of the form $1/m$. This proposal covers neither all observed fractions nor spin polarizations. Its simple form, however, makes it easy to compare it to numerical results and I therefore consider it important to be mentioned. An (almost) complete picture of the observed fractions and polarizations appears within the composite fermion theories which will be mentioned later (Sect. 3.4).

Halperin wavefunctions: two–component systems

Regarding the possibility of not fully spin polarized wavefunctions, Halperin proposed the following WFs [41]

$$\Phi_{mm'n}[z] = \prod_{i<j\le N_\uparrow} (z_i - z_j)^m \prod_{k<l\le N_\downarrow} (z'_k - z'_l)^{m'} \prod_{i\le N_\uparrow} \prod_{k\le N_\downarrow} (z_i - z'_k)^n \prod_{i,j} \exp(-|z_i|^2/4\ell_0^2) \exp(-|z'_j|^2/4\ell_0^2) \tag{3.29}$$

with m, m' odd. The state assumes $N_\uparrow$ ($N_\downarrow$) particles with spin up (down) and z_i (z'_j) describe their positions. The filling factors of the two components are

$$\nu_\uparrow = \frac{m' - n}{mm' - n^2}\,, \qquad \nu_\downarrow = \frac{m - n}{mm' - n^2}\,,$$

or equivalently, they describe a state at filling $\nu = \nu_\uparrow + \nu_\downarrow$ and polarization $p = (\nu_\uparrow - \nu_\downarrow)/\nu$. For example, the choice $m = m' = 3$ and $n = 2$ leads to the total filling factor $\frac{2}{5}$ and zero spin polarization ($\nu_\uparrow = \nu_d n$). On the other hand, no choice of m, m', n leads to a fully spin polarized ($S = N_e/2$) state at the same total filling factor. Examples of some other filling factors which can be achieved in terms of $\Phi_{mm'n}[z]$ are given in the book of Das Sarma and Pinczuk [21] (pp. 165).

These trial wavefunctions are an extension to the Laughlin state for systems where Zeeman energy is negligible compared to Coulomb energy. On their basis, Jain's composite fermion wavefunctions were proposed (Sect. 3.4). In Chapter 4 I will use them for a reference to numerical results.

3.3 Other types of electron–electron interactions

Short–range interaction (SRI) and its model in fractional quantum Hall systems is the main objective of this section. We will first inspect a general two–particle interaction under the influence of a strong magnetic field which will lead us to *Haldane pseudopotentials* $\{V_m\}$. One particular choice of $\{V_m\}$ defines the SRI and we will also get acquainted to some other types of interactions which have been considered previously. Finally, we will introduce the following useful concept: by varying the Haldane pseudopotentials continuously and watching the ground state we may identify what part of the interaction determines the structure of the ground state. In particular, following [39], we will show that the Laughlin wavefunction (the ground state[27] at $\nu = \frac{1}{3}$) is completely determined by the short–range part of the interaction: regardless of the long–rangedness of the Coulomb force.

Last part of this Section will be devoted to transfer of the ideas above to particles moving on a torus.

3.3.1 Two particles, magnetic field and a general isotropic interaction

Let us consider two negatively charged particles on a plane subject to a perpendicular magnetic field B. Assume that their interaction is described by a potential (energy) $V(r)$ which depends only on their mutual distance. Classically, when starting from rest, the particles would move on a straight line towards or away from each other were it not for the magnetic field. The Lorentz force bends their trajectories and makes them orbit around their centre-of-mass on a circular trajectory. In quantum mechanics, this circular motion is quantized just as in the case of an electron orbiting around a hydrogen nucleus. *Roughly speaking*, only discrete separations r_m between the two particles are allowed. Interaction energies $V(r_m) = V_m$ rather than $V(r)$, $r \in (0; \infty)$ fully determine the spectrum of a many–body system of particles interacting via $V(r)$.

We will now derive and explain these claims more precisely. The Hamiltonian for two particles reads

$$H = \frac{1}{2m}(\mathsf{p}_1 + |e|\mathsf{A}_1)^2 + \frac{1}{2m}(\mathsf{p}_2 + |e|\mathsf{A}_2)^2 + V(|\mathsf{r}_1 - \mathsf{r}_2|)\,. \tag{3.30}$$

Within the following several derivations we will temporarily use dimensionless coordinates to make the formulae more transparent. Assume the symmetric gauge, $\mathsf{A} = (-\frac{1}{2}By, \frac{1}{2}Bx, 0)$ and take $x' = x/\ell_0$, where ℓ_0 is the magnetic length, $\sqrt{\hbar/|e|B}$.

[27] Precisely speaking: a very good approximation (99%) to the ground state.

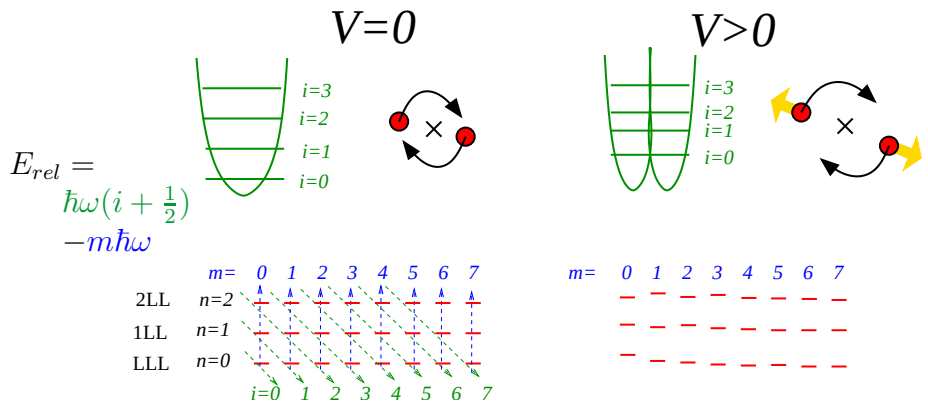

Figure 3.3: Spectrum of one particle confined to a plane subject to a perpendicular magnetic field or, equivalently, the spectrum corresponding to the relative motion of two particles (H_{rel}). *Left:* without particle–particle interaction, the two terms, 'harmonic oscillator' (quantum number i) and 'angular momentum' (quantum number m) combine into Landau levels (quantum number n). *Right:* interaction lifts the degeneracy. If the interaction potential is small compared to the harmonic oscillator term (i.e. $\langle V\rangle \ll \hbar\omega$), Landau levels are roughly preserved. The energy levels V_m *within* the lowest Landau level (sorted according to $m = \langle L_z/\hbar\rangle$) are then the Haldane pseudopotentials.

Just as for single particle (Sec. 3.1.1):

$$H/(\hbar\omega) = \frac{1}{2}(-i\nabla'_1 + \boldsymbol{\alpha}_1)^2 + \frac{1}{2}(-i\nabla'_2 + \boldsymbol{\alpha}_2)^2 + V'(|r'_1 - r'_2|)\,,$$

where $\omega = |e|B/m$ denotes the cyclotron frequency, $\boldsymbol{\alpha}(r/\ell_0) = A(r)/B$ is the dimensionless vector potential and $V'(r/\ell_0) = V(r)/(\hbar\omega)$. In the following we will skip the primes which indicate here that everything is expressed in dimensionless coordinates.

It is just a piece of standard handcraft to separate the Hamiltonian into centre-of-mass and relative parts (and we follow Laughlin [60]). We adopt coordinates

$$r_{CM} = \frac{r_1 + r_2}{2}\,, \qquad r_{rel} = \frac{r_1 - r_2}{\sqrt{2}}$$

and become rewarded by

$$H = H_{CM} + H_{rel} = \underbrace{\frac{1}{2}(-i\nabla_{CM} + \boldsymbol{\alpha}_{CM})^2}_{H_{CM}} + \underbrace{\frac{1}{2}(-i\nabla_{rel} + \boldsymbol{\alpha}_{rel})^2 + V(|r_{rel}|)}_{H_{rel}}\,.$$

The centre-of-mass (CM) part is identical to the Hamiltonian of a single particle in a perpendicular magnetic field and we will now focus only on the relative motion. Its kinetic part (also an electron-in-magnetic-field Hamiltonian) can be rewritten in the Fock–Darwin form (Eq. 3.10)

$$H_{rel} = -\frac{1}{2}\Delta_{rel} + \frac{1}{8}r_{rel}^2 - \frac{i}{2}\frac{\partial}{\partial\varphi_{rel}} + V(|r_{rel}|)\,,$$

or, back to dimensionful units (starting with this formula, all coordinates have again dimension, x rather than x/ℓ_0):

$$H_{rel}[\text{ J}] = \underbrace{\frac{p_{rel}^2}{2m} + \frac{1}{8}\hbar\omega(r_{rel}/\ell_0)^2 - \frac{1}{2}\omega L_{rel}^z}_{H_{rel,kin}} + V(|\mathsf{r}_{rel}|) \tag{3.31}$$

with L_{rel}^z denoting the (z–component of relative) angular momentum.

This is a Hamiltonian of one particle (in 2D) confined by a potential which is a parabola $\frac{1}{8}m\omega^2 r_{rel}^2$ plus an extra term $V(|\mathsf{r}_{rel}|)$. To be more illustrative, we will now assume that $V(r_{rel}) = (e^2/4\pi\varepsilon)\cdot 1/r$ but this particular choice is not essential for the following discussion. We could have taken (nearly) any other interaction.

Since $[H_{rel}, L_{rel}^z] = 0$, we can classify the eigenstates of H_{rel} by their angular momentum. In the *absence of interaction* ($V = 0$), the spectrum would be just Landau levels $\hbar\omega(n+\frac{1}{2})$, each of them containing states with angular momenta $m = 0, 1, 2, \ldots$ Now, in accord with our discussion in Sec. 3.2.1), we wish both particles (described by the full Hamiltonian, Eq. 3.30) to stay in the lowest Landau level (LLL). This can happen only if the centre-of-mass part lies in the LLL *and* the relative part lies in the LLL[28] . Thus we are restricted to angular momenta $m = 0, 1, 2, \ldots$, the eigenstates of H_{rel} being

$$\psi_{rel,V=0}^m(r,\varphi) = \exp(-im\varphi)\, r^m \exp(-r^2/2) \tag{3.32}$$

and they all have the same energy, $\frac{1}{2}\hbar\omega$. This is the highly degenerate lowest Landau level.

Now, we *switch the interaction on* and keep it small compared to the cyclotron energy, $e^2/(4\pi\varepsilon\ell_0) \ll \hbar\omega$. We may still look for the eigenstates of H_{rel} as of eigenstates of angular momentum

$$\psi_{rel}^m(r,\varphi) = R_m(r)e^{-im\varphi}$$

but the functions $R_m(r)$ will now be different from $r^m \exp(-r^2/4)$. Also, they will not have the same energy. Because $\langle r\rangle_m = \langle\psi_{rel}^m|r|\psi_{rel}^m\rangle$ grows[29] with increasing m, we can expect that their energies V_m drop at the same time (we consider repulsive interaction between particles). However, in spite of the lifted degeneracy, the range of energies V_m should be still $\ll \hbar\omega$.

The operator of the Coulomb interaction (in the lowest Landau level) can be then written in terms of its spectral decomposition

$$V(r_{rel}) = \sum_{m=0}^{\infty} |\psi_{rel}^m\rangle V_m \langle\psi_{rel}^m| \,.$$

As far as only spectrum of a *many–body* system *interacting* by $V(r_{rel})$ is concerned, the set of numbers V_m rules everything (regardless of the particular form of ψ_{rel}^m)[30].

[28] Then the total energy is $E_{CM} + E_{rel} = 2\cdot\hbar\omega(0+\frac{1}{2})$, i.e. two non-interacting particles in the LLL.

[29] A semiclassical estimate: $\hbar m = \langle L_z\rangle_m \propto \langle r\rangle_m\langle v\rangle_m = (\langle r\rangle_m)^2\omega$. The approximation $\langle rv\rangle_m \approx \langle r\rangle_m\langle v\rangle_m$ has been made.

[30] On the other hand, given $V(r)$, we need the wavefunctions ψ_{rel}^m to calculate V_m.

The quantities $\{V_m\}$ are called *Haldane pseudopotentials*. They were first introduced in [36] in the context of interacting electrons on a sphere.

3.3.2 Haldane pseudopotentials

In the previous subsection we arrived at the concept of Haldane pseudopotentials. Several remarks are due.

(1) Roughly speaking, the Haldane pseudopotentials $\{V_m\}$ can be interpreted as the interaction energy of two particles if they are orbiting around each other at distance $\langle r \rangle_m \approx \ell_0\sqrt{2m}$. A precise formulation is: V_m is the interaction energy of a two–particle state with angular momentum $m\hbar$ under the constraint of restriction to the lowest Landau level[31] . This is precisely the original definition from [36].

Thus, a *short–range interaction* can be modelled by setting all V_m's to zero except for the state where the two particles are nearest to each other (V_0 for bosons and V_1 for fermions).

(2) The claim $\langle \psi^m_{rel}|r|\psi^m_{rel}\rangle \approx \ell_0\sqrt{2m}$ is only approximate. The higher m, the better it is fulfilled (assuming that the particle-particle interaction decays with distance, $V \to 0$ when $r \to \infty$). This is a demonstration of the 'rule-of-experience' that for high values of quantum numbers semiclassical approaches are valid.

Fig. 3.4 illustrates this fact by comparing $\ell_0\sqrt{2m}$ and $\langle r \rangle_m$ of the non–interacting system ($V = 0$).

(3) *Fermions and bosons.* Careful reader may have noticed that we have spoken just about two *particles* so far. An additional constraint that e.g. (spatial part of the) wavefunction be antisymmetric implies

$$\psi_{rel}(\boldsymbol{r}_1, \boldsymbol{r}_2) = -\psi_{rel}(\boldsymbol{r}_2, \boldsymbol{r}_1) \qquad \Rightarrow \qquad \psi_{rel}(r, \varphi) = -\psi_{rel}(r, -\varphi)\,.$$

Therefore, only states with m odd are allowed in the case of two electrons with the same spin (cf. Eq. 3.32). In other words: only the values of $V_1, V_3, \ldots$ are needed when we describe motion of fully spin polarized electrons.

(4) *Uniqueness.* If $V(r)$ is given, the pseudopotentials V_m are uniquely determined. The opposite is however not true: if we know only the values of V_m, we cannot reconstruct $V(r)$ unless we know also the wavefunctions ψ^m_{rel}.

3.3.3 Particular values of Haldane pseudopotentials on a sphere

In this and in the next Subsection, we will classify various physical systems according to their Haldane pseudopotentials V_m. Or the other way round: some characteristic sets $\{V_m\}$ will be presented and the corresponding physical systems will be shown. This will lead us to a definition of some model interactions (like short–range interaction). Here we will deal with spherical systems, electrons on a torus will be discussed later (Subsection 3.3.6).

[31] Note that for each $L_z = m\hbar$ there is only one such state in each Landau level.

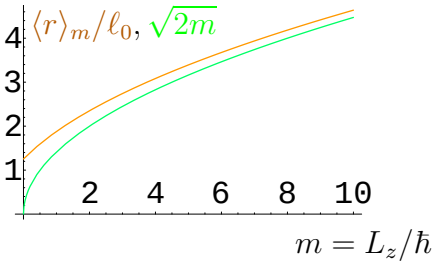

Figure 3.4: Mean interparticle distance $\langle r\rangle_m$ for free particles in the lowest Landau level (Eq. 3.32) compared to $\ell_0\sqrt{2m}$ (m is actually discrete variable, $m = 0, 1, 2, \ldots$). Match between the curves for large values of m demonstrates validity of quasiclassical approach.

Consider two electrons located in *arbitrary* Landau levels n_1 and n_2, respectively, in a state with total angular momentum m. Given these three numbers, the state is uniquely defined, up to the center-of-mass part of the wavefunction. Assuming interaction of the form $V(q)$ (in the Fourier space), their interaction energy can be shown to be (Haldane in [77])

$$V_m^{n_1,n_2} = \int_0^\infty q\mathrm{d}qV(q)L_{n_1}(q^2/2)L_{n_2}(q^2/2)L_m(q^2)\exp(-q^2)\,. \tag{3.33}$$

The *Laguerre polynomials* are defined by

$$L_n(x) = \frac{1}{n!}[x^n e^{-x}]^{(n)}e^x\,.$$

For the case of Coulomb interaction, $V(q) = \alpha/|q|$, integrals in Eq. 3.33 can be evaluated (easily and) analytically. Figure 3.5 shows their values for the cases (a) both particles in the Lowest Landau level ($n = 0$), (b) both particles in the first Landau level ($n = 1$) and (c) one in the lowest and one in the first Landau level.

It is not surprising that in the first case ($n_1 = n_2 = 0$) the coefficients V_m decay monotonically with increasing m, exactly as the Coulomb energy does with increasing distance. The non-monotonic structure of V_m for the case of particles in the first Landau level is due to the additional structure of wavefunctions in higher Landau levels (they have a node at $r = 0$ for $n = 1$).

3.3.4 Model interactions: hard core, hollow core

Why is a hard–core interaction (also known as the *short–range interaction*) that important for the physics of the lowest Landau level?

For (i) it is the strongest part of the Coulomb interaction, (ii) the Laughlin wavefunction is an exact gapped ground state for this interaction and (iii) the ground state changes only little if the other terms of the Coulomb interaction are considered.

Let us discuss this in more details. Short–range interaction (SRI) for *spin polarized electrons* is defined by Haldane pseudopotentials

$$\text{short–range int. (spin polarized electrons): } \{V_1, V_3, V_5, \ldots\} = \{1, 0, 0, \ldots\}\,. \tag{3.34}$$

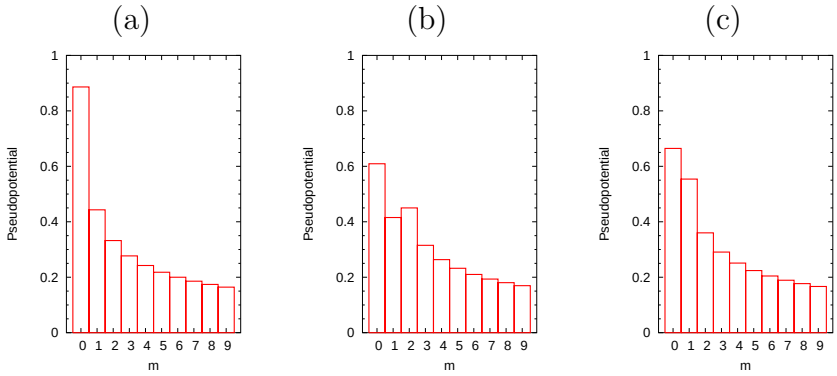

Figure 3.5: Values of Haldane pseudopotentials V_m on a sphere: interaction energy between two particles (a) both in the lowest Landau level, $(n_1, n_2) = (0, 0)$, (b) both in the first Landau level, $(n_1, n_2) = (1, 1)$, and (c) one in the lowest and another in the first Landau level, $(n_1, n_2) = (1, 0)$).

Even values of m are inaccessible for the sake of the antisymmetry of the wavefunction. Note that for the *Coulomb* interaction, Fig. 3.5a, V_1 is indeed the strongest pseudopotential (out of those with odd m).

On the other hand, considering the Laughlin wavefunction (of N particles), any pair of electrons in it is in a state with relative angular momentum $m = 3$: owing to factors $(z_i - z_j)^3$. As there are no pairs with angular momentum $m = 1$, the total energy of this state will be $V_1 \cdot 0 + V_3 \cdot N(N-1)/2 = 0$ for SRI. Also, this state is rigid: any excitation of this state must remove the triple zero from some of the electrons (leaving only a single zero required by antisymmetry) thereby creating some pairs with $m = 1$. The minimum excitation energy (gap) will thus be V_1.

These are analytical results. A surprising numerical result is that the many–body ground state changes only slightly if other pseudopotentials $V_3, V_5, \ldots$ are 'turned on' up to their Coulomb values (Fig. 3.5a). This has been confirmed by Haldane and Rezayi [39] (later also by others, e.g. [28]) by calculating the overlap between the real ground state and the Laughlin state for different sets of V_m. It is also shown in [39] that if V_1 is lowered beyond some critical value (while keeping other pseudopotentials on their Coulomb values), the gap collapses rendering the ground state compressible.

An advantageous property of the interaction (3.34) is that it is effectively non–parametric, the only present parameter V_1 can be factored in front of the Hamiltonian and determines only the overall scaling of the energy scale (assuming restriction to the lowest Landau level).

These results can be summarized by stating that the short–range interaction is the one component of a realistic interaction which determines almost completely the properties of the $\nu = 1/m$ spin–polarized ground states.

Obviously, for non–fully spin polarized systems it is not possible to keep $V_1 \neq 0$ only. Electrons of like spin are still closest in the state $m = 1$ (with energy V_1), electrons of

unlike spin are however closest in the state $m = 0$ with energy V_0. Such a model is obviously not as elegant as in the former case, it contains two parameters V_0, V_1 whose ratio cannot be factored out of the Hamiltonian. An alternative might be the following potential:

$$\{V_0, V_1, V_2, \dots\} = \{\infty, 1, 0, 0, 0, \dots\}\,. \tag{3.35}$$

Another typical model potential presented by Haldane and Rezayi [40] was inspired by the low value of V_0 in the first Landau level as compared to the lowest Landau level (Fig. 3.5). They suggested the hollow–core potential

$$\text{hollow–core interaction: } \{V_0, V_1, V_2, \dots\} = \{0, 1, 0, 0, 0, \dots\}\,.$$

and tried to explain the even–denominator fractional quantum Hall effect at $\nu = \frac{5}{2}$ in terms of this interaction.

3.3.5 Haldane pseudopotentials on a torus

Haldane introduced the quantities V_m for interacting electrons on a sphere [36]. In that case, m can be identified as the relative angular momentum of the electron pair (apart from the fact that with increasing m the separation between the particles increases). In contrast to that, configuration space rotational symmetry is lost on a torus and angular momentum is no longer a good quantum number. In this subsection we will introduce an alternative definition of Haldane pseudopotentials which is applicable also for particles on a torus.

First, recall that matrix elements of the *Coulomb* interaction (on a torus) can be conveniently evaluated in Fourier space (see Subsection 3.5.4) where

$$\text{Coulomb:}\quad V(\boldsymbol{r}) = \frac{e^2}{|\boldsymbol{r}|} \qquad \Rightarrow \qquad V(\boldsymbol{q}) = \frac{e^2}{|\boldsymbol{q}|}\,.$$

Consider now a more general (radial, bounded) interaction with its Fourier transforms $V = V(|\boldsymbol{q}|)$ and expand $V(|\boldsymbol{q}|)$ into a Taylor series. Owing to $V(\boldsymbol{r}) = V(-\boldsymbol{r}) = V(|\boldsymbol{r}|)$, the series will be free of odd powers q^{2k+1}. Now, go back to the direct space[32] [94]

$$V(q) = \widetilde{v}_0 + \widetilde{v}_2 q^2 + \widetilde{v}_4 q^4 + \dots \qquad \Rightarrow \qquad V(r) = \widetilde{v}_0 \delta(r) - \widetilde{v}_2 \nabla^2 \delta(r) + \widetilde{v}_4 \nabla^4 \delta(r) - \dots\,. \tag{3.36}$$

The coefficients $\widetilde{v}_i$ now fully characterize the particle–particle interaction and we are looking for a way how to translate them into V_m's. Let us take the functions ψ^m_{rel} from the planar system (Eq. 3.32 plus normalization) and let us calculate $V_m = \langle \psi_m | V(r) | \psi_m \rangle$. If $V(q) = q^{2k}$ then

$$V(q) = q^{2k}\ : \qquad V_m = (-1)^k \int \mathrm{d}r^2 \psi_m \psi_m^* \nabla^{2k} \delta(\boldsymbol{r}) = \frac{(-1)^k}{2^m m!} \left[\left(\frac{1}{r} \frac{\mathrm{d}}{\mathrm{d}r} r \frac{\mathrm{d}}{\mathrm{d}r} \right)^k r^{2m} \exp(-r^2/2) \right]_{r=0}\,. \tag{3.37}$$

[32] Note that $\mathcal{F}[f(r)]^{(n)} = q^n \mathcal{F} f(r)$.

	V_0	V_1	V_2	V_3	V_4	V_5
q^0 $(k=0)$	$1\cdot 2^0$	0	0	0	0	0
q^2 $(k=1)$	$1\cdot 2^1$	$-1\cdot 2^1$	0	0	0	0
q^4 $(k=2)$	$2\cdot 2^2$	$-4\cdot 2^2$	$2\cdot 2^2$	0	0	0
q^6 $(k=3)$	$6\cdot 2^3$	$-18\cdot 2^3$	$18\cdot 2^3$	$-6\cdot 2^3$	0	0
q^8 $(k=4)$	$24\cdot 2^4$	$-96\cdot 2^4$	$144\cdot 2^4$	$-96\cdot 2^4$	$24\cdot 2^4$	0

Table 3.1: Values of Haldane pseudopotentials corresponding to particle–particle interactions of the type $V(q) = q^{2k}$. These values are additive, e.g. $V(q) = -\frac{1}{2}q^2 + 1$ corresponds to 'hollow core interaction': $\{V_m\} = \{0, 1, 0, 0, 0, \ldots\}$.

This is a unique prescription of how an interaction of the type $V(q) = q^{2k}$ can be transcribed into the terms of V_m. The table 3.1 concludes these 'transcription coefficients' for several lowest powers of q [33]. Note especially that $V_m = 0$ for $m > k$.

In conclusion, an interaction potential defined by some particular set of values of Haldane pseudopotentials V_m can be recalculated into the coefficients $\widetilde{v}_i$ in Eq. 3.36 (Taylor series of $V(q)$) using Table 3.1 or, more generally using formula 3.37.

Again, several remarks should be made.

(1) Expansion in Eq. 3.36, being first suggested by Trugman and Kivelson [94], looks a bit unusual. In the distributional sense, we say that a non-zero ranged potential $V(r)$ can be written as a sum of terms with 'zero range' (δ function and all its derivatives are zero for $r \neq 0$).

Instead of a δ function imagine rather a sharp peaked function δ_b, a Lorentzian of width b, for instance. Functions $\nabla^{2k}\delta_b(\boldsymbol{r})$ will then have 'the longer range the higher k is'. This 'physical' statement[34] is illustrated in Fig. 3.6. In this sense, Eq. 3.36 is an expansion of $V(q)$ in terms of increasing ranges. Compare this with Tab. 3.1.

(2) When calculating the Coulomb matrix elements for particles on a torus (Subsection 3.5.4), we do not use the full function $V(q)$ but only its values in discrete 'lattice' points $\boldsymbol{q}$. This is obviously due to the periodic boundary conditions (i.e. confinement to the torus).

In particular, $\boldsymbol{q} = 0$ is missing among these points.

Thus, we need not worry about the long–rangedness of the Coulomb potential, $V(q \to 0) \to \infty$ which renders it unexpandable into power series of q. Instead of $1/q$ we may imagine to have considered any other polynomial in q which matches the values of $1/q$ at the 'lattice' points. Both interactions must lead to the same results.

(3) We employed ψ_m of an infinite system in order to calculate V_m for the particular $V(q) = q^{2k}$. These functions are appropriate for an infinite system (disc geometry). However, formula 3.37 includes $\psi_m(r)$ (and its derivatives) *only* at $r = 0$. At least for short distances

[33] If an interested reader will be looking for an expression giving the elements in the line k I recommend to start with $k!\binom{k}{m}(-1)^{m+k}$.

[34] 'Mathematical' = exact, 'physical' = less exact.

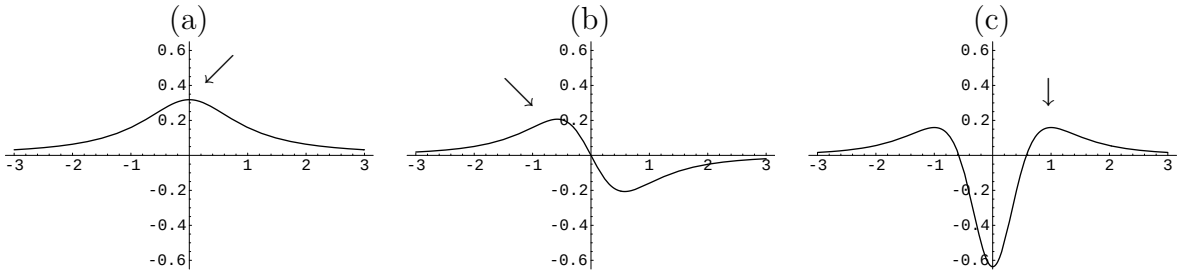

Figure 3.6: An approximation to the delta distribution in one dimension (Lorentzian of halfwidth b). *Left to right:* $\delta_b(x)$, $\delta_b'(x)$, $\delta_b''(x)$. The higher the derivative, the larger the 'range' of the function. (separation of the last maximum from origin)

we may expect that $\psi_m(r)$ on a torus and on a plane is the same, since both manifolds are locally flat (this may be explicitly verified by comparing Eq. 3.32 and Eq. 3.40 around $r = 0$).

Thus Tab. 3.1 is valid both for plane and torus geometry.

(4) *Example:* consider two electrons (in plane, on a sphere, on a torus) in the lowest Landau level and interacting via $V(q) = \alpha q^2$. Eigenstates (sorted according to increasing value of the particle–particle distance $\langle r \rangle$) in this system may be indexed by an integer, call it m. The state $m = 0$ will have energy $-\alpha$, the state $m = 1$ will have energy α and all other states (with larger interparticle separation) have zero energy.

The state with $m = 0$ will have a symmetric wavefunction and will be thus prohibited for electrons of like spin. Thus there will be only one state with non-zero energy for this case (and it is the state with the lowest interparticle separation) and $V(q) = \alpha q^2$ defines therefore a hard–core interaction.

On a plane and on a sphere, m will be the angular momentum of the Hamiltonian eigenstates.

3.3.6 Short–range interaction on a torus

The decomposition of the Coulomb interaction (in the lowest Landau level) into the Haldane pseudopotential has already been shown in Fig. 3.5. This is also the spectrum of two Coulomb–interacting particles on a sphere.

Let us focus on particles on a torus now, Fig. 3.7. The index m is no longer angular momentum of the pair as this is not a good quantum number. However, the mean distance between the two particles grows with rising m.

In the region of small interparticle distances the spectrum is analogous to the spherical system. Also the wavefunctions are similar to the spherical system, they preserve the circular symmetry (Fig. 3.8). Such states can be described as (almost exact) eigenstates to angular momentum $m\hbar$. Note however, that each level is now fourfold degenerate which

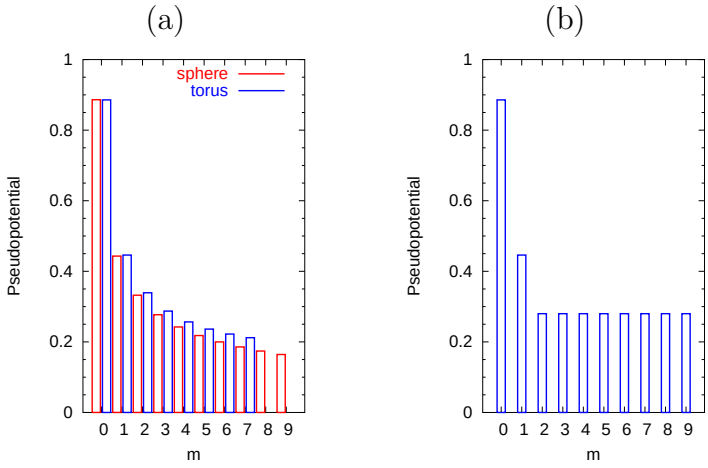

Figure 3.7: Haldane pseudopotentials on a sphere and on a torus. *Left:* comparison between sphere and torus. *Right:* definition of a short–range interaction (hard–core potential) on torus used in this work. Note the ill–definedness of m on a torus (see Fig. 3.8).

stems from the rotational symmetry of the square (with periodic boundary conditions) the particles are confined to. For higher–interparticle distances these quadruplets are no longer degenerate and it is meaningless to describe them in terms of a common m (see the enlarged region in Fig. 3.8a).

A reasonable model mimicking the short–range interaction is to keep the first two energies of the spectrum in Fig. 3.7, i.e. the pseudopotentials V_0, V_1 at their 'Coulomb' values while setting the other ones to zero. Table 3.1 gives a prescription how to encode such an interaction into $V(q)$. We thus arrive at an interaction potential defined by $V(q) = 0.34q^2 - 1.51$ which was used throughout this work to model a short–range interaction unless something else is explicitly stated.

3.4 Composite fermion theory, Chern-Simons, Shankar

In Subsection 3.2.3 a very basic observation about the Laughlin wavefunction Ψ_L (Eq. 3.20) has been made: three zeroes of Ψ_L are bound to each electron[35]. One zero is required by the Pauli principle (when $z_1 = z_2$, the wavefunction must vanish), the others were 'voluntary'. Now, compare this wavefunction to the exact ground state of $\nu = 1$ (at $B \to \infty$):

$$\text{GS, } \nu = 1 : \quad \Psi \propto \prod_{i<j}(z_i - z_j)\,, \qquad \text{Laughlin state, } \nu = \frac{1}{3} : \quad \Psi_L \propto \prod_{i<j}(z_i - z_j)^3\,,$$

where we omitted the exponential terms being the same for both wavefunctions.

[35] Recall that we fixed positions of $z_2, \ldots, z_n$ and used the last 'free' coordinate z_1 to inspect the wavefunction.

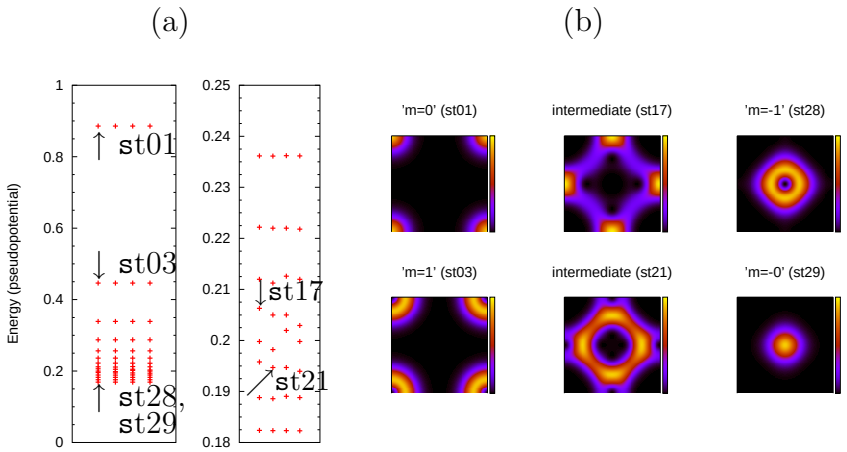

Figure 3.8: Two–particle eigenstates of Coulomb–interacting particles on a torus confined to the lowest Landau level. States are shown irrespective of the symmetry or antisymmetry of the wavefunction. *Left:* spectrum (horizontal axis has no meaning: levels are 'randomly' distributed into four groups in order to show degeneracies; each point displayed corresponds to one state). *Right:* density–density correlation functions $g(r)$ of several states. Conditional probability to find the second particle at r provided the first particle sits in the corner (the four corners are identical due to periodic boundary conditions). The states with the smallest interparticle distance can be characterised by a common $m = \langle L_z/\hbar \rangle$ (their $g(r)$ are almost identical to the eigenstates of L_z). Higher lying states are strongly affected by periodic boundary conditions. The highest states show again circular symmetry, but the second particle is not orbiting around the first one but rather around the opposite point on the torus.

It has been argued that a zero (just as a vortex) of the wavefunction is felt by electrons as a magnetic flux quantum (Subsect. 3.2.3). From this viewpoint, the Laughlin state can be interpreted just as the $\nu = 1$ state where two magnetic flux quanta are attached to each electron. These objects (electron dressed by two flux quanta) are called *composite fermions* (CFs)[36]. Note however that the precise definition of a composite fermion may vary in different theories. This will be explained below.

On an intuitive level, this concept explains the existence of a gapped ground state at filling factor $\nu = \frac{1}{3}$. Originally, there are *three* flux quanta per electron (Eq. 3.6) and the huge Hilbert space of many–electron states in the lowest Landau level is completely degenerate without interaction. In other words, we expect no gap without interaction. If we now assume, that the Coulomb interaction leads to the formation of composite objects, electron and *two* flux quanta, then there remains only *one* free flux quantum per each such object (CF). This in turn implies the filling factor of $\nu_{CF} = 1$ for CFs (Eq. 3.6) and we know that in this case the ground state of particles obeying Fermi statistics[37] will

[36]Similarly, Laughlin state at $\nu = \frac{1}{5}$ can be interpreted in terms of electrons with four flux quanta attached. We will however discuss mostly the ^{2}CF's here and will skip the 'two' unless confusion might arise.

[37]See comment [4].

be gapped: if a Landau level is completely filled, then any, even infinitesimal, excitation requires promoting at least one CF into a higher CF Landau level which costs finite energy $\geq \hbar\omega_{CF}$.

The last paragraph could be a good advertisement for composite fermion theories in *Sunday Times* or in *Bild Zeitung*. However, since this work is a thesis rather than an advertisement, let me try to introduce some of the current composite fermion theories in a little bit more detail.

3.4.1 Chern–Simons transformation

Looking at the Laughlin wavefunction in the way sketched above, it might occur reasonable to embody the flux attachment somehow already in the Hamiltonian.

The Chern–Simons (CS) transformation is just a gauge transformation of the magnetic field

$$\mathsf{a}_{CS}(\mathsf{r}) = \alpha\Phi_0 \int \mathrm{d}^2 r_1 \frac{\mathsf{e}_z \times (\mathsf{r} - \mathsf{r}_1)}{|\mathsf{r} - \mathsf{r}_1|^2} \Psi^\dagger(\mathsf{r}_1)\Psi(\mathsf{r}_1)\,.$$

It does not change the magnetic field (and it can be thus titled 'gauge transformation') felt by electrons only owing to the fact that two electrons cannot be simultaneously on the same place. Price for this is that the transformation is singular (a_{CS} diverges for $\mathsf{r} = \mathsf{r}_i$). $\Psi^\dagger(\mathsf{r})$ are the one–electron field operators and α is the number of attached magnetic fluxes.

After this transformation the full Hamiltonian

$$H = \frac{1}{2m} \int \mathrm{d}^2 \mathsf{r}\, \Psi^\dagger(\mathsf{r}) \left[-i\hbar\nabla_r + e\mathsf{A}(\mathsf{r}) - e\mathsf{a}_{CS}(\mathsf{r})\right]^2 \Psi(\mathsf{r}) \tag{3.38}$$

contains — apart from one particle terms — two particle terms (those containing a_{CS}) and also three particle terms $\Psi^\dagger(\mathsf{r})\Psi(\mathsf{r})\Psi^\dagger(\mathsf{r}_1)\Psi(\mathsf{r}_1)\Psi^\dagger(\mathsf{r}_2)\Psi(\mathsf{r}_2)$ (they originate from a^2_{CS}).

A mean field approximation can be made at this point where the density operator $\Psi^\dagger(\mathsf{r}_1)\Psi(\mathsf{r}_1)$ in a_{CS} is replaced by the mean value n_S. We arrive at a single particle problem with effective magnetic field $B_{CF} = B - \alpha\phi_0 n_S$. Let us give an example how this works

	CS transf.		mean field	
many–body system at $\nu = \frac{1}{3}$	$\longrightarrow$	a very complicated many–body problem at $\nu = \frac{1}{3}$	$\longrightarrow$	simple one–particle problem at $\nu = 1$

Since the final 'simple one–particle problem at $\nu = 1$' has a non–degenerate ground state, i.e. fully occupied lowest Landau level, the effect of the interaction between electrons can now be taken into account perturbatively.

Of course, a mean field approximation is not the only possible treatment of the Hamiltonian 3.38. Theories going beyond mean field, i.e. those treating fluctuations of the gauge field, are however very complex.

By the CS transformation we attach $2s = \alpha$ vortices[38](not zeroes) to each electron. In the mean field approximation the problem is equivalent to non–interacting particles in reduced magnetic field B_{CF} which then corresponds to filling factor ν_{CF}. It turns out that all experimentally observed fractions ν (except for the 'new fractions', Subsect. 3.2.6) correspond to integer ν_{CF}. Let us conclude with the overview of relations between quantities referring to electrons and to composite fermions (cf. Eq. 3.6)

$$B_{CF} = B(1-2s\nu) = B - 2sn_S\Phi_0\,, \qquad \ell^* \equiv \ell_{CF} = \frac{\ell_0}{\sqrt{1-2s\nu}}\,, \qquad \frac{1}{\nu_{CF}} = \frac{1}{\nu} - 2s\,, \quad (3.39)$$

$$\text{or} \quad \nu = \frac{p}{2sp+1}\,, \text{ assuming } p, s \text{ integer}\,.$$

3.4.2 Composite fermions à la Jain

Compared to the Chern–Simons transformation, Jain's suggestion goes in some sense the same way but opposite direction [44], [45]. It starts with a wavefunction of particles (fermions) at integer filling $\nu_{CF} = p$, attaches s zeroes (*not* vortices) to each particle and, after projection into the lowest Landau level, it presents the result as a trial wavefunction for the ground state at filling $\nu = p/(2sp+1)$ (Eq. 3.39). This procedure reproduces exactly the Laughlin wavefunction and at other fractions it gives wavefunctions with very high overlap with ground states calculated numerically (by exact diagonalization).

There are two central reasons why this approach is very popular. On one hand, it gives a simple single–particle picture of what is going on in the highly correlated many–body problem. On the other hand, it gives explicit formulae to work with since it is easy to write down a wavefunction of p full Landau levels. A very pleasant feature of this approach is that it allows to incorporate spin of electrons easily [99]. Just take $p_\uparrow$ full Landau levels with spin up and $p_\downarrow$ full Landau levels with spin down[39]. These Landau levels are then called *composite fermion Landau levels*. Magnetic field felt by the composite fermions, i.e. the field corresponding to filling factor $\nu_{CF} = p$ is called *effective magnetic field* B_{eff}. It is weaker than magnetic field B corresponding to the electronic state at ν (Eq. 3.39).

Note, that filling factors in Eq. 3.39 are all in range $\nu < \frac{1}{2}$. For $\frac{1}{2} < \nu < 1$, Jain *et al.* [99] suggest the idea of *antiparallel flux attachment*. It accounts to setting the effective field B_{eff} antiparallel to the real field B, the additional flux quanta are however added in parallel to B [40]. In terms of Eq. 3.39 this means $p \to -p$ or $\nu = p/(2sp-1)$.

An example of candidates for ground states and their polarization provided by Jain's composite fermion theory is given in Tab. 3.2. See Chakraborty [16] for a review regarding ground states with various spins (both from theoretical and experimental side).

[38]Condition α be even is dictated by Fermi statistics, for α odd we get composite bosons. [4]

[39]This is not just a hypothetic possibility: it can be arranged by a suitable ratio E_C/E_Z between cyclotron energy (Landau level separation) and Zeeman energy (E_C/E_Z can be changed e.g. by changing the Landé g factor). For $E_C/E_Z \to 0$ we expect only fully polarized states, for $E_C/E_Z \to \infty$ we expect spin singlet states (for p even).

[40]i.e. antiparallel to B_{eff}, that is how the name comes about.

$p_\uparrow$	1	2	3	-2	...	1	2	2	-1
$p_\downarrow$	0	0	0	0		1	1	2	-1
$p = p_\uparrow + p_\downarrow$	1	2	3	-2		2	3	4	-2
$\nu = p/(2sp+1)$	$\frac{1}{3}$	$\frac{2}{5}$	$\frac{3}{7}$	$\frac{2}{3}$		$\frac{2}{5}$	$\frac{3}{7}$	$\frac{4}{9}$	$\frac{2}{3}$
$S/\frac{n}{2}$	1	1	1	1		0	$\frac{1}{3}$	$\frac{1}{2}$	0

Table 3.2: The scheme of construction of the Jain's wavefunctions for composite fermions with two flux quanta attached: examples of composite fermion filling factors ($p_\uparrow$, $p_\downarrow$ are numbers of fully occupied spin up and spin down CF Landau levels) and corresponding electronic filling factors.

3.4.3 Composite fermions à la Shankar and Murthy (Hamiltonian theory)

Hamiltonian theory of FQHE (Shankar and Murthy [72]) builds on previous works of Jain and those concerning Chern–Simons transformations and, citing words of its authors, it combines the strengths of them both.

It provides a (projected) Hamiltonian of the lowest Landau level which scales only with Coulomb interaction. In addition to each electron a new independent object is introduced: a pseudovortex. Its definition[41] assures, that if an electron goes around a pseudovortex, it picks up the phase of $2\pi\, 2s$ (i.e. it has the same effect as an insertion of $2s$ flux quanta); note, it is *not* a zero of the wavefunction. The projected Hamiltonian is written in coordinates which are a combination of the electron and pseudovortex position ; this combination is then called *composite fermion coordinate*.

For this Hamiltonian an ansatz for a ground state can be written down. At filling $\nu = p/(2sp+1)$, it is just p Landau levels filled with composite fermions (in the sense as they have just been defined) and it is then possible to evaluate their Hartree–Fock energies.

The first substantial success of this theory is that it produces a correct scaling of spectra within the lowest Landau level ($\propto \sqrt{B}$). Compared to Jain's theory, it keeps track of the fact that the two fluxes (which sit exactly at each electron in the Laughlin state) can be only loosely bound to electrons. This happens by giving the pseudovortices their 'independence'. On the other hand, the electronic coordinates are actually the only really independent ones[42] and thus the price we must pay for the extension of the Hilbert space is that we must perform a projection to 'physical states' at the end.

However, this does not seem to be really a problem and thus the Hamiltonian theory seems to be the most advanced development in an effort to understand the many body physics in fractional quantum Hall effect.

[41] On the level of commutation relations (Eq. 129 in [72]).

[42] For instance in the Laughlin wavefunction, all the zeroes $(z_i - z_j)$ are expressed in terms of electronic coordinates.

3.5 Numerical methods or How to test the CF theory

The main part of this Section will concern the exact diagonalization (ED) as this was the method chosen in my study. It is not exact to say this is the only numerical method used in the context of the fractional quantum Hall effect. Basically, some numerics is at the end of nearly any method as soon as many–body problems are concerned, be it Hartree–Fock treatment of composite fermions or Monte Carlo simulations of the Laughlin state mapped onto a one–component plasma. What we rather mean here is that ED is a very low–level method: it solves the complete many–body Schrödinger equation. The only substantial[43] approximation of the model is to put the interacting electrons on a compact (finite–sized) surface, possibly without edges, instead of an infinite plane. The hope is that effects inflicted by the finite size can be separated from those generic to a two–dimensional electron gas.

Since there are no approximations in the Hamiltonian (in particular such ones derogating the many–body nature of the states), exact diagonalization has always been a standard to compare results of other theories with.

First, we will introduce the 'finite–sized surfaces'[44] of interest (torus [103] and sphere [36]), then exact–diagonalization will be discussed and finally remarks on possible extensions will be presented.

3.5.1 Torus geometry

One possibility to model an infinite plane by a finite manifold without edges is a rectangle (a by b) with periodic boundary conditions. Topologically, this is the same as a torus; let us, however, stay with the former picture (even if we sometimes use the word 'torus' as a shortcut for this model).

What are the single particle states (of the lowest Landau level) in this case? Recall Eq. 3.17 where single–particle states complying with translational symmetry along y are given[45]

$$\psi_{0,k'_y}(x', y') = \exp(-ik'_y y') \exp[-(x' + k'_y)^2/2] \,.$$

Periodic boundary conditions along y, i.e. $\psi(x', 0) = \psi(x', b/\ell_0)$, allow only discrete values of $k'_y = (2\pi\ell_0/b)j$ with j integer. At the same time, if we require $\psi_{0,k'_y}(x', y')$ to be centered within[46] $[0; a/\ell_0)$ (in the x direction), we have $0 \leq -k'_y < a/\ell_0$. Thus, up to sign,

$$0 < j < \frac{ab}{2\pi\ell_0^2} = m \,.$$

[43] Another usual yet not really necessary approximation is to neglect Landau level mixing, i.e. restriction to the lowest Landau level only. Also note, that there is a long way from an ideal 2D system which study here, to the experimental reality (impurities, effective mass approximation, etc.).

[44] We will not discuss the disc geometry here since it contains an edge. In rather small systems which are accessible to exact diagonalization it is then difficult to separate edge and bulk properties.

[45] Primed coordinates are in units of magnetic length, $x' = x/\ell_0$, $k' = k\ell_0$.

[46] This condition can be written also as $0 \leq X_j < a$, $X_j = k_y\ell_0^2$. Note that $x' = a/\ell_0$ is the same as $x' = 0$. We thus have to omit one of these two points to avoid double counting.

Eq. 3.6 has taught us that $ab/(2\pi\ell_0^2)$ is equal to number of magnetic flux quanta (Φ/Φ_0) which pass through the rectangle and it must be therefore an integer. This brings us to the central insight that *there is only a finite number m of states in a square with periodic boundary conditions* (subject to magnetic field and discarding all but the lowest Landau level). Later we will argue that m is equal to the number of magnetic flux quanta penetrating the rectangle (after Eq. 3.43).

States $\psi_{0,k'_y}(x',y')$ shown above are not periodic in the x direction and this can be accomplished by periodic continuation: $\psi(x,y) \to \psi(x,y) + \psi(x+a,y) + \dots$. The (non-normalized) single particle states we will be dealing with are thus (Yoshioka [103], [101], [104])

$$\varphi_j(x',y') \;=\; \sum_{k=-\infty}^{\infty} \exp\left[iy'(\frac{j}{m}+k)\zeta - \frac{1}{2}\left(x' - (\frac{j}{m}+k)\zeta\right)^2\right], \quad \zeta = \sqrt{\frac{a}{b}\cdot 2\pi m}\,, \\ j = 0,1,2,\dots,m-1\,. \tag{3.40}$$

These states constitute the (single–particle) basis of the lowest Landau level.

This sequence of arguments is sufficient for the purposes of this work, yet we camouflaged an important aspect about periodic boundary conditions. Let us have a closer look.

Twisted boundary conditions

It is relevant to require the $|\psi|^2$ rather than ψ itself to be periodic (Bloch's theorem). Thus, the wavefunction may acquire a non-trivial phase when going once around the torus. Mathematically, this can be described using the magnetic translation operators (Eq. 3.18):

$$T(a\mathsf{e}_x)\psi = \exp(i\phi_x)\psi\,, \qquad T(b\mathsf{e}_y)\psi = \exp(i\phi_y)\psi\,. \tag{3.41}$$

Fixing phases ϕ_x, ϕ_y, the correct (unnormalized) periodic single particle states are

$$\varphi_j(x,y) \;=\; \sum_{k=-\infty}^{\infty} \underbrace{\exp(ik\phi_x)}_{T(ka\mathsf{e}_x)} t(ka\mathsf{e}_x)\exp(-iX_j y/\ell_0^2 + i\phi_y y/b)\exp[-(x-X_j)^2/2\ell_0^2]\,, \\ X_j = \frac{j}{m}a\,, \qquad j = 0,1,\dots,m-1\,, \tag{3.42}$$

where $t(\xi\mathsf{e}_x)$ is an ordinary translation, i.e. turning $\psi(x,y)$ into $\psi(x+\xi,y)$. For $\phi_x,\phi_y = 0$ the original result (Eq. 3.40) is recovered. This choice of ϕ_x,ϕ_y is also used throughout this work.

Interpretation of ϕ_x,ϕ_y. By imposing the periodic boundary condition we arrived at the statement that wavefunctions must be centered (in x) at $X_j = (a/m)\cdot j$, $j = 0,1,\dots$ There is no *a priori* reason for the point $x = X_0 = 0$ to be more important than $x = X_? = (a/m)\cdot 0.5$ which is not among X_j's (i.e. there is no wavefunction centered at $X_?$ among the described states). By varying ϕ_x, the set $\{X_0, X_1, \dots\} = (a/m)\{0,1,\dots\}$ is

transformed into $(a/m)\{0+\phi_x/2\pi, 1+\phi_x/2\pi, \ldots\}$. Thus, sweeping ϕ_x from 0 to 2π, we probe all points in the x direction. Independently on this, we may sweep through all k_y points in the interval $[0; 2\pi/b]$ by changing ϕ_y. Thus, ϕ_x and ϕ_y are analogous to lattice wavevectors within the first Brillouin zone in an 'ordinary' periodic system (defined by ordinary rather than magnetic translations).

In summary: by considering only a finite system, we have only m states to probe the whole plane (i.e. $[0, a]$ in x and $[0, 2\pi/b]$ in y). Sweeping ϕ_x, ϕ_y from 0 to 2π we can access an arbitrary point in the plane.

Another interpretation of ϕ_x, ϕ_y was given by Tao and Haldane [93] in terms of additional magnetic fluxes[47] $(h/e)(\phi_{x,y}/2\pi)$. It was also shown that ϕ_x increasing linearly in time acts as a homogeneous electric field in x direction (see [38] or [43]).

General basis of single particle states on a torus: complex coordinates

A precise discussion of one–particle states on a torus (including the phases ϕ_x, ϕ_y) was first given by Haldane and Rezayi [38] (instead of a rectangle they even considered a general parallelogram). On a rigorous basis, they showed that the most arbitrary state is

$$\psi(x,y) = \exp(-\tfrac{1}{2}x^2) \cdot \underbrace{\exp(ikz) \prod_{l=1}^{m} \vartheta_1\left(\pi(z-z_l)/b|i\right)}_{\text{analytic}}, \qquad z = x+iy \tag{3.43}$$

where $\vartheta_1(u|\tau)$ is an elliptic theta function ([35], p. 921), k is a real number in range $|k| < \pi m/b$ and z_i are some fixed complex numbers within the rectangle $[0, a] \times [0, b]$. In terminology of Eq. 3.42, these states correspond to any j and any ϕ_x, ϕ_y. The most important thing to know about theta functions is that it $\vartheta_1(z-z_l|i) \propto z-z_l$ for $|z-z_l| \to 0$ and that this is its only zero in the rectangle (Fig. 3.10). In this form, it is also clear that m is equal to the number of flux quanta in the elementary cell (the rectangle): going once around the rectangle, the wavefunction gathers a phase of $2\pi\times$ number of zero points inside. That number is just m.[48]

By choosing fixed ϕ_x, ϕ_y, there arise m possible choices for the values of k and $z_0 = \sum_l z_l$, let us name them $j = 0, 1, \ldots, m-1$. For each pair (k, z_0) we can construct one function of the form (Eq. 3.43) and the resulting m functions will constitute a basis of the lowest Landau level, just as the basis in Eq. 3.42. There is naturally a large freedom in choosing one particular basis. This happens by choosing some particular position of the zero points z_l's (while observing the constraint on z_0). The basis in Eq. 3.42 can be obtained from Eq. 3.43 by putting the zeroes on a line, $z_l = ibl/m + j/ma$ and choosing $k = (2\pi/b)j$ for the state φ_j (with $\phi_x = \phi_y = 0$); even though it is by far not obvious from an inspection by bare eye. Fig. 3.9 shows a 2D plot of one of such functions.

[47] These come from two ideal anuloids (closed solenoids): one goes inside the torus and another around the torus outside.

[48] Linearly independent functions in the form of Eq. 3.43 which fulfil the boundary conditions.

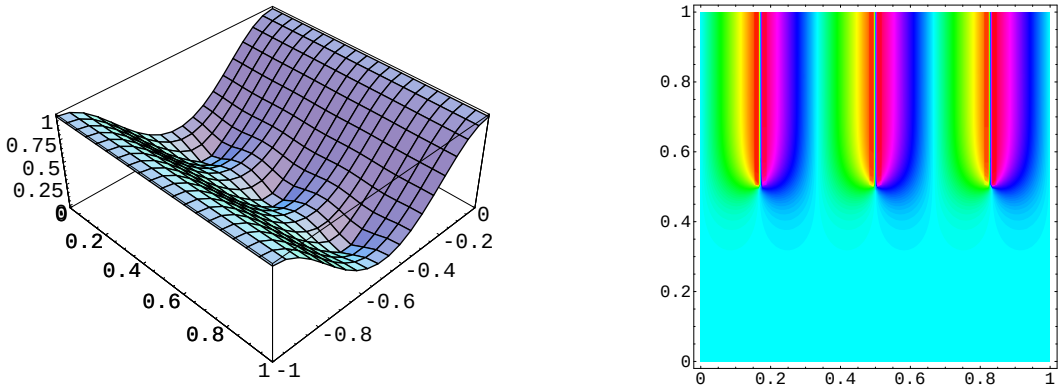

(a) Modulus.

(b) Phase.

Figure 3.9: One possible one–particle state on a torus pierced by three flux quanta (i.e. $m = 3$).

In principle, wavefunctions in Eq. 3.43 are very similar to those obtained in circular gauge (Eq. 3.14) except for substituting[49] z by $\vartheta_1(z|i)$. This is a manifestation of the fact, that even on a torus, circular symmetry is approximately preserved at short distances and deviations occur first when $\vartheta_1(z|i)$ diverts from z at larger distances z. One could say, $\vartheta_1(z|i)$ is the function $f(z) = z$ adapted to the torus (i.e. deformed to comply with periodic boundary conditions).

On the other hand (contrary to infinite plane), each single–electron wavefunction on a torus has as many zeroes as there are flux quanta passing through the torus.

3.5.2 Many–body symmetries on a torus

Center-of-mass

After Haldane and Rezayi [38].

What changes if we consider n–body states instead of single–particle ones? Given the considered Hamiltonian (homogeneous system plus interaction depending only on interparticle distances, Eq. 3.52), the most obvious symmetry is the separation of center-of-mass and relative part of the wavefunction[50]

$$\Psi(z_1, \ldots, z_n) = \Psi_{CM}(Z)\psi_{rel}\,, \qquad Z = z_1 + \ldots + z_n\,. \tag{3.44}$$

The center-of-mass part is just a one–particle wavefunction (it describes the motion of a particle with mass and charge equal to the total mass and total charge of all involved

[49] In Eq. 3.14 we could have taken as a basis not $1, z, z^2, \ldots, z^{m-1}$ but some other m linearly independent polynomials of m-th degree instead. They would have the form $\Pi_{l=1}^{m}(z - z_l)$.

[50] Remember that the Laughlin wavefunction (Eq. 3.20) is just the relative part.

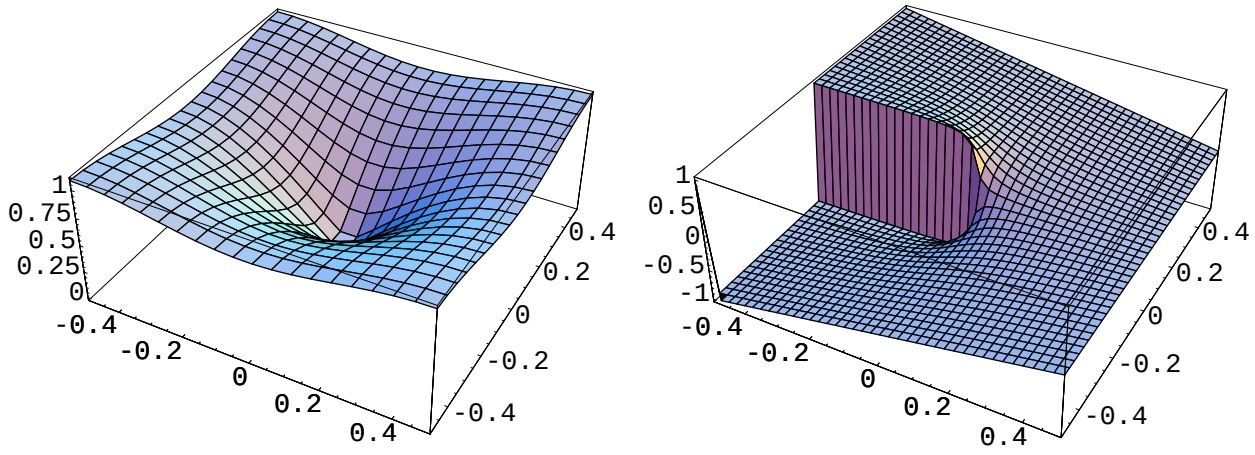

(a) Modulus, $|\vartheta_1|$.

(b) Argument, $\ln(\vartheta_1/|\vartheta_1|)$.

Figure 3.10: Theta function $\vartheta_1(z|i)$.

particles), hence it must have the form as shown in Eq. 3.43. Haldane and Rezayi [38] showed that it has q zeroes in the region $[0;a] \times [0;b]$ (given filling factor $\nu = N_e/(qN_e)$). Again (as for single–particle states), there are q basis states for Ψ_{CM}. Since the energy does not depend on the center-of-mass position (in a homogeneous system), these three states will lead to degenerate many–body states (provided, ψ_{rel} remains the same).

This introduces a delicate topic: of course, the electron density in a given state depends on the center-of-mass part of the wavefunction. Different choices of bases in the q-fold (i.e. threefold for $\nu = \frac{1}{3}$) degenerate space of center-of-mass wavefunctions may lead to a q-tuple of states with practically homogeneous density in some cases or with quite strongly varying density in other cases (Fig. 3.11). This is true in spite of that we always describe the same ground state subspace. Even worse: often (in homogeneous systems) we want to study only the relative part of the wavefunction, which must be the same in all cases (if it is the Laughlin WF, we know for example, it leads to a homogeneous density). The central trouble is then that Hamiltonian eigenstates obtained by exact diagonalization contain Ψ_{CM}.

A more detailed discussion of how Ψ_{CM} influences numerical results obtained on a torus is given in Subsect. 4.1.4.

Relative part of the wavefunction

After Haldane [37], see also more details in [17], Subsect. 7.2.

The discussion in the previous paragraph is based on (magnetic) translations of the center-of-mass $T_{CM}(\boldsymbol{u})$. In an n–body state, the translation of a single (i–th) particle $t_i(\boldsymbol{v})$

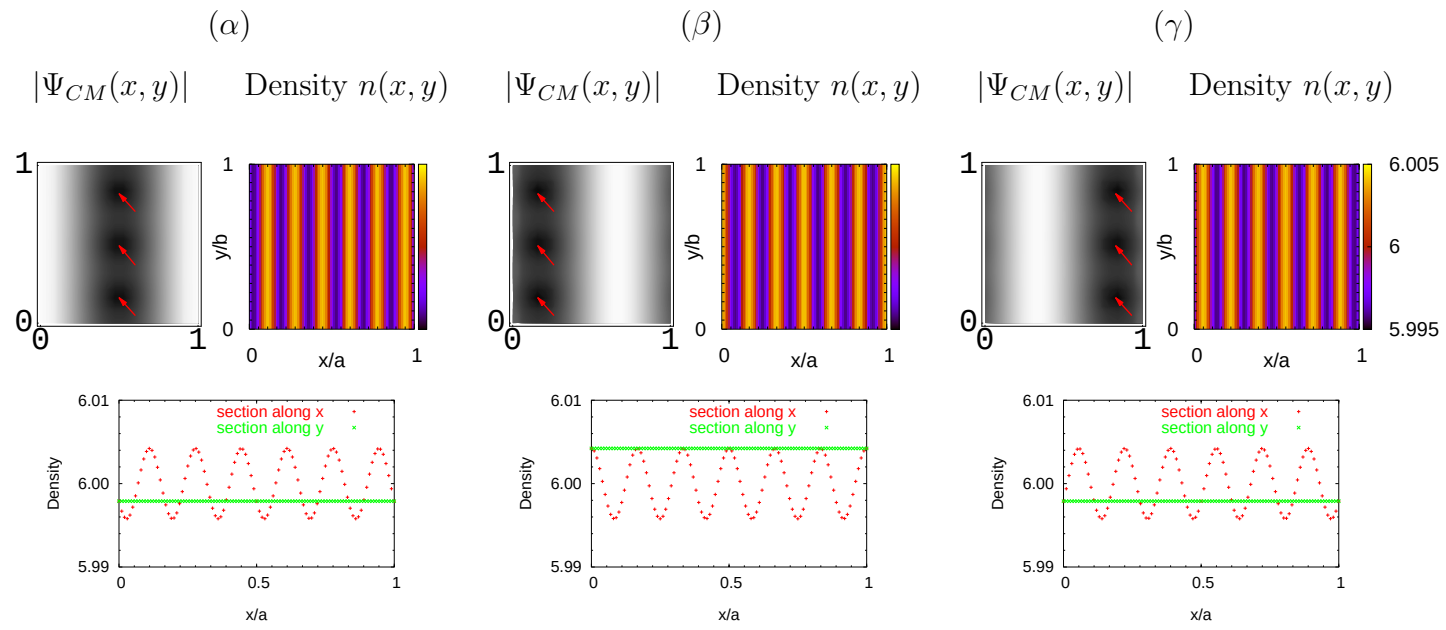

(a) A basis leading to inhomogeneous densities.

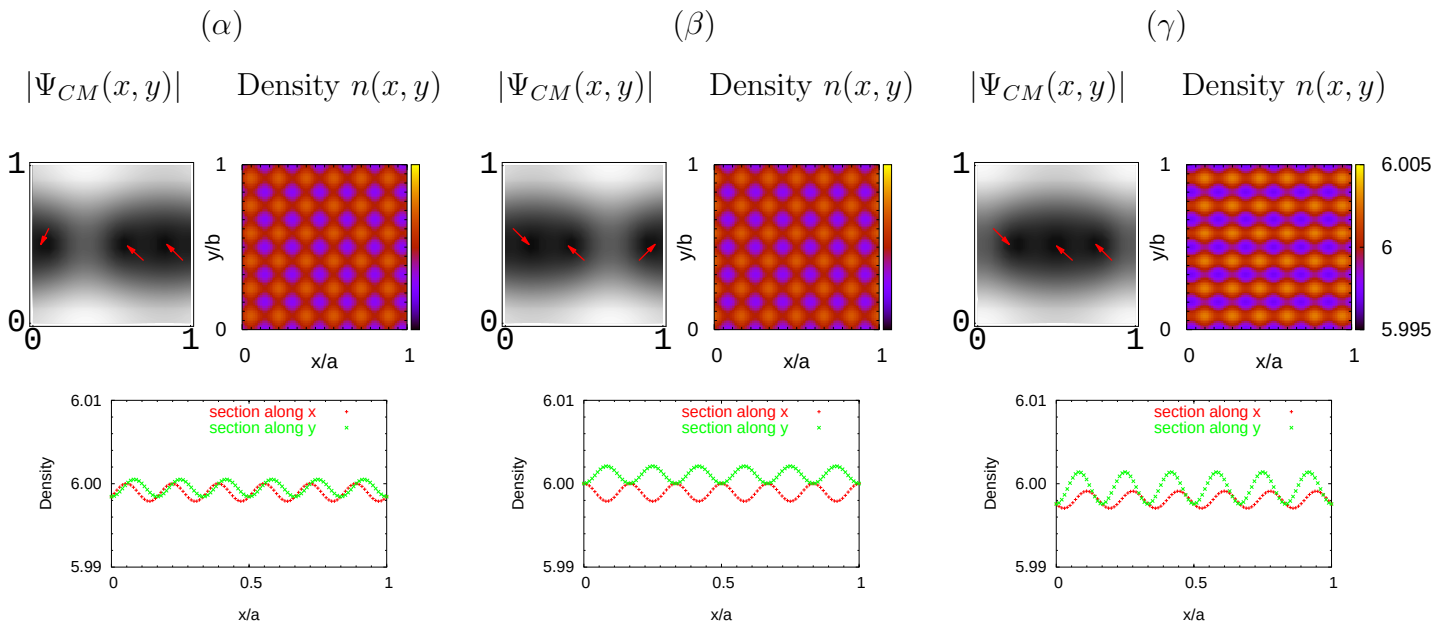

(b) A basis leading to less inhomogeneous densities.

Figure 3.11: Two different bases for Ψ_{CM}. At filling $\nu = \frac{1}{3}$ there are three allowed CM states on a torus. They are labeled α, β, γ in this figure. For each element of each basis we show the modulus of Ψ_{CM}, the density of the corresponding Laughlin state with six electrons, i.e. $\Psi_{CM}\Psi_L$, and section of the density along x and along y. Note the positions of the three zeroes in different Ψ_{CM}'s (marked by the red arrows).

can be split into a translation of the center of mass $T_{CM}(\frac{1}{n}\boldsymbol{v})$ and a relative translation $T_{rel,i}(\boldsymbol{v} - \frac{1}{n}\boldsymbol{v})$. Owing to the indistinguishability of particles, the effect of the relative translation $t_i(\boldsymbol{v})$ on a particular many–particle state is the same for any i; we may thus omit the index and imagine $i = 1$, for instance.

Again, just as in Bloch's theorem, a wavevector $\boldsymbol{k}^r$ can be attributed to these relative translations (Haldane [37])

$$T_{rel}(\boldsymbol{v})\psi = \exp(i\boldsymbol{k}^r \cdot \boldsymbol{v})\psi\,. \tag{3.45}$$

Since $T_{rel}(\boldsymbol{v})$ commutes with the Hamiltonian[51](Eq. 3.52), the Hamiltonian eigenstates can be sorted according to values of $\boldsymbol{k}^r$.

This concept is very similar to a single particle in a periodic potential. However, there is no real periodic potential in an infinite plane and we introduced one particular period artificially: the largest period possible within our model is the size of the rectangle.

The Brillouin zone for $\boldsymbol{k}^r$ is rectangular (Fig. 3.12) and its *size* grows with the size of the elementary cell. For filling factor $\nu = p/q$ (p, q without common divisor > 1) and number of flux quanta per cell $N_s = Nq$, the allowed values of $\boldsymbol{k}^r$ are

$$\boldsymbol{k}^r\ell_0 = \sqrt{\frac{2\pi}{N_s\lambda}}(s,t)\,, \qquad |s|, |t| \leq N/2 \text{ and integer.} \tag{3.46}$$

λ is the aspect ratio. For the sake of comparison between systems of different sizes we will sometimes use size-independent units for $\boldsymbol{k}^r$, where $\widetilde{\boldsymbol{k}}^r = (\pi, \pi)$ will mean the upper right corner of the Brillouin zone (i.e. $s = t = N/2$).

It can be verified ([17], p. 169), that application of the operator

$$\sum_j \exp(i\boldsymbol{q} \cdot \boldsymbol{r}_i) \tag{3.47}$$

to an arbitrary state (let it have a sharp value of $\boldsymbol{k}^r$) increases its wavevector by $\boldsymbol{q}$. On the other hand, the operator (3.47) generates a charge-density wave with wavevector $\boldsymbol{q}$, as can be best verified by the simple example of the Fermi gas.

Isotropic states are supposed to have $\boldsymbol{k}^r = 0$.

Momentum

So far, we have introduced two sorts of translational symmetries of states on a torus: one of the center-of-mass part of the wavefunction and another of the relative part. Since the corresponding (magnetic) translation operators commute with the (homogeneous) Hamiltonian, it would, in principle, be possible to split the basis of the whole lowest Landau level into several smaller bases and diagonalize in the subspaces separately. Each base would be characterized by a particular value of $\boldsymbol{k}_{CM}$ and $\boldsymbol{k}^r$.

[51] In Bloch's theorem, the allowed translations are given by an arbitrary lattice vector $\boldsymbol{v}$. Not all of them are allowed for T_{rel} though [37].

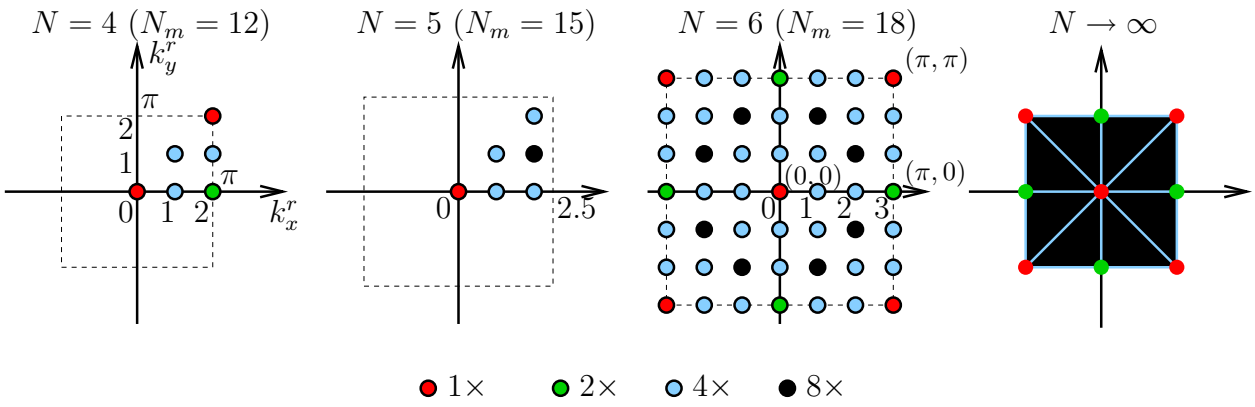

Figure 3.12: The first Brillouin zone for relative translations on torus (square with periodic boundary conditions). Its size depends on the number of particles in the system. At filling factor $\nu = p/q$ with $N_e = Np$ particles (and $N_m = Nq$ fluxes), number of allowed $\boldsymbol{k}^r$–points is N^2 and the upper right corner is $\boldsymbol{k}^r = \gamma(\pi, \pi)$, $\gamma = \sqrt{N/2\pi}$. Different colours indicate points of different symmetry (or degeneracy number of a state with this $\boldsymbol{k}^r$ in a homogeneous system), the rightmost figure shows the limit of large N.

This procedure can help to treat larger systems but it costs some extra effort to implement it and moreover it is only possible in homogeneous systems. We will now discuss another symmetry of the Hamiltonian which is a combination of the previous two and is preserved with a certain class of inhomogeneities.

The homogeneous Hamiltonian (Eq. 3.15) in Landau gauge (i is particle index, V_{int} is e.g. Coulomb interaction between particles)

$$H = V_{int} + \sum_i H_0^i\,, \qquad H_0 = \frac{1}{2}\hbar\omega\left[-\frac{\partial^2}{\partial x'^2} + \left(-i\frac{\partial}{\partial y'} + x'\right)^2\right], \qquad (x', y') = (x/\ell_0, y/\ell_0)$$

obviously conserves the total momentum in y direction. Due to the periodic boundary conditions[52] allowed values of k_y are $(2\pi/b)j$, $j = 0, 1, \ldots, m-1$ (cf. Subsect. 3.5.1). In an n-body state constructed as a Slater determinant of single–electron states φ_{j_i} (Eq. 3.40), the total momentum (along y) is thus

$$(b/2\pi)K_y = (b/2\pi)\sum_{i=1}^{n} k_y^i = j_1 + \ldots + j_n (\mod m) \equiv J\,. \qquad (3.48)$$

Values of J thus range for instance from 0 to $m-1$.

It is useful to keep in mind, that j_i is (up to the factor) the point in x–direction at which φ_{j_i} is centered ($X_{j_i} = (j_i/m)a$). Thus, J can also be interpreted[53] as the x–coordinate of the center-of-mass of the n-electron state.

[52] Periodicity in y enforces integer j and periodicity in x maps j onto $j + m$.
[53] This would be exact if the gaussian in $\varphi_j(x, y)$ were very narrow.

Without proof, let us now present the precise connection between J and the wavevectors following from T_{CM} and T_{rel} (i.e. $\boldsymbol{k}_{CM}, \boldsymbol{k}^r$).

Be again $\nu = p/q$ (p, q without common divisor > 1) and $m = Nq$ the number of flux quanta per cell. An arbitrary J can be decomposed into two parts

$$J = J_{CM} \cdot N + J_{rel}\,, \quad |J_{rel}| \leq N/2\,,\ J_{CM} \text{ integer}, \tag{3.49}$$

i.e. J_{rel} is J modulo N and J_{CM} is J divided by N. J_{rel} is directly the y-component of $\boldsymbol{k}^r$ (more precisely $J_{rel} = t$ or $J_{rel} = N/2 - t$ in Eq. 3.46, the former for $pq(n-1)$ even, the latter for $pq(n-1)$ odd [17]).

J_{CM} distinguishes states which differ *only* in the center-of-mass coordinate: by a successive application of T_{CM} to one state Ψ we can go through all possible values of $J_{CM} = 0, 1, \ldots, q-1$.

In each subspace with definite J, states of all different k_x^r are contained. Since T_{rel} (by allowed translation vectors) commute with the total momentum in y, it is in principle possible to split a basis to particular J into subspaces with $k_x^r = -N/2, \ldots N/2$. However, the basis state will not have the simple form of (antisymmetrized) product states of φ_j (in Eq. 3.40) anymore.

3.5.3 Other popular geometries: sphere and disc

Spherical geometry

Apart from the torus, the electrons might be confined to a sphere [36] (a review in [17], Sect. 5.3). Together with the torus, these have been the two geometries used to model an infinite plane as they are both locally flat and have no edges. For very large finite systems, results calculated on a torus and on a sphere should coincide.

The basic difference between the two geometries are the symmetries. In a rectangle with periodic boundary conditions, translational symmetries are preserved (see Subsect. 3.5.2). On a sphere, angular momentum $\boldsymbol{L}$ is preserved. Its length $L = |\boldsymbol{L}|$ corresponds to an effective wavevector $|\boldsymbol{k}^r| = (|\boldsymbol{L}|/\hbar)/R$, where R is radius of the sphere (Haldane [36], or [17] Sect. 7.1). The direction of $\boldsymbol{L}$ (or alternatively L_z, for instance) is related to the direction of $\boldsymbol{k}^r$: for example a wave going around the equator will have $\boldsymbol{L}$ pointing to the pole.

It has been demonstrated, that spectra calculated on a torus and those calculated on a sphere very nicely agree if the former is plotted against $|\boldsymbol{k}^r|$ and the latter against $(|\boldsymbol{L}|/\hbar)/R$ ([17], Sect. 7.1,7.2).

Disc geometry

Laughlin wavefunction in the form given by Eq. 3.20 is in fact not translationally invariant, owing to the exponential factor. Rather, it describes N_e electrons localized in a disc of

area $N_e/\varrho = N_e \cdot 2\pi\ell_0^2 m$ (Eq. 3.21; $\nu = 1/m$) as we may expect already from the analogy to a classical plasma.

From the point of view of exact diagonalization (Subsect. 3.5.4), this geometry is less suitable for studies of homogeneous (infinite) systems. The reason is that contrary to torus or sphere, disc has an edge. For numbers of particles accessible for numerical studies ($N_e \lesssim 10$), relatively many particles will be influenced by the edge and relatively few particles will behave like 'bulk'. Disc geometry on the other hand suitable to study e.g. edge states in the fractional quantum Hall systems. It is also very popular for studies of quantum dots: the central notion is the 'maximum density droplet' (MDD) which is basically a round quantum dot filled with electrons of constant density corresponding to filling factor one (see review of Reimann and Manninen [79]). Analogy of the MDD in the fractional filling regime ($\nu = \frac{1}{3}$), the Laughlin droplet, was studied for example by Mitra *et al.* [66].

It is possible to 'translate' the Laughlin wavefunction in Eq. 3.20 to torus [38] or spherical geometry [36]. These wavefunctions can be then compared to numerical results of exact diagonalization (Subsect. 3.5.4) in the particular geometry. Overlaps found to lie very close to unity for different sizes and different geometries are then the final proof of correctness of Laughlin's wavefunction [28] (cf. also Figs. 4.4 and 4.3).

3.5.4 Exact diagonalization

Many (n) interacting electrons in a rectangle with periodic boundary conditions can be described in the following way.

- Choose the number of flux quanta penetrating the rectangle (m). All allowed single–particle states φ_j are those written in Eq. 3.40 (or Eq. 3.42 for nontrivial boundary–condition phases ϕ_x, ϕ_y). Their number is m.

- Construct all possible n–particle states (for the given number of flux quanta m). Most conveniently, these can be antisymmetrized products (Slater determinants) of n states φ_{j_i}, denote them by

$$|j_1 \dots j_n\rangle = a^\dagger_{j_1} \dots a^\dagger_{j_n} |0\rangle \,. \tag{3.50}$$

- Filling factor is then fixed to $\nu = n/m$ (see Eq. 3.6).

- Take an arbitrary (exact[54] many–body) Hamilton operator and calculate its matrix elements in basis $|j_1 \dots j_n\rangle_k$, $k = 1, \dots, N$ (dimension of the matrix is thus N).

[54] Keep in mind that 'exact' refers only to its many–body nature. Substantial approximations are needed to get from the experimental reality to an ideal $2D$ system.

- Diagonalize the Hamilton matrix. Eigenvalues are the total energies E_i, eigenvectors $\mathsf{v}_i = (v_i^1, \ldots, v_i^N)$ are related to the many–body eigenstates by

$$H|\psi_i\rangle = E_i|\psi_i\rangle\,, \qquad |\psi_i\rangle = \sum_{k=1}^{N} v_i^k |(j_1 \ldots j_n)_k\rangle\,. \tag{3.51}$$

Remarks. (i) This procedure is *exact* if we consider a system where electrons in the lowest Landau level form a periodic system. The approximation lies therefore in representing an infinite system by a periodic repetition of a 'representative' finite cell, a procedure which has been very successfully applied in condensed matter theory. Formulated in other words: the Hamiltonian is exact and all approximations[55] are implemented by the choice of the basis. (ii) The dimension of the matrix is finite by construction (e.g. m choose n for spin polarized particles). No cut–off for one particle states is needed.

In the rest of this Subsection we will present the particular form of the Coulomb matrix elements (after [17], Sect. 5.1 or original [103]).

The exact Hamilton operator in first and in second quantization is

$$\begin{aligned} H &= \frac{e^2}{4\pi\varepsilon}\sum_{i<j} V(|\mathsf{r}_i - \mathsf{r}_j|) \qquad (3.52)\\ H &= \sum_j \mathcal{W} a_j^\dagger a_j + \sum_{\substack{j_1,j_2\\ j_3,j_4}} \mathcal{A}_{j_1,j_2,j_3,j_4} a_{j_1}^\dagger a_{j_2}^\dagger a_{j_3} a_{j_4}\,, \end{aligned}$$

where $a_j^\dagger$ create single–electron states. The latter expression assumes already periodic boundary conditions: the first sum is the 'Madelung energy' of the electron interacting with its own periodic images[56] [15], Eq. 2.17.

$$\mathcal{W} = -\frac{e^2}{\sqrt{ab}}\left[2 - \sum_{\substack{l_1,l_1\\ (l_1,l_2)\neq(0,0)}} \varphi_{-\frac{1}{2}}\left(\pi(l_1^2\lambda + l_2^2/\lambda)\right)\right]\,, \qquad \varphi_n(z) \equiv \int_1^\infty \mathrm{d}t e^{-zt} t^n\,. \tag{3.53}$$

Choosing the single–electron basis according to Eq. 3.40 (or 3.43), the interaction matrix elements are given by

$$\begin{aligned} \mathcal{A}_{j_1,j_2,j_3,j_4} &= \frac{1}{2}\int \mathrm{d}\mathsf{r}_1 \mathrm{d}\mathsf{r}_2 \varphi_{j_1}^*(\mathsf{r}_1)\varphi_{j_2}^*(\mathsf{r}_2) V(|\mathsf{r}_1 - \mathsf{r}_2|)\varphi_{j_3}(\mathsf{r}_2)\varphi_{j_4}(\mathsf{r}_1) =\\ &= \frac{\pi e^2}{2\pi\ell_0^2 m} \sum_{\substack{q_x=(2\pi/a)s\\ q_y=(2\pi/b)t\\ s,t\in\mathbb{Z}\\ (s,t)\neq(0,0)}} \delta'_{j_1+j_2,j_3+j_4}\delta'_{s,j_1-j_4} V(\mathsf{q}) \exp\left[-\frac{1}{2}\mathsf{q}^2\ell_0^2\right] \times \qquad (3.54)\\ &\qquad \times \exp\left[-2\pi i t(j_1 - j_3)/m\right] \times \alpha(j_1 + j_2 - j_3 - j_4, \phi_y)\,. \end{aligned}$$

[55] Number of particles, their placement on torus (including the phases ϕ_x, ϕ_y) and also restriction to the lowest Landau level.

[56] If only the electrons were considered, this energy would diverge at least as $\sum_n 1/n$. To keep it finite, a neutralizing positive background must be considered (Eq. 2.8 in [15]).

with both integrals taken over the rectangle $[0;a]\times[0;b]$. Primed Kronecker δ compares the two arguments *modulo* m. The last factor α is solely due to the boundary condition phase ϕ_y

$$\alpha(\Delta J,\phi_y)=\delta_{J,0}+\delta_{\Delta J,m}\exp(i\phi_y)+\delta_{\Delta J,-m}\exp(-i\phi_y)\,,$$

the matrix elements do not depend on ϕ_x.

The periodic continuation of the Coulomb interaction in two dimensions is given by

$$V(\boldsymbol{r})=\frac{e^2}{|\boldsymbol{r}|}\bigg|_{per}=\frac{1}{ab}\sum_{\boldsymbol{q}}\frac{2\pi e^2}{|\boldsymbol{q}|}\exp(i\boldsymbol{q}\cdot\boldsymbol{r})\,,\qquad \boldsymbol{q}=\left(\frac{2\pi}{a}s,\frac{2\pi}{b}t\right)\,,\ s,t\in\mathbb{Z}\,,\tag{3.55}$$

hence the Fourier series of $V(\boldsymbol{r})$ used in Eq. 3.54 is $V(\boldsymbol{q})=2\pi e^2/|\boldsymbol{q}|$.

Hamiltonian 3.52 assumes spin–polarized particles. Its extension to particles which may have different spin is straightforward, since the Coulomb interaction conserves spin [108].

$$H=\sum_j \mathcal{W}a_j^\dagger a_j+\sum_{\substack{j_1,j_2\\ j_3,j_4\\ \sigma,\sigma'}}\mathcal{A}_{j_1,j_2,j_3,j_4}a^\dagger_{j_1\sigma}a^\dagger_{j_2\sigma'}a_{j_3\sigma'}a_{j_4\sigma}\,.\tag{3.56}$$

σ,σ' can take on two values: up and down. Creation operators $a^\dagger_{j\sigma}$ must be extended appropriately: they create a particle in state φ_j either with spin up or spin down.

Symmetries and choices of bases

Regarding the structure of the basis of my choice (Eq. 3.50) there are two Hamiltonian symmetries which are easy to use: conservation of total momentum along y (described by J, Eq. 3.48) and conservation of the z–component of the total spin (S_z).

'Easy to use' means here that the basis of the whole lowest Landau level in the form $|(j_1\sigma_1\ldots j_n\sigma_n)_k\rangle$ (Eq. 3.50 with spin) can simply be sorted into groups corresponding to particular values of J and S_z.

Sorting according to J splits the basis into m subspaces of approximately the same size $\approx\binom{m}{n}/m$. Utilisation of S_z brings a bit smaller profit, since the $S_z=0$ subspace is larger than the $S_z=n/2$ subspace by a factor of about $\binom{n}{n/2}\approx 2^{n-1}/\sqrt{2\pi n}$. Thus size of the largest group is not simply number of all states divided by the number of subspaces.

Other symmetries of the homogeneous Hamiltonian would correspond to conservation of the total spin S^2 and conservation of k^r_x (Subsect. 3.5.2). Eigenstates to these operators, however, are generally not of the simple 'product' form (Eq. 3.50), but they are linear combinations of such states. More importantly, these symmetries are gone if inhomogeneous systems are considered. Cleverly chosen inhomogeneities can however preserve the symmetries mentioned previously (see Subsect. 5.2).

If the aim is to choose n as high as possible, then the largest accessible systems have about ten electrons. At filling $\nu=\frac{1}{3}$ with J symmetry employed and $S_z=n/2$, the basis counts

1 001 603 elements[57] for $n = 10$. The largest bases I was able to handle contained 3×10^6 elements, extremely elaborate programs can handle bases up to sizes about an order of magnitude larger [68]. An alternative to the classical exact diagonalization is presented below.

3.5.5 Density matrix renormalization group

Exact diagonalization as it has just been presented, boasts of taking the complete basis of the lowest Landau level on a torus. As long as the low–energy states are considered, many of the basis states will be almost absent in the product–state expansion (Eq. 3.51): especially those which place many electrons close to each other and thus contribute with a large Coulomb energy. Leaving out such states from the basis will not affect the calculated ground state noticeably while it reduces the matrix sizes considerably.

Density matrix renormalization group (DMRG) is a systematic method to leave out irrelevant basis states. Roughly, its basic idea is to successively enlarge the considered system and for calculating the $(n+1)$–particle ground state to use only the most important n–particle states.

The idea was used originally for one–dimensional systems (see e.g. a nice review by Schollwöck [85]). Shibata and Yoshioka [86],[87],[88],[89],[105] noticed that the single-electron basis of the lowest Landau level *is* in principle one-dimensional (Eq. 3.42) and adapted this method as an extension of the exact diagonalization for studies of the lowest Landau level. They were thus able to study systems with up to about 20 particles at fillings close to $\nu = \frac{1}{3}$.

3.6 Quantum Hall Ferromagnets

Consider the following situation: $\nu = 1$ and vanishing Zeeman energy. What is the ground state? (see a nice review by Girvin [31])

In the absence of Zeeman splitting, the lowest Landau levels ($n = 0$) for spin up and for spin down have the same energy, thus (without interaction) there are $2eB/h$ states available with energy $\frac{1}{2}\hbar\omega$, which is the lowest energy an electron can have in the presence of a magnetic field B. Filling factor one means that only eB/h states (per unit area) are occupied. Hence there is a vast number of degenerate ground states without interaction.

One of these states has the form

$$\Psi_H = \Phi(z_1, \ldots, z_n)|\uparrow\uparrow \ldots \uparrow\rangle\,.$$

Antisymmetry of Ψ_H implies antisymmetry of Φ, or in other words Φ vanishes when (any) z_i approaches (any) z_j. Each particle is surrounded by a correlation hole (cf. Eq. 4.5).

[57] In the $J = 5$ subspace where the ground state is (cf. Eq. 3.49).

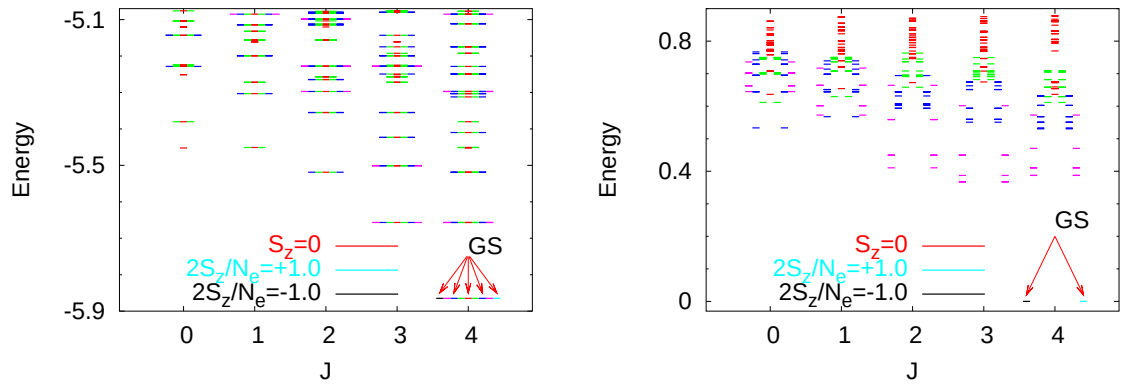

(a) $\nu = 1$ QHF, Heisenberg ferromagnet.

(b) $\nu = 2$ QHF, Ising ferromagnet. ($n = 0, \uparrow$ and $\nu = 1, \downarrow$ LL crossing; $n = 0, \downarrow$ full)

Figure 3.13: Spectra of two examples of quantum Hall ferromagnets (exact diagonalization). For Ising ferromagnet, only to the two crossing Landau levels are considered (the deep lying $n = 0, \downarrow$ level is fully occupied and treated as inert).

Therefore, in the presence of a sufficiently repulsive interaction, energy of this state will be lower than the energy of any state which does not have this property.

For Coulomb interaction, the energy cost of a single electron flip (which implies violation of Φ's antisymmetry) can be evaluated analytically: $E = (e^2/\varepsilon\ell_0)\sqrt{\pi/8}$. Quantitatively, this number is comparable to the cyclotron energy[58] $\hbar\omega$ and the fully polarized state thus becomes the ground state stabilized by the huge gain in exchange energy.

For Pauli principle to apply (Φ vanishes as $z_i \to z_j$), it is only important that all spins have the *same* direction, not that they are all up. Thus, the ground state is characterized by full spin polarization ($S = n/2$) and arbitrary S_z: all states $(S^-)^k\Psi_H$, $k = 0, 1, \ldots n$ are degenerate ground states.

It therefore turns out, that the $\nu = 1$ system in the absence of Zeeman splitting constitutes an example of a Heisenberg ferromagnet. An exact spectrum in a small system is shown in Fig. 3.13(a): in agreement with the argumentation above, the ground state has $S = n/2$ and it is well separated from excited states.

Other types of integer quantum Hall ferromagnets are possible, but they all share the common scheme: two degenerated Landau levels which provide $2eB/h$ 'free places' and only eB/h of them should be occupied. Depending on *which* Landau levels are degenerate, different types of ferromagnets can follow. A classification of possible cases was given by Jungwirth and MacDonald [46].

Let us introduce one more example, the $\nu = 2$ QHF which turns out to be an Ising type ferromagnet. By changing the ratio between Zeeman and cyclotron energy, $n = 0, \uparrow$ and

[58] In GaAs at magnetic fields in the range of few tesla.

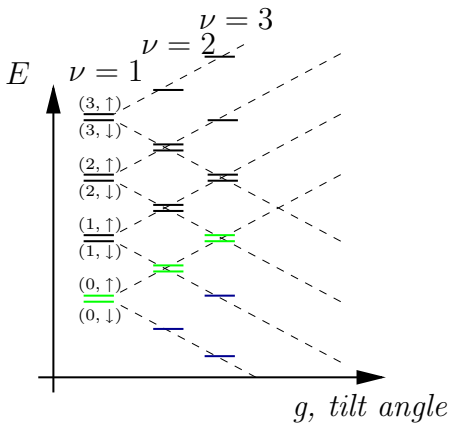

Figure 3.14: Integer quantum Hall ferromagnets occur when two crossing Landau levels should be only half–filled ($2eB/h$ free states, eB/h electrons to occupy them). Blue (black) levels indicate completely filled (empty) Landau levels, green levels are 'active'. Depending on which Landau level crossing is active, different types of ferromagnets occur: Heisenberg type for $\nu = 1$, Ising type for $\nu = 2, 3$ (the latter type was described in Ref. [47] for example).

$n = 1, \downarrow$ Landau levels can be brought to coincidence (Fig. 3.6). Experimentally, this can be accomplished either by changing the g–factor (it decreases with pressure [19]) or by tilting the magnetic field (cyclotron energy depends only on the component perpendicular to the 2DEG plane, Zeeman energy depends on the total field; the ratio between these two thus depends on the tilt angle) [22]. The low lying $n = 0, \downarrow$ Landau level is fully occupied (eB/h states) and can be taken as inert. The remaining eB/h states (giving in total $\nu = 2$) can be distributed among the $2eB/h$ available places of the *two* crossing Landau levels (Fig. 3.13(b)). Contrary to the $\nu = 1$ QHF, there are only two ground states now: either $n = 0, \uparrow$ is full or $n = 1, \downarrow$ is full (Fig. 3.6). To obtain this result we should use the exact diagonalization due to the large degeneracy present when interaction is switched off. However, the fact that putting some electrons to the $n = 0, \uparrow$ level and some to the $n = 1, \downarrow$ level costs extra energy, is probably a consequence of the fact that spin up orbitals are not the same as spin down orbitals [46] (they lie in different Landau levels).

A more detailed discussion of the spectra of a Heisenberg and an Ising QHF (Fig. 3.13) is given in Subsec. 4.3.3.

Quantum Hall ferromagnets which occur at integer filling factor have the advantage that they can often be well described by Hartree–Fock models, at least as far as ground state is considered. Even here, exact diagonalization studies can sometimes unveil unexpected ground states, as shown by Nomura [75] in bilayer systems (spin degree of freedom is substituted by pseudospin which refers to the two layers).

The principial question which is addressed in this thesis is, whether quantum Hall ferromagnetism can also occur at fractional filling factors. Experimentally, there are strong hints that the answer is yes [90], [27] (Sec. 2.3). It is then tempting to interpret these findings in terms of system with integer filling of composite fermions. It is a great challenge to confirm this hypothesis.

4 Structure of the incompressible states and of the half–polarized states

4.1 Basic characteristics of the incompressible ground states

Where to start with telling the story... An answer of universal validity to this question is: at the beginning [63]. Being interested in phenomena occurring at the transition between two incompressible ground states, the spin-polarized and the singlet one, it is reasonable to get acquainted with these two ground states first.

In the very illustrative model of non-interacting composite fermions (NICF; Sec. 3.4 and especially Subsect. 3.4.2), the ground state at electronic filling factor $\nu = \frac{2}{3} = 2/(2 \cdot 2 - 1)$ corresponds to two Landau levels (LLs) filled with CFs. If, in some particular situation, the CF cyclotron energy is smaller than the Zeeman splitting, these will be the $n = 0, \uparrow$, $n = 1, \uparrow$ CF Landau levels and the ground state will be fully spin polarized (Fig. 4.1). If the ratio between Zeeman and CF cyclotron energies is reversed, the ground state has $n = 0, \uparrow$, $n = 0, \downarrow$ CF Landau levels filled and is therefore a spin singlet[1]. Here, the CFs are electrons with two flux quanta attached *antiparallel* to the effective magnetic field B_{eff} [99] (Subsect. 3.4.2), which leads to a minus sign in the denominator of the CF filling factor formula 3.39.

A similar situation, i.e. occurrence of two incompressible ground states, the singlet and the polarized one, occurs also at filling factor $\nu = \frac{2}{5}$. Here, the ground state can be interpreted as two filled CF LLs where the two flux quanta were attached *parallel* to B_{eff}. Thus, these ground states should be completely equivalent to the ground states at $\nu = \frac{2}{3}$ within the NICF approximation.

Let us compare this picture (attempting to describe an infinite two-dimensional system) with 'exact results', i.e. with a finite system treated exactly. Looking at the exact spectra of a $\nu = \frac{2}{3}$ and a $\nu = \frac{2}{5}$ (finite) system (Fig. 4.2) we readily recognize ground states in the $S = 0$ and the $S = N/2$ sector which are well separated from excited states, as compared to the typical level separation within the excitation spectrum or in subspaces with other values of the total spin. Also, as the NICF model predicts, the spin singlet ground state

[1] Consider the action of the S^- (lowering operator for the z-component of spin) on the ground state: flipping a spin $\uparrow \rightarrow \downarrow$ must annihilate the state, because there is no room for an extra spin down in the lowest CF LL which is completely filled. Finally, $S^-|\Psi, S_z = 0\rangle = 0$ implies that $|\Psi, S_z = 0\rangle$ is a $S^2 = 0$ state.

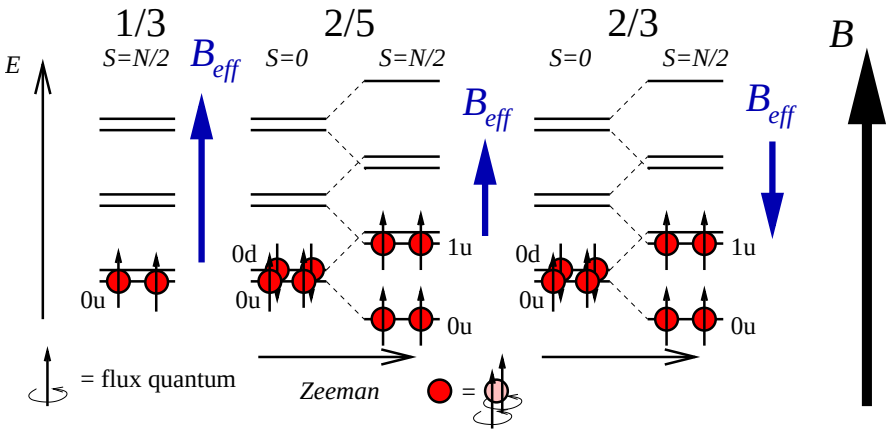

Figure 4.1: Systems at filling factors $\nu = \frac{1}{3}, \frac{2}{3}$ and $\frac{2}{5}$ correspond to $\nu_{CF} = 1, 2$ and 2 within the non-interacting CF picture. The composite fermions (CF) are electrons with two magnetic flux quanta attached parallel (for $\nu = \frac{1}{3}, \frac{2}{5}$) or antiparallel (for $\nu = \frac{2}{3}$) to the effective magnetic field B_{eff} (but always parallel to the real external field B). When Zeeman splitting is increased crossings between CF Landau levels occur and spin polarization of the ground state changes.

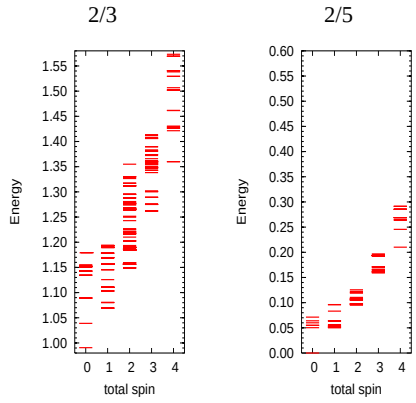

Figure 4.2: Energy levels of 8 particles on torus at filling factors $\frac{2}{3}$ and $\frac{2}{5}$ without Zeeman splitting. Obviously, up to an inessential shift, the short–range interaction used here (cf. section 3.3) produces quite similar spectra like the Coulomb interaction. Note the large excitation energies for the ground states at $S = 0$ and $S = 4$ (as compared to other inter-level separations): these produce the gaps needed for incompressibility of the ground states in the thermodynamical limit.

$(n = 0, \uparrow, n = 0, \downarrow)$ has a lower energy $E(S = 0)$ than the polarized one $(n = 0, \uparrow, n = 1, \uparrow)$, $E(S = N/2)$ if the Zeeman energy is set to zero. Both ground states have $k^r = (0, 0)$ which corresponds to $L = 0$ in a system with circular symmetry (Subsect. 3.5.2, 3.5.3). Angular momentum equal to zero is in turn a property inevitable in any state with only completely filled Landau levels. This is another *hint* that what we deal with here are states with completely filled CF Landau levels.

In the following, I will continue discussing properties of both incompressible states at $\nu = \frac{2}{3}$ and at $\nu = \frac{2}{5}$ obtained by exact diagonalization and I will occasionally mention links to composite fermion theories.

$$\Psi = \sum_i c_i \mathcal{A}|j_{i1}\rangle \otimes |j_{i2}\rangle \otimes |j_{i3}\rangle \otimes |j_{i4}\rangle =$$
$$= \begin{array}{rl} 0.423556 & |\cdots\bullet\bullet\cdots\cdots\bullet\bullet\cdot\rangle \\ -0.423556 & |\bullet\bullet\cdots\cdots\bullet\bullet\cdots\cdots\rangle \\ +0.335551 & |\cdots\bullet\cdots\bullet\cdots\bullet\cdots\bullet\rangle \\ -0.328373 & |\cdots\bullet\bullet\cdots\cdots\bullet\cdots\bullet\rangle + \ldots \end{array}$$

(a) Four–electron wavefunction as an expansion of Slater determinants (product states antisymmetrized by $\mathcal{A}$). In each of them, each $\bullet$ indicates an occupied state and position of $\bullet$ signifies $j = 1, 2, \ldots 12$ of this one–particle state.

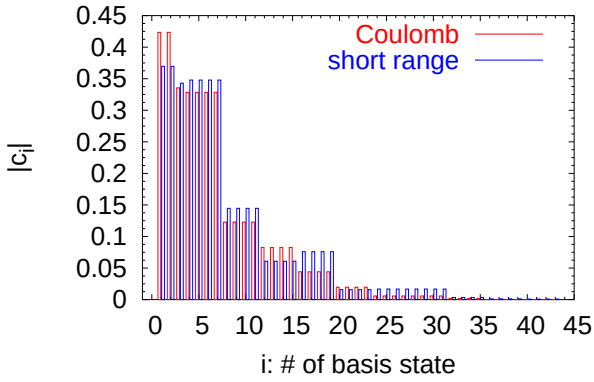

(b) Moduli of coefficients of all terms in the expansion (dimension of the four–electron basis is 43). For comparison, coefficients for a short–range interacting state, Subsect. 3.3.4, are also shown. Overlap between these two states is -0.9893.

Table 4.1: The ground state at $\nu = \frac{1}{3}$ is highly correlated, i.e. it is a superposition of many Slater determinants. Here it is demonstrated for a four electron state on a torus (with Coulomb interaction). In this case, there are 12 one–particle states available ($N_e/N_m = 4/12$) and they are centered around $X_j = a \cdot j/N_m$ in the x–direction in the basis chosen for our calculations (Eq. 3.40).

4.1.1 Densities and correlation functions

Having computed a many-particle wavefunction numerically usually does not automatically mean that we can say much about the nature of the state it describes. Very often, the only statement to be made is that the state is highly correlated, or entangled. By this we mean that the state cannot be written as a single Slater determinant [5], not even approximately, and thus its description goes far beyond any Hartree–Fock model. An illustrative example of this is the Laughlin state, Tab. 4.1 (note the comment [6]).

To learn more about the state it is apt to evaluate expectation values of observables such as density or density-density correlation functions. In the first quantization formalism these are the following operators

$$n(r) = \sum_i \delta(r - r_i) \tag{4.1}$$

$$g(r) = \frac{1}{N_e(N_e-1)} \sum_{i \neq j} \delta\big(r - (r_i - r_j)\big)\,, \tag{4.2}$$

summations running over all particles in the system. For inhomogeneous systems it is also

useful to consider an 'unaveraged' density-density correlation operator

$$g(\boldsymbol{r}'', \boldsymbol{r}') = \frac{1}{N_e(N_e-1)} \sum_{i \neq j} \delta(\boldsymbol{r}' - \boldsymbol{r}_i)\delta(\boldsymbol{r}'' - \boldsymbol{r}_j)\big) \,.$$

This is the probability (density) of finding a particle at place $\boldsymbol{r}'$ provided there is a particle at place $\boldsymbol{r}''$. The function $g(\boldsymbol{r})$ is just $g(\boldsymbol{r}+\boldsymbol{r}', \boldsymbol{r}')$ averaged over all $\boldsymbol{r}'$, hence $g(\boldsymbol{r}) \propto g(\boldsymbol{r}+\boldsymbol{r}', \boldsymbol{r}')$ for homogeneous systems, i.e. both quantities are the same up to a proportionality constant.

For not fully spin polarized states it is also useful to watch quantities $n_\uparrow(\boldsymbol{r})$, $g_{\uparrow\downarrow}(\boldsymbol{r})$, etc. defined by the operator

$$g_{\uparrow\downarrow}(\boldsymbol{r}) = \frac{1}{N_e(N_e-1)} \sum_{i \neq j} \delta_{\sigma_i\uparrow}\delta_{\sigma_j\downarrow}\delta\big(\boldsymbol{r} - (\boldsymbol{r}_i - \boldsymbol{r}_j)\big) \,. \tag{4.3}$$

and analogous relations[2].

The normalization of density and density–density correlation functions we chose in Eqs. 4.1,4.2,4.3 is the following:

$$\int \mathrm{d}\boldsymbol{r} n(\boldsymbol{r}) = N_e \,, \qquad \int \mathrm{d}\boldsymbol{r} g(\boldsymbol{r}) = 1 \,, \qquad \int \mathrm{d}\boldsymbol{r} g_{\sigma\sigma}(\boldsymbol{r}) = \frac{N_\sigma(N_\sigma-1)}{N_e(N_e-1)} \,,\ \sigma \in \{\uparrow, \downarrow\} \,, \tag{4.4}$$

where integrals are taken over the whole system (elementary cell).

As long as homogeneous systems are concerned we naturally expect density and also polarization to remain constant. For the incompressible states this is true only up to finite size effects: the density shows a slight modulation which decays rapidly as the system size is increased. Discussion of these effects which have no relevance for the real infinite 2D system will be presented later (see section 4.1.4).

In the following, by $g(r)$ we mean $g(\boldsymbol{r})$ with $r = |\boldsymbol{r}|$ for isotropic and homogeneous systems. Also, whenever we will speak about 'correlation functions' we mean (equal time) density–density correlation functions.

Fully occupied Landau levels

The density-density correlation function can be analytically evaluated for a state with $\nu = n$ fully occupied Landau levels [49] (for spin polarized electrons). This is the ground state of non-interacting electrons (at integer filling factor). In this case

$$g(r) = 1 - \frac{1}{n^2} \exp(-[(rk_F)^2/4n]) \left[L^1_{n-1}\left(\frac{(rk_F)^2}{4n}\right)\right]^2 \,, \tag{4.5}$$

[2]Quantities $g_{\uparrow\downarrow}(\boldsymbol{r})$ and $g_{\downarrow\uparrow}(\boldsymbol{r})$ obey $g_{\uparrow\downarrow}(\boldsymbol{r}) = g_{\downarrow\uparrow}(-\boldsymbol{r})$. For isotropic systems it thus makes no sense to distinguish these two quantities.

where $L_n^\alpha(x)$ are the associated Laguerre polynomials [7],[35]. In particular, for $n = 1$ and $n = 2$:

$$\begin{aligned} &\nu = 1 \ : \\ &\qquad g_{\nu=1}(r) = 1 - \exp(-r^2/2\ell_0^2) \qquad (4.6) \\ &\nu = 2 \ : \\ &\qquad g_{\nu=2}(r) = 1 - \exp(-r^2/4\ell_0^2) \cdot \frac{1}{4}[2 - r^2/4\ell_0^2]^2 \, . \end{aligned}$$

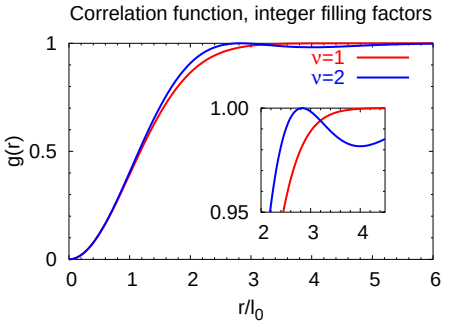

The Fermi wavevector k_F for a system subjected to a perpendicular magnetic field is defined as k_F in exactly the same system (i.e. the same areal density of electrons) just with magnetic field switched off. In this scheme

$$(k_F\ell_0)^2 = 2\nu \, , \ \text{or} \qquad k_F = \sqrt{2\nu}\ell_0^{-1} \, . \qquad (4.7)$$

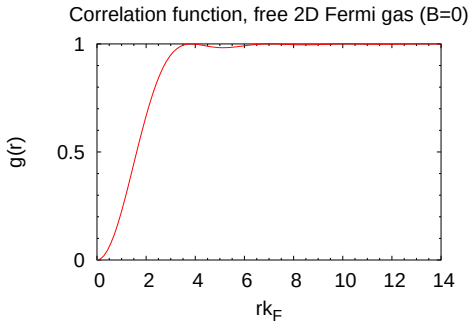

It is a pleasant news that by taking the limit $\nu = n \to \infty$ in Eq. 4.5 we obtain

$$g_{FS}(r) = 1 - \left[\frac{2}{k_F r} J_1(k_F r)\right]^2 \, , \qquad (4.8)$$

which is the correlation function of free electrons in two dimensions (Fermi sea). It should not be anything else because $\nu \to \infty$ with k_F kept constant means that B is decreased to zero at a given areal density of electrons.

Filling factor $\nu = \frac{1}{3}$

Provided Landau level mixing is absent and considering only the short-range interaction between particles (Sec. 3.3), the ground state at filling factor $\nu = \frac{1}{3}$ is described by the Laughlin wavefunction $\Psi_L(z_1, \ldots, z_n)$, Eq. 3.20. Up to my knowledge, no *closed* [8] analytical expression of the correlation function in this state is available. Only the short range behaviour can be determined analytically[3], $g(r) = cr^6 + o(r^6)$ for $r \to 0$.

Numerically, $\langle \Psi_L | g(r) | \Psi_L \rangle$ can be evaluated by various Monte Carlo techniques (see end of Sec. 3.2.2), Fig. 4.3. These results are closer to the thermodynamic limit — referring to larger numbers of particles — than $g(r)$ which can be obtained from exact diagonalization (Fig. 4.4) but this is only because we have an analytic WF of the GS in this case (Ψ_L). Exact diagonalization can be performed only for systems with $N_e \lesssim 10$ electrons, but it is not necessary to know anything about the ground state in advance apart of that it lies in the lowest Landau level. Therefore, exact diagonalization provides us a way to confirm that

[3]For $z_1 - z_2 \to 0$, $|\Psi_L|^2$ vanishes proportional to $(z_1^* - z_2^*)^3(z_1 - z_2)^3 = |z_1 - z_2|^6$.

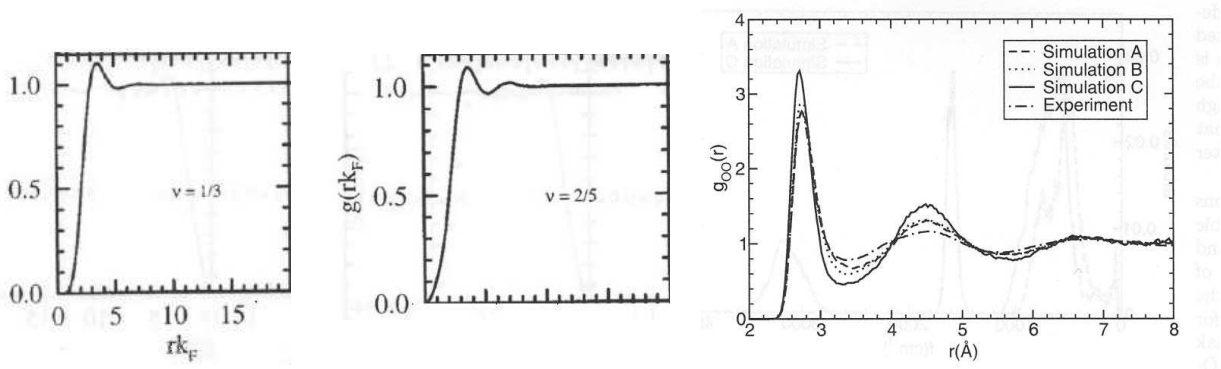

$\nu = \frac{1}{3}$ $\nu = \frac{2}{5}$ Water

Figure 4.3: *Left and middle:* Correlation functions of the ground states of 50-60 particles at filling factors $\frac{1}{3}$ and $\frac{2}{5}$ of the principal Jain's sequence, $\nu = p/(2p+1)$ (cf. Subsect. 3.4.2). The wavefunctions (WF) predicted by composite fermion theory were taken (for $\nu = 1/3$ this is identical with the Laughlin WF) and $g(r)$ was calculated by a Monte Carlo method. Taken from Ref. [49]. *Right:* correlation function between oxygen atoms in liquid water as an example of a density–density correlation function in a well–known liquid (see text on p. 75). Results of both numerical simulation and experiments are shown, see the original paper by Allesch *et al.* [12] for details.

Ψ_L is indeed the ground state or a good approximation to it, e.g. for Coulomb–interacting electrons. Note also that Figs. 4.4 refer to electrons on torus whereas Fig. 4.3 refers to the disc geometry (see Subsect. 3.5.3). The fact that correlation functions are very similar in both geometries (compare Fig. 4.4(b) and Fig. 4.3) supports the hypothesis that the corresponding states are universal and hence basically the same as the ground state in an infinite 2D system.

Several points should be mentioned here.

(i) The correlation function $g(r)$ in Fig. 4.4 is rather isotropic, at least on distances smaller than $a/2$. This distinguishes the Laughlin state from a Wigner crystal (Subsect. 4.4.1) or a unidirectional charge density wave (Subsect. 4.1.3) in which some special directions exist. This fact motivates also the 'incompressible *liquid*' terminology[4].

(ii) The first maximum in $g(r)$ occurs at $r_1 \approx 4.4\ell_0$ (Fig. 4.4(b)) and this separation can be taken as a typical interparticle distance in the Laughlin state[5]. After r_1,

[4]Liquids and gases differ in the strength of interparticle interaction. Whereas negligible in gases, the interaction in liquids is strong compared to kinetic energy. In the lowest Landau level, kinetic energy is zero (or constant, more precisely, Subsect. 3.2.1).

[5]It is an interesting fact that this distance lies close to the mean interparticle distance determined by the filling factor, $r_{mean}/\ell_0 = \sqrt{2\pi/\nu} \approx 4.35$ (cf. Eq. 3.6). This quite precise match between 'pure geometry' (r_{mean}) and a property of Ψ_L (r_1) probably considerably contributes to the exceptional stability of the Laughlin state.

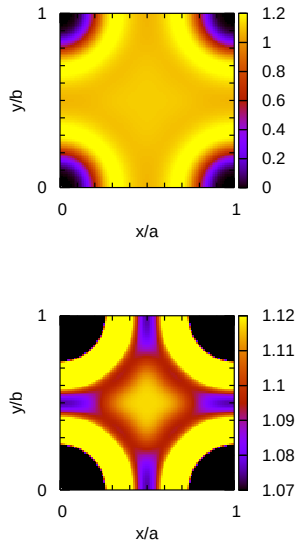

(a) $N_e = 10$. Due to the absence of circular symmetry on the torus, $g(\boldsymbol{r})$ is in general not only a function of $r = |\boldsymbol{r}|$. For $|\boldsymbol{r}| \ll a$, $g(\boldsymbol{r})$ is however quite isotropic (inset in Fig. 4.4(b)). The first electron is sitting at the corner (the four corners are identical owing to the periodicity). The lower plot differs from the upper one only by a finer z–scale which highlights the structures in $g(\boldsymbol{r})$ at larger distances.

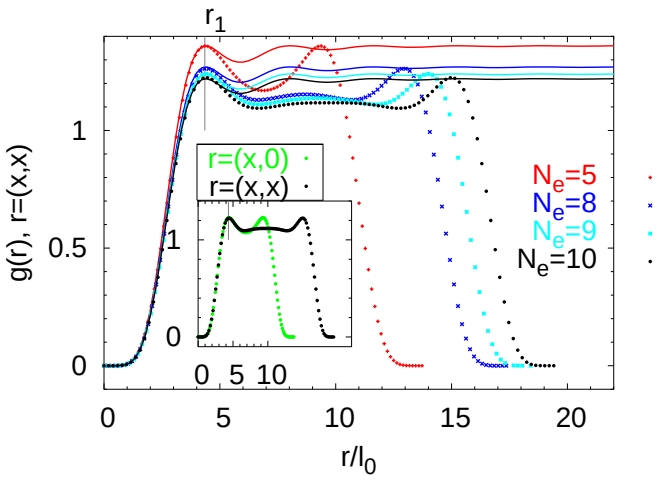

(b) Section of $g(\boldsymbol{r})$ for $N_e = 5, 8, 9, 10$–electron ground states along $\boldsymbol{r} = (x, x)$; the perfectness of match to $g(r)$ in Fig. 4.3 gives us a feeling how little the ground state is affected by the finiteness of the system. It is noteworthy that $g(r)$ can be astonishingly well fitted by the $[g_{FS}(r)]^3$ (Eq. 4.8) up to distances beyond the first maximum (up to vertical scaling, only k_F must be fitted, see the text). *Inset:* sections along diagonal and side of the square for the $N_e = 10$ system. $g(\boldsymbol{r})$ is isotropic well beyond the first maximum.

Figure 4.4: Correlation functions in the ground state of N_e electrons on a torus (square, length of sides $a = b$, with periodic boundary conditions) at filling factor $\nu = \frac{1}{3}$. The function $g(\boldsymbol{r})$ gives the probability of finding an electron at position $\boldsymbol{r} = (x, y)$ provided there is an electron sitting at $\boldsymbol{r}' = (0, 0)$. For a homogeneous system the choice of $\boldsymbol{r}'$ does not influence the probability distribution of finding the second electron.

oscillations in $g(r)$ decay rapidly. The overall form of $g(r)$ in the Laughlin state clearly differs from the correlation function of a free 2D Fermi gas (Eq. 4.8):

1. Laughlin state (Fig. 4.4(b)): the first peak of $g(r)$ is relatively high, measured for instance by ratio $g(r_1)/g(r \to \infty) \gtrsim 1.1$ [6]. 2D Fermi gas (Fig. next to Eq. 4.8): the first structure of $g(r)$ is about ten times weaker. Here, it is more appropriate to watch the depth of the first minimum, see the next point.
2. 2D Fermi gas: all maxima (at r^i_{FS}) of $g(r)$ have the same value, $g(r^i_{FS}) = 1$.

[6] In a finite system like in Fig. 4.4(b), we must substitute $r \to \infty$ by the largest distance possible. It is $r = a/\sqrt{2}$, that is about $10\ell_0$ in the $N_e = 10$ system.

Laughlin state: the first maximum $g(r_1) \approx 1.1$ (for $N_e \to \infty$) is much higher than other maxima.

3. 2D Fermi gas: $g(r) \propto r^2$ for $r \to 0$. This is purely the effect of Pauli exclusion principle; mathematically, it comes from the antisymmetry of the wavefunction (Ψ), in other words, Ψ is a Slater determinant. Laughlin state: $g(r) \propto r^6$. This is a manifestation of correlations in the state, i.e. of the fact that Ψ_L cannot be written as a single Slater determinant. $g(r) \propto r^6$ also means that any two electrons avoid being close to each other very efficiently and this helps to minimize the Coulomb energy which is high at short inter–particle distances ([39]; some details are also in Subsect. 3.3.4).

Just as an illustration, a correlation function $g(r)$ of liquid water is shown in Fig. 4.3, right. Of course, it is not possible to directly compare water and a 2D electron gas in the fractional quantum Hall regime. I hope though, the reader shares my impression that $g(r)$ of the Laughlin state (Fig. 4.3, left) is similar to $g(r)$ of *liquid* water (Fig. 4.3, right) rather than to $g(r)$ of a 2D Fermi *gas* (Eq. 4.8).

(iii) The Laughlin state (Fig. 4.4(b)) also differs from integer filling factor states apparently (Fig. next to Eq. 4.6). The latter ones ($i = 1, 2, \ldots$) namely have always $g_{\nu=i}(r) \propto r^2$ at $r \to 0$. Also $g_{\nu=i}(r)$ has exactly $i - 1$ maxima, i.e. $g_{\nu=1}(r)$ is free of maxima.

This demonstrates the fact, that in the $\nu_{CF} = 1$ composite fermion (CF) state, which is the model of the $\nu = \frac{1}{3}$ electronic ground state (Sect. 3.4), the *electron–electron* correlations are different to those in a $\nu = 1$ electronic state. This is a bit counterintuitive, since the CFs were created by adding two zeroes to electrons *in the* $\nu = 1$ *state* and we could have therefore expected that the electrons 'remained at their original positions' under this transformation. Figures 4.4(b) and (the one next to Eq.) 4.6 however show that even though the CF density equals the electronic one the electron–electron *correlations* are different in both states.

(iv) On 'intermediate length scales', the correlation function of the Laughlin state $g(r)$ in Fig. 4.4(b) can be strikingly well fitted by

$$c \cdot [g_{FS}(r)]^3 \,, \tag{4.9}$$

where $g_{FS}(r)$ is the correlation function of a free 2D Fermi gas, Eq. (4.8). Herefore, we put $k_F \approx 0.874\ell_0^{-1}$ which is only by about 7% more than what we would expect for filling factor $\nu = \frac{1}{3}$, Eq. (4.7).

The quality of the match relies on the choice of $m = 3$ for the exponent in Expr. 4.9 (for $r \to 0$) and on the fitting constants c and k_F (around $r \approx r_1$). The surprising fact is therefore only the good match *between* $r = 0$ and $r = r_1$. Also note that long–range ($r \gg r_1$) behaviours of Expr. 4.9 and $g(r)$ of the Laughlin state are different. This again emphasises the differences between the Laughlin state and the Fermi gas.

Expression 4.9 provides therefore only another representation of the exchange hole, parallel to approximate formulae given e.g. by Girvin [30].

In conclusion, we have seen that the correlation function of the correlated $\nu = \frac{1}{3}$ ground state (Fig. 4.3) has a strong first maximum (near to $4.4\ell_0$) and an unusual exchange hole $g(r) \propto r^6$. These features distinguish the $\frac{1}{3}$ state from both free 2D Fermi gas and completely filled Landau levels and indicate the *liquid–like* and *correlated* nature of the Laughlin state.

Filling factor $\nu = \frac{2}{3}$

Provided the Landau level mixing is absent, the particle–hole symmetry in one Landau level gives a direct relation (isomorphism) between Hilbert subspaces of fully polarized states at $\nu = \frac{2}{3} = 1 - \frac{1}{3}$ and $\nu = \frac{1}{3}$ (Subsect. 3.2.4). Owing to this relation eigenvectors of any radial two–particle interaction are exactly the same[7] in both spaces and corresponding eigenvalues are identical up to a constant shift (see section 3.2.4).

The correlation function in the *fully polarized* $\nu = \frac{2}{3}$ ground state (Fig. 4.5) is thus linked to the one of the Laughlin WF by an analytical formula (Eq. 3.26) . For a system with N_m flux quanta[8] it reads

$$\frac{2}{3}N_m(\frac{2}{3}N_m - 1)g_{\nu=\frac{2}{3}}(\boldsymbol{r}) = \frac{1}{3}N_m(\frac{1}{3}N_m - 1)g_{\frac{1}{3}}(\boldsymbol{r}) + \frac{1}{3}N_m^2 g_{\nu=1}(\boldsymbol{r})\,. \tag{4.10}$$

The $g(r) \propto r^6$ short range behaviour is thus obscured by the second term.

The *spin singlet* ground state at $\nu = \frac{2}{3}$ has a different character. Here, we can distinguish between correlation functions for electrons of like spin, $g_{\uparrow\uparrow}(\boldsymbol{r})$, and for electrons of opposite spin, $g_{\uparrow\downarrow}(\boldsymbol{r})$, Fig. 4.6. Neither of them bears any apparent resemblance to either the $\nu = \frac{2}{3}$ or $\nu = \frac{1}{3}$ polarized ground states. I should like to point out some of their particular features.

(i) The ring-like form of $g_{\uparrow\downarrow}(\boldsymbol{r})$ suggests that the state consists of pairs of particles with opposite spin with average separation $r_{\uparrow\downarrow} \approx 3.3\ell_0$.

(ii) There is a deep hole in $g_{\uparrow\downarrow}(r)$ around zero. This can*not* be due to Pauli exclusion principle which applies only to electrons of like spin, but rather solely due to Coulomb repulsion. As a check (not presented here), a further comparison between $g_{\uparrow\downarrow}(r)$ in Fig. 4.6 and the 'lowest LL Pauli hole' $g_{\nu=1}(r)$ (Eq. 4.6) shows that they have indeed

[7] In the following sense: Take an eigenvector for $\nu = \frac{1}{3}$. This is a linear combination of Slater determinants from the $\nu = \frac{1}{3}$ space. Replace each of them by its particle–hole counterpart and the resulting state from the $\nu = \frac{2}{3}$ space is an eigenstate.

[8] I.e. rectangular elementary cell of area $2\pi\ell_0^2 N_m$. Note that number of electrons in one system is equal to number of holes in the conjugated system. Therefore, in Eq. 4.10, $g_{\nu=1/3}$ and $g_{\nu=2/3}$ refer to systems with different numbers of electrons, $N_e = N_m/3$ and $N_e = 2N_m/3$, respectively. Recall $\nu = N_e/N_m$, Eq. 3.6.

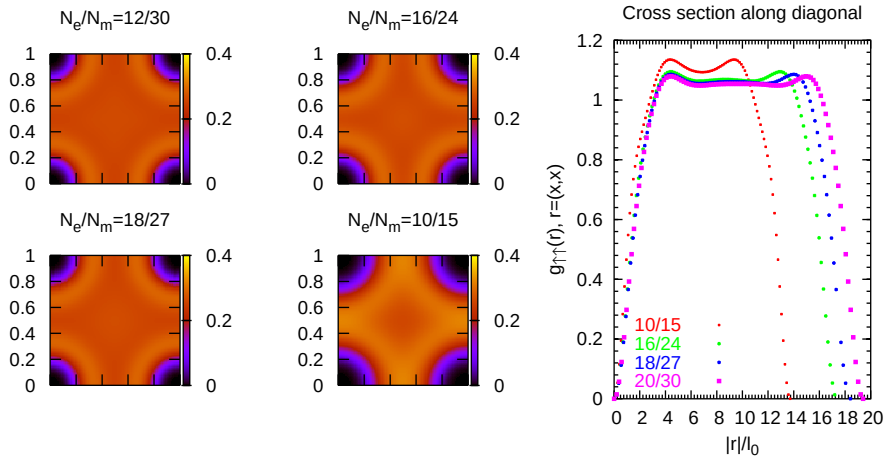

Figure 4.5: The $\nu = \frac{2}{3}$ polarized ground state: correlation functions in systems of different sizes.

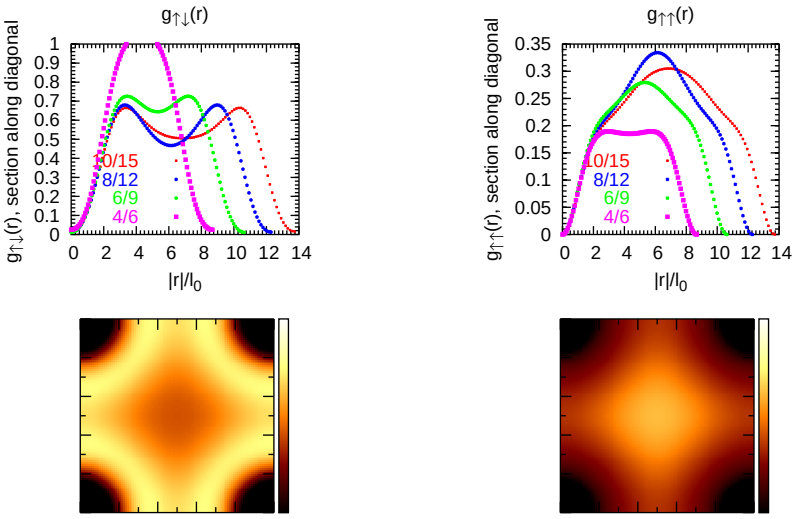

Figure 4.6: Correlation functions of electrons with like (right) and unlike spin (left) in the $\nu = \frac{2}{3}$ singlet GS. Systems of different sizes are compared. *Below:* $g_{\uparrow\downarrow}(\boldsymbol{r})$ and $g_{\uparrow\uparrow}(\boldsymbol{r})$ in the whole primitive cell (system with 10 particles). *Above:* section along diagonal.

different form. Also note that the value of $g_{\uparrow\downarrow}(0)$ is not exactly zero, it is several percent of the maximal value of $g_{\uparrow\downarrow}(r)$ (see also Subsect. 4.1.2).

(iii) There is a well pronounced shoulder in $g_{\uparrow\uparrow}(r)$ around $r \approx 2\ell_0$. It is very suggestive, how well this shoulder can be fitted by the correlation function of a full lowest LL (the 'lowest LL exchange hole'), Eq. 4.6. This is shown in Fig. 4.10(a).

This feature reminds of the relation between $\frac{1}{3}$ and $1 - \frac{1}{3}$ systems Eq. 4.10. This is also supported by the fact, that after the shoulder is subtracted, $\widetilde{g}(r)$ the remaining part of $g_{\uparrow\uparrow}(r)$ is $\propto r^6$ at short distances (Fig. 4.10(a)), just as it is the case in the $\frac{1}{3}$ Laughlin state. However, particle–hole conjugation between filling factors $\frac{1}{3}$ and $\frac{2}{3}$ is applicable only for spin–polarized states[9].

(iv) The sum of $g_{\uparrow\uparrow}(r)$ and $g_{\uparrow\downarrow}(r)$ properly scaled[10] for $N_e \to \infty$ lies very close to $g_{\nu=1}(r)$ with ℓ_0 substituted by $\ell_0\sqrt{2}$, Fig. 4.7. Therefore, if spin is disregarded, the singlet ground state at $\nu = \frac{2}{3}$ (created by magnetic field B) strongly resembles the state of a completely filled lowest LL (at magnetic field $B/2$).

Summary: the *polarized* ground state at $\nu = \frac{2}{3}$ is the particle–hole conjugate of the Laughlin state at $\nu = \frac{1}{3}$. The electronic correlation function of the $\frac{2}{3}$ state reproduces the 'liquid–like' maximum at $r_1 \approx 4.4\ell_0$ but the $\nu = \frac{1}{3}$ broad exchange hole with $g(r) \propto r^6$ is hidden behind the 'lowest LL exchange hole', $g_{\nu=1}(r)$.

The *singlet* GS seems to consist of pairs of spin up and spin down electrons with characteristic size of $3.3\ell_0$. Together with the 'sum rule', point (iv) above, this could be interpreted as that N_e electrons in the singlet GS form $N_e/2$ pairs, each with total $S_z = 0$ and these pairs form the same state as $N_e/2$ fermions at $\nu = 1$ (in the ground state).

In particular, I would like to stress that the singlet state can*not* be described as a mixture of two mutually uncorrelated $\nu = \frac{1}{3}$ Laughlin liquids, one with spin up, another with spin down, as we could wrongly infer from the picture of non–interacting composite fermions, see comment [9].

Filling factor $\nu = \frac{2}{5}$

This filling factor should be the counterpart to $\nu = \frac{2}{3}$ within the CF picture. The two magnetic fluxes are attached parallel rather than antiparallel to the effective magnetic field and in both cases the CF filling is two (Sect. 3.4). In spite of this relation the density–density correlations between electrons show significant differences.

The correlation hole of the *polarized* ground state (Fig. 4.8 or Fig. 4.3, middle) is much broader for $\nu = \frac{2}{5}$. The first maximum occurs in both systems ($\frac{2}{5}$ and $\frac{2}{3}$) at about the same distance $\approx 4.1\ell_0$, it is however much better pronounced in the $\frac{2}{5}$ system and also more

[9] For electrons with spin, states at ν and $2 - \nu$ can be particle–hole conjugates.

[10] $g_{\uparrow\uparrow}(r)$ and $g_{\uparrow\downarrow}(r)$ should have the same norm, e.g. equal to one, in sense of Eq. 4.4. With the current notation (Eq. 4.3) this is true only for $N_e \to \infty$.

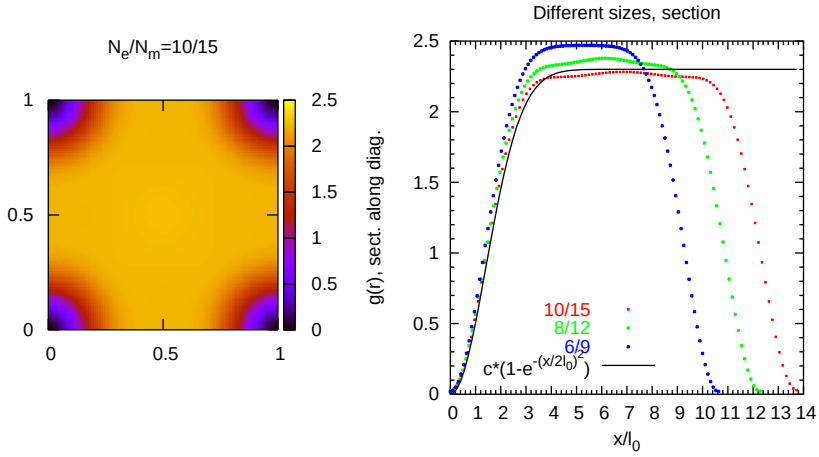

Figure 4.7: Different density-density correlation functions in the $\nu = \frac{2}{3}$ singlet state seem to be related to each other: $g_{\uparrow\downarrow}(r) + g_{\uparrow\uparrow}(r)$ (properly normalized, see text) is very similar to the function $1 - \exp(-r^2/4\ell_0^2)$, the density-density correlation in a full Landau level with $\ell_0\sqrt{2}$ in the place of ℓ_0.

structure is present beyond the first maximum here. Around $r = 0$ both systems follow $g(r) \propto r^2$; however, whereas $g(r)$ for $\nu = \frac{2}{3}$ is obviously dominated by the 'exchange hole', i.e. $g_{\nu=1}(r)$ (cf. Eq. 4.10), the $\frac{2}{5}$ state has a much broader minimum around $r = 0$.

These findings are not unexpected: consider two systems of the same area $2\pi\ell_0 N_m$, one at fillings $\frac{2}{3}$ and $\frac{2}{5}$, respectively. The latter will be more diluted ('emptier'), since it contains only $\frac{2}{5}N_m$ electrons, compared to $\frac{2}{3}N_m$ in the $\nu = \frac{2}{3}$ system (Eq. 3.6). Therefore, the correlation hole in $g(r)$ can be broader in the $\frac{2}{5}$ system. Rather, it is a warning that many claims which are true for electronic Landau levels are no longer true for composite fermion Landau levels.

There is also a close relation between the polarized $\frac{2}{5}$ GS and the Laughlin $\frac{1}{3}$ state according to the CF picture: the latter one corresponds to filling factor one, the former one to filling factor two of composite fermions. Comparing these two states, we find a bit stronger structures in the density–density correlation of the $\nu = \frac{2}{5}$ GS and also the first maximum shifts to smaller distances ($4.4\ell_0$ at $\nu = \frac{1}{3}$ and $4.1\ell_0$ at $\nu = \frac{2}{5}$). Both effects are quite similar to what happens when going from $\nu = 1$ to $\nu = 2$, cf. Figure next to Eq. 4.6. Comparing the $\nu = 2$ and $\frac{2}{5}$ systems, we again (cf. $\nu = 1$ and $\frac{1}{3}$) find much stronger structures of $g(r)$ in the latter case, just as we expect for a liquid state.

Some marked differences occur also in the *singlet ground states* at both filling factors. At $\frac{2}{5}$, correlation functions $g_{\uparrow\uparrow}(r)$ as well as $g_{\uparrow\downarrow}(r)$ seem to be quite flat beyond $r_m \approx 6\ell_0$. It

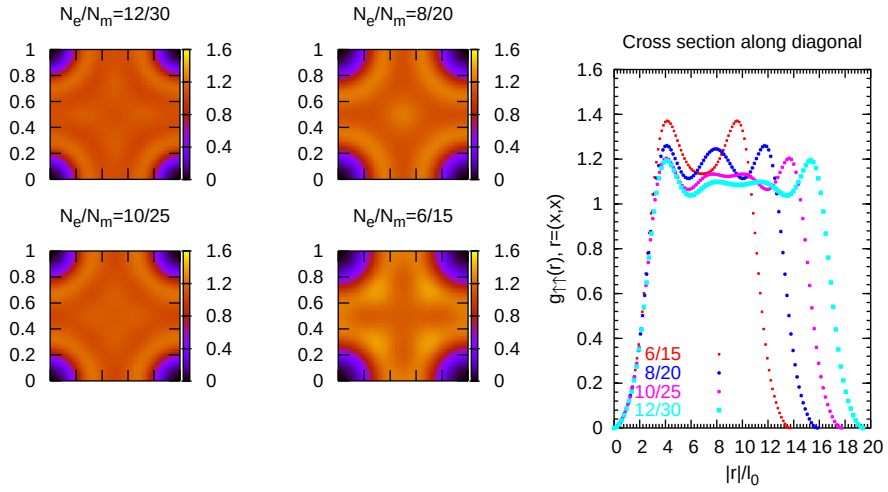

Figure 4.8: The $\nu = \frac{2}{5}$ polarized ground state, correlation functions. Note the good match between states in systems of different sizes.

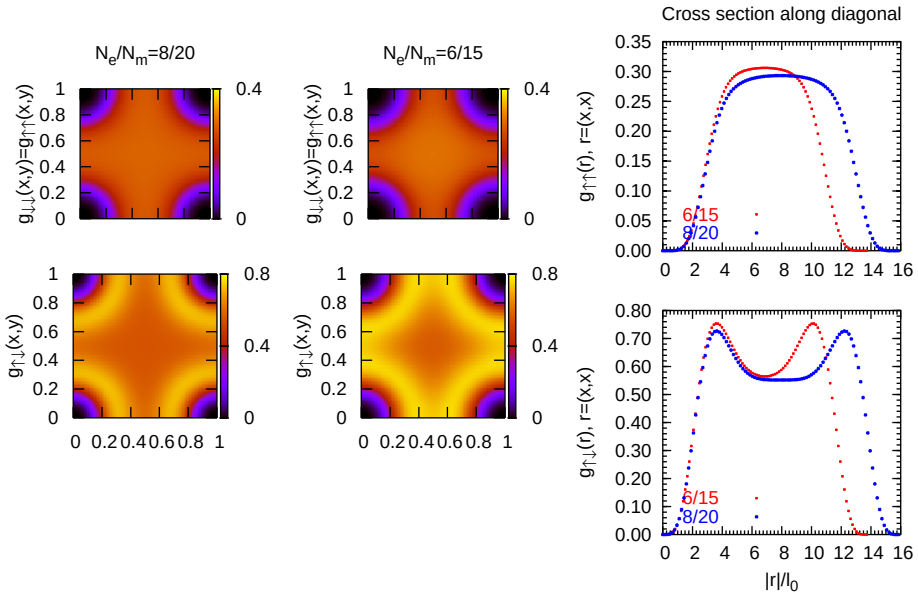

Figure 4.9: The $\nu = \frac{2}{5}$ singlet ground state, correlation functions.

may well be that the same is true for the filling $\frac{2}{3}$ (Fig. 4.9; the shoulder in $g_{\uparrow\uparrow}$ would probably have to be subtracted first), but then the plateau would occur first beyond some larger r_m and exact diagonalization is not applicable to confirm this with systems large enough.

It is remarkable that after subtracting the shoulder from $g_{\uparrow\uparrow}(r)$ of the $\frac{2}{3}$ singlet state (point (iii) in the discussion of $\frac{2}{3}$), the rest $\widetilde{g}(r)$ is $\propto r^6$ near to $r = 0$. This is the same behaviour as we find in $g_{\uparrow\uparrow}(r)$ of the $\frac{2}{5}$ singlet state, see Fig. 4.10.

Correlations of unlike spins exhibit one clear maximum which is, as compared to $\frac{2}{3}$, slightly but perceptibly shifted to a bit larger $r_{\uparrow\downarrow} \approx 3.7\ell_0$. This agrees with the above argument that $\frac{2}{5}$ systems are more diluted than the $\frac{2}{3}$ ones, but quantitatively this shift is too small. It is only $\approx 30\%$ of what we would naively expect from comparing the areal electron densities.

Finally, the $r \to 0$ behaviour of the $\frac{2}{5}$ singlet state, $g_{\uparrow\downarrow}(r) \propto r^4$ and $g_{\uparrow\uparrow}(r) \propto r^6$, matches the behaviour of the $\{3, 3, 2\}$–Halperin wavefunction (Eq. 3.29) and this $\Phi_{332}[z]$ is in turn identical[11] with the ground state wavefunction proposed by Jain's theory (Subsect. 3.4.2).

Summary: From the viewpoint of composite fermion theories, the *polarized* $\frac{2}{5}$ state ($p = 2$; see Tab. 3.2) is related both to the $\frac{1}{3}$ Laughlin state ($p = 1$) and $\frac{2}{3}$ polarized ground state ($p = -2$). The electron–electron correlations in exactly diagonalized systems clearly support the former relation, the latter one ($\frac{2}{5}$ with $\frac{2}{3}$) is however far from being obvious in this way.

Neither is the analogy between $\frac{2}{5}$ and $\frac{2}{3}$ apparent for the *singlet* ground state. Although similarities exist (pairing between electrons of unlike spin), short range behaviour of correlation functions is very different.

4.1.2 Ground state for Coulomb interaction and for a short–range interaction

Short–range interactions as they were introduced in Section 3.3 have a special significance for the FQHE. It has been repeatedly emphasised that the Laughlin WF is on one hand an *extremely good* approximation of the ground state of a Coulomb–interacting (CI) system while on the other hand, it is the *exact* ground state of electrons feeling only a short–range mutual interaction (SRI) as it was defined in section 3.3. Consequently, it is very popular to say that 'a short–range interaction Hamiltonian captures the essential physics of the FQHE by inducing the correct correlations[12] in the ground state'.

The SRI was used in most of the calculations presented in this work. This choice has been made for two reasons: it brings better chances in finding analytical results (like the

[11] This is because $\Phi_{nn'm}[z]$ lies completely in the lowest LL and thus the last step of Jain's procedure, namely the projection to the LLL, is out of effect. Seen from the opposite direction: the singlet $\frac{2}{5}$ state corresponds to filling only the lowest CF LLs (spin up and spin down).

[12] By correct correlations we mean the $\Psi \propto (z_i - z_j)^3$ behaviour of the GS wavefunction at $\nu = \frac{1}{3}$ when particles i and j come close together. For more general remarks on SRI and CI, see section 3.3.

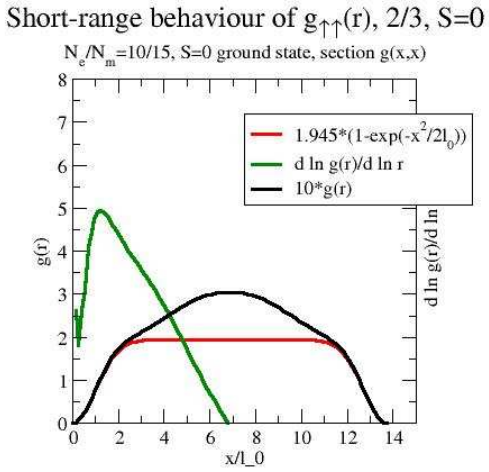

(a) Filling factor $\frac{2}{3}$. The shoulder at $r \approx 2\ell_0$ is apparently caused by a term proportional to $1 - \exp(-r^2/2\ell_0^2)$, i.e. $g_{\nu=1}(r)$, Eq. 4.6, which contributes to the total $g_{\uparrow\uparrow}(r)$. After this term was subtracted, a local power analysis of $g_{\uparrow\uparrow}(r)$ has been performed (green line).

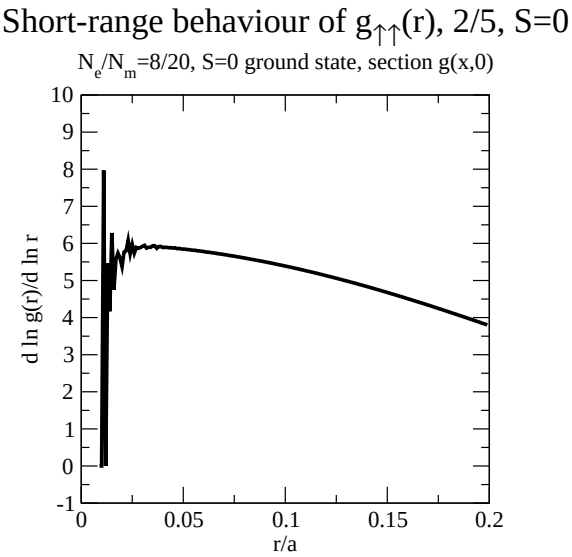

(b) Filling factor $\frac{2}{5}$. Local power analysis near to $r = 0$. Noise at very small distances is purely due to numerical inaccuracies: values of $g(r)$ are already very small there.

Figure 4.10: Correlation of like spins, $g_{\uparrow\uparrow}(r)$, of the singlet ground states at filling factors $\frac{2}{3}$ and $\frac{2}{5}$. Local power analysis (Eq. 4.11) shows, that both correlation functions are $\propto r^6$ for $r \to 0$; however, the shoulder in the state at filling factor $\frac{2}{3}$ has to be subtracted first.

Laughlin WF). Moreover we may hope that the results in finite systems converge faster to the thermodynamical limit ($N \to \infty$) because the electrons 'see' only as far as their interaction reaches and thus — sooner than for a long–range interaction — they will not 'realize' anymore that they live on a torus and not in an infinite plane. Aim of the following section is to show and discuss how the ground states at $\nu = \frac{2}{3}$ change if the character of the interaction changes.

The ground state energies for CI and SRI are naturally quite different. This is however for the largest part only an unessential shift; a part of it is the missing 'Madelung' constant, Eq. 3.53: under SRI an electron of course cannot interact with its own image in the neighbouring primitive cell[13]. More importantly, the gap energies are quite similar in both

[13]This fact is not completely trivial but still quite intuitive. We will not discuss it here and put it rather as an assumption that the distance between an electron and its image due to periodic boundary condition

cases (see also discussion in Subsect. 5.3.1).

Since the density of the incompressible ground states should always be constant (up to finite size effects to be discussed later) let us now focus on correlation functions. The three plots in Fig. 4.12 show $g_{\uparrow\uparrow}(r)$ and $g_{\uparrow\downarrow}(r)$ of the singlet state and $g(r)$ of the polarized state; in all three cases, the correlation functions of the CI state and the SRI state are quite similar. Most apparent differences appear at large distances; on a torus, the largest possible separation between two electrons is $r = a/\sqrt{2}$. On the other hand, the correlation functions are very precisely identical for small r. This shows that, e.g. in the polarized GS, the wavefunction contains the factor[14] $(z_i - z_j)^3$ for CI as well as for SRI. In other words, the Laughlin state (as the GS for SRI) describes *exactly* the short–range behaviour of an incompressible state of even long–range interacting electrons. Fig. 4.12 demonstrates that this is true (at least in a very good approximation) also for other ground states where the analytical wavefunction is not available (e.g. the singlet GS).

In fact, for the singlet GS there is a tiny but perceptible difference in $g_{\uparrow\downarrow}(0)$ for the two types of interaction. Since $g_{\uparrow\downarrow}(0)$ is almost zero, this observation suggests that a yet modified interaction might lead to analytical results: $\{V_0, V_1, \ldots\} = \{\infty, \alpha, 0, 0, \ldots\}$ in terms of pseudopotentials (Sect. 3.3). Such an interaction enforces $g_{\uparrow\downarrow}(0) = 0$, which is anyway almost fulfilled for the current SRI, and on the other hand it retains the pleasant property of SRI in polarized systems, i.e. it is one–parametric.

There is yet another significant difference between SRI and CI which is not obvious in Fig. 4.12 at first glance. The difference concerns the placement of zeroes in the wavefunction and we will concentrate on the $\nu = \frac{1}{3}$ ground state now (see Sec. 3.3).

In a general fermionic state, there must always be a zero bound to each electron in order to fulfil the Pauli exclusion principle: two electrons (of the same spin) cannot be at the same point in space simultaneously, *ergo* if $z_1 = z_i$ then the wavefunction must vanish. Factors $(z_i - z_j)^3$ in the Laughlin state mean that there are two extra zeroes exactly at the position of each electron. That is why[15] $g(r) \propto r^6$ for small r's (see Fig. 4.11, right; procedure to obtain this graph is explained at Eq. 4.11). For CI, the Laughlin WF is only an *approximation* to the ground state. In the real ground state, the one 'obligatory' zero is still sitting on each electron and the two others are only near rather than exactly on the top of the electron; in Fig. 4.11 left we can even see how far they are on average (these two extra zeroes are now mobile and their position depends on the position of all other electrons, see section 3.2.3). Note that this 'distance' depends on the system size [69].

(a or b) is much bigger than the interaction range.

[14] This is true for $\nu = \frac{1}{3}$ Laughlin state. But the polarized GS at $\nu = \frac{2}{3}$ is particle–hole conjugated to it and the g's of both states must be equal up to a trivial function, see sec. 3.2.4.

[15] Recall that $g(r) \propto \langle\Psi|\delta(z_1 - z_2 - z)|\Psi\rangle$ and '$r = |z| = |z_1 - z_2|$'. That is if $\Psi \propto r^3$, then $g(r) \propto r^6$.

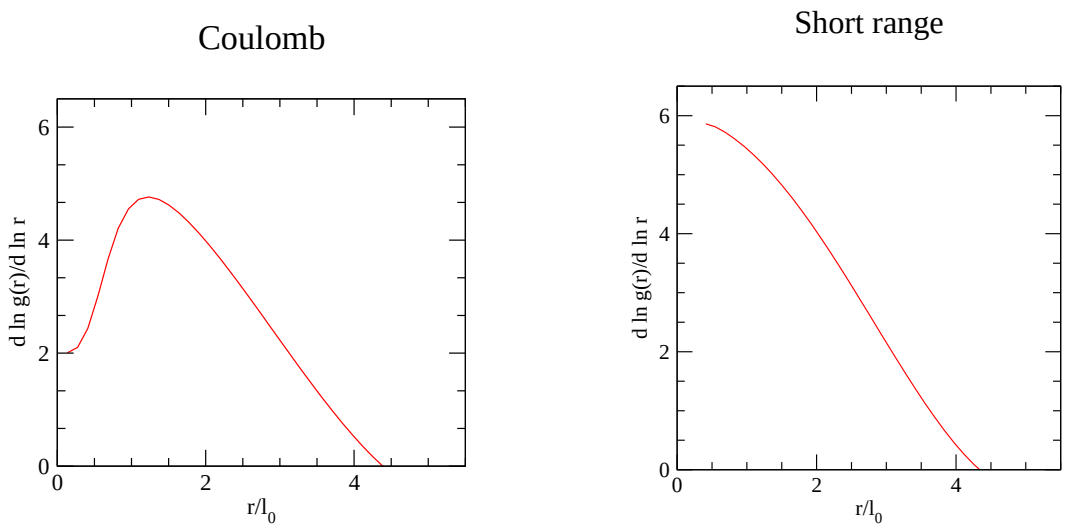

Figure 4.11: The incompressible ground state at $\nu = \frac{1}{3}$ (with ten electrons), Coulomb interaction (left) and a short–range interaction (right). Section through the density–density correlation function $g(\boldsymbol{r})$ along $\boldsymbol{r} = (x, x)$ is taken and the 'local degree' of the polynomial behaviour is determined (see the text). Whereas for SRI the local behaviour around $r = 0$ is obviously $g(r) \propto r^6$, indicating that there is exactly a **triple** ($6 = 2 \cdot \mathbf{3}$) zero of the wavefunction on on each electron, we can clearly see only **one** zero at each electron's position for Coulomb interaction, $g(r) \propto r^2$ and $2 = 2 \cdot \mathbf{1}$. However, going away from zero the 'local degree' grows (and goes tendentially up to six) showing that there are two other zeros near each electron; the position of the maximum gives an approximate size of the 'electron plus two zeroes complex'.

Local power analysis

A comment is due on the way how the plots in Figs. 4.11,4.10 were obtained. It is basically a section of $g(\boldsymbol{r})$ along one straight line[16] (going through $\boldsymbol{r} = 0$); this function was then transformed by

$$g(r) \;\longrightarrow\; \frac{\mathrm{d}\ln g(r)}{\mathrm{d}\ln r} \tag{4.11}$$

which gives a 'local degree of the polynomial behaviour'. Let me explain this: if $g(r)$ were αr^n then obviously $\mathrm{d}\ln g(r)/\mathrm{d}\ln r = n$; if $g(r) \propto (r - r_0)^n$ then $\mathrm{d}\ln g(r)/\mathrm{d}\ln r = nr/(r - r_0) \to n$ for $r \gg r_0$. In other words, if there is a dominant r^n term in $g(r)$, the quantity plotted in Fig. 4.4(b) gives the exponent. Of course, it is only approximate except for the case $g(r) = \alpha r^n$ but it is quite easy to evaluate and moreover it gives a global property of the wavefunction as compared to fixing electron positions $z_2, \ldots, z_n$ and examining the WF as a function of z_1 (where results depend on where we fix the electrons $z_2, \ldots, z_n$).

[16] Its orientation is not essential, for small r the states are quite isotropic even on torus, see section 4.4(b).

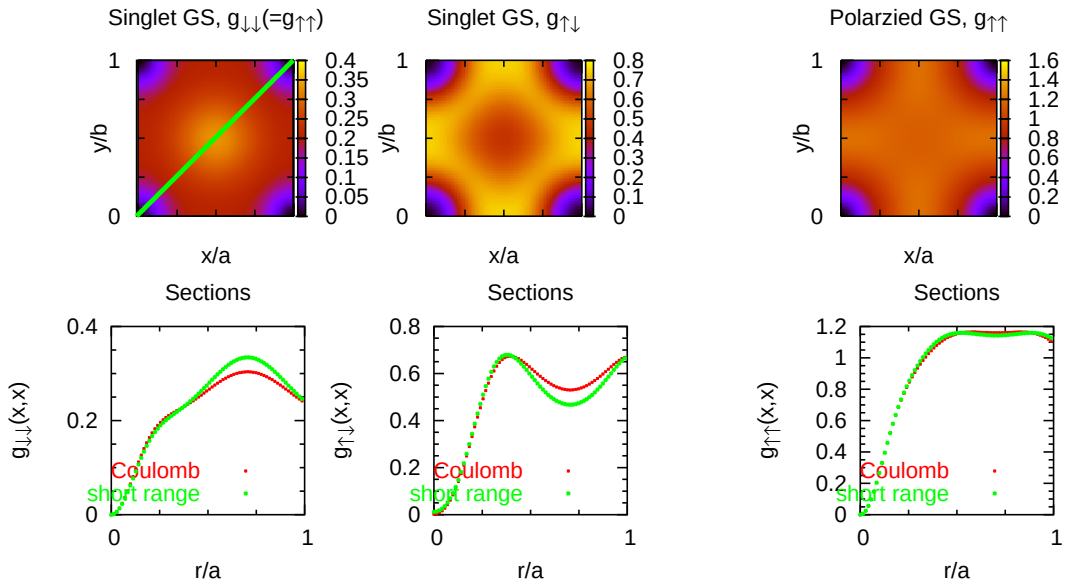

Figure 4.12: Correlation functions of the singlet and polarized ground states at $\nu = \frac{2}{3}$: comparison between the Coulomb and short–range interaction. The curves are identical for small r and slight deviations occur at longer scales. This is another way to demonstrate that it is sufficient to consider short–range interaction in order to get (almost) correct ground states under FQHE conditions.

4.1.3 Some excited states

There is a rich variety of excitations to the incompressible FQH states: for instance quasi-holes, excitons (quasihole–quasielectron pairs), charge density waves (CDW) or spin density waves (SDW), all of them can be described analytically (at least to some extent), and then of course all the rest of excitations which has not been understood up to now. Following the introduction given in Subsect. 3.2.5, we will now see how to identify some of these excitations in spectra obtained by exact diagonalization.

Charge density waves

Polarized ground state

CDWs can be excited for example in the liquid GS at $\nu = \frac{1}{3}$. Disregarding the possibility of spin flips (as it may be reasonable when Zeeman energy is too high), it turns out that these are the lowest excitations.

In Fig. 4.13 spectra of several short–range–interacting $\nu = \frac{1}{3}$ systems (tori of different sizes) are presented. The horizontal axis is modulus of $\boldsymbol{k}^r$, i.e. the 'crystallographic k–vector'

described in Subsec. 3.5.2. The Laughlin state has $\boldsymbol{k}^r = 0$ and a CDW of wavevector $\boldsymbol{Q}$ excited from this state has $\boldsymbol{k}^r = \boldsymbol{Q}$; beware however, that not every state which has $\boldsymbol{k}^r \neq 0$ must be a charge density wave! Apart from other possible periodic excitations, there are also basically nonperiodic excitations (e.g. quasiholes) and such states are forced into periodicity only 'artificially' by the periodic boundary conditions imposed in our exact diagonalization model.

The lowest excitations in Fig. 4.13 form a well developed branch $E(\boldsymbol{k}^r)$, which is usually called *magnetoroton branch*, and other excited states form a quasicontinuum. As mentioned in Subsect. 3.2.5, the dispersion of the magnetoroton branch can be calculated analytically in the single mode approximation. The original calculation by Girvin *et al.* [32] for *Coulomb* interacting systems at $\nu = \frac{1}{3}$ showed a well pronounced minimum in $E(|\boldsymbol{k}^r|)$ of the magnetoroton branch at $\boldsymbol{k}^r\ell_0 \approx 1.4$. In a short–range interacting system, shown in Fig. 4.13, the situation is slightly different: having reached its minimum value, $E(|\boldsymbol{k}^r|)$ remains constant beyond $\boldsymbol{k}^r\ell_0 \approx 1.4$.

A point worth of emphasis is that the magnetoroton branch in Fig. 4.13 contains points (energies) from exactly diagonalized systems of *different* sizes. This confirms our hope that these states are not bound to some particular geometry of the elementary cell and that they appear also in an infinite system.

Dealing with finite systems, we will always have only a finite, and usually quite small, number of allowed values for $\boldsymbol{k}^r$ (Eq. 3.46). On the other hand, the more points in $\boldsymbol{k}^r$–space we can access, the better we can recognise modes in exact diagonalization spectra, just like the magnetoroton branch in Fig. 4.13. Note also the large space between $\boldsymbol{k}^r = 0$ and the next smallest $|\boldsymbol{k}^r| \approx 0.5\ell_0^{-1}$ in Fig. 4.13 which corresponds to the longest wavelength compatible with the periodic boundary conditions.

The traditional way to improve these limits (few $\boldsymbol{k}^r$–points, too large smallest $|\boldsymbol{k}^r| > 0$) is to study larger systems. This is however prohibitively difficult with exact diagonalization. An alternative approach may be to study systems with aspect ratios $\lambda = a : b$ slightly deviating from one. This allows us to deform the lattice of allowed $\boldsymbol{k}^r$–points continuously (Eq. 3.46 contains λ), and on the other hand, we can expect that the states will not suffer from the *slight* asymmetry in $a : b$ in line with the argument that these states are not bound to any particular geometry of the elementary cell. This method is demonstrated in Fig. 4.13 by the blue points. There, I varied the aspect ratio from one up to 1.3. Since the energies of the CDW states still lie well on the magnetoroton branch, we can conclude that this aspect ratio variation is still only a small perturbation, i.e. acceptable for studying this branch.

Correlation functions of several states in the magnetoroton branch (Fig. 4.13) are shown in Fig. 4.14. The first look at $g(\boldsymbol{r})$ (upper row in Fig. 4.14) may be sometimes not enough to distinguish their charge density wave nature: the CDW is superimposed on the structure of the 'mother' Laughlin state, which these states are an excitation of. The periodic structure of $g(\boldsymbol{r})$ is thus more clear if we subtract the corresponding correlation function of the Laughlin state first (Fig. 4.14, lower row): we recognise three periods in y direction in the state A or 4 periods in y and one period in x in the state C, in agreement

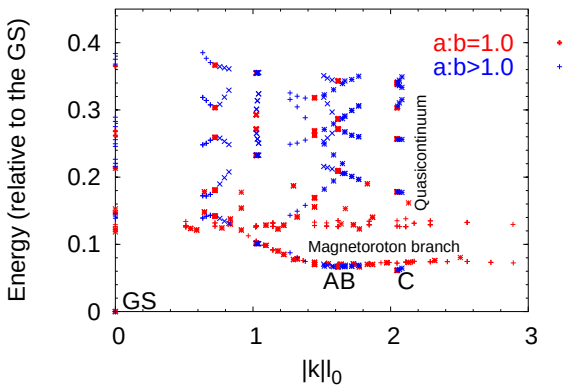

Figure 4.13: The ground state (at $k = 0$) and low excitations in SRI fully polarized $\nu = \frac{1}{3}$ systems of different sizes (4–10 electrons). Energy plotted against the $|\boldsymbol{k}^r|$, see Sec. 3.5.2. To be able to study more points in k space, systems of different sizes are compared and also systems with aspect ratios slightly varying from one, see text. Note the well pronounced magnetoroton branch. Note that energies calculated in systems of *different* sizes lie on the *same* branch indicating that these states are not much system–size–dependent (and therefore relevant even in infinite systems). The correlation functions for three states lying on this branch (A,B,C) are depicted in Fig. 4.14.

with the value of $\widetilde{k}^r/k_0 = \widetilde{k}^r/(N_m\pi/6)$ of these states. Note, that it is harder to distinguish the periodic structure in the $\widetilde{k}^r = (0, \pi)$ state (B), which may be partly because this is a point of high symmetry in the $\widetilde{k}^r$–space (Fig. 3.12).

In conclusion, we have shown how (the best known type of) charge density wave states on a torus can be identified in the exact diagonalization spectra and in correlation functions. Generally, we can expect that charge density waves excited from incompressible liquid states will form branches in $E(|\boldsymbol{k}^r|)$, provided of course that their energy is not hidden in a quasicontinuum of other excited states. Correlation functions show indeed the expected periodicity of a CDW superimposed on the structure of the ground state.

4.1.4 Finite size effects

It was the ultimate goal of this work to elucidate phenomena occuring in infinite 2D systems. Being tied to finite systems during numerical calculations we ought to distinguish which effects in the results have been introduced only by the finiteness of the system and which effects are proper to electrons in strong magnetic field regardless of the periodic boundary conditions. This problem is quite delicate and we may hope to learn a lot from observing how properties of e.g. the ground state (GS) change when the size of the system is increased.

Let us start with the perfect example, a $\nu = \frac{1}{3}$ system with its exact GS written as Ψ_L,

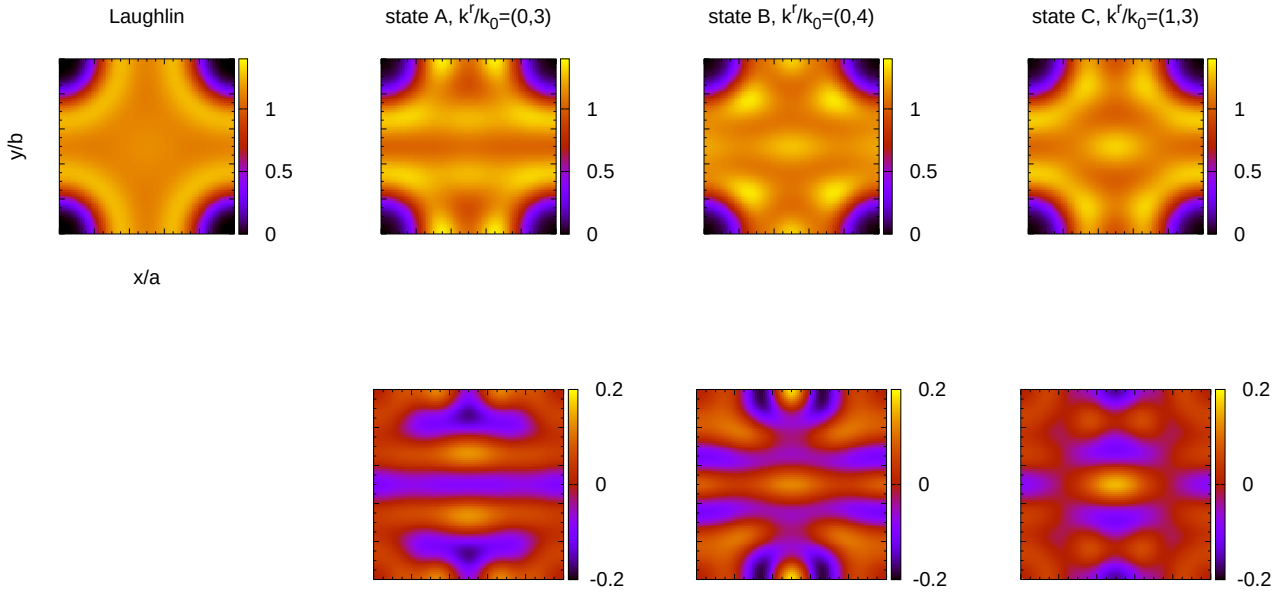

Figure 4.14: Correlation functions of the ground state (Laughlin) and several CDW states which lie on the magnetoroton branch of a $\nu = \frac{1}{3}$ system with short–range interaction (eight electrons). *Upper row:* correlation functions $g(r)$, *lower row:* $g(r)$ of the CDW states from which the Laughlin state $g(r)$ has been subtracted.

the Laughlin wavefunction (WF), Eq. 3.20. Particle density in the state Ψ_L is constant[17]. The first striking observation is that the density of the ground state obtained from exact diagonalization varies quite strongly (Fig. 4.15). At the same time we notice that the ground state, which is claimed to be incompressible, is actually triply degenerate.

Fortunately, this does not mean that finite size calculations are completely wrong. Both facts can be attributed to the centre-of-mass part of the wavefunction (CMWF) which is *not* present in Ψ_L but it *is* present in numerical calculations (see also section 3.2.3). It is not always easy to purge numerical results from the effects imposed by CMWF so that this topic deserves its own subsection.

Centre-of-mass part of the wavefunction: influence on density

Once again, recall that some theoretical background is given in Subsec. 3.2.3 and 3.5.1. Here we will concentrate on the effects the centre-of-mass part of the wavefunction (CMWF) introduces into numerical results for a system with periodic boundary conditions.

[17]Strictly taken, it is constant only if Ψ_L describes $N \to \infty$ particles. Otherwise, the N particles are confined to a finite disc (Subsect. 3.5.3), but within the disc, the density is constant up to very high precision.

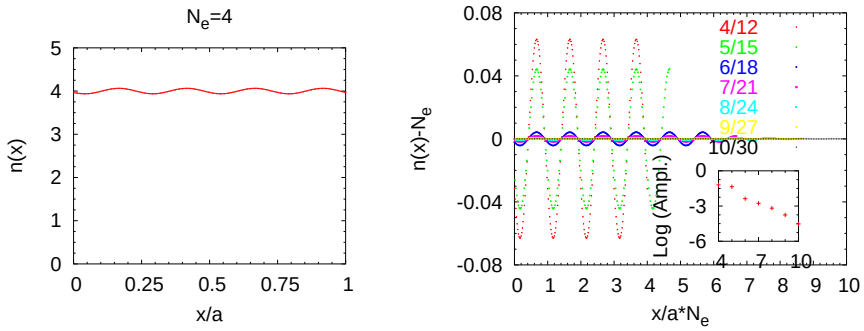

(a) Inhomogeneous density in an $N_e = 4$ system.

(b) Comparison between systems of different sizes. Note the scaling of the x axis.

Figure 4.15: Density of the $\nu = \frac{1}{3}$ incompressible ground state as obtained in torus geometry for different system sizes. The oscillations can be traced back to the centre-of-mass part of the wavefunction. As far as this effect is considered, differences between Coulomb interaction and short-range interaction are small.

The complete WF of the Laughlin state at $\nu = \frac{1}{3}$ (for n particles) in the disc geometry (Subsec. 3.5.3) might be

$$\Psi_{1/3}(z_1,\ldots,z_n) = \underbrace{F(Z)\exp(-|Z|^2/2\ell_0^2)}_{\Psi_{CM}(Z)} \times \underbrace{\exp\big(-(|z_1|^2+\ldots+|z_n|^2)/4\ell_0^2\big)\prod_{i<j}(z_i-z_j)^3}_{\Psi_L(z_1,\ldots,z_n)} \tag{4.12}$$

$$Z = z_1+\ldots+z_n \quad \text{and for example } F(Z) = Z^3\,,$$

or any other analytic function with three zeroes Z_1, Z_2, Z_3. The CMWF Ψ_{CM} has the form (Sec. 3.2.3) of a WF for one particle (somewhere) in the lowest Landau level to which a single variable Z is attributed.

Now, in torus geometry, the WF must be changed in order to comply with periodic boundary conditions (PBC, see Section 3.5.1): for Ψ_{CM} this can be summarized as

$$\prod_{i=1}^{3}(Z-Z_i) \to \prod_{i=1}^{3}\vartheta\big(\pi(Z-Z_i)/a|i\big)\,,$$

where $\vartheta(z|i)$ behaves like z on short distances but for longer distances it deviates so that $\vartheta(z+a|i) = \vartheta(z|i)$ (Subsec. 3.5.2).

Placement of the three zeroes Z_i within the elementary cell is in principle arbitrary. However, if we require the state $\Psi_{1/3}$ to have some particular symmetry[18], stringent conditions

[18]It is very popular to say that it is the choice of *gauge* what determines the form of Ψ_{CM}. This is a bit

on the position of the zeroes may apply. As an example, observe Ψ_{CM} obtained from the numerically calculated ground state Ψ_{GS} in a system with four particles, Fig. 4.16. The translational symmetry along y described by the quantum number J, Eq. 3.49, implies that Z_i's lie equally spaced on a line parallel to the y–axis (cf. [38]). Regardless of symmetries we ask for, there are always three linearly independent Ψ_{CM}'s at filling factor $\frac{1}{3}$ (Subsect. 3.5.2), once we fixed the periodic boundary conditions[19]. The companions of Ψ_{CM} in Fig. 4.16 as obtained from *analytical expressions* are shown in Fig. 3.11. On an intuitive (and mathematically incorrect) level, we could say that Z_1, Z_2, Z_3 in a particular Ψ_{CM} are the three complex coefficients in the linear combination which constitutes Ψ_{CM} (see comment [10]).

Let me briefly explain, how $\Psi_{CM}(Z)$ can be extracted from the numerically determined four–electron wavefunction $\Psi(z_1, \ldots, z_4)$. I arbitrarily chose complex numbers $z_1, \ldots, z_4$ with $\sum_i z_i = 0$ and used the fact

$$\Psi_{CM}(4\Delta) = \frac{\Psi(z_1 + \Delta, \ldots, z_4 + \Delta)}{\Psi(z_1, \ldots, z_4)} \Psi_{CM}(0)\,.$$

Once again, the reader is invited to check that Ψ_{CM} which we obtain from the exact diagonalization (Fig. 4.16) fully matches the function we expect from analytical considerations (α in Fig. 3.11(a)).

Let us now illustrate how Ψ_{CM} influences the one–particle density $n(z)$. The integral

$$\begin{aligned} n(z) &= \langle\Psi|\delta(z_1 - z)|\Psi\rangle = \int \mathrm{d}z_2\mathrm{d}z_3\mathrm{d}z_4 |\Psi(z, z_2, z_3, z_4)|^2 = \\ &= \int \mathrm{d}\widetilde{z}_2\mathrm{d}\widetilde{z}_3\mathrm{d}\widetilde{z}_4 |\Psi_{CM}(\underbrace{4z - \widetilde{z}_2 - \widetilde{z}_3 - \widetilde{z}_4}_{Z})|^2 |\psi_r(\widetilde{z}_2, \widetilde{z}_3, \widetilde{z}_4)|^2\,, \text{ with } \widetilde{z}_i = z - z_i\,, \\ &\qquad\qquad\qquad\qquad\qquad\qquad\qquad\qquad\qquad\qquad Z = z_1 + z_2 + z_3 + z_4 \end{aligned}$$

is in principle just a multi–variable convolution of the relative, ψ_r, and CM part, Ψ_{CM}, of the total wavefunction. If we denote the relative coordinates $\widetilde{z}_i$ by symbolic variable $[\widetilde{z}]$, we can rewrite the last expression as

$$n(z) = \int \mathrm{d}[\widetilde{z}] |\Psi_{CM}(4z - [\widetilde{z}])|^2 |\psi_r([\widetilde{z}])|^2 \tag{4.13}$$

In order to understand, what happens in this complicated integral, imagine that both z and $[\widetilde{z}]$ are simple one dimensional (real) variables. Function $\Psi_{CM}(x)$ will have the form

misleading: regardless of the gauge, we still have three degenerate states at $\nu = \frac{1}{3}$ and we are free to choose *any* basis in this three dimensional subspace. Rather, when we choose a particular gauge (which reflects some *symmetry*), we are *lead* to make some simple product ansatz from which wavefunction of this symmetry follows. However, the choice of this ansatz is never really necessary, we make it only for our convenience.

[19] By sweeping the phases ϕ_x or ϕ_y (Eq. 3.41) applying to boundary conditions imposed on Ψ_{CM}, we would continuously shift the zeroes Z_i right or up, respectively. Thus, e.g. for ϕ_x going $0 \to 2\pi$, the $J = 2$ state (α in Fig. 3.11(a)) moves to the $J = 6$ state (β in Fig. 3.11(a)).

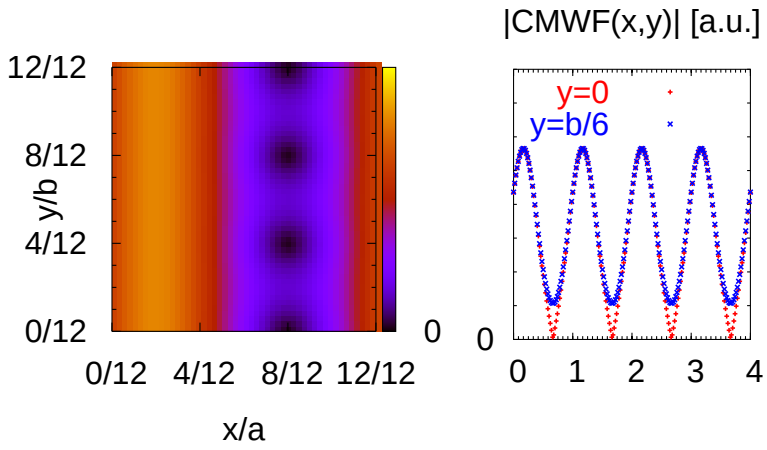

Figure 4.16: Centre-of-mass part of the wavefunction (modulus), $\Psi_{CM}(Z)$, $Z = z_1 + z_2 + z_3 + z_4$ as determined in the $\nu = \frac{1}{3}$ ground state of four particles ($J = 2$) on a torus. *Left:* $\Psi_{CM}(X, Y)$, *right:* $\Psi_{CM}(X, 0)$ and $\Psi_{CM}(X, b/6)$.

shown in Fig. 4.16 right, the form of function $\psi_r(x)$ is for the moment unimportant, let us *imagine* that it is a simple peak at $x = 0$ (see comments below).

Since $|\Psi_{CM}(x)|^2$ has period one (see Fig. 4.16), the period of $n(x)$ will be 1/4, just as we observe in Fig. 4.15. The value of $n(x)$ will be maximal when $4x = \frac{1}{6} + k$ with k an integer, since then the maxima of the two functions in the convolution 4.13 coincide. On the other hand, $n(x)$ will reach its minimum for $4x = \frac{4}{6} + k$, since then the maximum of $|\psi_r|^2$ is just shifted to the minimum of $|\Psi_{CM}|^2$.

This procedure can be repeated for variable y instead of x. The periodicity of $n(y)$ will be 1/12 since $|\Psi_{CM}(y)|^2$ has period 1/3 rather than 1 (Fig. 4.16 left) and the difference between maximal and minimal values of $n(y)$ will be much smaller than along x, since the same is true for the function $|\Psi_{CM}|^2$ (also Fig. 4.16 left).

In fact it is true that $\psi_r([\widetilde{z}])$ vanishes for '$[\widetilde{z}] = 0$' due to Pauli principle, but this modifies the previous discussion only quantitatively. In reality $|\psi_r([\widetilde{z}])|^2$ has a peak at some finite nonzero value. The essential facts are that (i) it is nonnegative, (ii) even and (iii) it vanishes for $\widetilde{z}_i \to \infty$.

Conclusion: even though e.g. the Laughlin state is translationally invariant, the CM part of the wavefunction which is always present in the exact diagonalization studies, will cause the density to be inhomogeneous. If the calculated states are eigenstates of J (see Eq. 3.49 for explanation), the density $n(z)$ of an N_e–electron state

- will be $1/N_e$ periodic along x (cf. Fig. 4.15)
- will be $1/3N_e$ periodic along y (cf. Fig. 4.19 right)
- will rapidly converge to a constant for $N_e \to \infty$.

The last statement is taken from Haldane and Rezayi [38] and it is completely in agreement with the numerical results in Fig. 4.15. A qualitative explanation is given in comment [11].

Centre-of-mass part of the wavefunction: influence on correlation functions

As stated at the very beginning of this chapter, $g(\boldsymbol{r}) \propto \delta(\boldsymbol{r}_1 - \boldsymbol{r}_2 - \boldsymbol{r})$ and $g(\boldsymbol{r}, \boldsymbol{r}') \propto \delta(\boldsymbol{r}_1 - \boldsymbol{r})\delta(\boldsymbol{r}_2 - \boldsymbol{r}')$ should be 'the same' for a homogeneous systems: we mean $g_{\boldsymbol{r}_0}(\boldsymbol{r})$ should be independent of $\boldsymbol{r}_0$ and equal to $g(\boldsymbol{r})$, using the notation $g_{\boldsymbol{r}_0}(\boldsymbol{r}) = g(\boldsymbol{r}_0, \boldsymbol{r}_0 + \boldsymbol{r})$. However, whereas the former quantity depends only on the relative coordinate $z_1 - z_2$ (and it is thus untouched by the integration over Z and consequently by the CM part), the latter quantity has the form 'density at $\boldsymbol{r}_1$ times density at $\boldsymbol{r}_2$' and it may thus suffer from the fact that the density is not constant[20] . This is indeed the case (we focus on a $\frac{1}{3}$ GS as an example): we find that although $g_{(x_0,y_0)}(x, y)$ is similar to $g(x, y)$ (Fig. 4.17a), it slightly varies with (x_0, y_0) (Fig. 4.17b,c). These variations have the following periodicities (within numerical accuracy)

$$\frac{\partial}{\partial y_0} g_{(x_0,y_0)}(x, y) = 0\,, \qquad g_{(x_0+1/N_e,y_0)}(x, y) = g_{(x_0,y_0)}(x, y)$$

and thus reflect the periodicity of the density modulation (constant along y and N_e periods along x; Fig. 4.17).

The form of $g_{(x_0,y_0)}(x, y)$ as a function of x, y is more complicated. The quantity $g_{(x_0,y_0)}(x, y)/g(x, y)$ which should be constant in an infinite system shows stripe-like structures along y but it is far from being constant along x (Fig. 4.18). Also the periodicity (number of stripes) is different from the one for the density. Fortunatelly, these finite size effects also decay rather fast with increasing system size, although not as fast as in the case of the density (Fig. 4.15): even for a ten-electron Laughlin state $g_{(x_0,y_0)}(x, y)$ may deviate from $g(x, y)$ by several percent (Fig. 4.18). Also note that the isotropy is lost in $g_{(x_0,y_0)}(x, y)$ and it is recovered first in $g(x, y)$ which may also be regarded as an average of the former quantity with respect to x_0, y_0.

In conclusion, the difference between $g(x, y)$ and $g_{(x_0,y_0)}(x, y)$ is a finite size effect (unless spontaneous symmetry breaking occurs). It is definitely related to the CM part of the WF, but the relation is not as straightforward as for the density and may be subject to further analysis.

How to suppress the effect of the CM part of the WF

As stated above, for homogeneous systems, we wish to study only the relative parts of WFs whereas numerical calculations give the product of the relative $\Psi_r(z_1, \ldots, z_n)$ and CM part $\Psi_{CM}(Z)$ in a form where they are not easy to separate. If we calculate quantities like the

[20] In mathematical terms: integrations over the CM and relative part cannot be separated.

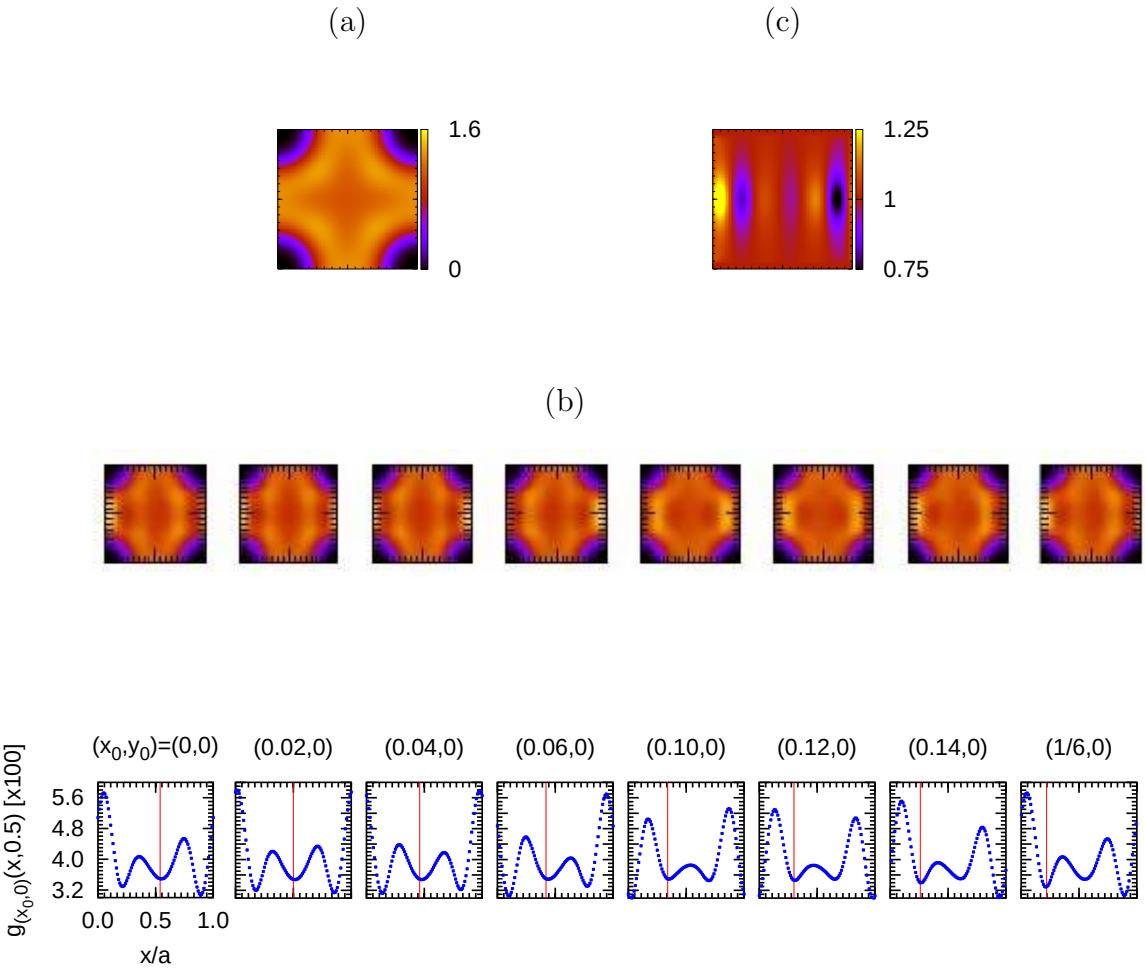

Figure 4.17: Density-density correlation functions $g(\boldsymbol{r})$ and $g(\boldsymbol{r},\boldsymbol{r}')$: demonstration of finite size effects (Laughlin state with 6 particles on a torus). *Left to right:* (a) $g(\boldsymbol{r})$; (b) $g_{\boldsymbol{r}_0}(\boldsymbol{r}) \equiv g(\boldsymbol{r}_0, \boldsymbol{r}_0+\boldsymbol{r})$ with $\boldsymbol{r}_0$ varying from $(0,0)$ to $(\frac{1}{6},0)$ (*above*: in the whole primitive cell as a function of x, y, *below*: section through $y_0 = 0.5b$); (c) $g_{(0,0)}(\boldsymbol{r})/g(\boldsymbol{r})$. In the absence of finite size effects, (c) would be equal to one everywhere.

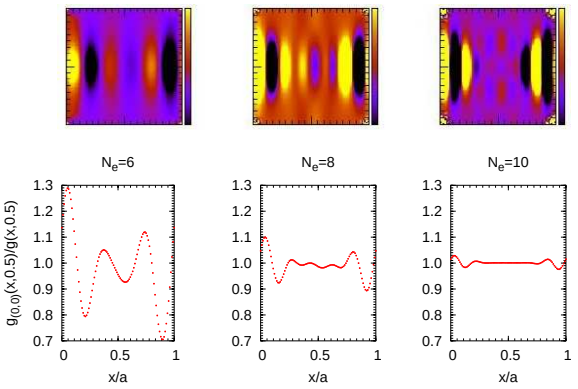

Figure 4.18: Decay of finite size effects in $g(r, r')$ with increasing system size (on the example of the Laughlin $\nu = \frac{1}{3}$ state). *Above:* $g_{(0,0)}(r)/g(r)$ in a very sensitive scale (in order to highlight the structures); *below:* section of this quantity along $y = 0.5b$ (normalized to one). For increasing system size $g_{(0,0)}(r)/g(r)$ approaches a constant as we expect for a homogeneous (infinite) system.

density or correlation function in the state $\Psi = \Psi_r \Psi_{CM}$, we evaluate integrals of the type

$$n_{\Psi_r \Psi_{CM}}(z) = \int \mathrm{d}z_1 \ldots \mathrm{d}z_n |\Psi_r(z_1, \ldots, z_n)|^2 |\Psi_{CM}(z_1 + \ldots + z_n)|^2 \delta(z_1 - z)\,.$$

Our aim is to rather get the quantity

$$n_{\Psi_r}(z) = \int \mathrm{d}z_1 \ldots \mathrm{d}z_n |\Psi_r(z_1, \ldots, z_n)|^2 \delta(z_1 - z)$$

or, in other words, to replace $\Psi_{CM}(z_1 + \ldots + z_n)$ by a constant in the numerically calculated wavefunction $\Psi_r \Psi_{CM}$.

Even though we could numerically calculate Ψ_{CM} and then calculate the density in the state Ψ/Ψ_{CM}, this is technically quite labourious (and requires numerical evaluation of $(n-1)$-fold integrals). Instead we can make the following trick; consider again the example of the $\nu = \frac{1}{3}$ GS. The state is triply degenerated (in the CM part) and the three different $\Psi_{CM}^{1,2,3}$ (as they come from ED in subspaces with sharp J) have the pleasant property that the sum of their squared moduli is nearly constant, or in a more restrained (and honest) terminology, its variations are much weaker than those of individual $|\Psi_{CM}^i|^2$ (see Fig. 4.19).

With this in mind we expect that the sum $n_{\Psi^1_{CM}\Psi_r}(z) + n_{\Psi^2_{CM}\Psi_r}(z) + n_{\Psi^3_{CM}\Psi_r}(z)$ will be a good approximation to $n_{\Psi_r}(z)$. The reader may check with Fig. 4.19 how well this is fulfilled.

Other finite size effects

Here, we will try to abstract from the effects due to the CM part of the calculated wavefunctions. Since the operator for density–density correlation depends only on relative coordinates we expect that $g(r)$ will be free of the finite size effects described in previous paragraphs. Since the curves for $g(r)$ obtained from the $\nu = \frac{1}{3}$ ground state in systems of different sizes (Fig. 4.4(b)) match very well for $|r|$ going at least to one third of the elementary cell we may have good confidence in these results even within the scope of

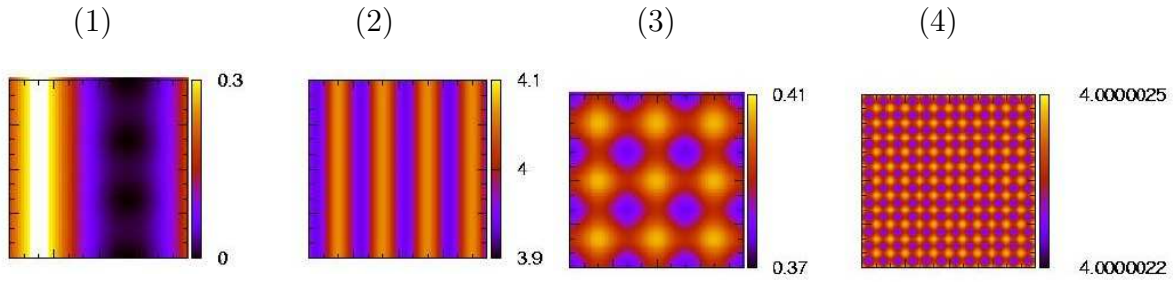

Figure 4.19: *Left to right:* (1) $|\Psi_{CM}(Z)|^2$, $Z = z_1 + z_2 + z_3 + z_4$ for one of the three degenerate ground states in a 4 particle $\nu = \frac{1}{3}$ system and (2) the density $n(\boldsymbol{r})$ of this state. (3) $|\Psi^1_{CM}(Z)|^2 + |\Psi^2_{CM}(Z)|^2 + |\Psi^3_{CM}(Z)|^2$ of those three states and (4) the sum of their densities (divided by three). Note that the last density is nearly constant (as it should be for the Laughlin state) and thus by adding up densities of the three states differing only in the CM part, we eliminated the effect of the CM part of WF.

infinite systems. In clear terms, we may believe that $g(r)$ of the infinite system is nearly the same as $g(r)$ obtained in a finite system (with $a : b = 1$) as far as up to $r \approx 0.35a$.

Another type of finite size effects which are 'finer' than those originating from the CM part of the WF is shown in Fig. 4.19, the rightmost plot. The density plotted should be constant (after averaging over the three states degenerated in the CM part) in the infinite system. The weak $(1/N_m)$-periodic structure ($N_m = 12$ in Fig. 4.19) which we still observe reflects the quantization of one particle momenta by the PBC: one particle can be localized only around one of N_m discrete set of points in the x–direction. This effect is the same along x and y, since we 'lost' the quantum number J, Eq. 3.49, by averaging over the three states (which belong to $J = 2, 6, 10$ in the present case). Note, how extremely small this finite size effect is.

4.1.5 Conclusion: yet another comparison to composite fermion models

For a large part we were concerned with the $\nu = \frac{1}{3}$, $\frac{2}{3}$ and $\frac{2}{5}$ incompressible ground states in this section. All these states, including their possible spin polarizations, can be described in terms of Landau levels (LL) filled with composite fermions (CF), Fig. 4.1 and Sec. 3.4. In particular, wavefunctions suggested by Jain (Subsec. 3.4.2) are very close to the many–electron ground states calculated by exact diagonalization, as it is demonstrated by comparing the wavefunctions calculated by the two approaches in terms of overlaps which approach unity (Wu *et al.* [99], for instance) or of correlation functions shown in this Section (Fig. 4.3 with Fig. 4.4, 4.8).

However, we have seen in this Section that this picture is not as intuitive as someone may believe. Correlation functions of states with p filled CF LLs are quite different from those of states with p filled electronic LLs. Changing orientation of the effective magnetic field (the one following from the 'CF LL quantization') alters the correlation functions

drastically: even worse, it is hard to establish a relation between the ground states at $\nu = \frac{2}{3}$ and $\frac{2}{5}$ on the level of comparing the *electronic* correlation functions. We should also mention a discrepancy in the CF model for the $\nu = \frac{2}{3}$ polarized state. It is both a particle–hole conjugate to the $\nu = \frac{1}{3}$ Laughlin state and a state with two filled CF Landau levels and effective magnetic field antiparallel to the real magnetic field (or attached flux quanta). As already Wu, Dev and Jain [99] noted in their original work about antiparallel flux attachment, these two models give two non–equivalent[21] microscopic wavefunctions. Surprisingly enough, both wavefunctions have high overlaps (≈ 0.99) with the polarized ground state obtained by exact diagonalization [99]. Thus, either both models are in fact indeed equivalent or this result shows that even such high overlaps may be not enough to prove the correctness of a trial many–body wavefunction.

Another point worth of notice is that the 'CF cyclotron energies' extracted from exact diagonalization with electrons are not quite the same in $\frac{2}{3}$ and $\frac{2}{5}$ systems. In the picture of non–interacting CFs, only the direction of the effective field B_{eff} is reversed. Thus, if B_{eff} has the same modulus in both cases and Zeeman energy vanishes then $E_p(N_e = 8) - E_u(N_e = 8)$, i.e. the difference of energies of the polarized and singlet GSs for 8–electron systems, should be equal to four times the CF cyclotron energy in the both systems. As long as the GS energies of $N_e = 8$ systems are regarded, the difference of CF cyclotron energies is small, about 5%, Fig. 4.20, the scaling factor $5 : 3$ makes B_{eff} equal in both systems. However, the agreement becomes worse when we attempt to extrapolate the energies to larger systems.

Also comparing $\frac{2}{5}$ to $\frac{2}{3}$, differences in the lowest excitations from the polarized and singlet ground states are quite apparent (Fig. 4.20).

All these facts demonstrate that it can be misleading to think of the $\frac{2}{3}$ and $\frac{2}{5}$ states as of an exact copy of Landau levels completely filled with electrons. Composite fermion models must be taken seriously since they provide us with many very good predictions (explicite forms of wavefunctions, e.g.) but apart of that they are not exact, they fail to describe some phenomena like e.g. position of zeroes in Coulomb interacting states, Subsect. 4.1.2, the analogy between electronic and CF Landau levels is sometimes weak[22].

The nature of many incompressible FQH states is therefore still not completely clear, for example the ground states at $\nu = \frac{2}{3}$ and $\frac{2}{5}$. Results in this Section indicate that the singlet states at these filling factors comprise of pairs of spin up and spin down electrons which we would not expect from the CF analogy — at least not at first glance. Furthermore, in the $\nu = \frac{2}{3}$ singlet (with electron density n), the $\uparrow - \downarrow$ pairs seem to form a state which could be constructed by taking a system with the lowest LL completely filled with electrons (with electron density $n/2$) and then replacing each electron by an $\uparrow - \downarrow$ pair. This behaviour is not observed in the $\nu = \frac{2}{5}$ singlet. We may again conclude, that even though the $\frac{2}{5}$ and $\frac{2}{3}$ ground states are very closely related on the level of composite–fermion

[21] At least to the best of my knowledge noone was able to show their equivalence.

[22] One of the inherent problems I did not mention so far is the question of mixing between CF Landau levels: whereas LL mixing can be neglected for electrons in the limit $B \to \infty$, there is no such case for CFs.

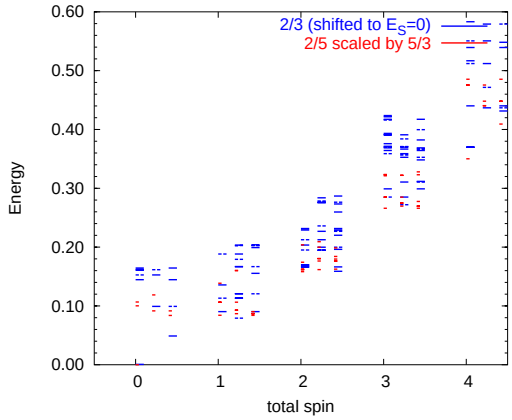

Figure 4.20: Spectra of $\nu = \frac{2}{3}$ and $\frac{2}{5}$ systems with eight electrons, zero Zeeman energy. In the picture of non–interacting composite fermions, the energies of the polarized ($S = 4$) ground states (the $\frac{2}{3}$ and $\frac{2}{5}$ ones) should be the same when B_{eff} is correctly rescaled.

theories, their electronic properties are different. It can thus be misleading to extend our intuition concerning the (completely filled) electronic Landau levels to states interpreted as (completely filled) composite fermion Landau levels.

4.2 The half–polarized states at filling factors $\frac{2}{3}$ and $\frac{2}{5}$

In the previous section we dealt with the spin singlet and polarized ground states at filling factors $\frac{2}{3}$ and $\frac{2}{5}$ and it was mentioned that it is the Zeeman splitting (or better, $E_Z/E_C \propto \sqrt{B}$) which determines which of them is the actual ground state. It is the singlet state for vanishing Zeeman splitting (low magnetic fields) and the polarized state if the Zeeman term dominates (limit $B \to \infty$). All this can be understood within the composite fermion concept (Fig. 4.1) where we even obtain the prediction that there is a *direct* transition (crossing) between these two ground states at some critical value of E_Z/E_C or equivalently, at some critical magnetic field B_C, if we sweep magnetic field and keep the filling factor constant (cf. also Sect. 5.1).

However, experiments by Kukushkin et al. [56] (Sect. 2.4) indicate that this picture may be incomplete. They suggest that some exactly half–polarized state becomes a stable ground state in the vicinity of B_C. In this Section I will describe one candidate for such a half–polarized state ground state and discuss its properties.

4.2.1 Ground state energies by exact diagonalization

At first glance, spectra of homogeneous small finite systems with Coulomb interaction (Sect. 5.1, Fig. 5.1) do not suggest any intermediate state at the transition. The picture

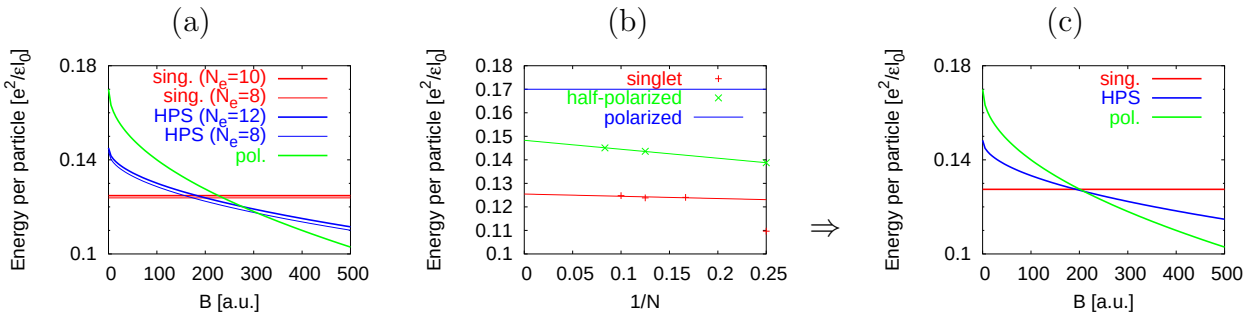

Figure 4.21: Ground state energies at $\nu = \frac{2}{3}$: the half–polarized state may become the absolute ground state in a narrow interval of magnetic fields. *Left:* Energies of SRI ground states in the subspaces $S = 0$ (singlet), $S = N_e/4$ (half-polarized) and $S = N_e/2$ (fully polarized) as a function of Zeeman splitting (or magnetic field; note the energy units $e^2/\varepsilon\ell_0 \propto \sqrt{B}$). In all cases, energies of the two largest systems available to calculations are shown. *Middle:* extrapolation of the GS energies to infinite systems ($1/N \to 0$). *Right:* The energy–versus–magnetic field diagram for extrapolated ground state energies. This indicates that even then the HPS will be a ground state close to the transition.

is quite different when short–range interaction is considered: in an interval of magnetic fields around B_C the GS is a state with total spin equal to $N_e/4$ (Fig. 4.21a), i.e. a half-polarized state (HPS). This holds for all system sizes accessible to numerical calculation and, by extrapolating energies to $1/N \to 0$ (Fig. 4.21b), it seems to hold also for infinite systems.

I suggest that it is only through the finiteness of the system that a half polarized ground state did not appear in Coulomb interacting systems (Fig. 5.1). The SRI systems may be less sensitive to this generical drawback of exact diagonalization models. On the other hand, SRI models predict wrong values of B_C (see Subsec. 5.3.1) and thus the scheme presented in Fig. 4.21(a) must be checked in systems with Coulomb interaction.

Considering Coulomb–interacting systems, the scheme suggested in Fig. 4.21(a) is supported by extrapolations of GS energies performed by Niemelä, Pietiläinen and Chakraborty [73] in spherical geometry (Fig. 4.22a) and it is not supported by analogous calculations on a torus presented here (Fig. 4.22b). I should like to stress that the extrapolation of the energy of the HPS is based on solely two (or three[23]) points. Therefore the question of whether the HPS becomes the absolute GS or not remains basically open until exact diagonalizations of larger systems become possible.

Nonetheless I will assume in this Section that a half–polarized state can indeed make it in energy down to the absolute ground state and I will therefore focus on the $S = N_e/4$ sector of systems at filling factor $\frac{2}{3}$ (and in Subsec. 4.2.5 also $\frac{2}{5}$). Studies were mostly focused on the SRI states where it is easier to identify the best candidate for the half–polarized ground state. Its Coulomb–interacting counterpart is discussed later, in Subsec. 4.2.6.

[23]Note that the third point in Fig. 4.22(b), the one from $N_e = 4$ half–polarized system, is not very reliable. For $N_e = 4$ it is not quite clear which state we should consider (Subsec. 4.2.3).

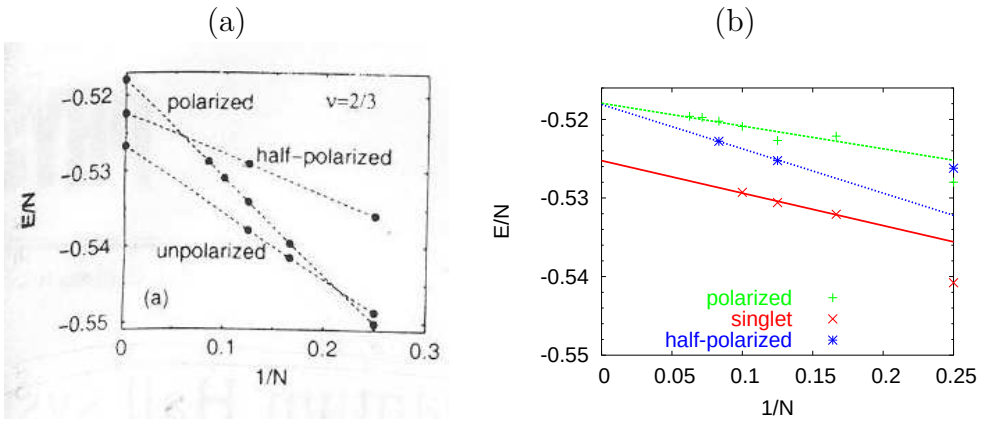

Figure 4.22: Extrapolation $1/N \to 0$ of the GS energies for Coulomb interacting systems at $\nu = \frac{2}{3}$. *Left:* on a sphere (taken from [73]), *right:* on a torus.

By convention[24], a half–polarized state with 12 (8) electrons will consist of 9 (6) electrons with spin up (majority spin) and 3 (2) electrons with spin down (minority spin).

4.2.2 Identifying the HPS in systems of different sizes

Provided some particular physical half–polarized state $\mathrm{GS}_\infty$is the ground state in an infinite system, we may ask what its realizations in finite systems of different sizes are. Vice versa: given the half–polarized states calculated in a system of $N_e = 12$ (4, 8...) electrons, which state corresponds to GS_∞? In this way we can think of states which 'correspond to each other' in systems of different sizes. The trouble is, of course, that we do not know GS_∞. Regarding the computational capacity available, I could study $\nu = \frac{2}{3}$ systems with 4, 8 and 12 particles[25], the next larger system would require diagonalization in spaces of dimension many hundred million. It seems likely that the analogues to $\mathrm{GS}_\infty$are the GSs in $N_e = 12$ and $N_e = 8$ systems (GS_{12}, GS_8) and that it is a low lying excited state (`st03`) in the smallest system, $N_e = 4$. In the following I should like to give some reasons for this.

- GS_{12} and GS_8 belong to the same symmetry class defined by the 'crystallographic $\boldsymbol{k}^r$' (Eq. 3.46). They have both $\widetilde{k}^r = (\pi, \pi)$, i.e. they lie in the 'corner of the Brillouin zone' (Fig. 3.12, Subsec. 3.5.2). This is also closely related to the fact that both GS_{12} and GS_8 are non–degenerate.

- The states GS_{12} and GS_8 are well separated from excitations within the $S = N_e/4$ sector and the energy of the lowest excitation is similar ($0.01\ (e^2/\varepsilon\ell_0)$) in systems of

[24]Note that this definition implies only $S_z = N_e/4$ and not necessarily $S = N_e/4$. Unless stated otherwise, we will always speak about $S = N_e/4$ states.

[25]In order to get a state with $S_z = N_e/4$, numbers of spin up and spin down electrons must be in ratio 3 : 1. Therefore the total number of electrons must be a multiple of four.

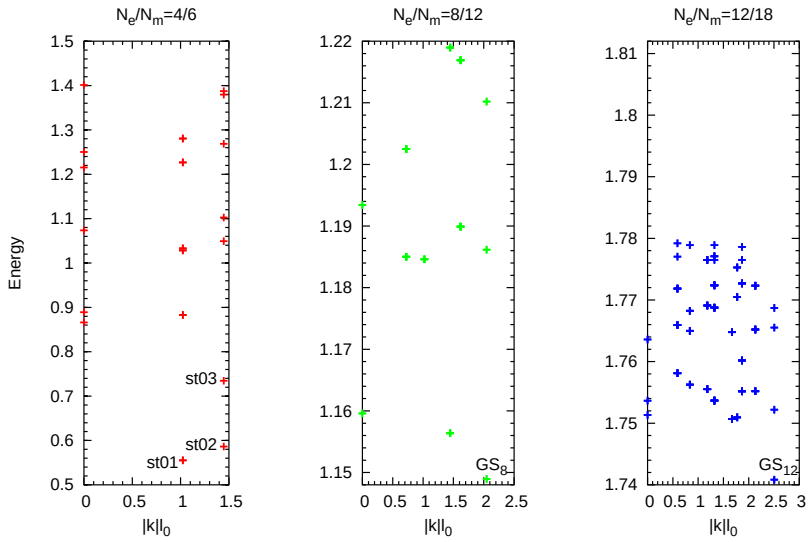

Figure 4.23: Low lying energy levels in the $S = N_e/4$ (half–polarized) sector of $\frac{2}{3}$ systems with (*left to right*) $N_e = 4$, 8 and 12 particles. The states are sorted according to $|\boldsymbol{k}^r|$ (Subsec. 3.5.2). The GS of an infinite system is likely to have $\widetilde{\boldsymbol{k}}^r = (\pi, \pi)$ which is a point of very high symmetry in the $\boldsymbol{k}^r$–space. This symmetry class is however distinct from the one of the singlet and polarized incompressible ground states.

different size.

- Though not completely identical, the inner structure of GS_{12} and GS_8 is very similar as seen by the correlation functions, Fig. 4.24.

- The GS of the $N_e = 4$ system has a lower symmetry than the formerly described states. Looking for a state of inner structure (correlation functions) similar to the one of GS_{12} and GS_8 within the sector $\widetilde{\boldsymbol{k}}^r = (\pi, \pi)$, we find (Subsec. 4.2.3) remarkable similarities with the second excited state ('`st03`', marked in Fig. 4.25). However, we should bear in mind that for $N_e = 4$ there is only a single electron with reversed spin (note that e.g. $g_{\downarrow\downarrow}(r) \equiv 0$ as a consequence), in other words the system is indeed extremely small. Relevance of such states with respect to infinite systems is thus doubtful.

4.2.3 Inner structure of the half–polarized states

Focus of this part will be the correlation functions of the states GS_{12} and GS_8 and a brief comment will be made on $N_e = 4$ states. As mentioned above and as the kind reader may verify in Fig. 4.24, GS_{12} and GS_8 look indeed similar.

GS_{12} and GS_8 match in all three spin–resolved correlation functions, $g_{\uparrow\uparrow}(r)$, $g_{\uparrow\downarrow}(r)$, $g_{\downarrow\downarrow}(r)$, Fig. 4.24. The match is especially good (quantitative) on short distances, $r \lesssim 3\ell_0$. This suggests that states GS_{12} and GS_8 are not bound to some particular system size and we can thus hope that if we could make the system larger, they would eventually develop into the GS_∞.

Differences between correlation functions of GS_{12} and GS_8 at longer distances r are understandable, given the normalization (Eq. 4.4): the $N_e = 12$ system is 'larger' than the $N_e = 8$ one, yet the integral $\int \mathrm{d}r g(r)$ must be the same.

Some further points are worth of notice.

(i) $g_{\uparrow\downarrow}(r)$ is suppressed nearly to zero at $r = 0$ (in spite of the missing Pauli principle; only on account of the repulsive interaction) and it displays strong maxima around $r \approx 3.4\ell_0$.

(ii) Even though by far not identical, $g_{\uparrow\uparrow}(r)$ and $g_{\downarrow\downarrow}(r)$ are similar to each other. The clear shoulder around $r \approx 2\ell_0$ seems to stem from the 'exchange hole' (of the LLL) $g_{\nu=1}(r) = 1 - \exp(-r^2/2\ell_0^2)$, see Eq. 4.5. After subtracting a suitably scaled function $g_{\nu=1}(r)$ the shoulder completely disappears and the remaining parts of both $g_{\uparrow\uparrow}(r)$ and $g_{\downarrow\downarrow}(r)$ are $\propto r^6$ close to $r = 0$, Fig. 4.26 and discussion below.

(iii) Up to a high precision the sum of $g_{\uparrow\uparrow}(r)$, $g_{\downarrow\downarrow}(r)$ and $g_{\uparrow\downarrow}(r)$ (with appropriate scaling, see Fig. 4.7 for explanation) is identical with $g_{\nu=1}(r)$, however with ℓ_0 replaced by $\sqrt{2}\ell_0$. Not shown here.

Let us now turn to the smallest system where $S = N_e/4$ states may occur (at $\nu = \frac{2}{3}$), i.e. $N_e = 4$. Figure 4.25 shows correlation functions of the lowest two states in the sector of $\widetilde{k}^r = (\pi, \pi)$. Out of these, the second state (i.e. `st03`) seems to be analogous to $S = N_e/4$ GS's in the two larger systems ($N_e = 8$, 12): $g_{\uparrow\uparrow}(r)$ is again a sum of the 'correlation hole' and a function $\propto r^6$, $g_{\uparrow\downarrow}(r)$ shows a peaked structure with maximum around $2.8\ell_0$ (both of these features are missing for the lower state `st02`). However, as mentioned above, the $N_e = 4$ system is too small for a reliable study of $S = N_e/4$ states ($g_{\downarrow\downarrow}(r) \equiv 0$).

Back to the GS_{12} (called HPS here), it is very interesting to study the '$\propto r^6$ part' (P6P) of the like–spins correlation functions, $g_{\uparrow\uparrow}(r)$, $g_{\downarrow\downarrow}(r)$. What we mean by 'P6P' is the rest after we subtract the 'lowest LL correlation hole', i.e. the $g_{\nu=1}(r)$ part causing the shoulder in $g_{\sigma\sigma}(r)$ around $r \approx 2\ell_0$ (green line in Fig. 4.26a,b), see above.

One of many facts we can extract from Fig. 4.26 is that P6P/ $\uparrow\uparrow$ (refering to $g_{\uparrow\uparrow}(r)$) and P6P/ $\downarrow\downarrow$ are similar but not identical. For example, they both exhibit a peaked structure but the first maxima do not coincide, they occur[26] at $5.0\ell_0$ and $5.8\ell_0$ for P6P/ $\uparrow\uparrow$ and P6P/ $\downarrow\downarrow$, respectively (dark blue and grey lines in Fig. 4.26a).

[26] Note that the peak position is in fact unaffected by the procedure of subtracting the $g_{\nu=1}(r)$ part. Namely, the peak is situated in a region where $g_{\nu=1}(r)$ is almost constant both for $g_{\uparrow\uparrow}(r)$ and $g_{\downarrow\downarrow}(r)$ (Fig. 4.26).

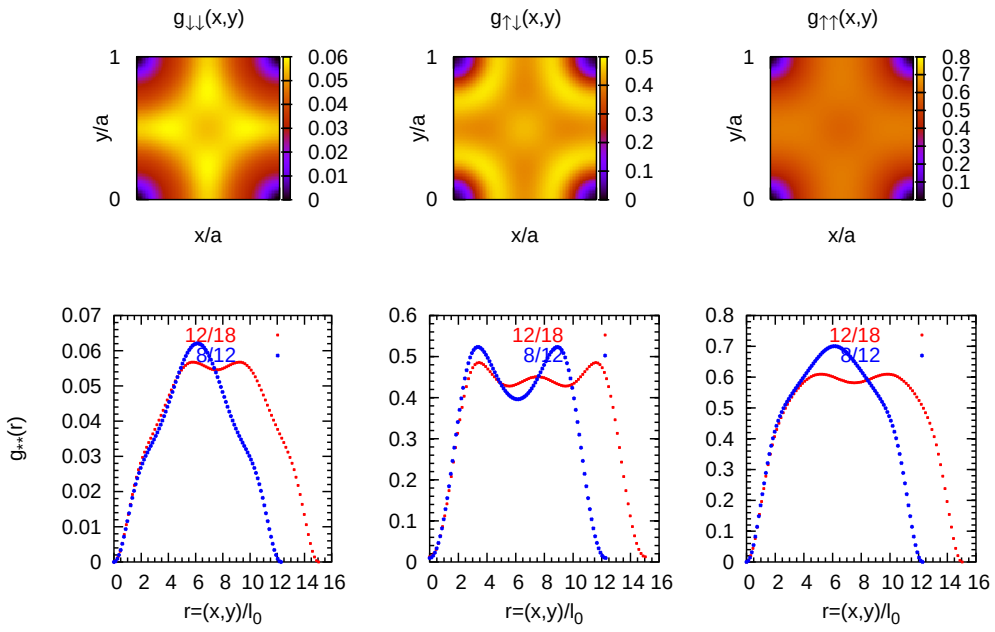

Figure 4.24: The likely analogues of the half-polarized ($S = N_e/4$) GS_∞(ground state in an infinite system) on a torus with $N_e = 8$ and $N_e = 12$ particles and filling factor $\frac{2}{3}$. *Left to right:* density–density correlation for ↑↑ (majority spins), ↑↓ and ↓↓ (reversed spins), *upper row:* in the whole primitive cell; *lower row:* sections along the diagonal. Note the isotropy of the state, i.e. visual manifestation of its high symmetry.

Let us compare the P6P/ ↓↓ of the HPS with P6P/↓↓ of the singlet incompressible $\frac{2}{3}$ GS (dark blue and cyan lines in Fig. 4.26a). Match of these two is very good up to $r \approx 4\ell_0$, the absence of the peak at $5.8\ell_0$ in the singlet state could be due to smallness of the system where the singlet state was determined ($N_e = 10$); it might appear in the next larger system, $N_e = 12$ (cf. similar situation in Fig. 4.24).

On the other hand, P6P/↑↑ of the HPS seems to resemble the singlet state less than P6P/↓↓ of the HPS. The form of P6P/↑↑ seems to be not very different from the one of the correlation function of the Laughlin $\frac{1}{3}$ state (cf. Fig. 4.4(b)) whose first maximum occurs however already at $r = 4.4\ell_0$ (red and blue lines in Fig. 4.26b). In any case, P6P/↑↑ of the HPS matches better $g_{\nu=\frac{1}{3}}(r)$, i.e. the Laughlin state, than P6P of the $\nu = \frac{2}{3}$ singlet state; here we mean especially behaviour on ranges $\lesssim 3\ell_0$.

Last but not least: the correlations between unlike spins are also very similar in the singlet state and in the HPS, Fig. 4.26c, in particular positions of the maxima differ by as little as $0.1\ell_0$ (both are around $r \approx 3.4\ell_0$).

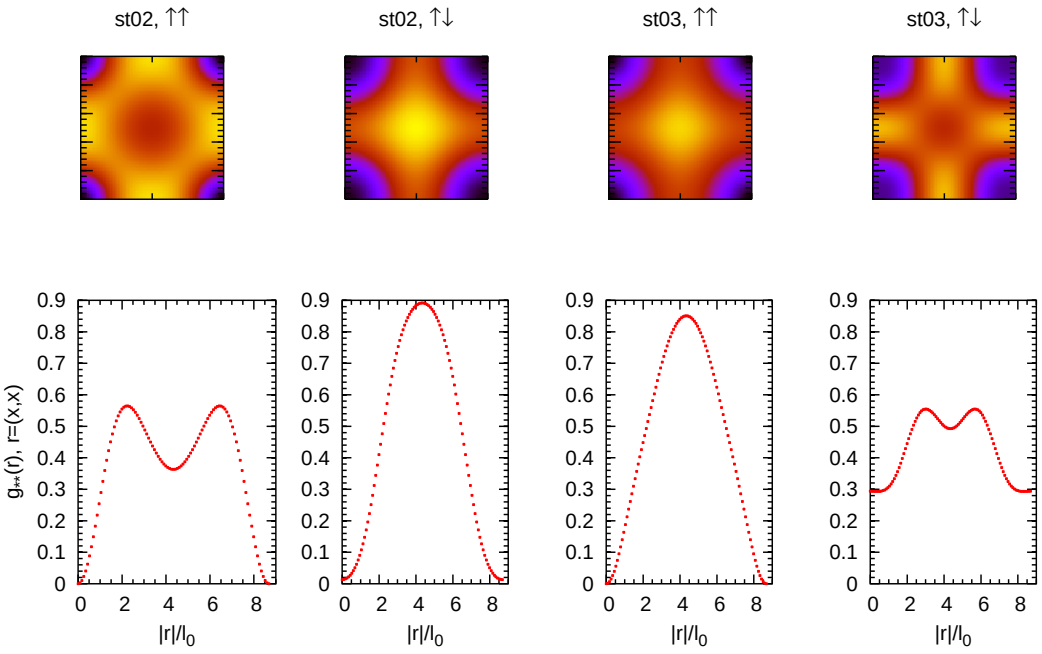

Figure 4.25: Two possible candidates for the $\nu = \frac{2}{3}$ HPS in $N_e = 4$ system. Correlation functions shown. Note that $g_{\downarrow\downarrow}(r) \equiv 0$, since there is only one spin down electron is such a small system.

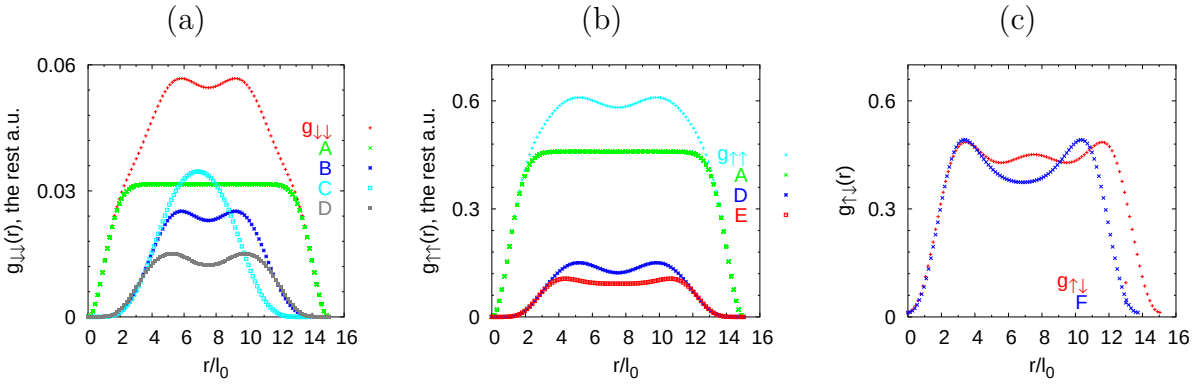

Figure 4.26: The half-polarized state (GS in the $S = N_e/4$ sector) for $N_e = 12$ particles, analysis of the correlation functions (details in text). *Left to right*: (a) $g_{\downarrow\downarrow}$ (minority spin), (b) $g_{\uparrow\uparrow}$ (majority spin) and (c) $g_{\uparrow\downarrow}$. Legend. A: lowest LL correlation hole, $g_{\nu=1}(r)$ scaled to fit the shoulder. B and D: $g_{\downarrow\downarrow}(r)$ and $g_{\uparrow\uparrow}(r)$ without shoulder. C and F: $g_{\downarrow\downarrow}(r)$ and $g_{\uparrow\downarrow}(r)$ of the singlet state ($N_e = 10$, $\nu = \frac{2}{3}$), $g_{\downarrow\downarrow}(r)$ without shoulder. E: $g(r)$ of the $\nu = \frac{1}{3}$ Laughlin state. 'Without shoulder' means, that the curve A was multiplied by a suitable constant to fit the shoulder and subtracted.

4.2.4 Discussion

Findings presented above suggest that the $\nu = \frac{2}{3}$ half–polarized ground state in short–range interacting systems is a gapped state in which the singlet and polarized incompressible states coexist. Below, some key points regarding the HPS are summarized.

Symmetry and energy

Both in eight– and twelve–electron systems, the ground state has $\widetilde{k}^r = (\pi, \pi)$. This is one of two points of the highest symmetry in the k^r–space: the another is $k^r = (0, 0)$ (Fig. 3.12). In particular, 'highest symmetry' means that this k^r–point is not related to any other point by a symmetry operation in the k^r–space corresponding to relative translations (Sec. 3.5.2). This in turn implies that states with $\widetilde{k}^r = (\pi, \pi)$ or $(0, 0)$ — and only such states — are non–degenerate, except for center-of-mass and incidental degeneracies. Together with the relatively large lowest excitation energy $\Delta(N_e = 8, 12)$ from both GS_{12} and GS_8 (10% of the gap of the Laughlin state, Fig. 4.23) , this suggests that the ground state is gapped. Also the relation $\Delta(N_e = 8) < \Delta(N_e = 12)$ speaks in favour of this hypothesis: if the gap were to vanish in an infinite system, we would expect the lowest excitation energy to decrease with system size. Naturally, we must be careful, since we can compare systems of only two different sizes and the function $\Delta(N_e)$ may be non–monotonous. On the other hand, $\Delta(N_e = 12) \approx 0.01$ $(e^2/\varepsilon\ell_0)$ is much larger than a typical level separation between excited states, Fig. 4.23 and for a mere finite size effect, this gap seems too large.

In spite of the similarities to the singlet and polarized incompressible ground states, $\widetilde{k}^r$ clearly distinguishes HPS from these two states, since they have both $\widetilde{k}^r = (0, 0)$. Also in spherical geometry, where $|\widetilde{k}^r| \propto L$ (Subsec. 3.5.3), these incompressible states have $L = 0$ while the HPS has $L = S$, where S is the total spin [73]. Thus, even though we showed that the HPS could be gapped, it is of different nature than the singlet and polarized ground states. Meaning of this different symmetry is however not clear.

It would be interesting to study this state in a system with hexagonal elementary cell [37]. This geometry is nearer to an isotropic 2D system than a torus (it has a six–fold rather than a four–fold rotational symmetry) while it is still compatible with plane waves (in CDWs). Most importantly, there is only one point of the highest symmetry in this geometry and a straightforward question is whether or not the HPS will maintain its high symmetry.

Inner structure again

Features of the HPS described by points (i–iii) in Subsec. 4.2.3 are actually strikingly similar to those of the incompressible singlet state at $\nu = \frac{2}{3}$. Investigation of the $g_{\uparrow\uparrow}(r)$ after the 'shoulder' was subtracted (P6P/$\uparrow\uparrow$) suggests again some relation to the Laughlin state which is the particle–hole conjugate to the polarized incompressible state at $\nu = \frac{2}{3}$. Especially manifest is the hint at pairing between unlike spins (maximum around $3.4\ell_0$ in $g_{\uparrow\downarrow}(r)$). On the other hand, the shoulder in correlation functions of like spins seems to be

rather a manifestation of filling factor $> \frac{1}{2}$, since it occurs also for other states at filling $\nu = \frac{2}{3}$ (than just for the singlet, polarized and half–polarized GS) and it does not occur at filling $\nu = \frac{2}{5} < \frac{1}{2}$ (cf. Subsec. 4.2.5). It suggests that some $\nu = \frac{2}{3}$ states with less than full polarization can be interpreted in terms of holes rather than electrons even though particle–hole symmetry applies only for fully polarized states (cf. Subsec. 4.1.1).

In the following Sections I will continue investigating the half–polarized states at filling factor $\frac{2}{3}$ by other methods and continue discussing the hypothesis of 'coexisting singlet and polarized states'. First, however, we look at two different minor issues.

4.2.5 Half-polarized states at filling $\nu = \frac{2}{5}$

At filling $\frac{2}{5}$, the situation is much less transparent than at filling $\frac{2}{3}$. First, only systems with four and eight particles are accessible to exact diagonalization, the twelve particle system implies matrix dimensions in the order of hundreds of millions. Second, the spectrum of the eight particle system (in the $S = N_e/4$ sector) is quite different from that of a $\frac{2}{3}$ system (Fig. 4.2.5):

(i) the ground state lies at a different point in the k^r–space, $(0, 0)$, than the $\frac{2}{3}$–HPS which has $\widetilde{k}^r = (\pi, \pi)$.

(ii) The excitation energy from this GS is very small (less than a third of that one of the $\frac{2}{3}$ HPS).

(iii) The symmetry of the low excited states is lower than for $N_e = 8$, $\frac{2}{3}$ system.

Regarding the possibility that (within the 8 electron calculations) the half-polarized GS at $\nu = \frac{2}{5}$ is not the counterpart to the GS at $\nu = \frac{2}{3}$, there are two $\frac{2}{5}$ states displayed in Fig. 4.28: (a) the one with the lowest energy (in $S = N_e/4$ sector) and (b) the lowest state with the same symmetry as the $\frac{2}{3}$ HPS, i.e. $\widetilde{k} = (\pi, \pi)$.
Similarly, as for the $\nu = \frac{2}{3}$ states, the $\frac{2}{5}$ HPS bear features of the polarized and singlet ground states. Let us regard the state (a):

- Near $r = 0$ the functions $g_{\downarrow\downarrow}$ (minority spin), $g_{\uparrow\downarrow}$ and $g_{\uparrow\uparrow}$ (majority spin) are $\propto r^6$, r^4 and r^2, respectively. In this respect, $g_{\downarrow\downarrow}$ and $g_{\uparrow\downarrow}$ resemble the singlet state and $g_{\uparrow\uparrow}$ resembles the polarized state.

- Up to the first maximum, $g_{\uparrow\uparrow}$ of the HPS is the same as in the polarized state, but shifted by about $0.2\ell_0$ outwards. Positions of the first maxima mismatch slightly more (by $0.4\ell_0$). The strong maximum in the centre of the cell is not present in the HPS.

- $g_{\uparrow\downarrow}$ of the HPS and the singlet GS match very well even beyond the first maximum (positions of the maxima are identical, $r \approx 3.5\ell_0$). On contrary to the previous point,

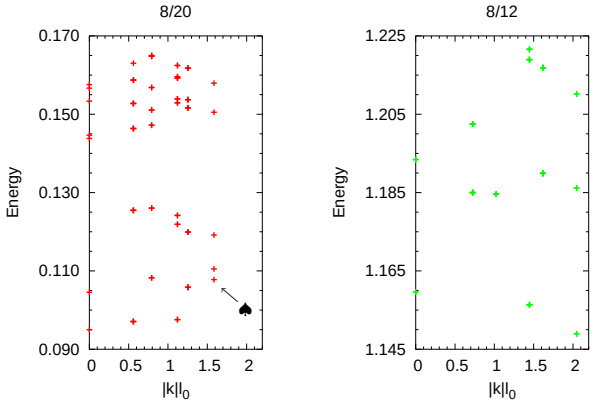

Figure 4.27: Low lying half-polarized (i.e. $S = N_e/4$) states of a $\frac{2}{5}$ system. The lowest state with the same symmetry as the HPS of $\nu = \frac{2}{3}$ is marked by ♠.

there is another maximum in the centre of the cell in the HPS state (and nothing in the singlet state).

- $g_{\downarrow\downarrow}$ of the HPS and the singlet GS also match very well up to $r \approx 4\ell_0$. Then there is a deep minimum in the HPS which is absent in the singlet GS.

Turning to the state (b) we might say that it is less alike to the singlet state: the minimum in $g_{\downarrow\downarrow}$ is much deeper than for state (a), the first maximum in $g_{\uparrow\downarrow}$ does not match the maximum seen in the singlet state. On the other hand, $g_{\uparrow\uparrow}$ seems to be more similar to the polarized state.

Lowest excitations (in the high symmetry sectors) show even less similarities to the singlet and polarized GSs, especially $g_{\downarrow\downarrow}$ is quite dissimilar beyond the $r \approx 0$ range and maxima in $g_{\uparrow\downarrow}$ match less well .

In conclusion, if there is a counterpart to the $\frac{2}{3}$ HPS at filling $\frac{2}{5}$ at all, I expect it to be the state (a) (the absolute GS), even though hints for this are not very convincing.

4.2.6 Short–range versus Coulomb interaction

Let me conclude with observations regarding the Coulomb– and short–range–interacting (SRI) systems in the sector of half–polarized states.

- the spectra do not look very similar, Fig. 4.29(a); however, the absolute ground states have in both cases the same symmetry (they lie in the same point of the k space).

- the Coulomb and SRI ground states (in the largest system available, $N_e = 12$) have very similar structure. The correlation functions $g_{\uparrow\uparrow}$ and $g_{\uparrow\downarrow}$ match nicely while $g_{\downarrow\downarrow}$ show some differences between the CI and SRI states. In spite of this, the overlap between the two states is as large as 95%. This allows for the following conclusions

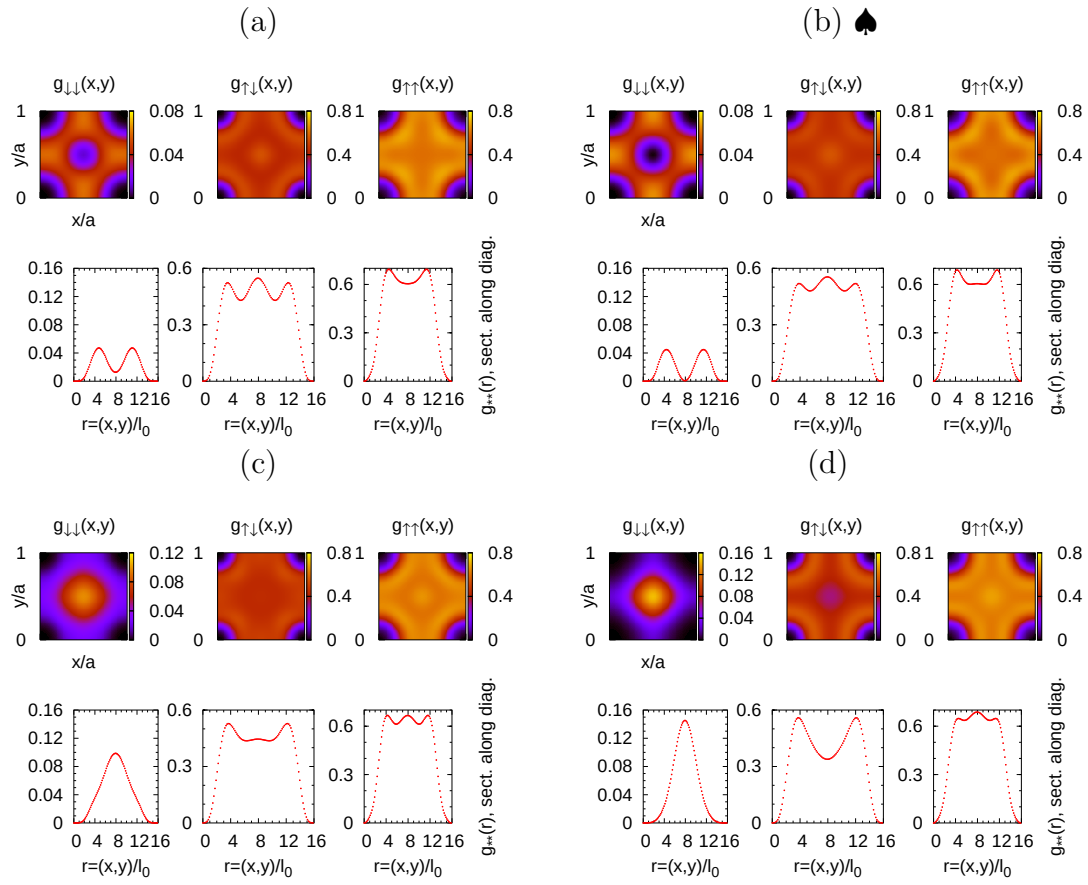

Figure 4.28: Half–polarized states at filling $\frac{2}{5}$ and their inner structure (density–density correlation functions); eight electron system. *Upper row:* (a) the GS in the $S = N_e/4$ sector is non-degenerate but it has a different symmetry, i.e. $(0,0)$, than the HPS of $\nu = \frac{2}{3}$. (b) the lowest half-polarized state (at $\frac{2}{5}$) with the same symmetry, i.e. $(\frac{\pi}{2}, \frac{\pi}{2})$ as the HPS of $\nu = \frac{2}{3}$ (marked by ♠ in Fig. 4.2.5). *Lower row:* (c,d) Lowest excited states in the sector $(0,0)$ and $(\frac{\pi}{2}, \frac{\pi}{2})$, respectively.

  - The two states 'correspond to each other'.
  - The short–range part of the interaction seems to be essential for this state (very similar as for the Laughlin state).
  - Deviations in $g_{\downarrow\downarrow}$ (minority spin) might come from the fact that spin–down electrons are very far separated from each other (they have an effective filling of only $\nu = \frac{1}{6}$). Thus the long–range part of the interaction substantially influences their motion.

- in $N_e = 8$ systems, the most likely analogue to the $N_e = 12$ ground state is the state ♢, Fig. 4.29(a) . This is the lowest 8–electron state with the same symmetry (value of $\widetilde{k}^r$) as the $N_e = 12$ ground state. Correlation functions of the two states (8–

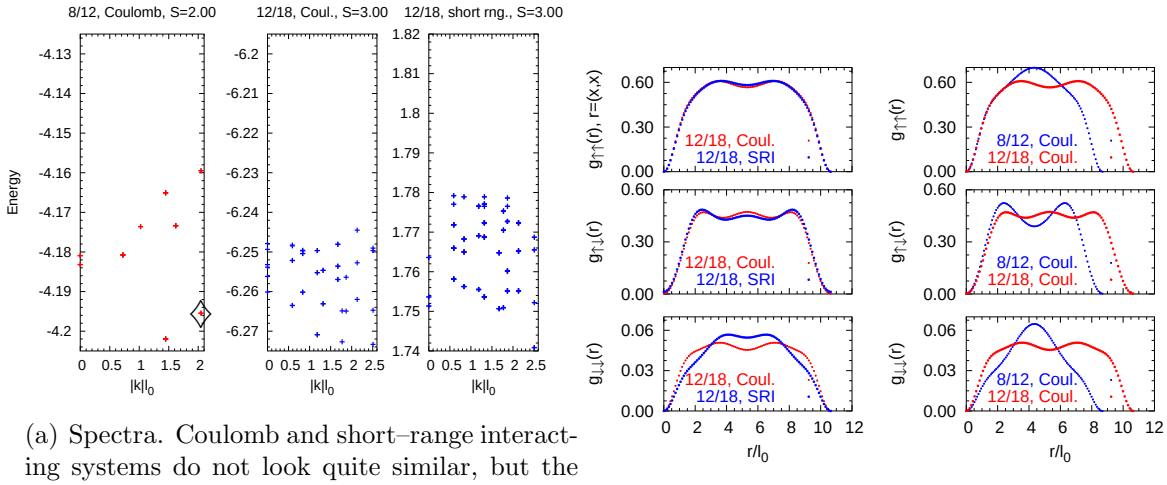

(a) Spectra. Coulomb and short–range interacting systems do not look quite similar, but the ground state is always at the maximum $|k|$.

(b) The ground state

Figure 4.29: Half–polarized states in Coulomb interacting systems.

and 12–electron ones) match reasonably, Fig. 4.29(b) (compare also with differences between $N_e = 8$ and $N_e = 12$ short–range ground states, Fig. 4.24).

- among the excited states the level order is often modified, comparing the $N_e = 12$ Coulomb and short–range systems. When trying to assign CI to corresponding SRI states, calculating overlap between two states seems to be a more reliable tool than comparing correlation functions.

In summary: in spite of differences in the excitation spectrum, the half–polarized ground states of Coulomb and short–range systems seem to be basically the same. Differences in the excited states and in the correlations between the minority spin electrons indicate that the definition of the short–range interaction should be improved when we study the half–polarized states: since the minority spin electrons are relatively far from each other, non–zero values of higher pseudopotentials (V_m, $m > 1$; cf. Subsect. 3.3.6) should probably be considered.

4.3 In search of the inner structure of states: response to delta impurities

Now that some candidates for the half–polarized ground state at filling $\frac{2}{3}$ have been introduced we wish to look at them more closely and learn more about their inner structure. The ultimate goal of such efforts is to propose trial wavefunctions just as the Laughlin wavefunction at filling $\nu = \frac{1}{3}$.

Even though I did not accomplish this aim, I will present in this Section more hints at relations between the half–polarized state and the singlet and polarized incompressible states.

As a probing tool, the homogeneous states are subjected to a δ–line impurity and response in density and polarization is observed. In first quantization,

$$H_{impurity} = \sum_{i=1}^{N_e} W(\boldsymbol{r}_i)\,, \qquad W(x,y) = \delta(x - x_0) \tag{4.14}$$

This inhomogeneity profile (Fig. 4.30) was chosen since it is compatible with the torus symmetry. For studies of point–like impurities, spherical geometry is more suitable since it preserves the rotational symmetry, cf. references in Subsec. 4.3.1. The δ–line form is particularly apt to unveil a tendency of the state to build plane charge or spin density waves. We should keep in mind, that due to the restriction to the lowest Landau level, even a δ–like potential has an effective cross section of ℓ_0 (see [80]).

As we are dealing with spinful electrons, inhomogeneities can be principially of four distinct types:

$$\begin{aligned} H_{EI} &= W(r)\cdot(\delta_{\sigma\uparrow} + \delta_{\sigma\downarrow})\,, \qquad & H_{MI,\uparrow} &= W(r)\cdot\delta_{\sigma\uparrow}\,, \\ H_{MI} &= W(r)\cdot(\delta_{\sigma\uparrow} - \delta_{\sigma\downarrow})\,, \qquad & H_{MI,\downarrow} &= W(r)\cdot\delta_{\sigma\downarrow}\,, \end{aligned} \tag{4.15}$$

where the function $W(r)$ describes the spatial form of the impurity (as it is shown in Fig. 4.30 for instance). It is important to note that these impurities fail to conserve S^2 but they do conserve S_z. Also, owing to the form of $W(\boldsymbol{r}) = W(x)$, they conserve $\boldsymbol{k}^r_y$ and thus also J (Eq. 3.49) and they spoil only the $\boldsymbol{k}^r_x$–symmetry. This is very convenient from the computational point of view as matrix sizes remain tractable. From the physical point of view, this inhomogeneity is a 'gentle' tool which does not completely destroy the high symmetry of the studied states. For example, it allows us to stay in the $S_z = N_e/4$ sector when we study the half–polarized states.

The first type (H_{EI}, electric impurity) is an ordinary non–magnetic impurity or external electric potential. The magnetic impurity (H_{MI}) favours particles with correct spin ($\downarrow$, if $W(r) > 0$) and costs energy for particles with wrong spin ($\uparrow$ in this case). The last two types describe an impurity which is seen only by one group of spins. In case that a system consists of two separated subsystems, one of spin up particles and another of spin down particles, these impurities allow to test only one of them without directly disturbing the other one.

Note that some inhomogeneity types in Eq. 4.15 may be redundant, depending on the state we apply them to. For instance, the effect of $H_{MI,\uparrow}$ and $H_{MI,\downarrow}$ must be the same up to a sign for all states in the $S_z = 0$ sector.

Before we turn to the exact diagonalization results, let us briefly think about what types of responses to general inhomogeneities we can expect at all. Most importantly, consider the difference between compressible and incompressible states. As a classical *compressible*

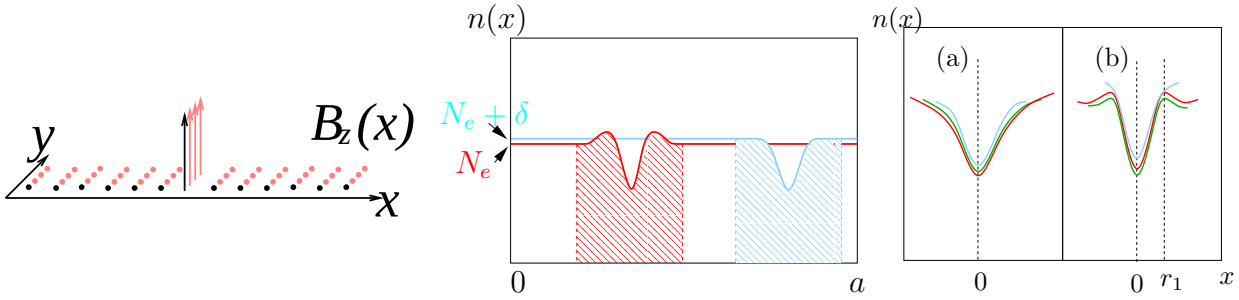

(a) δ–line impurity of the type $\delta_{\sigma\uparrow} - \delta_{\sigma\downarrow}$.

(b) A compressible–like response (blue line) and an incompressible–like response (red line). Note that density integrated over the hatched area remains unchanged for the incompressible system when the inhomogeneity is switched off.

(c) Two possible ways of how a response to an inhomogeneity can change with system size; different lines in one sketch refer to the same state in systems of different sizes.

Figure 4.30: δ–line inhomogeneity and sketches of possible resulting effects.

system imagine a playground of fixed size filled with a gas of negatively charged footballs of density $n(r)$, $\langle n(r)\rangle = N$. A negative impurity at $r = 0$ will repel the gas causing $n(0) < N$, Fig. 4.30(b) (cyan line). Beyond some distance r_h, the density will reach a constant level again and this level will be slightly higher than the original density, $N + \delta = n(r) > N$, $|r| > r_h$, so that the constraint $\langle n(r)\rangle = N$ remains preserved. Some charge has been depleted away from the impurity, thereby compressing slightly the gas in the rest of the system. If the depleted charge equals the charge of the impurity, the charge distribution (charge of the footballs plus charge of the impurity) in the system will remain constant in spite of non–constant $n(r)$ and the gas particles far away from $r = 0$ will not 'see' the impurity anymore. This is the case of ideal *screening*.

A classical *incompressible* liquid, say again charged footballs, will not react at all. Simply because it cannot change its density. Even though particles of the liquid feel repulsion from $r = 0$, the density will remain constant $n(r) = N$. We can also encounter a bit different behaviour, Fig. 4.30(b) (red line). Though the density decreases directly at $r = 0$, an oscillatory structure develops in $n(r)$, so that the integral density in the region $|r| < r_h$ remains as it was without the impurity. The density then also remains at its original value N beyond r_h. This is a non–ideal incompressible behaviour: at very short distances, the density can slightly vary, but averaged over distances of at least r_h, the density remains constant. Also, since not net charge was depleted from the region $|r| < r_h$, the impurity is *completely unscreened* on distances larger than r_h.

Compressible–like response as shown in Fig. 4.30(b) can be combined with quantum interferences (Friedel oscillations) and it is also possible to think of some overscreening effect which would lead to an oscillatory $n(r)$. This means the sole fact that $n(r)$ exhibits

oscillations does not necessarily have to imply incompressibility. A more reliable criterion is that the integral density over $|r| < r_h$ remains the same with and without impurity. This procedure is delicate in finite systems where r_h can be comparable to the system size.

The last Figure, 4.30(c), shows two possible ways of how responses change with system size. The right panel suggests that the state is not fixed to a particular size of the finite system and especially we could expect oscillations with period r_1 also in an infinite system. On the contrary, the left panel shows a state with no intrinsic length scale and e.g. the width of the peak is related to the (finite) size of the particular system.

Now, let us proceed to fractional quantum Hall states.

4.3.1 Electric (nonmagnetic) impurity

The effect of electric impurities on incompressible ground states has been under investigation since the historic times of the fractional quantum Hall effect. The main reason is that disorder (not too much — not too little) is essential for the occurrence of the integer quantum Hall effect (see Chap. 2.1 and references therein). For the fractional quantum Hall effect, two of the basic questions were, (i) how strong impurity potentials may be so that they do not destroy the gap and (ii) how does it change the ground state. Basic studies with the Laughlin state were performed as early as in 1985 [80], [109], [32].

Since we are limited to finite, and actually quite small systems, it is very daring to make here statements about the infinite 2D electron gas. When we speak about 'incompressibility' of some state we actually mean rather 'incompressible–like' in terms of Fig. 4.30. In fact, the main purpose of the following Subsections is to see how the polarized and singlet state respond to impurities in a *finite system* and later to compare them to the half–polarized state again in a *finite system*. We will focus on *short-range interacting* systems here.

The Laughlin state or the fully polarized $\frac{2}{3}$ state

The fully polarized $\nu = \frac{2}{3}$ state is a particle–hole conjugate to the $\nu = \frac{1}{3}$ Laughlin state in a homogeneous system (Subsect. 3.2.4). In this part we will study the latter state[27].

The response of a $\nu = \frac{1}{3}$ system to an impurity of the form Eq. 4.14, a δ–line along y, is shown in Fig. 4.31. Different curves show the ground state density $n(x)$ in systems of different sizes ($N_e = 4$ to 10 particles). The repulsive impurity is always located at $x = 0$ and it is 'weak', its strength is $\sim 10\%$ of the gap. These results agree very well with the densities presented[28] by Zhang *et al.* [109], who considered a δ rather than a δ–line

[27] Strictly taken, the particle–hole symmetry is lost when an arbitrary impurity is considered since the Hamiltonian is no longer translationally invariant. Differences between the $\nu = \frac{1}{3}$ and $\frac{2}{3}$ polarized states are however small if the impurity is weak. In particular, for inhomogeneities considered in this paragraph, it has been checked numerically that $n(x) - N_e$ are almost the same for the two states. Moreover, the larger N_e, the smaller are the differences.

[28] Note also that findings in Fig. 4.31 assume short–range interaction whereas Zhang *et al.* [109] and

impurity, though for $N_e = 4$ systems only. Comparison between rectangular, spherical and also disc geometry showed in all cases very similar behaviour [109].

Results in Fig. 4.31(a) support the conclusions of Zhang and Rezayi: the oscillatory response of $n(x)$ is size–independent and it has a period $r_1 \approx 2.5\ell_0$. The response, measured by $n(0)$, does *not* vanish with increasing system size but it decays with distance from the impurity. Comparing $n(x)$ in Fig. 4.31(a) to the model cases in Fig. 4.30(b), we may tend to classify the Laughlin state as an incompressible one. Incompressibility of the Laughlin state is locally not perfect, otherwise $n(x)$ would remain constant, at least in infinite systems. However, if some net charge were accumulated even in a larger region (of the order r_h) around $x = 0$, we would expect $n(x)$ at large distances to be consistently higher[29] than the no–inhomogeneity value $n(x) \equiv N_e$. This is not seen in Fig. 4.31(a).

Zhang *et al.* suggest that the observed response is a local charge density wave (Subsec. 3.2.5), a strong argument supporting this idea is given in the discussion below, point (iv). Under this view, it is not surprising that the response to a δ–line shown in Fig. 4.31(a) is very similar to the response to a δ–peak studied by Zhang: only the 'envelope function', not the wavelength depends on the particular form of the exciting impurity.

We should again add several comments:

(i) oscillations observed in $n(x)$ (Fig. 4.31(a)) are not related to Friedel oscillations. The latter appear in a Fermi gas where a sharp Fermi surface exists giving rise to interferences, just as in correlation functions of a free Fermi gas (Subsec. 4.1.1).

(ii) small wiggles on the $N_e = 4$ density in Fig. 4.31(a) are due to the center–of–mass (CM) part of the wavefunction. Being a finite size effect, they fall off rapidly with system size as we indeed see in Fig. 4.31(a). Cf. also Subsec. 4.1.4.

(iii) the ground state of the homogeneous system is triply degenerate in the CM part (Subsec. 4.1.4). This degeneracy is lifted by the inhomogeneity, but energy differences between these three states remain much smaller than their separation from the lowest excited states (for the inhomogeneity strength considered; cf. [109]).

The response $n(x)$ (of any of the three states) depends slightly on the position of the impurity within the elementary cell, but this dependence and also differences among the three states in energy and in $n(x)$ quickly vanish with increasing system size. In Fig. 4.31(a) always the impurity giving the strongest response in $n(x)$ was chosen.

(iv) Period of oscillations: As Rezayi and Haldane [80] note, numerical calculations as in Fig. 4.31 agree with results of the single mode approximation proposed by Girvin *et al.* [32]. The linear response function $\chi(q)$ (in the $\nu = \frac{1}{3}$ Laughlin state) is dominated by the magnetoroton collective mode around $q_0\ell_0 \approx 1.4$. Would it be $\chi(q) = \delta(q - q_0)$,

Rezayi *et al.* [80] considered Coulomb interaction.

[29] Recall the difference N to $N + \delta$ in Fig. 4.30(b). If just a unit charge is depleted from the impurity, then $\delta = 1/N$. In infinite systems, the difference δ will vanish, but data in Fig. 4.31(a) come from rather small systems $N \leq 10$ where δ is not negligible.

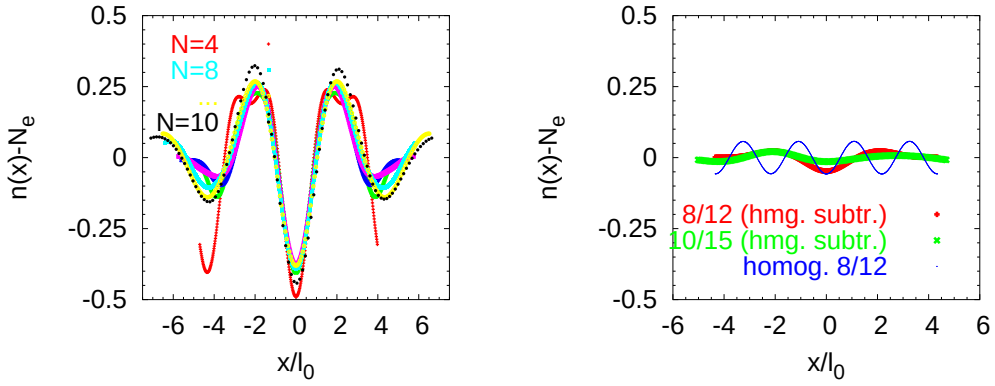

(a) The polarized state ($\nu = \frac{1}{3}$ considered, see text).

(b) The singlet state. The thin line shows the CM oscillations in a homogeneous system, thick lines show responses to an impurity with CM oscillations subtracted.

Figure 4.31: Polarized and singlet $\frac{2}{3}$ state and (non-magnetic) impurity in the form of a δ-line (along y). Normalized density along x plotted.

the density response to a point impurity potential would be $n(r) \propto J_0(q_0 r)$. This density profile looks like damped oscillations with the first node at $r = 1.7\ell_0$.

Regarding a more realistic profile of $\chi(q)$, this estimate for $n(r)$ is a very good approximation to $n(x)$ in Fig. 4.31(a)

As the purpose of the present work was to study systems with spin, we will now continue to spin singlet states at $\nu = \frac{2}{3}$. Some quite new results for the $\nu = \frac{1}{3}$ Laughlin state have been achieved by Müller [69].

The singlet state

The $\frac{2}{3}$ singlet ground state shows basically the same signs of incompressibility as the polarized state. The period of the density oscillations incurred by a δ–line impurity is almost the same ($r_1 \approx 2\ell_0$), and also in terms of classification of Fig. 4.30(b), the singlet state shows an incompressible–like behaviour (cf. discussion of the polarized state). The striking feature of the singlet state is, that the strength of the response is about an order of magnitude less than in the polarized state: thus in an 8–electron system, the density response is 'hidden' under the center-of-mass oscillations, Fig. 4.31(b).

This strong difference between the singlet and polarized ground states is unexpected since 'incompressibility' gaps of both states are similar.

This hints at unusual stability of the singlet state with respect to charged inhomogeneities.

In terms of perturbation theory, this is not due to energetic reasons but rather owing to small matrix elements of H_{EI} between the ground state and excited states. Energy of the first excited state, however, decreases when impurities are present and thus, in spite of the quite stable density of the GS, the gap will eventually collapse.

Regarding the response in systems of different size, we find a considerable attenuation when going from eight to ten–electron systems, Fig. 4.31(b). Nevertheless I assume that the response remains finite even in the thermodynamic limit. To support this hypothesis I would like to emphasis that the $N_e = 8$ (10) singlet state occurs in systems with $N_m = 12$ (15) flux quanta[30] and these are the two smallest systems considered in Fig. 4.31(a). For the these two systems we also observe a considerable attenuation of the $n(x)$ response when going from the $N_e = 4$ to $N_e = 5$ state (Fig. 4.31(a)) and this reduction in response is definitely only a finite size effect. As close as this analogy is, observations presented in Fig. 4.31(b) are not conclusive and an investigation of the singlet state in a larger system ($N_e = 12$) would be needed.

Let us just briefly mention, that non–magnetic impurities have no effect on the polarization of the singlet ground state.

4.3.2 Magnetic impurity in incompressible $\frac{2}{3}$ states

As far as spin polarized states are considered, magnetic impurities (Eq. 4.15) will not furnish us with any new information, see the comment on redundancy of some types of impurities, Eq. 4.15. Hence only the $\frac{2}{3}$ singlet ground state will be discussed here as the half–polarized states deserve to be considered separately (Subsec. 4.3.4).

Considering the *density*, Fig. 4.32(a), we find a yet weaker response than for non–magnetic impurities, Fig. 4.31(b). The response reminds of an incompressible system (in terms of Fig. 4.30(b)) and may remain finite in the thermodynamic limit, cf. discussion of non–magnetic impurities.

Polarization $n_\downarrow(x)/n(x)$ behaves quite differently, Fig. 4.32(b): the response is large and it looks compressible[31]. Electrons with 'correct spin' ($\uparrow$) accumulate around the impurity, $n_\downarrow(0)/n(0)$ drops from the homogeneous value (0.5) by as much as by 5%, whereas the average polarization off the impurity slightly increases so as to keep the overall average value 0.5 (as required by $S_z = 0$). This behaviour differs strongly from the density response (Fig. 4.32(b)).

It should also be noted that both density and polarization are here much less system–size dependent than in the case of non–magnetic impurities.

These are quite remarkable findings: it seems that the singlet state is *locally* much more 'incompressible' than the polarized state. On the other hand, the singlet state is relatively

[30] Number of flux quanta is a measure for system area $A = 2\pi\ell_0^2 N_m$, Eq. 3.6.

[31] Again in terms of Fig. 4.30(b). In particular, note that the polarization $n_\downarrow(x)/n(x)$ in Fig. 4.32(b) approaches ≈ 0.51 as we go 'far away' from the impurity, i.e. a different value than the polarization in the homogeneous case, 0.5.

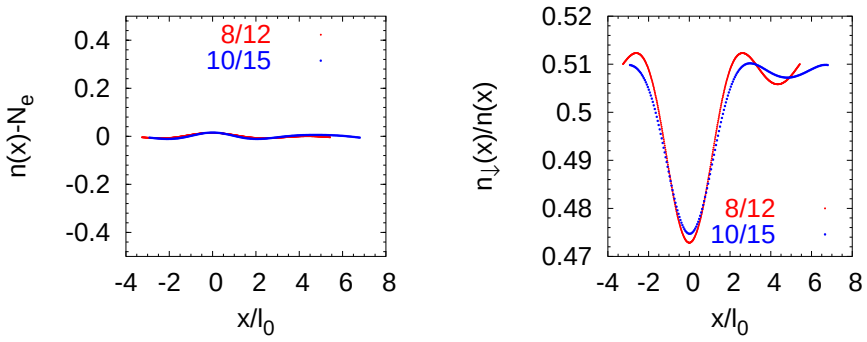

(a) Density. (b) Polarization.

Figure 4.32: Singlet $\frac{2}{3}$ ground state for an attractive magnetic impurity $H_{MI,\uparrow}$ (see Eq. 4.15) in the form of a δ-line (along y). Normalized density and polarization along x are plotted.

easily polarizable, at least compared to the rigid density[32]. This again confutes the picture of 'two uncorrelated $\frac{1}{3}$ Laughlin liquids, one spin up, another spin down' which we could wrongly infer[33] from the view of filled composite fermion LLs.

4.3.3 Integer quantum Hall ferromagnets

A brief introduction to integer quantum Hall ferromagnets (QHF) was given in Subsec. 3.6.

Here we will focus on the $S_z = 0$ sector in prototypes of Ising and Heisenberg QHFs with neglected LL mixing. These states ($S_z = 0$) are analogues of the half–polarized states at filling $\frac{2}{3}$, the explanation follows. Disciples of CF teachings deem the $\nu = \frac{2}{3}$ ground states to have $\nu_{CF} = 2$ completely filled CF LLs (Fig. 4.2). Transitions between the singlet and polarized GSs occur, when the $n = 0, \downarrow$ CF LL crosses the $n = 1, \uparrow$ CF LL. It is then plausible to neglect the low lying $n = 0, \uparrow$ CF LL and look only at the two crossing CF Landau levels. The two ferromagnetic Ising states — the singlet, and polarized electronic GS at $\nu = \frac{2}{3}$ — correspond to *all* CFs placed in the $n = 0, \downarrow$, and $n = 1, \uparrow$ CF LL, respectively. Hence the half–polarized state ($\nu = \frac{2}{3}$) corresponds to half–filled $n = 0, \downarrow$ and half–filled $n = 1, \uparrow$. Disregarding the fully occupied $n = 0, \uparrow$ CF LL, i.e. counting only particles in the two crossing CF LLs (in total N_e CFs), the ferromagnetic Ising states are $S_z = \pm N_e/2$ and the 'half–half' state is $S_z = 0$.

[32] If we assume the density in Fig. 4.31(b) to be the response of two independent liquids, then the polarization in Fig. 4.32(b) should be (i) smaller by a factor of five for $N_e = 8$ than what is observed and (ii) considerably smaller for $N_e = 10$ compared to the $N_e = 8$ case.

[33] Remind that in fact it is not the claim of CF theories, that particles of $n = 0, \uparrow$ and $n = 0, \downarrow$ CF LLs are uncorrelated.

In this Subsection we aim to study the same situation as the one occuring at the $\nu = \frac{2}{3}$ ground state transition (within the picture of crossing CF LLs) but for *electronic* Landau levels, i.e. with electrons instead of composite fermions. We therefore study a $\nu = 1$ [34] system with spin degree of freedom, where spin down (spin up) electrons lie in the $n = 0$ ($n = 1$) Landau level, respectively[35]. Without electron–electron interaction, these two Landau levels are set to equal energy so as to model the LL crossing. Mixing to the fully occupied $n = 0, \uparrow$ LL (as well as to all higher LLs) is neglected, since all these levels are well separated from the two crossing levels.

Heisenberg QHFs are not related to $\nu = \frac{2}{3}$ and we investigate them just for the sake of comparison between Ising– and some other type of QHF. In the integer QHE regime, Heisenberg QHF occurs e.g. when $n = 0, \uparrow$ and $n = 0, \downarrow$ LLs cross (and $\nu = 1$) as it is the case for instance at vanishing Zeeman splitting. With CFs, this happens at $\nu = \frac{1}{3}$, i.e. $\nu_{CF} = 1$ (cf. Fig. 4.2).

We will first briefly discuss homogeneous states in these QHF systems and then we will turn to their response to magnetic inhomogeneities (δ–lines).

Ising quantum Hall ferromagnet

There are two degenerate ground states of an Ising ferromagnet: both with $S = N_e/2$, one $S_z = N_e/2$ and another $S_z = -N_e/2$. Excited states are in general no eigenstates[36] to S^2 and may only be classified according to S_z. They are all well above the ground states (Fig. 3.13(b)) and in general, their energy grows with $N_e/2 - |S_z|$. In the following we will only speak about $S_z = 0$ states. The whole $S_z = 0$ sector is quite high in the complete spectrum. Unlike for a Heisenberg ferromagnet there is nothing like a $S = N_e/2, S_z = 0$ ground state for an Ising ferromagnet.

Low lying $S_z = 0$ states of the considered Ising QHF are apparently arranged into a flat dispersion branch[37], Fig. 4.33(a). The anomalous form of this branch in a $N_e = 8$ system, seems to be of finite–size origin, since $N_e = 10, 12$ and 14 spectra are similar to each other. States of the lowest branch have $\widetilde{k}^r$ of the form $(2\pi n/N_e, 0)$, $n = 0, \pm 1, \ldots, N_e/2$, or $(0, 2\pi n/N_e)$. This is in agreement with the symmetry between x and y (we consider a square elementary cell) and it shows that rotational symmetry is absent in the low energy sector[38]. The lowest branch flattens and becomes well separated from excited states with increasing system size, and the minimum energy remains at $\widetilde{k}^r = (0, 0)$. Also, other branches develop, the second lowest branch is described by $\widetilde{k}^r = (\pi n/N_e, \pm 2\pi/N_e)$ (plus the x–y symmetric partner) and minimum energy at points $(\pi, \pm 2\pi/N_e)$ ($N_e = 12$ spectrum in Fig. 4.33(a)).

[34] Again, we disregard the fully occupied $n = 0$, spin up level. Counting also electrons in this level, the total filling factor is two.

[35] Technically, this requires only implementing modified values of pseudopotentials, see Fig. 3.5.

[36] This is a consequence of the omission of the fully occupied $n = 0, \uparrow$ level.

[37] For a fully occupied Landau level, J 'coincides' with k_y^r. Precisely, $k_y^r = (N_e/2 - J)\sqrt{2\pi/N_m}$ for N_e even in the sense of Eq. 3.46. Centre–of–mass degeneracy is absent.

[38] Otherwise we would observe also states with $\widetilde{k}^r = (k_x, k_y)$, $k_x, k_y \neq 0$.

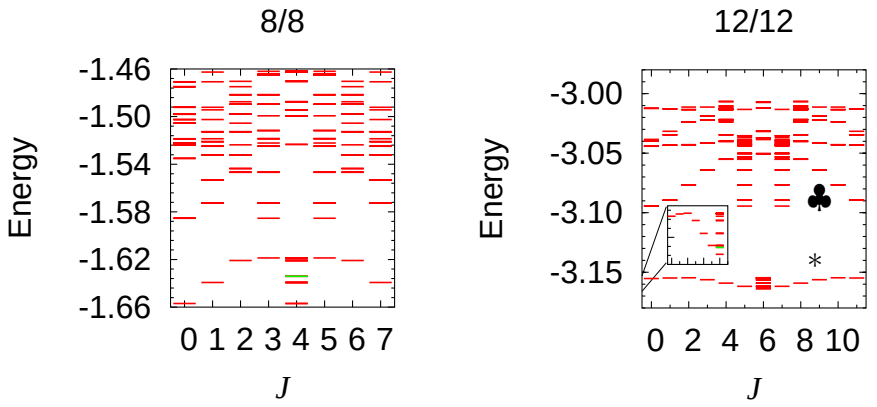

(a) Spectra. The lowest branch is marked by $*$, the second lowest by ♣. The green state does not belong to the lowest branch.

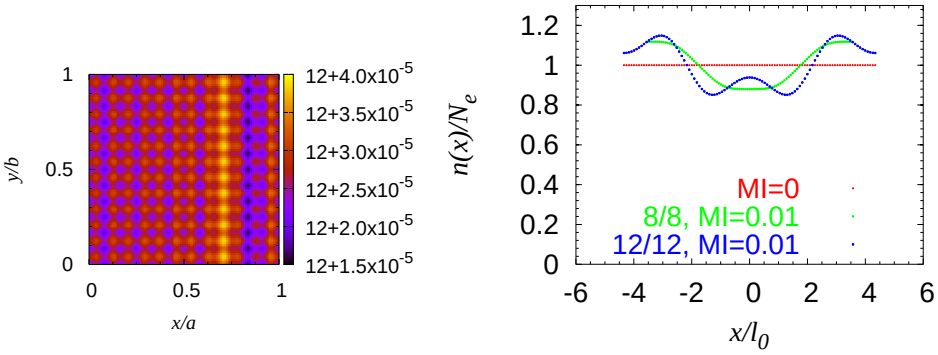

(b) *Left:* Density in the ground state, 12 particle system; *right:* change in density in response to a δ–line impurity (see Fig. 4.35(b).

Figure 4.33: Half–polarized states ($S_z = 0$) of an Ising quantum Hall ferromagnet. $\nu = 2$

Apart from these branches an isolated $\widetilde{k}^r = (0, 0)$ state is present (marked in green in Fig. 4.33(a)) and it is hidden within the branch. It could be that this state becomes the absolute ground state (and is separated from the lowest branch) in sufficiently large systems.

The flat branch is reminiscent of results of Rezayi[39] *et al.* [82] and could correspond to

[39]The cited work concerns the situation when the lowest and the third Landau levels of different subbands cross. Rezayi *et al.* had first to show that this system is an Ising QHF. See subsection 3.6 for more details. In the $S_z = 0$ sector of his system Rezayi *et al.* found a multiply (almost) degenerate ground state with $\widetilde{k}^r$ just of the sequence $(2\pi n/N_e, 0)$, similar as we see in Fig. 4.33(a) for $N_e = 12$.

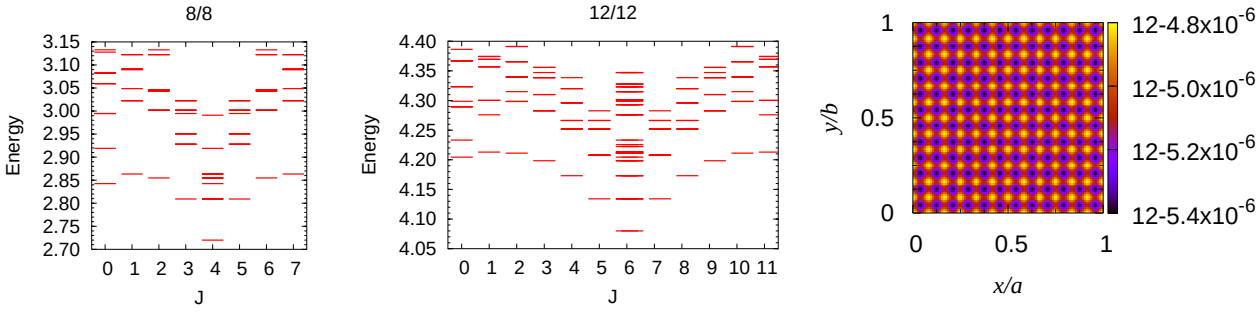

(a) Spectra.

(b) Density, 12 particle system.

Figure 4.34: Half–polarized states ($S_z = 0$) of a Heisenberg quantum Hall ferromagnet. $\nu = 1$

domain states, i.e. stripes along x or y with alternating spin polarization, in a system which does not prefer any particular domain size. The origin of the highly symmetric isolated ('green') state is unknown.

As it can be expected, low lying states have homogeneous density[40] and it is true even for the whole lowest branch, as an example we show density in the ground state ($k^r = 0$), Fig. 4.33(b). States in the second lowest branch show unidirectional charge density waves.

In summary, in a homogeneous Ising QHF (corresponding to $\nu = 2$, see description at the beginning of this Subsection) we observe

- a flat branch of low lying states, which could become degenerate in infinite systems. This first branch (Fig. 4.33(a)) probably consists of stripe domains[41] — or spin density waves — of all possible wavelengths $\lambda = a/n$, $n = 0, 1, \ldots N_e/2$ just as in the system studied in [82]. Contrary to isotropic states (like Laughlin liquid), the wave must be parallel to one side of the square elementary cell.

- second branch (Fig. 4.33(a)) with pronounced dispersion, which could be a charge density wave

- continuum of excited states above the two branches and

- another state, with high symmetry, $k^r = (0, 0)$, which lies among the states of the lowest branch.

[40] The anticipated domains would probably be visible first in correlation functions.

[41] In a homogeneous system, all these states have constant both density and polarization. Domains should be visible first in correlation functions.

Heisenberg quantum Hall ferromagnet

The situation here is quite different from the Ising ferromagnets. The Hamiltonian (Coulomb interaction projected to the lowest Landau level) conserves the total spin S and it even commutes with S^+ and S^- which change S_z while keeping the length of the total spin. The ground state is fully polarized, $S = N_e/2$, but its z–component of spin is arbitrary (Fig. 3.13(b)).

Looking at the sector $S_z = 0$, Fig. 4.34(b), the lowest state is thus the ferromagnetic $S = N_e/2$ state. Other low–energy states form again a branch, $\widetilde{k}^r = (\pm\pi n/N_e, 0)$ and $(0, \pm\pi n/N_e)$, $n = 0, \ldots, N_e/2$ (x–y symmetry present, rotational symmetry absent). Contrary to the Ising QHF, this branch does not seem to flatten. States in the branch fulfil $S = N_e/2 - n$: the ferromagnetic (ground) state is polarized and going up the branch, the polarization decreases. In this respect, the excitations of the lowest branch markedly differ from spin density waves. What we observe in the Heisenberg QHF are most likely states with n weakly interacting spin waves which were observed under the same conditions on a sphere by Wójs and Quinn [98].

Half–polarized QHF states and magnetic impurity

If a homogeneous state cannot be established and domains formation is more favourable, then no particular domain size is preferred. This is the central message of the following paragraph and it applies to both Ising and Heisenberg QHFs (described at the beginning of Subsection 4.3.3).

The two systems were subjected to a δ–line magnetic inhomogeneity, just as the incompressible singlet ground state in Subsec. 4.3.2. However, QHF systems and incompressible liquid states at $\nu = \frac{1}{3}$ or $\frac{2}{3}$ behave quite differently. Looking at a QHF and comparing the response in systems of different sizes, we observe no intrinsic length scale (Fig. 4.35). Rather, the form of the response reflects the size of the system (like in the left panel of Fig. 4.30(c)). This statement applies both to the Ising (Fig. 4.35(b)) and the Heisenberg QHF (Fig. 4.35(a)), where we show the polarization of the energetically lowest state in a system subject to the inhomogeneity.

It is also interesting to look at the *density* of the disturbed QHF states. The density of the Heisenberg QHF remains almost unchanged (it is constant) unlike the density of the Ising QHF state, Fig. 4.33(b) right. This is understandable: whereas in the Heisenberg QHF spin up and spin down one–particle states have exactly the same density[42], this is not the case for the Ising QHF. In that case, spin up and spin down states come from different Landau levels. Thus, even when the magnetic impurity shuffles the spin up and spin down particles somehow in the Heisenberg QHF, the density does not change.

Finally, we comment on densities in the inhomogeneous states (in the Ising QHF). Results shown in Fig. 4.33(b) belong to quite small systems (12 particles at most). In the largest system studied, we observe a maximum in the density direct at the position of the impurity

[42] And also wavefunction: both spin up and spin down states are from the lowest Landau level.

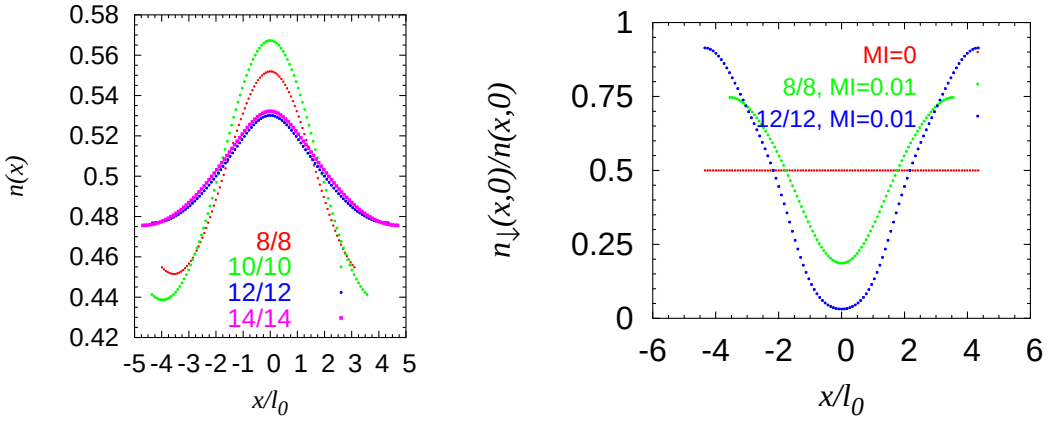

(a) Heisenberg QHF ($\nu = 1$).

(b) Ising QHF ($\nu = 2$, crossing of $n = 0, \uparrow$ and $n = 1, \uparrow$ levels.

Figure 4.35: Different quantum Hall ferromagnets (QHF), half–polarized states: polarization response to a magnetic δ-line impurity in systems of 8 and 12 particles.

($x = 0$) and the maximum approaches the value of density in a homogeneous system. With some imagination this allows for a hypothesis that — if domains are formed in an infinite system — the density will be inhomogeneous close to the domain boundary while remaining homogeneous inside a domain. However, we would have to study larger systems to confirm this speculation.

4.3.4 The half-polarized states

The inner structure of the half–polarized ($S = N_e/4$) ground state at filling $\frac{2}{3}$ is investigated in this Subsection. I would like to argue that this state (assuming short–range interaction) resembles rather the incompressible singlet and polarized ground states at $\nu = \frac{2}{3}$ than the Ising quantum Hall ferromagnet in the $S_z = 0$ sector as described in Subsection 4.3.3.

In this Subsection, by 'half–polarized ground states' we mean the 8– and 12–electron $S = N_e/4$ states GS_8 and GS_{12} as introduced in Sec. 4.2 (cf. correlation functions in Fig. 4.26).

The ground state in a homogeneous system has a nearly constant density (oscillations due to the center-of-mass part wavefunction are less than 0.1% in the 12–electron system). This changes when a weak δ–line magnetic impurity along y is applied: not only the polarization but also the *density* becomes inhomogeneous, Fig. 4.36. The first minima of $n(x)$ are at the same position $r_1 \approx 2.2\ell_0$ in the two system sizes considered and decaying oscillations are likely to follow at larger distances. Comparing the two system sizes in Fig. 4.36(a), we find a much weaker response in the larger system, but this still does not have to imply a vanishing response in an infinite system (cf. discussion of the singlet state in Subsec.

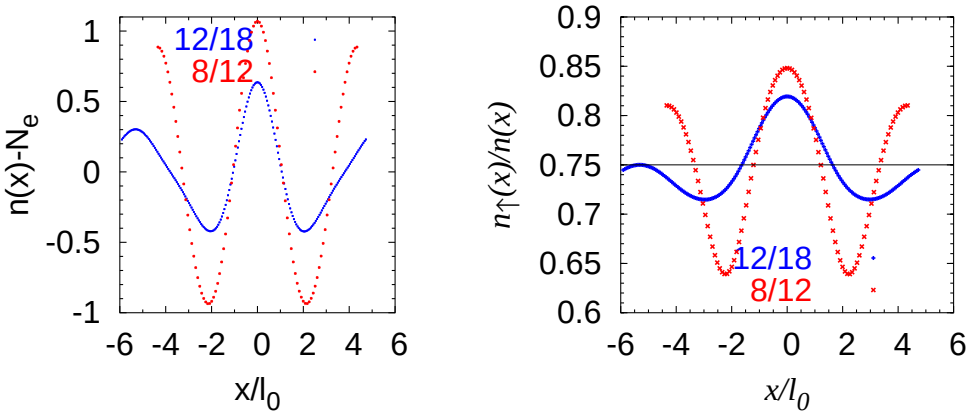

(a) Density.

(b) Polarization.

Figure 4.36: Half–polarized ground state ($S = N_e/4$) responding to a δ–line magnetic impurity, $H_{MI,\uparrow}$ (see Eq. 4.15).

4.3.1).

Unlike the Ising quantum Hall ferromagnet discussed in Subsect. 4.3.3, the half–polarized states seem to have an intrinsic length scale in $n(x)$ (of the order of r_1), Fig. 4.36(a). It is remarkable that this r_1 matches quite well the position of the first maximum in the density of the Laughlin state ($\frac{1}{3}$) responding to an impurity, Fig. 4.31.

Contrary to the density, the *polarization* does not show an intrinsic length scale as positions of the first minima in $N_e = 8$ and $N_e = 12$ systems mismatch considerably, Fig. 4.36(b). However, the polarization response here differs from the behaviour of the singlet state, Fig. 4.32(b). Rather, Fig. 4.36(b) suggests that $n_\downarrow(x)/n(x) \to 0.75$ as we go away from the impurity for the half–polarized states. This behaviour was classified as 'incompressible' in Fig. 4.30(b).

These observations bring me to the conclusion that the presence of the impurity will not lead to a splitting of the state into two domains (one with spin up, second with spin down), which we could expect for Ising QHF (Fig. 4.35). Rather it seems that an impurity will change the polarization of the system only locally, in an 'incompressible manner', Fig. 4.30(b). Finally, the density response has the same characteristic length scale as the singlet and polarized $\nu = \frac{2}{3}$ ground states and such a length scale is absent in the polarization (in agreement with behaviour of the singlet state, Fig. 4.32(b)).

A state with $S_z = N_e/4$ comprises of $\frac{1}{4}N_e$ electrons with spin down ('minority spins') and $\frac{3}{4}N_e$ electrons with spin up ('majority spins'). Since the two populations are not balanced, we may gain extra information by speaking to them separately. The simplest concept, assuming non–interacting electrons, would be: $H_{MI,\downarrow}$, $H_{MI,\uparrow}$ and H_{MI} (see Eq. 4.15) give rise to responses in ratio $\frac{1}{4} : \frac{3}{4} : 1$. *Very roughly*, this is indeed the case. Heights of the central peak ($x = 0$) for these three types of inhomogeneities are indeed approximately in

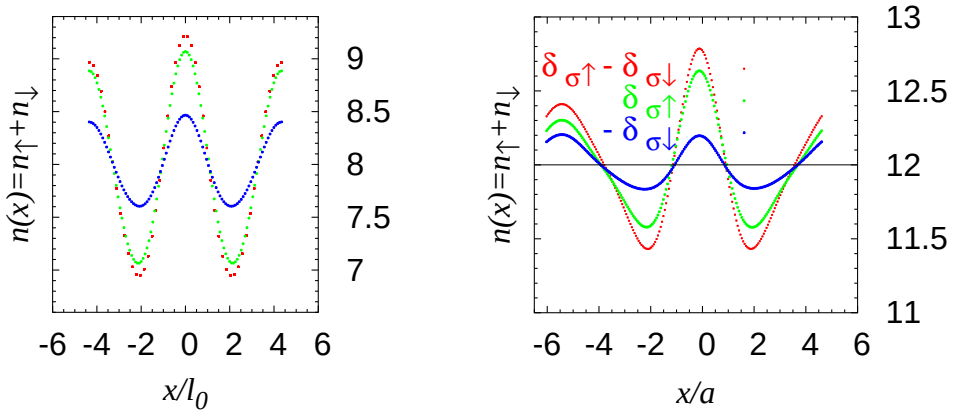

(a) 8 electrons, density.

(b) 12 electrons, density.

Figure 4.37: Half–polarized ground state ($S = N_e/4$) responding to a δ–line magnetic impurity. Different impurity types are considered: H_{MI}, $H_{MI,\uparrow}$ and $H_{MI,\downarrow}$ (see Eq. 4.15).

this ratio, both for the density and for the polarization, Fig. 4.37. In the following we will discuss investigations with spin–dependent perturbations in more detail.

Let us separate the density of majority and minority spins, Fig. 4.38. I would like to argue that the half–polarized state with N_e electrons consists of two coexisting and weakly interacting liquids: $N_e/2$ electrons in a fully polarized liquid (with $S_z^p = N_e/4$) and $N_e/2$ electrons in a $S_z^u = 0$ state. Minority spins are thus present only in the $S_z^u = 0$ liquid whereas majority spins occur in both of them. Concentrate on Fig. 4.38(c).

- Minority spins ($\downarrow$) react almost equally to $H_{MI,\uparrow}$ and $-H_{MI,\downarrow}$: they namely reflect only changes in the $S_z^u = 0$ liquid and there are as many up as down spins in it[43]. The combined effect of $H_{MI,\uparrow} - H_{MI,\downarrow}$ causes a response of about the sum of these two.

- Majority spins ($\uparrow$) react differently to $H_{MI,\uparrow}$ and $-H_{MI,\downarrow}$; keep in mind that $n_\uparrow$ reflects changes in both (polarized and $S_z^u = 0$) liquids. The latter impurity inflicts changes only on the $S_z^u = 0$ part, whereas the former impurity acts on both liquids. If both liquids would have the same sensitivity to the considered impurities, we could expect responses in ratio $4 : 3 : 1$ (H_{MI} to $H_{MI,\uparrow}$ to $H_{MI,\downarrow}$). The fact that responses observed in Fig. 4.38(c) (measured by the height of the central maximum) are in ratio $3 : 2 : 1$ could be an indication that the polarized liquid is less sensitive than the $S_z^u = 0$ liquid.

- Note also, that responses are the same (up to an inversion) for attractive and repulsive

[43] In fact, the $H_{MI,\uparrow}$ impurity influences also the polarized liquid component, but we cannot see it in the density of minority spins provided the two liquids do not interact appreciably.

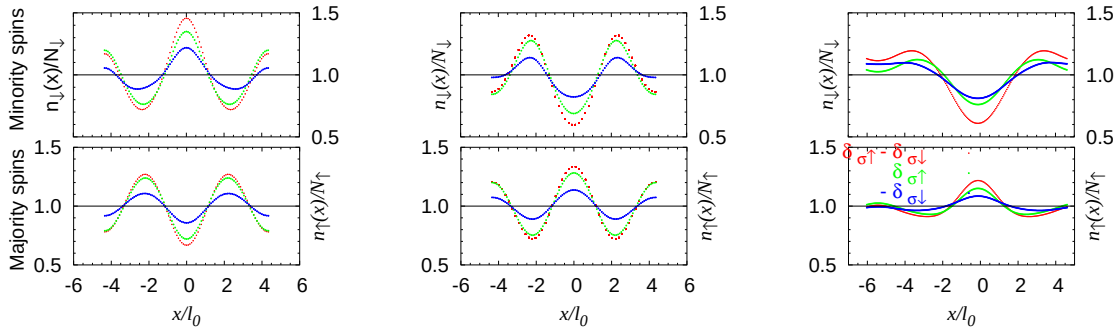

(a) 8 electrons, repulsive. (b) 8 electrons, attractive. (c) 12 electrons, attractive.

Figure 4.38: The same as Fig. 4.37, but the density is decomposed into the density of majority spins ($n_\uparrow$) and minority spins ($n_\downarrow$). By attractive (repulsive) is meant that the δ–impurity at $x = 0$ is attractive (repulsive) for the majority spin.

impurities, Fig. 4.38(a) and 4.38(b), provided the impurities are weak.

Studies of the eight electron half–polarized state, Fig. 4.38(b) is not in conflict with this interpretation, responses in densities are quantitatively different though. We should, however bear in mind that these systems (with primitive cell of size 12 flux quanta) correspond to the smallest system ($N_e = 4$) considered in Fig. 4.31 ($\nu = \frac{1}{3}$ state plus an impurity) and in that case finite size effects are already very strongly pronounced. Thus, the twelve electron system can be considered as the smallest system with finite size effects *not* playing a major role.

Conclusion

The hypothesis of the coexistence of the spin singlet and polarized liquids in the half–polarized states (HPS) seems to be supported. We have pointed out some similarities between the HPS and the former two incompressible states. In contrast, response to magnetic impurities seems to be different for the HPS and the Ising quantum Hall ferromagnet (in the $S_z = 0$ sector) which would be the direct counterpart of the HPS if composite fermions are substituted by electrons.

In general, it is not very surprising that electronic systems ($\nu = 2$ Ising QHF) differ strongly from the CF–counterparts. We have already seen this in correlation functions in Subsec. 4.1.1. However, the observed differences seem to be too deep to allow us to establish a relation between QHF states and the half–polarized states introduced in Sec. 4.2.

4.4 Deforming the elementary cell

In this Section we discuss another way of how to investigate fractional quantum Hall states: we will exactly diagonalize $\nu = \frac{1}{3}$ and $\nu = \frac{2}{3}$ systems in elongated rectangular elementary cells with dimensions a by b, i.e. those with aspect ratio $a : b > 1$. In this case, however, the area of the rectangle is always kept constant, $ab = 2\pi\ell_0^2 N_m$ (cf. Eq. 3.6), and therefore

$$ab = 2\pi\ell_0^2 N_m\,, \qquad \Rightarrow a = \ell_0\sqrt{2\pi N_m \lambda}\,,\ b = \ell_0\sqrt{2\pi N_m/\lambda}\,,\ \lambda = a : b\,. \tag{4.16}$$

What can we expect? In the first approximation, we would say (i) nothing happens for an isotropic state like the $\nu = \frac{1}{3}$ Laughlin liquid and (ii) crystalline or wave–like states will change both in energy and in density. The reason is, that structures in homogeneous liquid states (as we saw for example in correlation functions in Subsec. 4.1.1) are intrinsic and not incurred by the finite system size. That is why we expect it to change neither in energy nor in correlation function (at least on short distance) if a and b slightly change. On the other hand, an integer multiple of the period of a wave–like or crystalline state must be necessarily equal to a and/or b, hence by varying the aspect ratio we force it to change its period. In a classical crystal this means compression (or better deformation, since total 'volume' ab remains constant) and we expect it to cost energy.

During this investigation of $\nu = \frac{2}{3}$ systems I was motivated by the work of Rezayi *et al.* [82] who investigated one particular type integer quantum Hall ferromagnet. Their exact diagonalization on a torus showed an N_m–fold nearly degenerate ground state and the authors argued that these states comprised of stripes of alternating spin polarization (Subsec. 4.3.3) oriented parallel to one side of the rectangle, for example a. As they varied the aspect ratio, the states still remained degenerate[44], and their energy $E(\lambda)$ changed proportional to b. This was a strong argument for the stripe order, since then $\mathrm{d}E(\lambda)/\mathrm{d}b$ can be interpreted as energy per unit length of an interface between a spin up and spin down stripe.

With this in mind, let us look at the half–polarized states and see what we can learn about their nature. First, however, we start with their better understood relatives.

4.4.1 Incompressible ground states

As usual, we will start with $\nu = \frac{1}{3}$, being probably the best understood system. This will also be the only case where we will discuss Coulomb interacting systems, in the rest we will stay with short–range interacting systems.

Coulomb versus short–range interaction: $\nu = \frac{1}{3}$

The spectrum of a Coulomb–interacting system has a quite rich structure, Fig. 4.39(a). The ground state energy exhibits several minima as a function of the aspect ratio of the

[44] In fact, the degeneracy even improved: the small energy differences between the N_m states dropped.

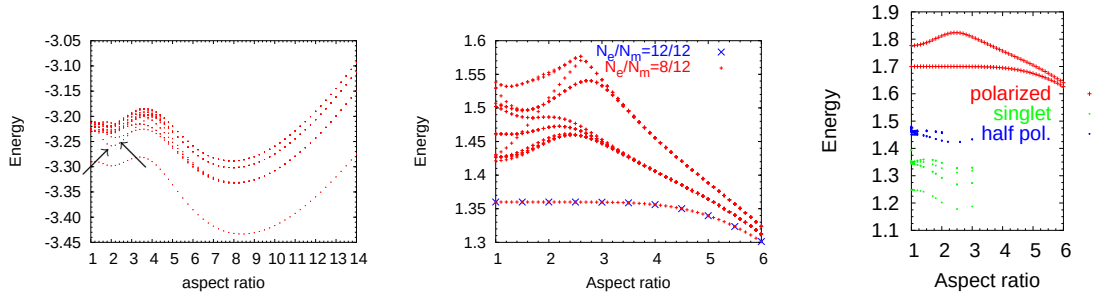

(a) Coulomb interaction ($\frac{1}{3}$).

(b) Short–range interaction ($\frac{2}{3}$). Blue crosses mark the energy of a full Landau level.

(c) Polarized, singlet and half–polarized states at $\nu = \frac{2}{3}$. Overview.

Figure 4.39: Spin polarized eight electrons at filling factor $\frac{1}{3}$ and $\frac{2}{3}$. Energy of the lowest states versus aspect ratio of the primitive cell. An overview of the polarized, singlet and half–polarized states in the same scale is presented in the last panel.

elementary cell; in fact even more structure seems to appear in larger systems, as far as I could infer from comparing 6, 8 and 10 electron systems. In the following, I will explain that this structure occurs mainly due to the long–range part of the Coulomb potential, it should be possible to describe it mainly by the Hartree part of the total energy or simply that it is due to formation of charge density waves (CDW) resembling Wigner crystals[45]. In a second step, we will discuss how correlations (and energy due to correlations) depend on the aspect ratio, Fig. 4.39(b).

Perhaps the best way to understand the energy–versus–aspect–ratio dependence of the Coulomb–interacting ground state is to look at two low excited states (marked by arrows in Fig. 4.39(a)). These two states are just the CDWs mentioned above and they look almost like Wigner crystals: one hexagonal, another square, as density–density correlation shows, Fig. 4.40. It is then no wonder that the energy of such states is minimal, when the aspect ratio matches its geometry. For eight electrons considered here, this happens for[46] $4d : 2d = 2$ and $4d : (2\sqrt{3}/2d) = 4\sqrt{3}/3$ for the square and hexagonal crystal, respectively. Perhaps the most apparent difference between a CDW and an (unpinned) Wigner crystal is that for the latter state we expect the correlation function to drop almost to zero between the 'lattice sites'. Obviously, this is not the case here, Fig. 4.40. This is also understandable: at filling factor $\nu = \frac{1}{3}$, the system is too densely populated, or mean interparticle distance is too small, $r_{mean}/\ell_0 = \sqrt{2\pi/\nu} \approx 4.35$ (cf. Eq. 3.6) to allow

[45] Differences between Wigner crystals and CDWs are discussed below. In fact, energy of the states in question (Fig. 4.40) will contain strong exchange contributions. Nevertheless, these states are very similar to the *classical* states which minimize the Coulomb energy.

[46] d is the 'lattice constant'.

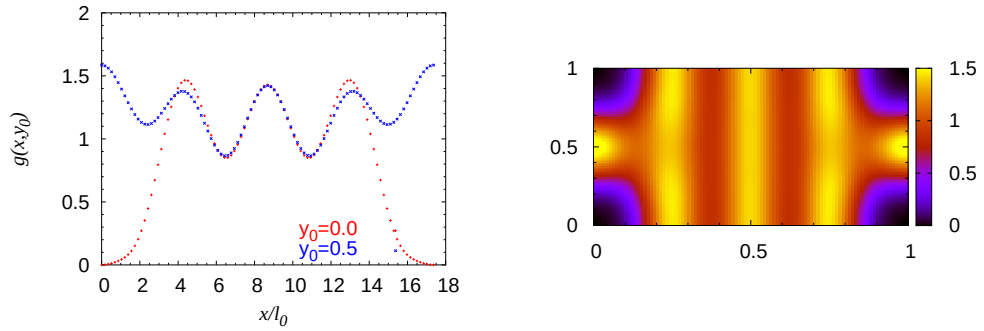

(a) The 'square' crystal state (aspect ratio 2).

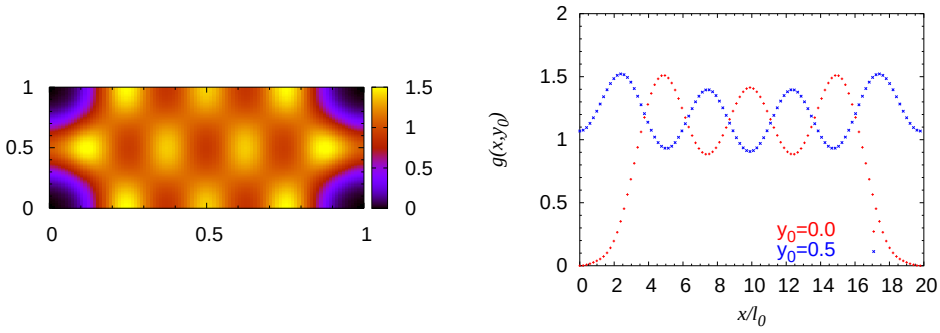

(b) The hexagonal crystal state (aspect ratio $4/\sqrt{3} \approx 2.31$.

Figure 4.40: Charge density waves resembling Wigner crystal states are among the lowest excitations in a Coulomb interacting $\frac{1}{3}$ system. Their energy is minimized (as a function of aspect ratio) when the elementary cell matches the crystal geometry. Correlation functions in eight–electron systems are shown, length of x– and y–sides corresponds to the particular aspect ratio.

the electron density (or correlation function) to vanish between two sites[47]. Even if we 'assembled a hexagonal Wigner crystal at $\nu = \frac{1}{3}$', the wavefunctions at neighbouring sites would strongly overlap and it is then more favourable for the electrons to retain something of the Laughlin correlations; as a result we obtain a CDW (or a 'strongly correlated crystal' [58]) like the state in Fig. 4.40(b). At lower filling factors, r_{mean}/ℓ_0 is larger and Wigner crystal states become possible. This can be interpreted as a quantum phase transition from liquid to solid as the filling factor is decreased and the extensive studies in this field suggest the critical value $\nu \approx \frac{1}{7}$, see Sec. 5.7 in Chakraborty [17] for a review.

The ground state (GS) energy reflects these geometrical conditions. This state also minimizes its energy when the square crystal can easily be formed, but at short distances it

[47] An electron *within the lowest Landau level* cannot be localized more strongly than on a length scale of the order of unity (magnetic length ℓ_0).

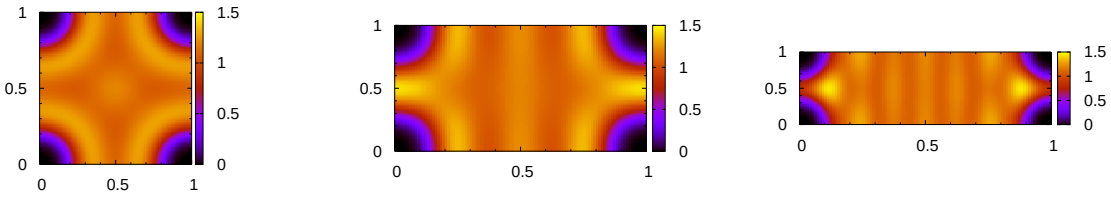

(a) Aspect ratio 1.00. (b) Aspect ratio 2.00. (c) Aspect ratio $2\sqrt{3} \approx 3.46$.

Figure 4.41: Evolution of the Laughlin state with aspect ratio of the elementary cell (Coulomb interaction). Correlation functions are shown.

quite strictly preserves the liquid–like correlations, Fig. 4.41: it is isotropic at least at short distances (in Fig. 4.41(b), the ring corresponding to the first maximum is round, not deformed; compare to Fig. 4.40) and also $g(r) \propto r^6$ (not obvious in Fig. 4.41). It seems plausible that the increase of GS energy around $a : b \approx 3$, Fig. 4.39(a), is due to the loss of isotropy at shorter distances: the ring of the first maximum in $g(r)$ disappears, Fig. 4.41(c); $g(r) \propto r^6$ however remains. It is important to know, that unlike the energy, the *structure* (correlation functions) of the ground state is quite insensitive to the type of interaction (Coulomb or short–range).

Let us now concentrate on short–range interacting states. The crystalline states disappear from the realm of low–energy excitations. The ground state energy is completely independent on aspect ratio, it is zero. This shows Figure 4.39(b); energies of fully polarized $\frac{2}{3}$ states displayed therein are equal to those of $\frac{1}{3}$–systems up to a constant shift[48] . In fact, the ground state is rigid in the following sense: a state can have zero energy only if there are three zeroes on the position of each electron in the wavefunction. By this (together with confinement to the lowest Landau level), the wavefunction is completely determined. It is even surprising, that given this, the ground state looks that similar to a CDW state at higher aspect ratios like the one in Fig. 4.41(c).

Assuming fully spin polarized electrons, $\frac{2}{3}$ and $\frac{1}{3}$ systems (e.g. 8/12 and 4/12) are particle–hole conjugated. Thus, spectra of these systems are identical up to a constant energy shift, which is just the Coulomb (or short–range interaction) energy of a completely filled lowest Landau level[49] (see Subsect. 3.2.4). In simple numbers, this is shown in Fig. 4.39(b): the $\nu = \frac{1}{3}$ Laughlin state has zero energy for any aspect ratio (not shown), the $\frac{2}{3}$ ground state energy is then simply just the Hartree–Fock energy of a completely filled Landau level.

[48]This constant depends on aspect ratio, but the dependence is imperceptible up to $a : b \approx 4$ (for 4 electron system).

[49]Note that this energy *varies* with aspect ratio (both for Coulomb and for short–range interaction). The common statement that interaction energy of a full LL is a constant is valid in a broad range of aspect ratios, but not everywhere. In Fig. 4.39(b), this holds up to $a : b < 4$.

Beyond $a : b \approx 4$, this energy is no longer constant, indicating that the deformation of the elementary cell becomes pathologic and latest at this point, such a model describes no longer a 2D system but rather an effective 1D system.

Consider $a/b \gg 1$. Then the N_e electrons are located on a very thin cylinder[50] of length $\propto \sqrt{a/b}$ (area of the cylinder is fixed by filling factor, $ab = 2\pi N_m$) and single electron states resemble 'rings on a pole'. The mean distance between electrons is then $\propto \sqrt{a/b}/N_e$ and Coulomb energy is then obviously proportional to $(a/b)^{-1/2}$. The increase of the ground state energy for very large aspect ratios, Fig. 4.39(a), is due to the repulsion between an electron and its own periodic image in the 'short–direction'.

Excited states are even more sensitive to deformation of the elementary cell. Energy levels group into branches beyond $a/b \approx 2$, Fig. 4.39(b), which, thinking of the effective 1D model, correspond to 0, 1, 2, etc. pairs of 'rings on pole' sitting at neighbouring sites. In figurative terms: there is no longer enough room for two electrons to be positioned in 'vertical' direction (along y axis, i.e. the shorter side of the elementary cell) except when they freeze into a crystal.

In conclusion, going beyond aspect ratio ~ 2 (in a $N_m = 12$ system) the system cannot be taken as a faithful model for an isotropic infinite system.

The singlet state

Apparently, the singlet ground state is more sensitive to varying the aspect ratio. Its energy changes at much smaller deformation than that of the polarized state, Fig. 4.39(c). However, comparison between systems of different sizes shows, that its energy is also constant provided that the aspect ratio is not too far from one and the system is large enough, Fig. 4.42. This is another hint at isotropy of the state. A crystalline state responds more strongly to a change of a/b, since this is in principle an attempt to compress the lattice in one direction while expanding it in the other direction: recall just the CDW states in $\nu = \frac{1}{3}$ systems marked by arrows in Fig. 4.39(a).

This is in agreement with a direct observation of correlation functions, Fig. 4.43. In particular, the ring structure in $g_{\uparrow\downarrow}(r)$ (or maximum at $r_0 \approx 3.4\ell_0$) remains preserved even for aspect ratios $a : b \approx 3$, Fig. 4.43(b). This is similar to how the ring structure of the first maximum was preserved in the deformed $\nu = \frac{1}{3}$ Laughlin state (Fig. 4.41(b)). Also, looking at $g_{\uparrow\uparrow}(x)$ and $g_{\uparrow\downarrow}(x)$ in the deformed singlet state, the *sum* of these two seems to remain constant beyond r_0 even in deformed systems (in spite of that $g_{\uparrow\downarrow}(x)$ decreases beyond $x = r_0$). This was just the conclusion in $a : b = 1$ systems (Fig. 4.7) and it suggests that the singlet state did not change much even in a quite strongly deformed system ($a : b \lesssim 3$). Moreover, given this is true, it allows us to use deformed systems to see what happens on a bit larger distances[51] than in a square cell.

[50] Such models were studied by Rezayi and Haldane [81].

[51] Maximum distance between two electrons in a deformed elementary cell, $\frac{1}{2}\ell_0\sqrt{2\pi N_m}(\lambda + 1/\lambda)$, grows with increasing λ.

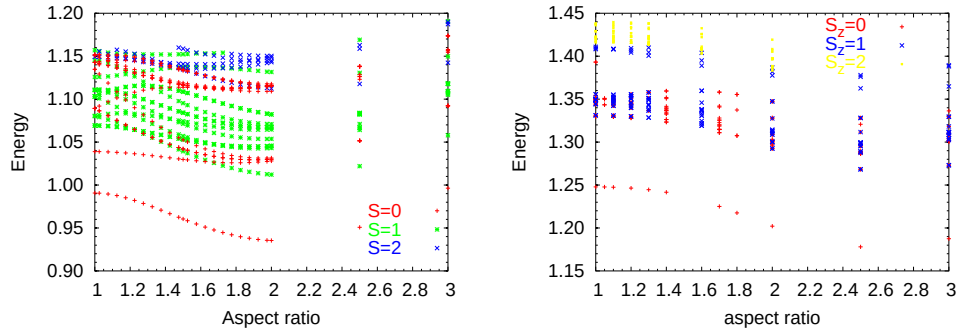

(a) Eight electrons.

(b) Ten electrons.

Figure 4.42: Low lying states at filling $\frac{2}{3}$ under vanishing Zeeman splitting versus aspect ratio of the primitive cell. Note that energy of the singlet ground state remains about constant for aspect ratios $\lesssim 1.4$ in the larger system.

Regarding the energy, which seems to react more sensitively to deformations than the correlation functions, the following speculation seems plausible. If the singlet state is a liquid of $\uparrow - \downarrow$ pairs of characteristic size $r_0 \approx 3.4\ell_0$ (cf. Subsec. 4.1.1), it ought to be more sensitive to aspect ratio variations than the Laughlin state just because such a pair in the $\nu = \frac{2}{3}$ singlet state is larger than a single electron in the $\nu = \frac{1}{3}$ Laughlin state.

4.4.2 Half-polarized states

The half–polarized states can be expected to suffer severely under the finite size of the system. Most obviously, a system with eight electrons contains only two electrons with minority spin. Contrary to fully polarized systems (where eight particles is already fair enough), it is thus the smallest system with $S = N_e/4$ where many–body effects can be studied.

Let us compare how systems of two different sizes respond to varying aspect ratio. In an eight–electron system, Fig. 4.44(a), there are four low lying states: the ground state at $a/b = 1$ with $\widetilde{k}^r = (\pi, \pi)$, a $(0, 0)$ state which becomes the ground state at $a/b > 1.5$ and a pair of degenerate states, $(0, \pi)$ and $(\pi, 0)$ ($\widetilde{k}^r$ is defined in Subsec. 3.5.2). The former two states are isotropic (and lie in high symmetry points of the Brillouin zone), the other two are spin–density waves in x and y direction, judging by the correlation functions (not shown). Moving away from aspect ratio one, degeneracy of the latter two is lifted — just as the 90 deg rotational symmetry of the elementary cell is broken — and the wave along x (the longer side) becomes energetically more favourable. It is quite conspicious that this state evolves parallel to the (π, π) state for aspect ratios above ≈ 1.4. For these values of $a : b$, the inner structure of these two states seems very similar, too.

In the low–energy sector, a $(0, 0)$ state is absent in a 12–electron system, Fig. 4.44(b).

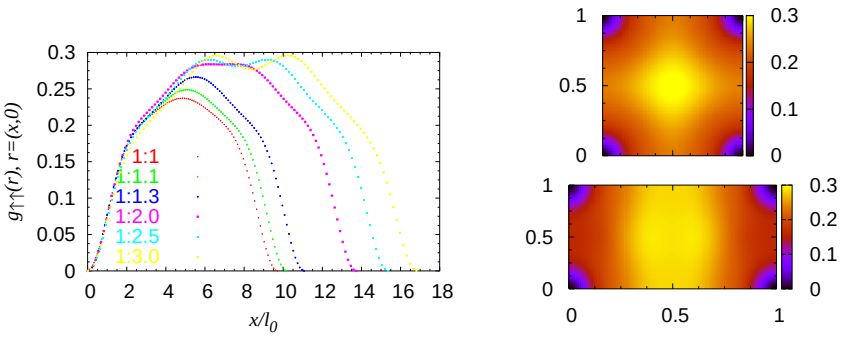

(a) Same spins.

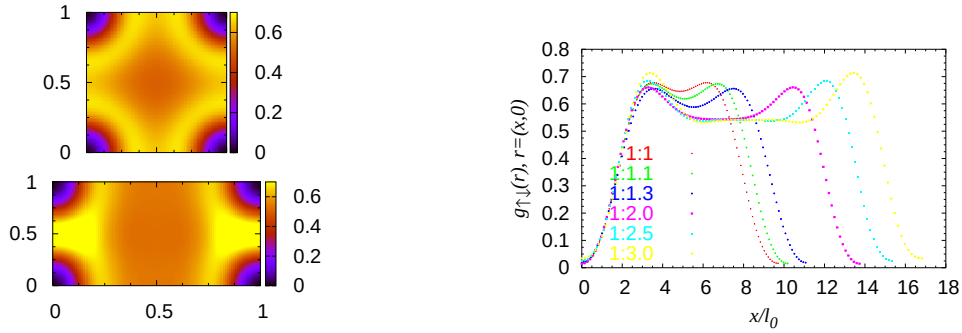

(b) Opposite spins.

Figure 4.43: The singlet $\frac{2}{3}$ state in elementary cells of different aspect ratios: density–density correlation between like and unlike spins (the two aspect ratios shown in 2D plots are $a : b = 1$ and 2).

In other respects, the situation is however quite similar to the smaller system. There is a well–separated (π, π) ground state in a square cell and this state becomes nearly degenerate with a $(0, \pi)$ state for aspect ratios $\gtrsim 1.4$. Also, the energy of these two states decreases with increasing aspect ratio and eventually reaches its minimum; in contrast to the smaller system, the minimum occurs later, at $a : b \approx 2.4$ (Fig. 4.44(b)) compared to ≈ 1.6 in Fig. 4.44(a), but this occurs also for the incompressible states, e.g. the singlet at $\nu = \frac{2}{3}$ (Fig. 4.42(a) vs Fig. 4.42(b)). The correlation functions of these two states, $(0, \pi)$ and (π, π), are similar to those of the $(0, \pi)$ and (π, π) states in the eight–electron system (not shown).

Now turn to the correlation functions of the $(0, \pi)$ and (π, π) states in a 12–electron system, Fig. 4.45. Both states are quite isotropic, for a square elementary cell[52]. However, already under slight variation of the aspect ratio, stripe structures parallel to the shorter side evolve ($a : b = 1.2$, Fig. 4.45(a)). In this respect, both states look quite similar (4.45(d)

[52]At a very close look, we find a slight x versus y anisotropy in the $(0, \pi)$ state.

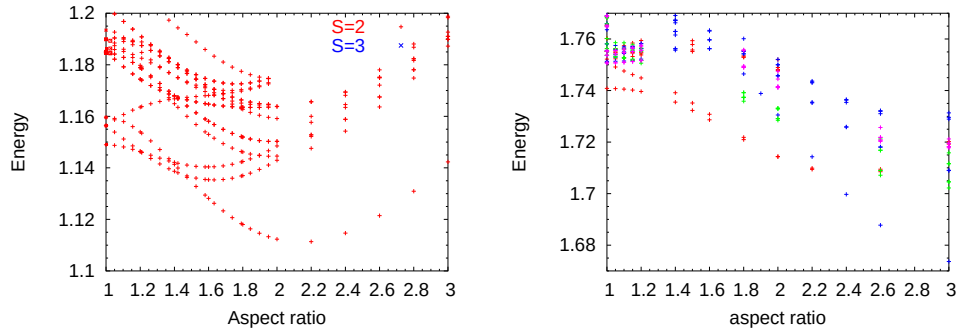

(a) 8 electrons.

(b) 12 electrons. Colours indicate different J's.

Figure 4.44: Half–polarized states ($S = N_e/4$) at filling $\frac{2}{3}$ versus aspect ratio. States with next larger spin are well above (out of scale here).

or compare Figs. 4.45(a) and 4.45(b)) and I would like to stress that the differences in the correlation functions between the isotropic (at $a : b = 1$) and the wave–like state ($a : b = 1.8$) are very large: both in isotropy/anisotropy and in the short–range behaviour (Fig. 4.45(d)). This is in a stark contrast to the behaviour of the incompressible states, e.g. the Laughlin state which preserves lot of its original isotropy even at $a : b \approx 2$ (Fig. 4.41).

These observations suggest the following interpretation: the half–polarized ground state at $\nu = \frac{2}{3}$ is an isotropic state which however inclines to the formation of a spin–density wave. The wave has the shortest period allowed by the number of electrons, i.e. it resembles an antiferromagnetic ordering ($\uparrow\downarrow\uparrow\downarrow\ldots$ rather than e.g. $\uparrow\uparrow\downarrow\downarrow\ldots$) as the correlation functions in the rightmost column in Fig. 4.45(a) suggest: since there are just three $\downarrow$–electrons in the system, we expect two[53] stripes in $g_{\downarrow\downarrow}(x, 0)$ in the case of $\uparrow\downarrow\uparrow\downarrow\ldots$ ordering[54]. However, the amplitude of oscillations in $g_{\downarrow\downarrow}(x, 0)$ is moderate (Fig. 4.45(d)) and hence we should rather term the state a 'spin density wave' than e.g. a state with stripe domains of alternating spin polarization.

Just on the basis of the present investigation, it is not clear whether in a large enough system, this spin wave state is the ground state, a low–energy excitation or it is degenerate with the isotropic ground state: even though the GS at $a : b > 1$ (spin wave) has a lower energy than the isotropic state at $a : b = 1$ (Fig. 4.44(b)), this does not say much about which state would be the ground state in a larger system. We saw a similar situation for the $\nu = \frac{1}{3}$ Laughlin state (Fig. 4.39(a)) or the singlet $\nu = \frac{2}{3}$ state (Fig. 4.42): the energy of the ground state was not at its minimum at $a : b = 1$, yet the isotropic (corresponding to $a : b = 1$) state is probably the ground state in the thermodynamic limit. The question how to decide which state — isotropic or anisotropic — will be preferred in infinite systems

[53] The third $\downarrow$–electron is just at the origin.

[54] In more detail, see Fig. 4.45(c): the minima/maxima in $g_{\uparrow\uparrow}(x, 0)$ match well with the maximum/minima in $g_{\uparrow\downarrow}(x, 0)$. In other words, spin up is followed by spin down.

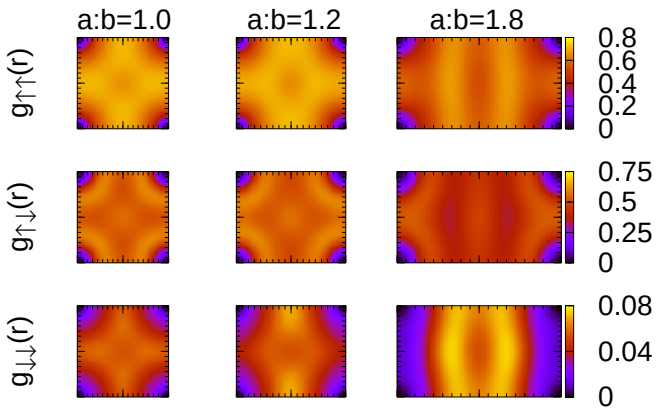

(a) The lowest state, $\widetilde{k}^r = (\pi, \pi)$.

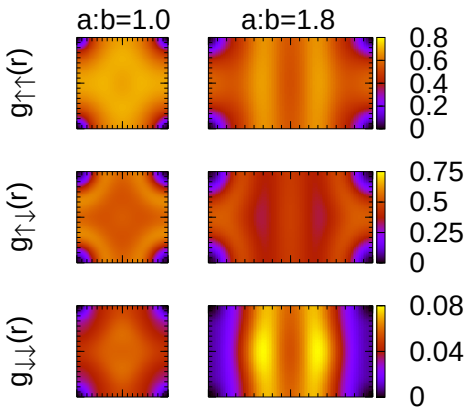

(b) The first excited state, $\widetilde{k}^r = (0, \pi)$.

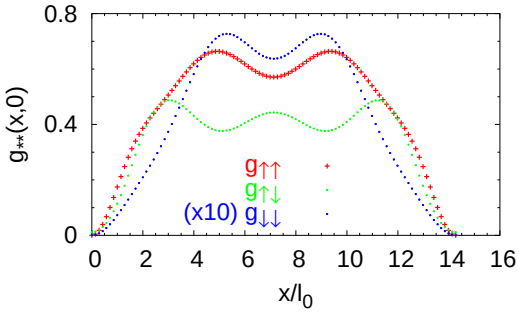

(c) $g_{\uparrow\uparrow}$, $g_{\uparrow\downarrow}$ and $g_{\downarrow\downarrow}$ of the lowest state in a deformed cell.

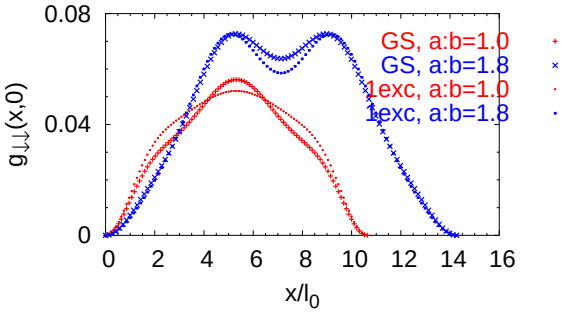

(d) $g_{\downarrow\downarrow}$, section along x for square and deformed elementary cell.

Figure 4.45: Evolution of two half–polarized states lowest in energy with growing aspect ratio of the elementary cell (12 electrons, $\nu = \frac{2}{3}$, short–range interaction). Correlation functions are shown.

remains open, but comparison between systems of more different sizes could be very helpful.

4.4.3 Conclusions

It has been demonstrated that isotropic states like the fully polarized or singlet incompressible $\nu = \frac{2}{3}$ ones tend to be insensitive to slight deformations. The 'response' was observed in the energy of the state and in its correlation functions, where we saw that especially the short–range behaviour remains basically unchanged. The insensitivity improves with increasing the system size (number of particles). We also registered some differences be-

tween the singlet and polarized state: in systems of equal size (area) the former state was disturbed by smaller deformations. This agrees with our previously mentioned hypothesis (Sec. 4.1) that the singlet ground state consists of pairs of electrons with unlike spin: since the typical size of such a pair was rather large ($3.4\ell_0$), the singlet state will suffer under the finite size of the system more than the polarized state where the 'relevant particles' are still electrons (whose 'size' is about ℓ_0)[55].

Investigation of the half–polarized state revealed that while the state is isotropic in a square cell, it tends to build a unidirectional spin density wave for aspect ratios not far from one. In this regime, it becomes also degenerate with *one* other state. Correlation functions of the both states (in deformed elementary cells) are quite similar to each other. We suggested that these states have an antiferromagnetic ordering in agreement with both correlation functions and wavevectors of these two states, $\widetilde{k}^r = (0, \pi)$ and (π, π). The question which state (isotropic or spin wave) is the real ground state in an infinite system remained unanswered.

4.5 Summary and comparison to other studies

4.5.1 The incompressible states: the polarized and the singlet ones

We studied various properties of the fractional quantum Hall states with spin degree of freedom at filling factors $\frac{1}{3}$, $\frac{2}{3}$ and $\frac{2}{5}$: correlation functions, response to magnetic and non–magnetic δ–line impurities or to deformation of the elementary cell. Briefly summarized:

- the results are in agreement with the concept of incompressibility of these states and also (in the case of $\nu = \frac{1}{3}$) with some earlier studies, e.g. [109].

- even though these states can be imagined as composite fermion systems with integer filling, the analogy to Landau levels completely filled with *electrons* can often be misleading. For instance: electrons of unlike spin are strongly correlated in the $\nu = \frac{2}{3}$ singlet state while they are completely uncorrelated in a $\nu = 2$ singlet state.

- we inferred pairing of spin up and spin down electrons in the $\nu = \frac{2}{3}$ singlet state. In the spin–unresolved density–density correlations, this state looks as if the two electrons in each pair were located exactly at the same position and the pairs then formed a $\nu = 1$ state. This conclusion was not possible for the $\nu = \frac{2}{5}$ singlet state thereby highlighting differences between fillings $\frac{2}{5}$ and $\frac{2}{3}$ which are very closely related within composite fermion theories.

[55] Imagine filling a container once with ten tennis balls ($\sim$ polarized state) or with five footballs ($\sim$ singlet state). Slightly deforming the container will probably affect the latter system stronger.

4.5.2 Half–polarized states

We identified a highly symmetric half–polarized state at filling factor $\frac{2}{3}$ which *could* become the absolute ground state in a narrow range of Zeeman energies (or magnetic fields). Such a state is completely unexpected in mean–field composite fermion theories. Extending earlier studies (exact diagonalization on a sphere) we showed that extrapolating the energy of this state from finite size exact diagonalizations to the thermodynamic limit is problematic and the question whether the half–polarized state really becomes the absolute ground state remains open.

Investigations on this state both for short–range and Coulomb interacting systems showed strong similarities to the incompressible singlet and polarized states at $\nu = \frac{2}{3}$. Consequently, we suggested that the singlet and the polarized state coexist within the half–polarized state. The state *might* be gapped for short–range interacting electrons but even if yes, it is probably not gapped for Coulomb interacting systems. These differences in spectra accentuate the fact that extrapolations to infinite systems should be taken with extreme caution. It also means, that the definition of the short–range interaction should be reconsidered as it may be an oversimplified model to study the half–polarized states (since the mean distance between two minority spin electrons is rather large, higher pseudopotentials should also be taken into account).

The half–polarized state forms a pronounced spin–density wave, or antiferromagnetic order, when anisotropy is introduced from outside (deformation of the elementary cell) but we could not conclude whether this spin–wave will be more energetically favourable than the isotropic form in much larger systems.

4.5.3 Half–polarized states: other studies

Let us first briefly recall other suggestions which appeared on the market since Kukushkin *et al.* presented their experiment showing a plateau of the polarization at one half (see Sect. 2.4). All works mentioned below can be applied both to filling factor $\frac{2}{3}$ and $\frac{2}{5}$ in principle. Unless necessary, we will not distinguish between these two cases.

Ganpathy Murthy [70] was attracted by the idea that correlations favour either the spin singlet or the fully polarized state. At the point where the two ground states cross (recall Figures 4.21 and 4.1), electrons could prefer to form a translationally non–invariant state consisting of regularly alternating areas of (locally) singlet and (locally) polarized states arranged into a partially polarized density wave (PPDW). He argues that this structure ought to have square rather than a hexagonal symmetry. The energy of the PPDW state is evaluated within the Hamiltonian theory of composite fermions[56] [72] and it is shown that the PPDW state is stable (against one–particle excitations) and lower in energy than the (homogeneous) singlet and polarized states. The period of the density wave should be $2\sqrt{\pi}\ell^*$ (see Eq. 3.39) which is $7.93\ell_0$ for filling $\frac{2}{5}$ and $6.14\ell_0$ for $\frac{2}{3}$. Charge modulation in

[56] It is basically a self consistent Hartree–Fock calculation with composite fermions which are treated in a concept admitting of vortices bound loosely to electrons.

the wave should be quite weak (in the order of 1%).

Apal'kov, Chakraborty, Niemelä and Pietiläinen [13] object that the energy of the PPDW is too high and claim that a homogeneous Halperin state in the two crossing CF Landau levels (see below) should have a lower energy[57]. As the mentioned Halperin state cannot account for the half–polarized states, Apal'kov *et al.* suggest another candidate for the half–polarized state, a non–symmetric excitonic liquid. They consider only the 'active levels' meaning the two CF Landau levels which cross. These (*two*) levels have total filling of *one*, i.e., there are only N_m electrons for N_m places in the $\uparrow$ level and N_m places in the $\downarrow$ level. By convention, they define a $\uparrow$–particle as an 'electron' and a missing $\downarrow$–particle as a 'hole'; an 'electron'–'hole' pair is an 'exciton' and a pair of a $\downarrow$–particle and a missing $\uparrow$–particle is 'vacuum'. Owing to the constraint $N_\uparrow + N_\downarrow = N_m$, one–particle states can be mapped onto a system consisting solely of 'vacua' and 'excitons'. The partial filling factor $N_\downarrow/N_m \in [0;1]$ then gives simultaneously the polarization and the number of 'excitons' (by N_m). Note, that 'excitons' are bosons by virtue of an integer spin.

From this viewpoint, the $\nu = 1$ quantum Hall ferromagnet (being described by the Halperin $(1,1,1)$ state) is a Bose condensate of excitons. In that case, all the excitons have angular momentum[58] $L = 0$ and they are noninteracting. Apal'kov *et al.* suggest that the half–polarized state at $\nu = \frac{2}{3}$ or $\frac{2}{5}$ could be a condensate of excitons with $L = 1$ (for which they call it nonsymmetric).

To support this idea, they perform exact diagonalizations in a $\nu = 1$ system with several model interactions (which are meant to describe the two — active — crossing CF Landau levels). These interactions are derived from the Coulomb potential with suppressed short–range component, probably (without justification) with the intention to describe interacting composite fermions. Stability of the half–polarized state is substantiated by showing that the energy versus polarization curve has a downward cusp at half–polarization. On the other hand, $g_{\uparrow\downarrow}(0) \neq 0$ in the half–polarized state indicates that 'excitons' in it do not have $L = 0$ [59].

Finally, the idea of Eros Mariani [65] should be presented. Parallel to the previous two works, the two 'active' crossing CF Landau levels are considered. An assumption is made that they both have a partial filling of $1/2$ rendering (after a *second* Chern–Simons transformation) two Fermi seas of 'free' composite fermions (of second generation). Mariani *et al.* show that interaction of these objects with fluctuations of the gauge field leads to an attractive effective interaction between particles with opposite spin and momentum. In analogy to superconductive pairing, this implies a gapped ground state. An estimation of the gap is given.

[57] Without invalidating the following results, this estimation seems to be however incorrect [71].

[58] This is most easily seen by the fact that $g_{\uparrow\downarrow}(0) = 0$: on an 'electron' ($\uparrow$ particle), there is no $\downarrow$ particle, i.e. there *is* a 'hole'. In an exciton (hydrogen atom), the only wavefunctions with $\psi(r = 0) \neq 0$ are those with $L = 0$. In turn, $g_{\uparrow\downarrow}(0) = 0$ follows from the fact that the Halperin state has maximum polarization and thus the spatial part of the wavefunction must be totally antisymmetric.

[59] The particular value of $L = 1$ is demonstrated by other means.

4.5.4 What are the half–polarized states then?

Presently, it is not clear which (if any) of the candidates proposed in the previous subsection describes the half–polarized reality. As Murthy correctly mentions, the final instance of judgement would be an exact diagonalization in a large enough system. Unfortunatelly, we dispose of systems not larger than 12 particles. Nonetheless let us compare the candidates with what was presented earlier in this chapter.

The downward cusp in energy–versus–polarization dependence cannot be assured by the calculations presented here. However, if the lowest half–polarized state indeed becomes the absolute ground state at the transition between the singlet and polarized state (see extrapolations in Fig. 4.22), the cusp is likely to be present. In the other case, it will turn into an upward cusp, as the calculated spectra suggest.

Results presented here indicate, that the half–polarized ground state ($\frac{2}{3}$) has $(\widetilde{k}^r_x, \widetilde{k}^r_y) = (\pi, \pi)$ and that it shows similarities to the singlet and polarized ground states (Fig. 4.24). In particular $g_{\uparrow\downarrow}(0) \approx 0$, which is in contrast with the model of a nonsymmetric exciton liquid (cf. the correlation functions in [13]). Comparison between short–range interaction and Coulomb half–polarized states (Fig. 4.2.6) suggest that, similar to the Laughlin state, the short–range part of the interaction plays the major role. From this point, the model discussed by Apal'kov *et al.* [13] seems to be more appropriate rather for some other systems.

Positioning of the half–polarized state out of the centre of the Brillouin zone could be an indication that it is indeed a standing wave. This is also supported by spectral properties when the elementary cell is deformed (Fig. 4.44): the two lowest states becoming degenerate at aspect ratios larger than 1.4 could be a charge/spin–density wave (note also the correlation functions, Fig. 4.45). The fact, that the energy of the ground state lowers with increasing aspect ratio could indicate that this state is more stable than an isotropic one. However, caution is advised here, since the singlet incompressible ground state does the same (Fig. 4.42) while its isotropic form is the true ground state.

Theory of the 'superconductive' pairing was not addressed so far. Comparisons on the level of correlation functions, possibly in k^r–space, are in principle possible, but quite complicated because of the two Chern–Simons transformations involved.

5 Quantum Hall Ferromagnetism at $\nu = \frac{2}{3}$?

5.1 Transition between the singlet and polarized incompressible ground states

Also this Chapter starts from the fact that there are two distinct ground states at filling factor $\frac{2}{3}$: the spin–singlet and the fully polarized one. Their structure was studied in Chapter 4 and we also recalled their interpretation in terms of composite fermions (Fig. 4.1). Whichever of these two becomes the absolute ground state depends on the Zeeman splitting which favours spins aligned parallel to magnetic field. The singlet state was the lowest in energy for vanishing Zeeman splitting. However, increasing the Zeeman splitting, its energy remained unchanged while the energy of the fully spin polarized state decreased and eventually this other state became the absolute ground state. This simplest scenario, sweeping the Zeeman energy while magnetic field is kept constant, is not very usual, albeit it is experimentally possible (Subsect. 2.3). However, even if we simply sweep the magnetic field (and keep constant filling $\nu = \frac{2}{3}$ which requires a simultaneous change of the electron density), the Coulomb energy of the singlet state changes $\propto \sqrt{B}$ and that is slower than the Zeeman energy of the polarized state in the limit of large B; the qualitative discussion above is thus still valid. The total energy bilance of the two ground states (in SI units) is thus

$$\begin{aligned} \text{polarized:} \qquad & E_p(B) = \frac{e^2}{4\pi\varepsilon\ell_0} E_p^C - g\mu_B N_e B = -|C_p|\sqrt{B} - |D_p|B\,, \\ \text{singlet:} \qquad & E_s(B) = \frac{e^2}{4\pi\varepsilon\ell_0} E_s^C = -|C_s|\sqrt{B}\,, \end{aligned}$$

where N_e is the number of particles and $E_p^C > E_s^C$ are the total Coulomb energies in units $e^2/4\pi\varepsilon\ell_0$ (as calculated by exact diagonalization, for example; not per particle). Obviously, $E_p(B) < E_s(B)$ for B large enough. What the critical field B_c is, where both energies are equal, depends obviously on $(E_p^C - E_s^C)/N_e$. This quantity is accessible only numerically and it depends on N_e although we may hope that it stays nearly constant for N_e large enough.

Figure 5.1 demonstrates this singlet to polarized transition for $4, 6, 8$ and 10 Coulomb–interacting electrons on a torus. Note that energy units in Fig. 5.1, $e^2/(4\pi\varepsilon\ell_0) \propto \sqrt{B}$,

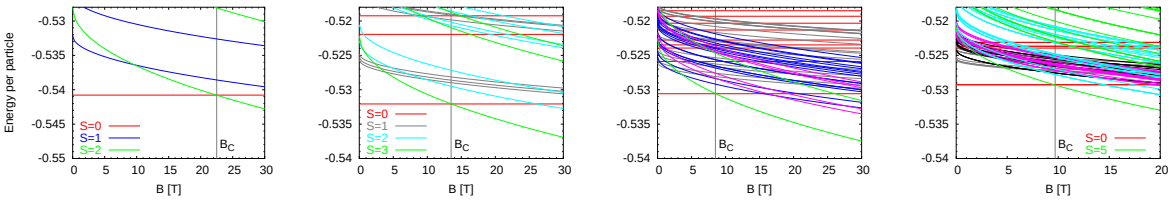

(a) $N_e = 4$ (b) $N_e = 6$ (c) $N_e = 8$ (d) $N_e = 10$

Figure 5.1: Energies of low lying states at $\nu = \frac{2}{3}$ in a homogeneous Coulomb–interacting system with Zeeman field: transition from an incompressible singlet ground state to a fully polarized incompressible ground state. Different numbers of particles in a square with periodic boundary conditions are considered, the scenario is however the same in all cases.

change with magnetic field. In these units, the potential (Coulomb) energy of all states stays constant (singlet state) and Zeeman energy scales as $\propto e^2/(4\pi\varepsilon\ell_0) \cdot \sqrt{B}$.

A close look at Fig. 5.1 shows that the magnetic field B_c, at which the ground state transition takes place, varies non–monotonically. However, an extrapolation of energies of the two ground states to $1/N \to 0$ allows for a rough estimate of $B_c \approx 7$ T in an infinite system (see also Subsect. 4.2). This is in quite good agreement with experiments [55], even though in some samples B_c as low as ≈ 2 T was observed [56], [90]. This could be due to deviations from an ideal 2D system (see Subsect. 5.2).

In following Sections I will investigate the ground state and low–lying excited states near to this transition. The central question is whether there are some spin structures in these states. In particular, I was looking for signs of domain formation. Let me explain why.

The ground state is always either a singlet or fully polarized in a homogeneous system; the energies of these two states are equal at the transition. This is similar to an Ising ferromagnet, if we label the polarized state by pseudospin up and the singlet state by pseudospin down. In an infinite system at non–zero temperature, however, the Ising ferromagnet prefers a state with domains (some with (pseudo)spin up, some down) to the two homogeneous states. First because entropy of the former is higher (cf. [47]) and second because the total magnetization of a domain state is approximately zero (while, locally, most spins are parallel to their neighbours) thereby minimizing the energy of magnetic stray fields [14]. None of these two mechanisms was included in the studied model of a $\nu = \frac{2}{3}$ system, nevertheless, I asked how the system will respond if such a 'domain–inducing' mechanism is modeled by a magnetic inhomogeneity. Will the ground state split into regions of different spin polarization? With this question in mind, the inhomogeneity should prefer the singlet ground state in one part and the polarized ground state in another part of the system.

From the experimental side, there are quite strong hints at ferromagnetism (Sect. 2.3). Hysteresis, saturation (in time) of magnetoresistance, Barkhausen jumps etc. hint at ferromagnetic states with domain structure near the transition point. The big challenge

for a theorist is thus either to support these views or give an alternative explanation of the observed phenomena.

5.2 Attempting to enforce domains by applying a suitable magnetic inhomogeneity

This and the following sections will be concerned with various attempts to induce the formation of domains close to the transition point. At the beginning we must discuss (i) how to enforce domains (what to add to the Hamiltonian, form of inhomogeneity) and (ii) how to detect them (which quantities should be observed).

5.2.1 First attempt: the simplest scenario

The simplest scenario is sketched in Fig. 5.2. In the homogeneous case, the Hamiltonian consists of two terms

$$H = H_{Coul} + H_{Zeeman} = \frac{e^2}{4\pi\varepsilon} \sum_{i<j} \frac{1}{|\mathsf{r}_i - \mathsf{r}_j|} + \sum_j g_0 \mu_B B \sigma_z^j \,, \tag{5.1}$$

the Coulomb interaction and the Zeeman term. If the Coulomb energy is fixed, energies of the two incompressible ground states can be shifted with respect to each other by varying the Zeeman term. If B is fixed at $B = B_c$ (i.e. the two ground state have the same energy), the Zeeman energy can be still varied by means of the g factor. Decreasing g slightly, the singlet state will become the absolute ground state, increasing g the polarized state will prevail.

The idea of a 'domain–enforcing' inhomogeneity is to the turn the constant g into $g(x_j) = g_0 + g_1(x_j)$ in Eq. 5.1 and $g(x) > g_0$ in one part of the system whereas $g(x) < g_0$ in another. Or, speaking in terms of Fig. 5.1: we slightly[1] modulate the magnetic field B: in one part of the system we consider $B > B_c$ and in another $B < B_c$.

The full Hamiltonian to consider is thus

$$\begin{aligned} H &= H_{Coul} + H_{Zeeman} + H_{MI} \,, \qquad (5.2) \\ H_{MI} &= \sum_j g_1(x_j) \mu_B B \sigma_z^j \,, \quad \langle \varphi_i | H_{MI} | \varphi_j \rangle = \delta_{ij} E_{MI} \begin{cases} i = 0, 1, \ldots, \frac{1}{4} N_m & : \quad 1 \\ i = \frac{1}{4} N_m + 1, \ldots, \frac{3}{4} N_m & : \quad -1 \\ i = \frac{3}{4} N_m + 1, \ldots, N_m & : \quad 1 \end{cases} \end{aligned}$$

where $|\varphi_j\rangle$ is a one–particle state localized around $x = (j/N_m)a$ (Eq. 3.40). This roughly corresponds to $g_1(x)$ having a 'rectangular wave' form ($g_1 = 1$ for $0 < x < \frac{1}{4}a$ and $\frac{3}{4}a < x < a$ and $g_1 = -1$ for $\frac{1}{4}a < x < \frac{3}{4}a$).

[1] By slightly we mean that only the spin degree of freedom is affected, not the orbital. This is then of course just an approximation.

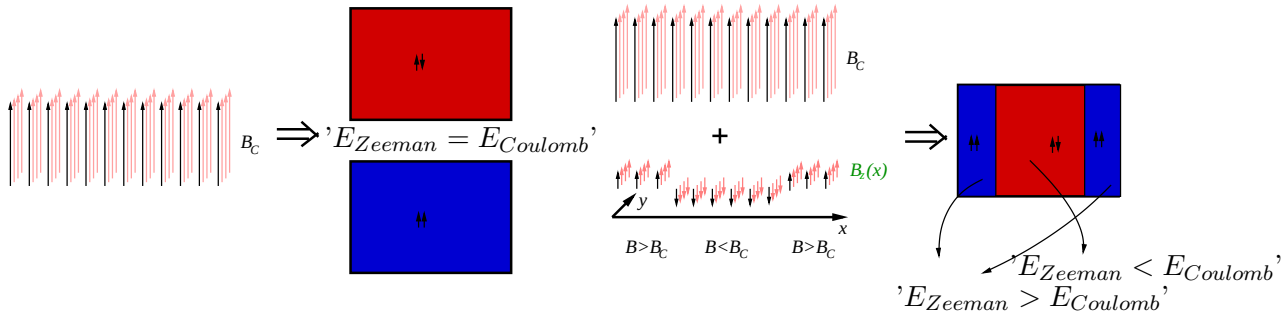

(a) Homogeneous system.

(b) System with 'domain-enforcing' inhomogeneity.

Figure 5.2: An idea of how to enforce domains at the crossing of singlet and polarized ground states of $\nu = \frac{2}{3}$. An average Zeeman field is chosen so that the both homogeneous states have the same energy. Modulation of the Zeeman field prefers the singlet state 'in the middle' and the polarized state 'at the edges' (note however the periodic boundary conditions).

Basic result of this model is: the ground states slightly change in accord with the inhomogeneity and nothing peculiar happens near the transition. As we sweep the magnetic field through $B = B_c$, the singlet state evolves 'smoothly and monotonously' into the polarized state, without any remarkable intermediate states, even in the presence of a weak inhomogeneity.

Typical results backing this conclusion are shown in Fig. 5.3. A magnetic inhomogeneity (Eq. 5.2) was applied to a ten–electron Coulomb–interacting system and its strength E_{MI} was chosen to be $\sim 10\%$ of the incompressibility gap. Regarding the ground states and the gap, the spectrum remains virtually unchanged (see Fig. 5.9(a) for a comparison of the spectra between homogeneous and inhomogeneous systems). Looking now at the singlet and polarized ground states, we find a spatially varying spin polarization[2] $n_\uparrow(x)/n(x)$, Fig. 5.3(a). However, the mean values of the polarization still remains at 0.5 (1) as it was in the homogeneous singlet (polarized) state, Fig. 5.3(a), leftmost (rightmost) inset. The polarization of the 'transition state' has a mean value of 0.75, i.e. just in the middle between the polarized and the singlet state. This is not surprising, since the 'transition state' was taken to be a symmetric linear combination of the two crossing states (see Subsect. 5.2.2). What is more interesting, is the *variation* of the polarization around the mean value (Fig. 5.3(b)): in this point, the 'transition state' lies just between the singlet and polarized states. Contrary to what we observe in Fig. 5.3(a) (middle inset), formation of domains near the transition would mean that the polarization of the transition state should vary between 0.5 and 1.

[2]Throughout this Chapter, we will refer to $p(x) = n_\uparrow(x)/n(x)$ as to polarization. In the literature, another definition is more common, $P(x) = [n_\uparrow(x) - n_\downarrow(x)]/n(x)$, both quantities are, however, equivalent: $P(x) = 2p(x) - 1$. In other words, p (our definition) ranges from 0 to 1 whereas P ranges from -1 to 1.

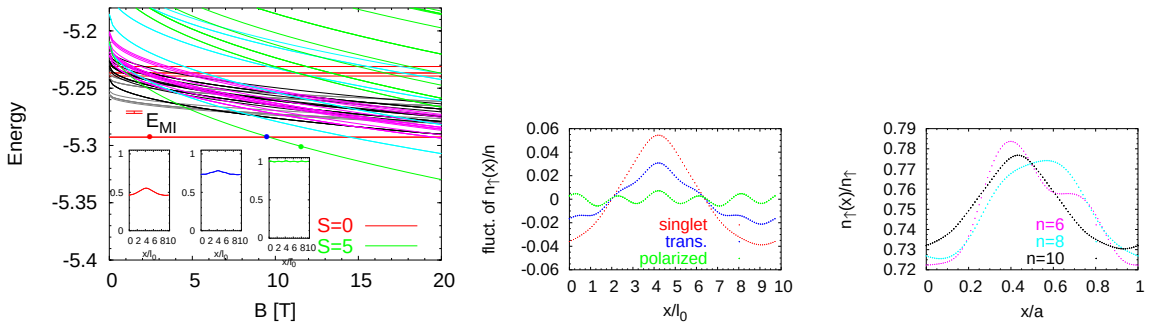

(a) An overview: spectrum and (inset) polarizations of the singlet, transition and polarized ground state (left to right).

(b) Polarization of the three states in detail ($n = 10$). Mean polarization subtracted.

(c) The transition in systems of different sizes.

Figure 5.3: Response of a ten–electron system to a weak ($E_{MI} = 0.002$) magnetic inhomogeneity of the form given in Eq. 5.2. No sings of domain formation observed: the transition state does not respond stronger than the incompressible states.

It could be that the system is simply too small for domains to evolve near the transition. However, this does not seem to be the case, since the response to the inhomogeneity does not grow with increasing system size but rather stays about the same (Fig. 5.3(c)).

Naturally, it could be that just the particular parameters of the model presented in Fig. 5.3 were chosen unluckily. Let us therefore discuss the inhomogeneous $\nu = \frac{2}{3}$ systems more thoroughly.

5.2.2 Turning crossing into anticrossing: inhomogeneous inplane field

At $B = B_C$ (blue point in Fig. 5.3(a)) there is actually a crossing between the singlet and polarized ground states rendering the transition jump–like just as in a homogeneous system. For the transition state (the blue curve in Fig. 5.3(b)), we took a fifty-fifty linear combination of these two ground states. We can say that the transition occurs in an infinitesimally small interval of magnetic field around B_c.

In a realistic system, the transition is unlikely to happen all at once in the whole system. I can imagine two mechanisms which cause a more continuous transition in a finite interval of B.

- 'weak inhomogeneities': spectrum (as a function of B) looks basically the same as in Fig. 5.3(a), *but* there is an anticrossing at $B \approx B_C$.
- 'strong inhomogeneities': the energy gap between the pair of the crossing ground states and the excited states at $B = B_c$ (Fig. 5.3(a)) is reduced compared to the incompressibility gaps of the singlet and polarized ground states far away from B_C,

i.e. for $B \to 0$ and $B \to \infty$. Under influence of stronger inhomogeneities, it could be that some originally excited state (or more states) become ground state around $B \approx B_C$ while singlet and polarized incompressible states remain lowest in energy only far away from B_C. If this turns out to be the case, it could be that more states (possibly of different S_z) can be mixed by the inhomogeneity, eventually rendering the ground state compressible.

In this Subsection we will discuss the former possibility, the latter will be the topic of Subsect. 5.2.3.

The ground state transition in Fig. 5.3(a) is a crossing even in the presence of the magnetic inhomogeneity H_{MI} (Eq. 5.2) because the symmetry of H_{MI} is too high and it does not mix the two crossing ground states. In particular, $[H_{MI}, S^2] \neq 0$ but $[H_{MI}, S^z] = 0$ and the singlet state $|S\rangle$ has $S_z = 0$ whereas the polarized state $|P\rangle$ is $S_z = N_e/2$ [3]. The inhomogeneity H_{MI} mixes states with different S but only those with equal[4] S_z.

How to break this symmetry by some plausible term in the Hamiltonian and what happens then?

Weak inhomogeneous[5] inplane magnetic fields will do. This scenario is not unlikely to occur in a realistic system. It merely means, that the extra fluctuating magnetic field (which speaks only to spins) is not pointing exactly in the direction of the (strong) external magnetic field causing the Landau level quantization. Existence of such symmetry–breaking inhomogeneities is very likely in realistic systems, although they might be very weak (e.g. hyperfine interaction with nuclear spins).

Let us consider a Hamiltonian with inplane magnetic inhomogeneities (IMI) of the form

$$H = H_{Coul} + H_{Zeeman} + H_{MI} + H_{IMI}\,, \tag{5.3}$$

$$H_{IMI} = \sum_j g_0 \mu_B B_x(x_j) \sigma_x^j\,, \quad \langle \varphi_i | H_{IMI} | \varphi_j \rangle = \delta_{ij} E_{IMI} \begin{cases} i = \frac{1}{4} N_m : & 1 \\ i = \frac{3}{4} N_m : & -1 \\ \text{otherwise}: & 0 \end{cases}$$

Main claim of this Subsection is that weak H_{IMI} only opens an anticrossing at the ground state transition. In other words, the relevant states still basically form a two–level system comprising of the (slightly disturbed) singlet and polarized ground states. The 'width' of the anticrossing (measured either by the level splitting, Fig. 5.4(b), or by the range of magnetic field where $\langle S_z \rangle$ noticeably changes, Fig. 5.9) grows with increasing E_{IMI} (strength of the inplane field inhomogeneity).

This fact is best demonstrated in Fig. 5.4. Inhomogeneities are weak there (compared to both incompressibility gaps $E_g^P \approx E_g^S$), i.e. $E_{MI}, E_{IMI} \ll E_g$, and the spectrum remains

[3] $S_z|S\rangle = 0$ and $S_z|P\rangle = (N_e/2)|P\rangle$, therefore $\langle P|H_{MI}|S\rangle = (N_e/2)^{-1}\langle P|S_z H_{MI}|S\rangle = (N_e/2)^{-1}\langle P|H_{MI}S_z|S\rangle = 0$.

[4] The fully polarized ground state ($S = N_e/2$, $S_z = N_e/2$) has also an $S_z = 0$ counterpart, since the homogeneous Hamiltonian commutes with spin lowering operator. This state, however, is a highly excited state at $B \approx B_C$, since its Zeeman energy is zero.

[5] Inhomogeneity of this field is not necessary for breaking the symmetry.

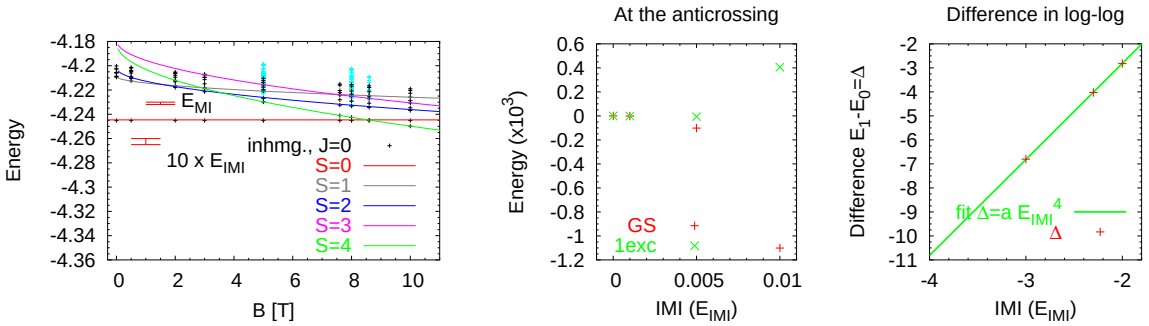

(a) Spectrum. Solid lines: homogeneous system; points: inhomogeneities switched on.

(b) Energy of the lowest two states at the anticrossing as IMI is being turned on. *Right:* level splitting

Figure 5.4: Response (of an eight–electron system) to a weak inhomogeneity in perpendicular and inplane direction (Eq. 5.3). Perpendicular component E_{MI} is the same as in Fig. 5.3. Exponent four comes from $N_e/2$, see explanations in the text.

almost unchanged (Fig. 5.4(a)). Only directly at $B \approx B_C$ an anticrossing opens and the level separation ΔE grows with increasing E_{IMI} (and E_{MI} is kept constant), Fig. 5.4(b). Even for a quite strong inplane inhomogeneity (of the order of E_g), the level splitting remains small ($\ll E_g$). The reason for this is simple: H_{IMI} couples only states which differ by ± 1 in S_z, since it is a one–particle operator (allowing for only one spin flip at once). Thus, a coupling of the two ground states occurs for a $N_e = 8$ system first in the fourth order of perturbation theory ($N_e = 8$ implies $S_z = 4$ for fully polarized system). This interpretation fully agrees with the finding $\Delta E \propto (E_{IMI})^4$ (Fig. 5.4(b)). We can therefore expect that, for an inhomogeneity of constant strength, the level splitting will vanish exponentially at $N \to \infty$ as long as E_{IMI} is much smaller than the gap at $B \approx B_C$.

Another view at the crossing for $E_{IMI} \neq 0$ is presented in Fig. 5.5. If we focus on the ground state and sweep B through B_C, we may observe how $\langle S_z \rangle$ (or $\langle S \rangle$) of the ground state smoothly passes from 0 to $N_e/2 = 4$. The transition observed in this way (i.e. $\langle S_z \rangle \approx 2 = N_e/4$) coincides with transition observed in spectrum (the 'anticrossing region'), Fig. 5.5(a), 5.5(b). The larger E_{IMI}, the smoother the transition and the broader the range of B in which the transition occurs, Fig. 5.5(c).

So as to conclude: most importantly, an inplane magnetic inhomogeneity (IMI) transforms the ground state transition into an anticrossing. This effect should fade away for larger systems ($N_e \gg 1$). IMIs also shift the transition point B_C to lower fields, Fig. 5.5(c), but this effect seems to be rather small for inhomogeneity strength not exceeding the incompressibility gap.

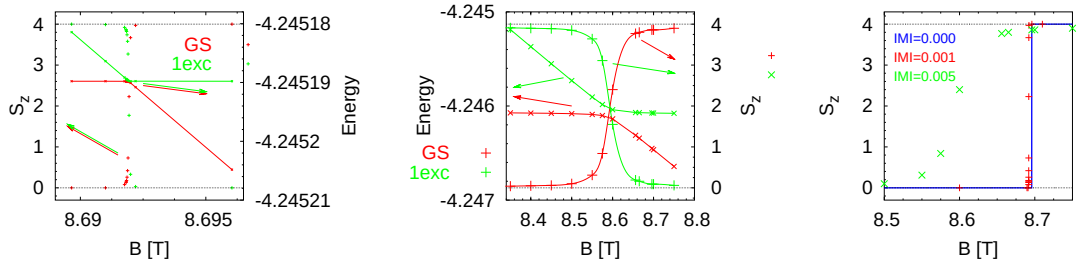

(a) Weak IMI. ($E_{IMI} = 0.001$)

(b) Intermediate IMI. ($E_{IMI} = 0.005$)

(c) Crossing at different values of IMI.

Figure 5.5: Inplane magnetic inhomogeneity (IMI) turns the crossing between the singlet ground state and the polarized ground state, Fig. 5.4(a), into an anticrossing. The cross–over between the two ground states can be observed either in the spectrum or in $\langle S_z \rangle$ of the ground state as B is swept through B_c.

5.2.3 Strong inhomogeneities

Let us again suppress inplane inhomogeneities and let us study stronger perpendicular inhomogeneities of the form Eq. 5.2.

If the strength of the 'rectangular wave' impurity becomes comparable to the gap at $B \approx B_C$, $E_{MI} \approx E_g$, the situation at the 'singlet-to-polarized' transition changes dramatically. The excitation gap closes and many states of different spin polarizations crowd near to the ground state. Even at zero temperature and in spite of lack of anticrossings of states with different S_z (i.e. S_z is a good quantum number again), the transition becomes more gradual, when measured by S_z of the ground state, Fig. 5.6(c).

Primarily, this is owing to the $S = 1$ state which profits best from the inhomogeneity. Keeping in mind its value of $k^r = (1.07, 0)\ell_0^{-1}$, this state seems to be a spin density wave in x–direction pinned by the inhomogeneity potential. However, states with other spins are very near to it.

This $T = 0$ transition can be again smoothened by an inplane inhomogeneity, as shown in Fig. 5.7. Here, the transition $S_z = 0 \to 1$ becomes much more gradual than the transition $S_z = 1 \to 4$. Reason for this is again that the inplane inhomogeneity couples directly only states with $\Delta S_z = \pm 1$. Other quantities than just S_z (e.g. polarization) are shown in Fig. 5.9.

A strong magnetic inhomogeneity has also another quite pronounced consequence: the singlet-polarized ground state transition B_C shifts to higher magnetic fields, Fig. 5.6. This effect is considerably stronger than the shift to lower fields in case of the inplane inhomogeneity (Fig. 5.5). Origin of this shift to higher B is the decreasing energy of the singlet ground state, Fig. 5.6 or Fig. 5.8(d).

Let us look at this issue more closely. Increasing E_{MI}, there is no apparent transition

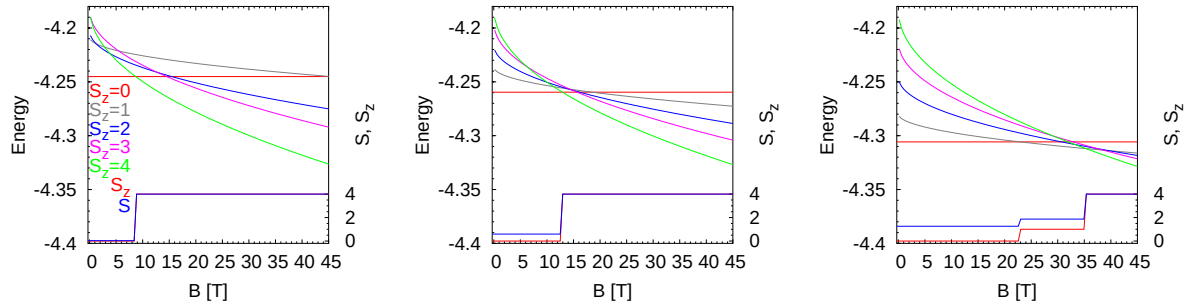

(a) Weak MI. ($E_{MI} = 0.002$)

(b) Intermediate MI. ($E_{MI} = 0.01$)

(c) Strong MI. ($E_{MI} = 0.02$)

Figure 5.6: Stronger MI's bring another ground state into play ($S_z = 1$) and the transition from the singlet to the polarized ground state becomes more gradual.

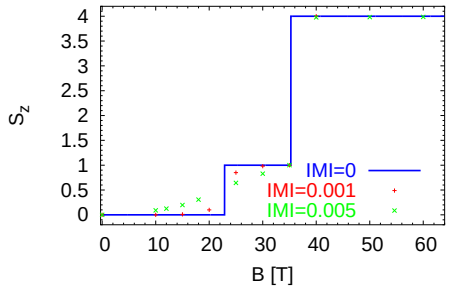

Figure 5.7: Strong perpendicular magnetic inhomogeneity, just as in Fig. 5.6(c), combined with inplane inhomogeneity (IMI). $\langle S_z \rangle$ of the ground state.

(crossing) in the ground state of the $S_z = 0$ sector. However, the total spin of the ground state increases from zero and saturates around $S \approx 1.6$ for $E_{MI} \approx 0.02$, Fig. 5.8(d). No later than at this point, the label 'singlet ground state' becomes inappropriate. At such values of E_{MI}, the polarization achieves the maximum variation between zero and one, Fig. 5.8(a). The eight electrons, four with spin up, four with spin down, split into two nearly independent groups: the spin up (down) electrons gather in the region where $g_1(x)$ is positive (negative), see Eq. 5.2. Such a state where e.g. no spin up electrons occur in the 'wrong region' (yellow line in Fig. 5.8(c)) is obviously no longer even remotely related to the homogeneous incompressible state, even though it has $S_z = 0$. Rather, we could interpret it as two $\nu = \frac{1}{3}$ systems living next to each other: one with spin up, another with spin down. The strong spatial variation of density in this system, Fig. 5.8(b), indicates that electrons try to avoid the 'interface region'; an alternative way to see this is to compare the 'spin–down domain region' (seen in the polarization, Fig. 5.8(a)) with the density of spin down electrons, Fig. 5.8(c). However, we must always be aware that we investigate only a finite system which are too small to observe the 'inside' of a domain where we expect the density to be constant (in a sufficiently large system, the maximum in Fig. 5.8(c) should spread into a plateau). Therefore, also conclusions about the interface

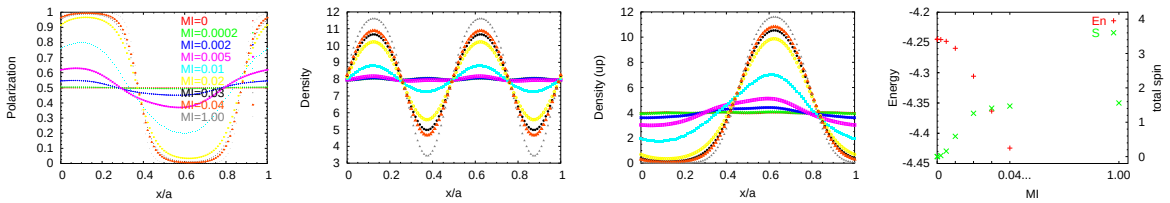

(a) Polarization $n_\uparrow(x)/n(x)$.

(b) Density.

(c) Density $n_\downarrow(x)$.

(d) Energy and S.

Figure 5.8: Destruction of the singlet state by very strong magnetic inhomogeneities: the system splits into two domains, one with spin up, another with spin down and the electrons avoid the 'interface region' (minima in the density).

region must be accepted with caution.

5.2.4 Quantities to observe

Polarization is the most natural quantity to study when we are looking for domains of polarized and singlet states. Nevertheless, it could be useful to search for other observables as they might bring some more information on what is happening in the states.

Here, I suggest to study the *local* expectation values (or densities) of otherwise 'global' operators such as S_z or S^2. These are defined by

$$S_{x,z}(\mathbf{r}) = S_{x,z} \otimes n(\mathbf{r})\,, \qquad S^2(\mathbf{r}) = S^2 \otimes n(\mathbf{r})\,, \text{ where } \qquad n(\mathbf{r}) = \sum_{i=1}^{N_e} \delta(\mathbf{r} - \mathbf{r}_i)$$

and they should be plotted in the form $S_z(\mathbf{r})/n(\mathbf{r})$. Their meaning is the following: Imagine an n–electron state which is an equal–weight superposition of two states: one localized in the region $0 < x < a/2$ which is fully spin polarized ($S_1 = n/2$) and another localized in $a/2 < x < a$ which is a spin singlet. This state is $S_z = n/4$, yet its $S_z(x)/n(x)$ is equal to $n/2$ or 0 in the two respective regions.

What these quantities reveal is demonstrated in the case of a strong magnetic inhomogeneity, both perpendicular and inplane, Fig. 5.9. The low–energy part of the spectrum does not change considerably, Fig. 5.9(a), even though the singlet state was separated almost completely into a spin–up and a spin–down domain by the inhomogeneity (seen in the polarization, Fig. 5.9(b)). Note that again the states near the transition have smaller variations in the polarization than the 'inhomogeneous singlet–state'.

The lower two plots of Fig. 5.9(b) show $S_z(x)/n(x)$ and $S_x(x)/n(x)$. Obviously, S_z stays quite constant with x, at least on the scale ranging from $S_z = 0$ (singlet) to $S_z = 4$ (fully polarized). Albeit polarization (or relative density of spin down electrons) varies strongly, $S_z(x) \approx$ const. This indicates that the state does not really separate into domains of locally different S_z. Observation of the quantity $S^2(x)$ (not shown) suggests the same conclusion.

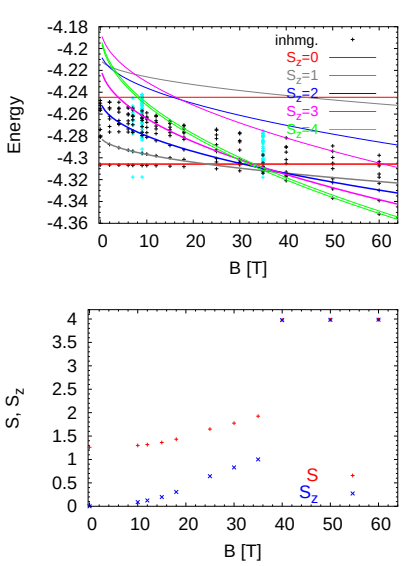

(a) Spectrum and $\langle S_z \rangle$, $\langle S \rangle$ of the ground state.

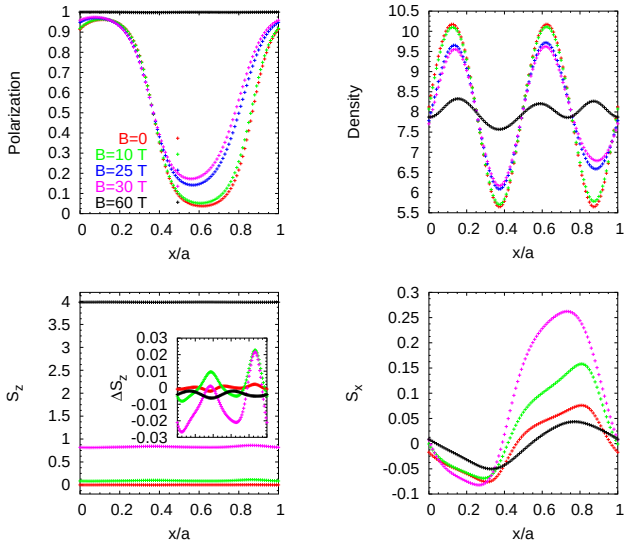

(b) The ground state in different quantities.

Figure 5.9: Response to strong inhomogeneity of the form in Eq. 5.3. $E_{MI} = 0.02$, $E_{IMI} = 0.005$.

Local expectation values of S_x indicate that states near the transition are more susceptible to inplane inhomogeneities. At any B, this response is much stronger than for perpendicular inhomogeneities. This is understandable: if we imagine a 'classical' spin vector pointing in z–direction and accept that it fluctuates by a small angle $\Delta\varphi$, then $S_z \propto \cos\Delta\varphi \approx 1$ whereas $S_x \propto \sin\Delta\varphi \approx \Delta\varphi$.

5.2.5 Different geometries of the inhomogeneity

Disregarding entropy, it is unlikely that a domain state will be the ground state in a homogeneous system. If it is an excitation we can hope to favour it energetically by including a suitable inhomogeneity like H_{MI} in Eq. 5.2. We do not a priori know, however, what 'suitable' means. So far, we divided the system into two *equal* parts by H_{MI}.

How the singlet state responds to inhomogeneities of different forms is shown in Fig. 5.10. Different lines correspond to the 'rectangular wave' inhomogeneities with different ratios of the 'plus' and 'minus' parts. All these inhomogeneities are thus a single stripe (per elementary cell) parallel to y of different width.

Also, response to H_{MI} consisting of two stripes is shown (i.e. 'rectangular wave' with half period).

Responses are basically very similar to each other and it seems that having focused on H_{MI} of the form of Eq. 5.2 we did not choose a particularly clumsy one. One particularly inter-

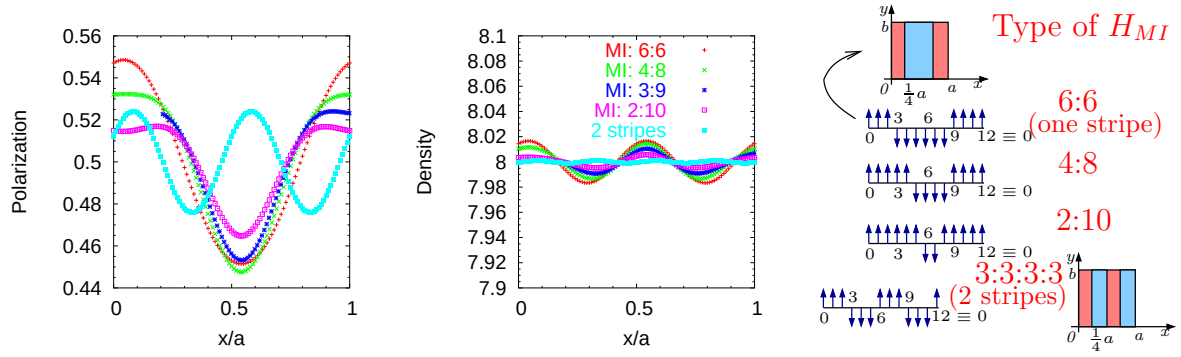

(a) Polarization.

(b) Density.

(c) Various inhomogeneities H_{MI} used.

Figure 5.10: Response of the singlet to various weak magnetic inhomogeneities. The inhomogeneity is similar to the one in Eq. 5.2 but it divides the system into two areas (stripes) of various ratios (6 : 6 through 2 : 10) or it consists of two stripes with size 3 : 3 : 3 : 3.

esting information which can be extracted from Figure 5.10 is that polarization response is always at least an order of magnitude larger than in density (10% against 0.3% in the present case). This only confirms the conclusion of Subsection 4.3.2 : even though singlet incompressible states try to maintain constant density, they can be fairly easily polarized.

A pronounced example of the influence of the form of the inhomogeneity are the half-polarized states, Fig. 5.11. The lowest level in the $S = 2$ sector is six–fold degenerate (factor of three from the centre-of-mass and factor of two from the relative part). The two states are mirror images of each other with respect to the diagonal of the elementary cell. We split them into two groups $J = 2, 6, 10$ and $J = 0, 4, 8$ (within each group the states differ only by the center-of-mass part) and subject each group to one-stripe and two-stripe inhomogeneities (stripes are always along y, Fig. 5.10(c)).

One group ($J = 2, 6, 10$) responds strongly to the two-stripe H_{MI} and is left almost unchanged by the one-stripe H_{MI}, upper row in Fig. 5.11(b). Nearly the opposite is true for the other group. This gives a clear picture of the structure of these states. They are spin density waves with two periods in one direction and one period in another direction. This is fully in agreement with the spin–spin correlation functions (not shown). This conclusion is also underlined by the markedly lowered energy of the $J = 2$ state when it is addressed by the two-stripe inhomogeneity, Fig. 5.11(a). This is a practical demonstration of one spin-density-wave state selected by an impurity from a degenerate manifold.

5.2.6 Transition at nonzero temperature

Regardless of how intensely we try to help an eventual domain state to become the ground state, it may still be, that it is hidden among the excitations. Therefore we may try to

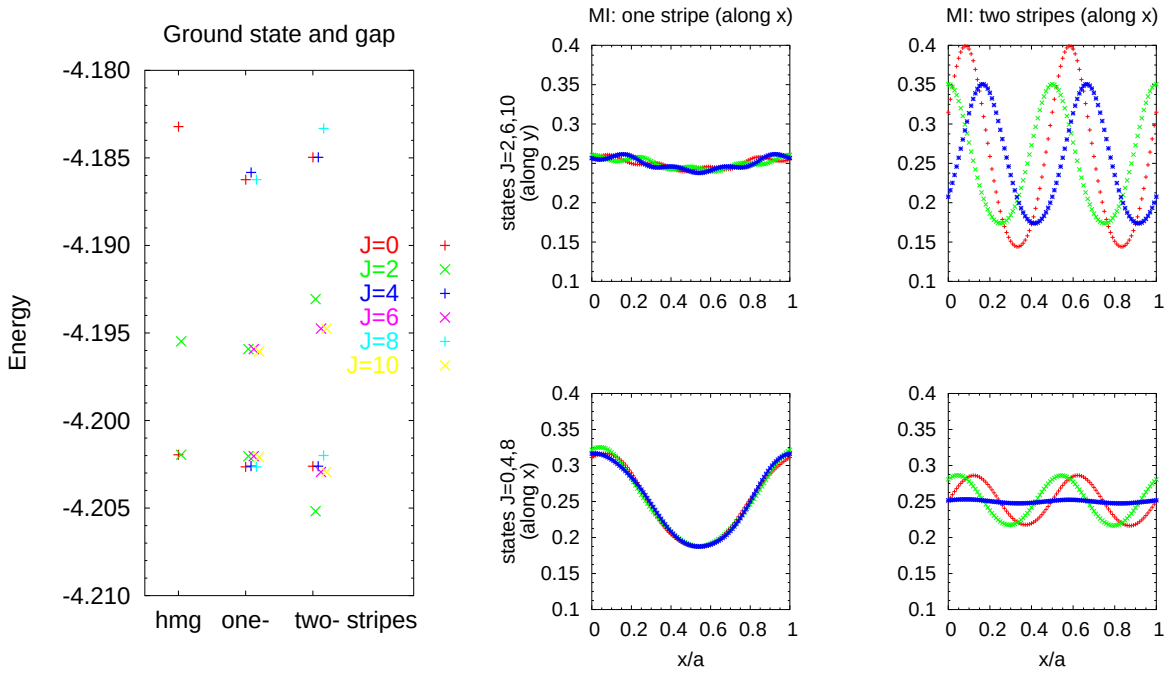

(a) Energies.

(b) Polarizations.

Figure 5.11: The half–polarized states ($S = 2$) and their response to a magnetic inhomogeneity of the form of one or two stripes.

take the excited states into account by means of thermal averaging.

The strong impurity mode ($E_{MI} = 0.02$) was chosen for this study. Three–fold degeneracy (in center-of-mass) of the incompressible ground states is lifted but the level splitting is still smaller than the incompressibility gap (cf. the black and blue points in the upper plot of Fig. 5.9(a) around $B = 10$ T).

Various temperatures were considered: $kT \ll E_g$ means than we do not average even over all states of the originally degenerate triple. Knowing that E_g means the gap energy at $B \to 0$ or $B \to \infty$, other temperatures shown in Fig. 5.12 are self-explaining.

Judging by polarization $n_\downarrow(x)/n(x)$, the state at the transition approaches a situation which we could call 'domain'. In the middle ($x/a \approx 0.5$), the polarization drops to zero and only spin up electrons are present. In the other region ($x/a \approx 0 \equiv 1$), polarization is about 0.5, meaning that the number of spin up as spin down electrons in this area is the same.

We should note though that an inhomogeneity which is strong enough to produce such nice 'domains' is also strong enough to change the originally incompressible singlet state completely, Fig. 5.12a. In other words, the response of the system at the transition is still weaker than the response of the singlet state. This manifests that spontaneous build-up of

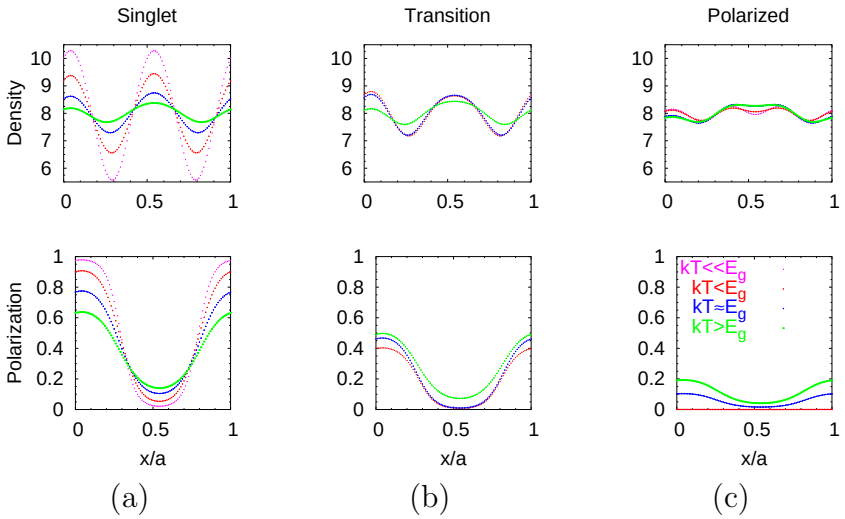

Figure 5.12: Density and polarization at different temperatures: filling factor 2/3 with magnetic inhomogeneity (corresponding to Fig. 5.6(c)). *Left to right:* before, at and after transition, i.e. $B \to 0$, $B \approx B_c$ and $B \to \infty$.

domains is not very likely within this model.

In the following Section we will try to suggest slightly different models which may put us on the trace of states which exhibit nontrivial behaviour at the transition between the incompressible singlet and polarized ground states.

5.3 Systems with short range interaction

As far as the transition between singlet and polarized ground state is concerned, the most obvious feature of the $\nu = \frac{2}{3}$ Coulomb–interacting systems is the energy 'gap' which separates the two degenerate ground states from excited ones even at the very crossing, Fig. 5.13(a) (or also 5.1). In the previous section we demonstrated that this picture may change when fairly strong magnetic inhomogeneities are applied, Fig. 5.6. It also completely changes if we replace Coulomb by short–range interaction, Fig. 5.13(b).

Let us first concentrate on the calculated spectrum of the *homogeneous* system with short–range interaction, Fig. 5.13(b). Again, we observe a gapped ground state with maximum spin and zero spin in the limit of $B \to \infty$ and $B \to 0$, respectively. In between, however, states with different spins become the absolute ground states. Aforemost, it is the half–polarized state ($S = 2$), although states with other spins ($S = 1$ and 3) are not very far. Alternatively, this can be expressed by the B–dependence of the spin of the ground state, Fig. 5.14(a).

The half–polarized states have been extensively discussed in Sec. 4.1 where they were studied as 'zero–temperature candidates' for the ground state in homogeneous systems.

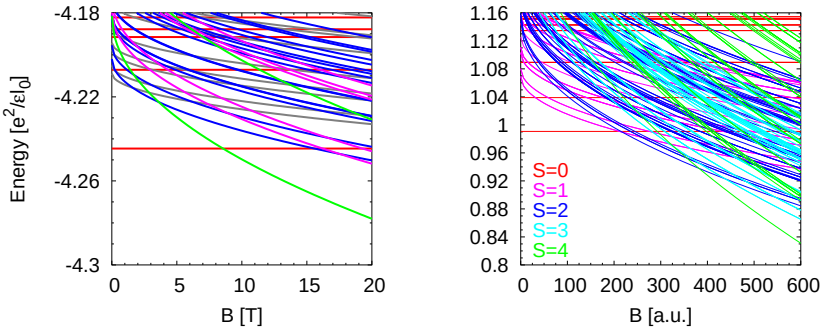

(a) Coulomb interaction.

(b) Short–range interaction.

Figure 5.13: Spectrum of a homogeneous system with Zeeman splitting (8 electrons, $\nu = \frac{2}{3}$).

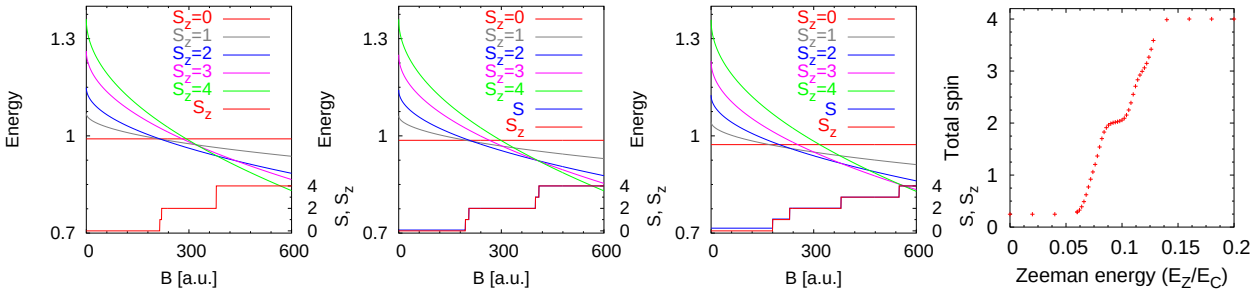

(a) Homogeneous.

(b) Intermediate inhomogeneity ($E_{MI} = 0.01$).

(c) Strong inhomogeneity ($E_{MI} = 0.02$).

(d) Spin at finite temperature, corresp. to Fig. 5.14(c).

Figure 5.14: Spectrum and the expectation value of the spin in the ground state in short–range interacting systems (eight electrons).

However, since inhomogeneities couple the ground state to the excited states, the properties of the lowest–lying state will not be determined solely by the those of the ground state.

Spectral properties of the short–range interacting (SRI) system subjected to a 'perpendicular' magnetic inhomogeneity (Eq. 5.2) are summarized in Fig. 5.14. In a similar fashion as for the Coulomb–interacting systems, states with other spins become the absolute ground state in some range of the magnetic field (cf. Fig. 5.6). This is also manifested in the expectation value of spin (or S_z) of the system even at nonzero temperatures: most significant is, however, still the 'half–polarized' plateau $S_z(B) \approx 2$, Fig. 5.14(d).

After this introduction let us look at the inhomogeneous states themselves. Their prop-

erties are highlighted especially in comparison to the Coulomb interacting (CI) states. When subjected to a 'rectangular cosine' magnetic impurity, those (CI) states showed a smooth monotonous transition from the singlet to the polarized state. The singlet was most strongly affected by the inhomogeneity, the polarized state was not affected at all (it was 'frozen' by its symmetry[6]) and the transition state was just in the middle. This is the finding both at $T = 0$, Fig. 5.3(b), and at temperature low enough to average only over the three states which were degenerated in the homogeneous system, Fig. 5.15(a).

The SRI systems give a different view: the response to the inhomogeneity is slightly stronger at the transition than in the singlet state, Fig. 5.15(a) (note the inset: the blue curve has a little bit larger amplitude than the red one). This is not very surprising given that there are quite many states near the ground state in the transition region. At slightly higher temperature (where we average over about 10 states in the singlet and polarized limit), this distinction between Coulomb and short–range interacting systems weakens, Fig. 5.15(b).

Regarding the Figure 5.15, I would like to stress once again, that the 'transition states' for the Coulomb and the short–range interaction are completely different. In the former case, this state is basically a superposition of the singlet and the polarized states, whereas it is a half–polarized state ($S_z = N_e/4$) for the SRI.

It seems we are on the track of the domain build-up here. In an ideal case, we would expect: negligibly affected singlet and polarized states while the polarization of the transition state varies between 0 (polarized domain) and 0.5 (singlet domain). Back in reality, however, we are still very far from such behaviour as the difference between polarizations of the singlet and transition state is quite small. Nevertheless, the direction seems correct, contrary to the Coulomb interacting systems. We may therefore conclude:

- if nontrivial effects at the transition are expected, there must be more states involved than just the singlet and polarized ground states;
- it is likely that the half–polarized states play a major role;
- at low temperatures inhomogeneous states as in Fig. 5.15(b) can be observed simultaneously with a plateau in $S_z(B)$, Fig. 5.14(d).

The last point is a consequence of the fact that not only the ground state but also the lowest excited states have $S_z = 2$ in a part of the transition region, Fig. 5.13(b).

[6]The polarized state has all spins up, $S_z = N_e/2$. Since magnetic inhomogeneity of the form in Eq. 5.2 preserves S_z, it does not couple the polarized state with any states which contain spin down electrons, since such a state must have $S_z < N_e/2$.

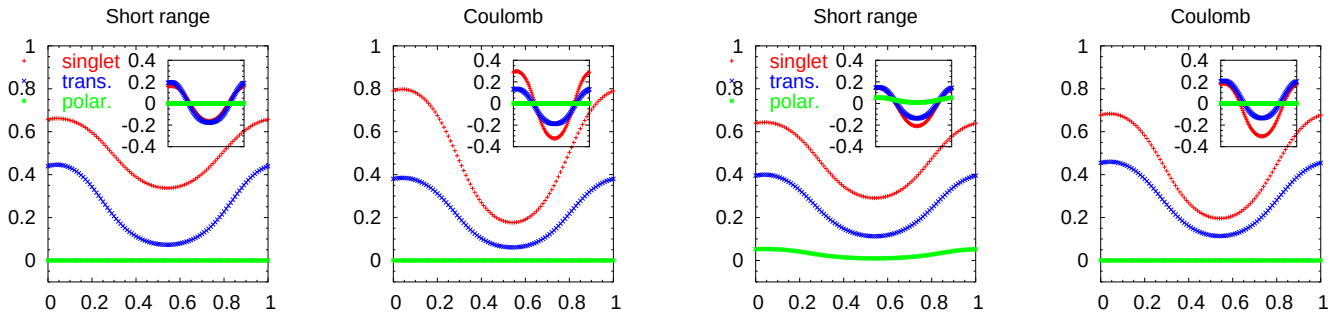

(a) 'Low' temperature.

(b) Slightly higher temperature.

Figure 5.15: Short–range interacting system with strong inhomogeneity (Eq. 5.2, $E_{MI} = 0.02$): polarization in the singlet sector, around the transition and in the polarized sector; cf. spectrum in Fig. 5.14(c). Insets show how polarizations fluctuate around anticipated mean values (0.5, 0.25 and 0 for the singlet, transition and polarized state).

5.3.1 Comments on the form of the short–range interaction

For a short–range interaction, I chose the form described in Subsect. 3.3.6, Fig. 3.7b. The basic idea there was to keep the pseudopotentials[7] V_0 and V_1 at their normal values while setting the others to zero. Reasons for doing so were given in Sect. 3.3.

As far as incompressible liquid states are concerned, not much happens during such 'pseudopotential engineering': the best measure for this are directly the density–density correlation functions, Fig. 4.12. The good match between correlation functions of Coulomb– and short–range–interacting states agrees with the common claim that their energy is determined mostly by effects occurring at short distances. Also excitation energies remain essentially unchanged as long as 'zero momentum' states are considered (as opposed to charge or spin density waves).

What strongly changes is the energy difference between the polarized and singlet state: it is 0.0632 for Coulomb and 0.3693 for short–range interaction (in an eight–electron system, with zero Zeeman energy). This happens because the average Coulomb potentials felt by electrons in a singlet state and in a spin polarized state differ: roughly, we take the average over set $\{V_0, V_1, 0, 0, \ldots\}$ in the former case (all m's allowed) and over $\{V_1, 0, 0, \ldots\}$ in the latter case (only odd m's allowed). This is a fundamental problem: requirement of equal averages is not compatible with preserving the ratio of V_0 and V_1 as in a Coulomb interacting system[8]. Therefore, with short–range interactions, we must be very cautious whenever we

[7] V_0 and V_1 give the energy of two interacting particles in the state with angular momentum 0 and 1. These are the states with smallest and second smallest interparticle separation possible and only the latter one is accessible if the particles have the same spin (relative wavefunction corresponding to V_0 is symmetric).

[8] We would have to use higher Haldane potentials to achieve this, losing thereby the simplicity of the

compare absolute energies of states with different spins (and thus parity properties of the wavefunction). Namely, position of the singlet-polarized transition depends directly on the energy difference of the singlet and polarized ground state (see Sec. 5.1).

This warning applies to spectra in this subsection (Fig. 5.14, Fig. 5.13(b)). However, the polarizations in Fig. 5.15 do not suffer from this, provided that half–polarized states indeed become the absolute ground state somewhere around the transition.

5.4 Systems with an oblong elementary cell

In this Chapter, we only considered square elementary cells a by a so far. If we somehow (e.g. by means of a magnetic inhomogeneity) manage to split such a system into two equally large domains, their size will be $a/2$ by a, cf. Fig. 5.10(c). Consequently, the spin singlet and spin polarized states which we expect to appear in these domains would necessarily have to be deformed as in a cell of aspect ratio 1 : 2. In principle, this could even suppress the formation of such domains or at least shift them among higher excited states[9]. In the following Section we will investigate systems in a rectangular cell with aspect ratio 2 : 1 which have the possibility of splitting into two square domains. All results in this Section refer to Coulomb interacting systems.

5.4.1 Overview of the transition: which states play a role

Going from square elementary cell to aspect ratio 1 : 2, the overall view of the transition changes. The crossing between singlet and polarized incompressible states is no longer well separated from excited states, Fig. 5.16.

Similarly, as for short–range interaction, states with different spin appear near the transition: most prominently $S = 1$ and $S = 2$. Again (cf. Figs. 5.6, 5.14) and these states are promoted by the 'rectangular wave' perpendicular magnetic inhomogeneities, Fig. 5.17. A consequence of this is a gradual change of the spin in the ground state as we sweep magnetic field (or simply increase Zeeman energy). Here, I would like to point out the difference of the present case to the Coulomb interacting system in a square elementary cell (Fig. 5.6): for an oblique elementary cell, (i) the $S = 1$ state becomes the absolute ground state near the transition even in homogeneous systems and (ii) a much weaker inhomogeneity is needed to make the $S = 2$ state the absolute ground state in some range of the magnetic field[10].

definition of short–range interaction (in other words, the Laughlin state would not have zero energy any more).

[9] We know that energy of any of the two incompressible ground states depends on aspect ratio (the stronger the smaller the system is), Subsect. 4.4.1. There is no reason to expect that energy of a domain wall between two such states is constant.

[10] Fig. 5.17(c) shows that $E_{MI} = 0.004$ is sufficient for this to happen in a 2 : 1 system, while $E_{MI} = 0.02$ is not strong enough for a square elementary cell, Fig. 5.6(c).

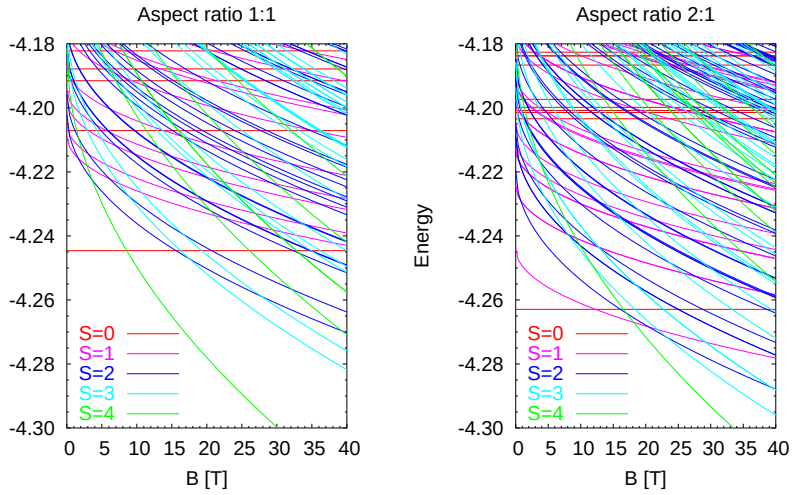

(a) Aspect ratio 1 : 1.

(b) Aspect ratio 2 : 1.

Figure 5.16: Spectra of homogeneous eight electron systems (with Zeeman splitting) for square and oblong elementary cell.

	asp. 1 : 1, hmg.	asp. 2 : 1, hmg.	asp. 2 : 1, $E_{MI} = 0.004$
$S_z = 0$ GS	0.713	0.976	
$S_z = N_e/2$ GS	0.750	0.9996	

Table 5.1: Incompressible ground states (polarized and singlet) in an eight–electron system. Overlaps between states in a square elementary cell, oblong elementary cell and oblong elementary cell with intermediate magnetic inhomogeneity.

By changing the elementary cell geometry we support eventual domain states, but it is adequate to ask how much the incompressible singlet and polarized states are affected by this procedure. The inner structure of these states under elementary cell variations was addressed in Subsect. 4.4.1 and we saw indications that the states are liquid like (and very similar to the original states from square elementary cell) even at aspect ratio 1 : 2. However, overlaps between the square–cell and deformed states are noticeably below unity and hence their behaviour is not representative if we are interested in infinite homogeneous systems. Recall, that the square–cell polarized state is extremely close to the Laughlin state (overlaps $\approx 99\%$).

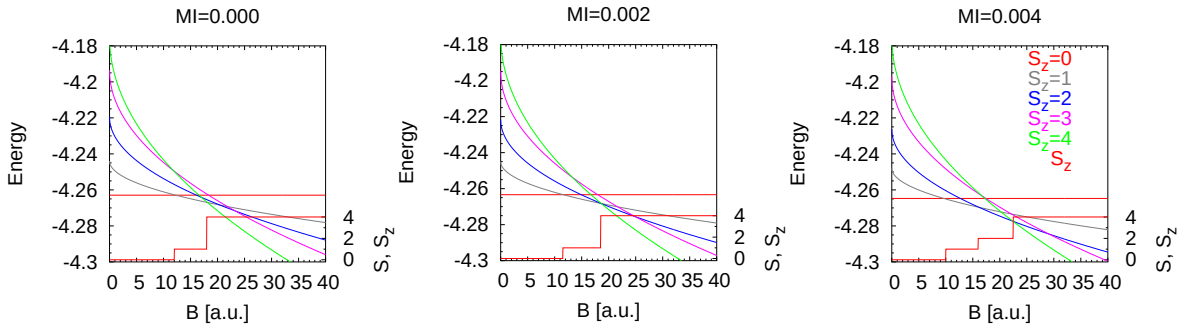

(a) Homogeneous. (b) $E_{MI} = 0.002$ (weak). (c) $E_{MI} = 0.004$ (intermediate).

Figure 5.17: Spectra and S_z of the ground state in a system with oblique rectangular elementary cell (aspect ratio 2 : 1, eight electrons). Magnetic inhomogeneities (Eq. 5.2) of different strengths are considered.

5.4.2 States at the transition

Here, I present the central result of investigations on systems with aspect ratio 2 : 1. The low–energy states near the transition ($S = 1$ and $S = 2$ in Fig. 5.17) respond very strongly to a 'rectangular cosine' magnetic inhomogeneity, Fig. 5.18 (blue and magenta lines). Already for intermediate strength of the inhomogeneity (15% of the singlet incompressibility gap in a square cell), polarization varies between ≈ 0.5 and ≈ 0.05, Fig. 5.18(a) (remember that values of 0.5 and 0 would mean a state with $S_z = 0$ and $S_z = N_e/2$, respectively). Equivalently, Fig. 5.18(b) shows that (a) the density of spin down electrons drops below 25% of its average value in the spin polarized region and (b) spin up and spin down densities are balanced up to 10% variations in the 'spin singlet region'. At the same time, variations of the total density remain small (less than 5%), but there is a clear deficit of electrons in the 'polarized region', Fig. 5.18(c).

As a check that the inhomogeneity is not too strong ('destructive') compared to the Coulomb interaction responsible for the formation of the incompressible ground states (far away from B_c), we should observe the incompressible states (red and green lines in Fig. 5.18). For both of them, responses are much weaker than for the transition states.

Let us now concentrate only on the half–polarized states and try to analyze their nature. Observe first the homogeneous system near the transition, Fig. 5.19 and focus on the half–polarized sector ($S_z = N_e/4 = 2$) with one particular value of J (Subsect. 3.5.2). The low lying states show pronounced spin structures and, moreover, several distinct types of spin structures appear in the low energy part of the spectrum. This is heralded by different values of k^r which is $(0, 0)$, $(\pm 1, 0)$ and $(2, 0)$ for the lowest three states (`st01`,`st02`+`st03`, `st04`, the middle pair is degenerate) and the different spin structures can be best seen in

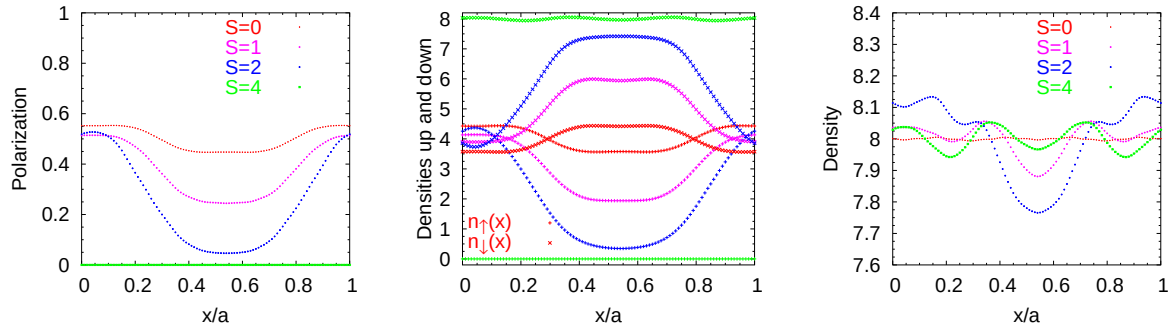

(a) Polarization.

(b) Densities of electrons with spin up (or down).

(c) Total density.

Figure 5.18: 'Domains' imprinted by a magnetic inhomogeneity of type 'rectangular wave' into a system with oblong rectangular elementary cell (aspect ratio 2 : 1). The strength of the inhomogeneity is about 20 % of the gap in the limit $B \to 0$ (in particular $E_{MI} = 0.004$). Plotted quantities are averaged over the three states which were degenerate in the homogeneous system (in the center-of-mass part).

the density–density correlation of minority spin[11], $g_{\downarrow\downarrow}(r)$, Fig. 5.20. The lowest state looks isotropic (as far as the rectangular elementary cell allows), the other two (`st02`+`st03` and `st04`) are different kinds of spin density waves in the 'long direction' (x). Keeping in mind that these states are energetically close to each other (compared to incompressibility gaps at $\nu = \frac{2}{3}$ in a square elementary cell, for example), we can indeed expect strongly modulated polarization in response to suitable not very strong inhomogeneities. Polarizations in Fig. 5.18 were a good demonstration of this prediction.

Now, a natural question arises: what types of spin structures can be imprinted into these states? Are they completely 'soft' or are some particular structures preferred? An answer[12] is given by polarizations in response to various types of inhomogeneities, Fig. 5.21. Briefly summarized: a variety of spin structures is possible but 'periodic' structures are preferred. Among the 'periodic' structures, the largest period available is preferred (one stripe, i.e. just the 'domains' as in Fig. 5.18). By 'periodic' we mean commensurate with the elementary cell period, for instance a 'rectangular wave' in contrast to a delta peak (since otherwise, any structure is periodic in our system due to periodic boundary conditions).

Looking only at polarizations, Fig. 5.21(a), responses to all types of inhomogeneities considered seem to be the same (in strength) within a factor of two. However, a closer look reveals some marked differences between those which are 'periodic' and the others, Fig. 5.21(b). The one–stripe and two–stripe inhomogeneities mix mostly only the lowest four states: (sum of squares of) projections of the inhomogeneous state to states `st01`–`st04`

[11] Half–polarized states contain 6 spins up and two spins down here, which we choose to call majority and minority spins respectively.

[12] Free of ambition to be complete.

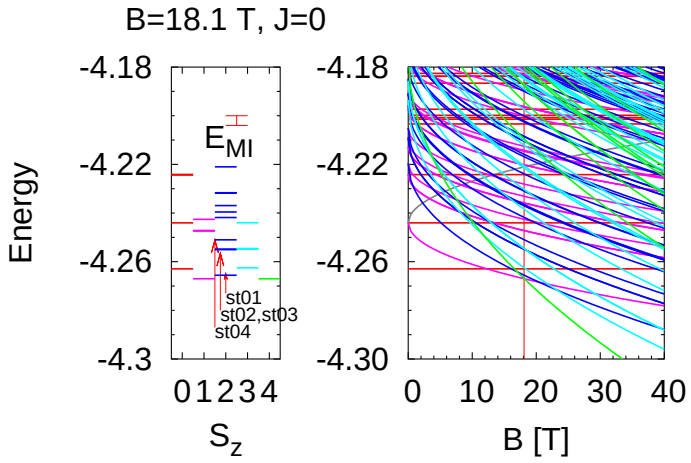

Figure 5.19: Low lying states near the transition (in absence of inhomogeneity, eight electrons). The $J = 0$ sector is where (a) both incompressible ground states (singlet and polarized) occur and (b) the lowest half–polarized state occurs.

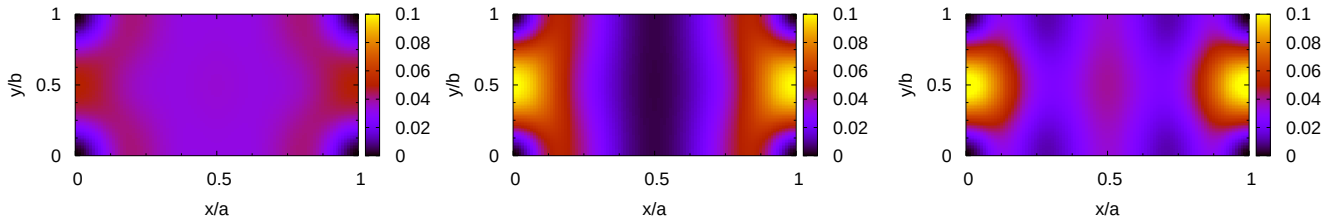

(a) The lowest state (`st01`).

(b) An SDW state (`st02`, `st03`).

(c) Another SDW (`st04`).

Figure 5.20: Density–density correlations ($g_{\downarrow\downarrow}$, i.e. minority spin) in the lowest half–polarized states. Coulomb interaction, a homogeneous system, aspect ratio 2 : 1.

give in these cases $\geq 90\%$. It seems that a one–stripe structure, or domain state in Fig. 5.18, stems from the $k^r = (\pm 1, 0)$ states (`st02`+`st03`) and the two–stripe structure comes from the $k^r = (2, 0)$ state (`st04`); in both cases, however, projections to the lowest state (`st01`) remain high.

A different situation occurs for 'non–periodic' structures like a delta peak. Inhomogeneous states are then 'constructed' largely from states which were originally energetically higher in a homogeneous system. Such states (e.g. with a delta peak in the polarization) only

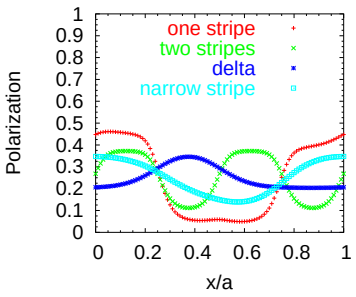

(a) Polarization. Impurity types are the same as in Fig. 5.10.

State	hmg.	one stripe	two stripes	δ–peak
Energy	-4.2656	-4.2713	-4.2695	-4.2439
`st01`	1	-0.82	-0.92	-0.04
`st02`	0	-0.51	0.00	0.03
`st03`	0	0.21	0.00	0.07
`st04`	0	0.03	0.22	0.64
cummul. $\Sigma(\langle\cdot\vert\cdot\rangle)^2$	1	0.98	0.90	0.41

(b) Projections of the inhomogeneous ground states to the lowest four homogeneous states (in Fig. 5.20).

Figure 5.21: Half–polarized state and different forms of inhomogeneity. Strength of the inhomogeneity is the same in all cases, $E_{MI} = 0.004$.

have a strong projection to the $k^r = (2, 0)$ state (`st04`), but still more than 50% of weight comes from higher states, Fig. 5.21(b).

This scheme, 'periodic–welcome, others–less welcome', is confirmed also in terms of energy. While the 'periodic' states (one– and two–stripes) profit energetically from the inhomogeneity, the delta–peak state is shifted to higher energy, Fig. 5.21(b).

Finally, the following conclusion about the $\nu = \frac{2}{3}$ system near the transition seems to be possible. The softening against magnetic inhomogeneities of different forms (as observed in Fig. 5.18(a)) stems not only from the spectral properties of the system (small level spacing, Fig. 5.19) but also from the fact that more different (inner) spin structures occur among the low lying states. States belonging to a single value[13] of S (e.g. $S = N_e/4$) are capable of generating a response as shown in Fig. 5.18(a).

5.4.3 What is inside the domains?

We will now only consider the 'one–stripe' inhomogeneity, in sense of Fig. 5.10, which has lead us to the states with polarization varying almost between zero and one half, Fig. 5.18. In other words, we could distinguish two domains of about equal areas in that state: one, where there were only spin up electrons and another where there were as many spin up as spin down electrons, whereby the total density was spatially nearly constant. Now, we are interested in the inner structure of these domains. One of the aims of this thesis was to find side-by-side domains comprising of the incompressible singlet and incompressible polarized states. Unfortunately, results presented in this Subsection cannot give a conclusive answer on whether the states discussed in the previous Subsection are of this type or not. Also,

[13] In the calculations presented here, this constraint is implied by the symmetry of the considered impurities (no inplane component, $E_{IMI} = 0$).

it would be surprising if they could, given how small systems (eight electrons) we study[14] Nevertheless, these results provide at least some basis for comparing the inside of the domains to the incompressible states and, in particular, highlight some differences between these two.

As a probing tool I chose density–density correlation functions. As we are dealing with inhomogeneous states, we must use $g(\boldsymbol{r}, \boldsymbol{r}_0) \propto \langle \delta(\boldsymbol{r}_1 - \boldsymbol{r}) \delta(\boldsymbol{r}_2 - \boldsymbol{r}_0) \rangle$ rather than $g(\boldsymbol{r}) \propto \langle \delta(\boldsymbol{r}_1 - \boldsymbol{r}_2 - \boldsymbol{r}) \rangle$. The former quantity is the conditional probability to find an electron at $\boldsymbol{r}$ given there is an electron at $\boldsymbol{r}_0$ and we will separately address the cases when both electrons have spin up or when they both have spin down. By convention, majority electrons are spin up (expected to be present in both domains) and minority electrons are spin down (absent in the fully polarized domain).

Roughly, we can say that the eight electrons are organized in four vertical stripes: two in the polarized and two in the unpolarized domain. For instance, if we catch a majority spin electron in the left stripe in the polarized domain, we will see another quite sharply localized (majority spin) electron in the same stripe and two delocalized electrons in the other stripe of the polarized domain, Fig. 5.22(c). In the unpolarized domain, we will see the two majority electrons distributed nearly equally into the two stripes.

Similarly, if we pin a majority spin electron in one stripe of the unpolarized domain, Fig. 5.22(a), we find another (majority spin) electron in the same stripe. Four electrons in the polarized domain are distributed homogeneously into the two stripes. We will see almost the same picture with minority spin electrons, if we catch a *minority* spin electron at the same place. Naturally, we will see almost nothing in the polarized domain, Fig. 5.22(b).

Summary. In eight electron systems, the domain states comprise of four vertical stripes (i.e. parallel to the short side of elementary cell), each occupied by two electrons. In the polarized domain, each stripe contains two electrons separated by $b/2$, and the two stripes can 'freely slide' besides each other. Stripes of the unpolarized domain are preferentially occupied by electrons of the same spin and both spins (majority and minority) seem to be equivalent: schematically $\langle\uparrow\uparrow|_L\langle\downarrow\downarrow|_R + \langle\downarrow\downarrow|_L\langle\uparrow\uparrow|_R$. The domains seem to be rather independent: for instance, regardless of where, within the unpolarized domain, we pin the majority spin electron, the density of electrons seen in the polarized domain does not change much.

I should like to stress that although the stripe structure is well pronounced in conditional probabilities, the density varies only weakly, Fig. 5.18(c). But, even so, it contains indications of the four stripes. This structure suggests that the interior of any of the domains is rather anisotropic and this is quite distinct from the liquid states at $\nu = \frac{2}{3}$ (polarized and singlet, Figs. 4.5, 4.6) where at least the first maximum in $g(\boldsymbol{r})$ occurs for all $\boldsymbol{r}$ with $|\boldsymbol{r}| = r_1$ (Subsect. 4.1.1) and not only in the x– or y–direction. The study of finite size effects comparing the averaged and non–averaged correlation functions (Fig. 4.17, Subsect. 4.1.4) suggests that for liquid states, the anisotropy of non–averaged correlation functions

[14] One of the reasons why studies of finite systems on a torus or on a sphere were so successful was that these models contain no edges. On contrary, there are 'edges' in the state with 'domains': the domain walls.

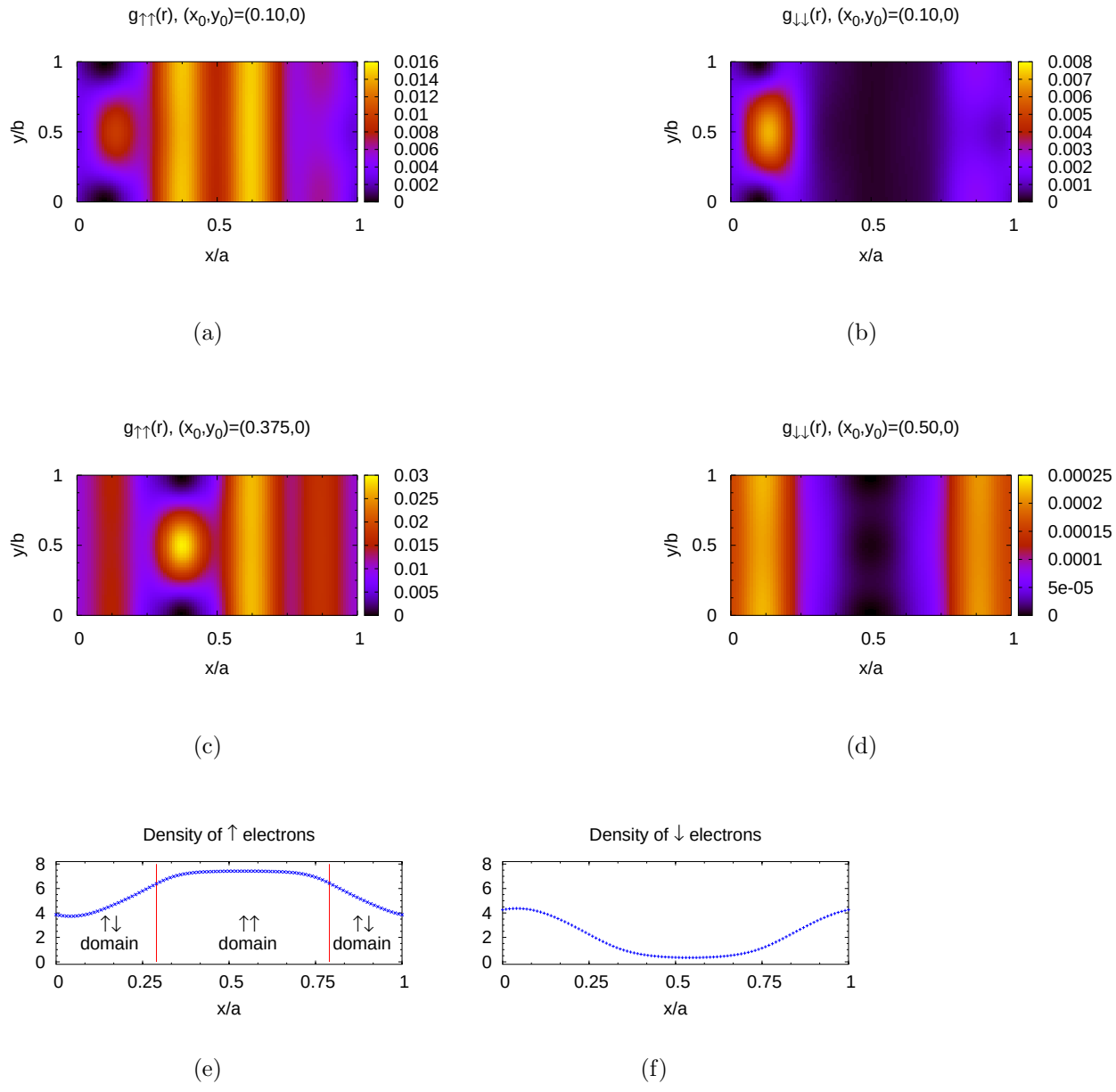

Figure 5.22: Half–polarized state with intermediate magnetic inhomogeneity ('rectangular wave', $E_{MI} = 0.004$), non–averaged density–density correlation functions.

should be much smaller than what we observe in Fig. 5.22. On the other hand, the results shown in Fig. 5.22 refer to a state which is inhomogeneous and which is strongly influenced by the aspect ratio being far from unity. A more thorough study of the non–averaged correlation functions in systems of various aspect ratios and comparison to systems of different sizes is therefore necessary to allow for more definite conclusions.

5.4.4 Comment on homogeneous half–polarized states

It is worth of emphasis that the half–polarized state we study here is not the same as the half–polarized states studied from the state discussed in Sect. 4.2.

The lowest state here, in an elongated elementary cell, has $\boldsymbol{k}^r = (0, 0)$, whereas the half–polarized ground state in a square cell has $\boldsymbol{k}^r = (2, 2)$ (see Sec. 4.2). These are the two inequivalent points of the highest symmetry.

In the present system (aspect ratio 2 : 1) all low lying half-polarized states belong to the $\boldsymbol{k}^r_y = 0$ sector. States with other values of $\boldsymbol{k}^r_y$ lie well above the four discussed states `st01`–`st04`, the lowest of these other states has an energy of -4.240, cf. the spectrum on the left in Fig. 5.19. Being interested in the states low in energy we may therefore stay restricted to the sector $\boldsymbol{k}^r_y = 0$. This is a pleasant fact since there is then no need to consider inhomogeneities of very low symmetry (implying handling larger Hilbert spaces).

Also note that a spatially fixed inhomogeneity couples the relative and center-of-mass (CM) coordinates. At filling $\nu = \frac{2}{3}$ there are three possible CM states on a torus, which however remain mutually decoupled owing to the high symmetry of the inhomogeneity. The chosen sector $J = 0$ corresponds to a combination of $\boldsymbol{k}^r_y = 0$ sector and the one CM state, which leads to the lowest energy. Differences to other CM states are, however, not too large.

5.5 Summary of studies on the inhomogeneous systems

Perhaps the most important conclusion of this Chapter is that the two incompressible ground states at $\nu = \frac{2}{3}$, the polarized and the singlet one, are alone not enough to create a state with 'domains', i.e. regions of polarization[15] zero existing side-by-side with regions of polarization one. We have demonstrated this in Subsection 5.2: when a 'domain–inducing' magnetic inhomogeneity is applied, the singlet ground state is more strongly affected than states near the transition. This claim remained true for different types of magnetic inhomogeneities, for different quantities used to detect the domains (apart from the polarization, also for $S_z(x)$, $S_x(x)$, etc.) and also for non–zero temperature.

Different conclusions apply when more than just the polarized and the singlet ground states are present in the low–energy sector. We have demonstrated, that near the transition, the gap could actually close in several different situations. In the present study, this happens for very strong magnetic inhomogeneities (Subsect. 5.2.3), for systems with an elongated elementary cell (Sect. 5.4) and for short–range interacting systems (Sect. 5.3). The states which closed the gap always belong to an intermediate value of spin, most prominent are those with $S = 1$ and $S = 2$ and since we considered only eight–electron systems, the latter value of spin corresponds to the half–polarized sector $S = N_e/4$. These states are considerably softer against magnetic inhomogeneities than the incompressible singlet and polarized states. On one hand, this fact follows from a small level spacing in the low energy sector when the gap closes. However, the magnetic inhomogeneities were also found to have

[15] Just for the moment here, the singlet state has a polarization equal to zero.

large (~ 0.1) matrix elements between most of the low lying states.

The states with the strongest tendency to form domains (i.e. the 'softest' ones) were found in systems with Coulomb interaction and an elongated elementary cell. Near the transition, even a moderately strong magnetic inhomogeneity (weaker than the incompressibility gap) was enough to make the polarization approach the values corresponding to the singlet and polarized states inside the domains. For these domain states, we have investigated the 'inside' of the domains by means of non-averaged correlation functions (Subsect. 5.4.3). We could not yet confirm that the domains comprise of an incompressible liquid, however, this system deserves a more detailed study. Especially in this case, a comparison with larger systems would be very helpful.

6 Conclusions

Fractional quantum Hall systems at filling factors $\nu = \frac{2}{3}$ and $\frac{2}{5}$ have been studied numerically by means of exact diagonalization techniques on a torus. In both systems, the existence of two different ground states is well established: one is fully spin polarized, another is a spin singlet and they are both strongly correlated. All four states can be visualised as composite fermion systems at integer filling factor ($\nu_{CF} = 2$). A transition between these two ground states can be induced by changing the Zeeman energy while keeping the filling factor constant (Sect. 2.2 and Sect. 5.1).

At the beginning of Chapter 4, we investigated the polarized and the singlet incompressible ground states in terms of their density–density correlation functions. First, we highlighted the fact that — even if these states were *exactly* described by some composite fermion model — the inner structures of the ground states at $\nu = \frac{2}{3}$ and $\frac{2}{5}$ differ strongly from the inner structure of a state comprising of two fully occupied Landau levels. In other words: in a composite–fermion state (e.g. $\nu_{CF} = 2$), the correlations between the *electrons* are different than in a corresponding electronic state ($\nu = 2$). A more important result is, however, that the electronic correlations differ strongly also between the $\nu = \frac{2}{3}$ and $\frac{2}{5}$ states themselves. This is surprising, since both filling factors map to the same filling factor of composite fermions ($\nu_{CF} = 2$) and only the orientation of the effective field is different. Study of the correlation functions allowed to suggest a new interpretation of the singlet $\nu = \frac{2}{3}$ ground state: the electrons move along in pairs of opposite spins and the pairs form a state equivalent to a fully occupied lowest Landau level. This conclusion does *not* apply to the $\nu = \frac{2}{5}$ singlet ground state.

The central focus of the present work was on the low–energy states occurring near the transition between the singlet and the polarized ground states. Some experimental results indicate that another ground state distinct from the two ground states already mentioned could exist near the transition (Sect. 2.4). In Sections 5.5 and 4.2 we found several arguments in favour of a half–polarized state ($S = N_e/4$) becoming the absolute ground state in a narrow range of the magnetic field. The systems available to exact diagonalization were however too small to allow for an unswerving prediction. Two candidates for the half–polarized ground state were identified. In Section 4.2 we concentrated on the 'isotropic candidate'. A study of its inner structure (correlation functions) combined with an investigation of the response to probing magnetic inhomogeneities (Sect. 4.3) produced results resembling both the singlet and polarized incompressible ground state. A hypothesis that both these states coexist within the half–polarized state has been presented.

Calculations with elongated rectangular elementary cells (Sect. 4.4) suggested another candidate for the half–polarized ground state: a spin–density wave along the longer side

of the elementary cell. A comparison between two systems of different size indicated that this state has the shortest period allowed by the finite size of the considered system (e.g. one third of the length of the cell for a state which contains three minority spins). Based on the present calculations it is not possible to decide which of the two candidates (if any) evolves into the ground state of an infinite system.

At $\nu = \frac{2}{5}$, no obvious analogue to the half–polarized state at $\nu = \frac{2}{3}$ was found.

Employing magnetic inhomogeneities to enforce domains of different spin polarization near the transition at $\nu = \frac{2}{3}$ (Chapter 5) we found that no signs of domain formation occur unless the energy gap closes. The loss of incompressibility could however still be compatible with the experimental observation of a plateau of polarization one half during the transition: it is enough if there are many states with $S = N_e/4$ and no (or only few) states with other values of S in the low–energy sector (Sect. 5.3).

The 'best' candidates for domain states were found to appear in systems with an elongated rectangular cell. The fundamental idea here was that the elementary cell with aspect ratio $2:1$ is divided by the inhomogeneity into two square parts which could be more convenient for the formation of isotropic states (the singlet and the polarized incompressible liquid). Examination of the domain state however showed that the inside of the domains does not resemble the incompressible ground states at $\nu = \frac{2}{3}$. Nevertheless, a more detailed study is necessary here, since systems with aspect ratio far from unity can suffer more from finite size effects than what was demonstrated in Sect. 4.1.

It took me a noticeable amount of time to conceive the final sentence of this thesis. After a thorough consideration, I decided for the following: All conclusions presented above should be verified in larger systems.

Bibliography

[1] The spatial part of the Hartree–Fock wavefunction in Eq. 1.1 is a product of two functions: one of the variable $\boldsymbol{r}_1$ and another of the variable $\boldsymbol{r}_2$. Within the probabilistic interpretation of $|\psi_{var}(\boldsymbol{r}_1, \boldsymbol{r}_2)|^2 = p_1(\boldsymbol{r}_1)p_2(\boldsymbol{r}_2)$ this implies that the phenomena described by the probabilities p_1 and p_2 are completely independent. On the contrary, the *correlations* correspond to conditional probabilities $P(\boldsymbol{r}_1, \boldsymbol{r}_2)$ which cannot be written as a product of two functions of one variable ($\boldsymbol{r}_1$ and $\boldsymbol{r}_2$). Therefore, correlated states cannot be described by a single 'product' state (like the one in Eq. 1.1) but, at best, by an expansion in terms of the product states.

If the two electrons have the same spin, then the spatial part of the wavefunction will be antisymmetric in accord with the Pauli principle. This in turn implies that $|\psi_{var}|^2$ cannot be written in the product form shown above and the electrons must be correlated. These correlations of a state described by a single Slater determinant will be, however, considered 'trivial', since they occur even in a non–interacting system and they are purely a manifestation of the fermionic nature of electrons. In most of the present work, we will study features of the correlations going beyond the 'bare' Pauli exchange hole.

[2] For some special values of β, analytical results regarding OCP are available (recent works are for instance [83], [84]). One of these, $\beta = 2$ (i.e. $m = 1$, $\nu = 1$) is dual to nothing but full (lowest) Landau level in absence of Landau level mixing. In this case, even the many–body (interacting) problem is exactly solvable since dimension of the Hilbert space is one (in full LL, simply all states are occupied). The result is then the same as the one of Hartree–Fock approximation.

[3] If we consider the lowest Landau level with zero Zeeman splitting, Laughlin state (which is fully polarized) still remains the ground state. However, the Hamiltonian has now $SU(2)$ symmetry (no direction of spin is preferred) and the Laughlin state breaks this symmetry (all spins point e.g. up). Goldstone theorem states [34], that if the ground state breaks a *continuous* symmetry, then there is a gapless (or zero mass) excitation.

[4] Going once around an s-fold vortex gives phase $2\pi s$ (see Subsect. 3.2.3). Exchange of two particles corresponds to one half of such a loop (for $\psi(r_1, r_2) \to \psi(r_2, r_1)$ corresponds to $\psi_{rel}(\varrho) \to \psi_{rel}(-\varrho)$ with $\varrho = r_1 - r_2$ in the relative part of the WF;

$\varrho \to -\varrho$ is half the way of going around zero). Thus exchanging two particles with s attached vortices, the wavefunction acquires phase πs. For two *fermions* with s attached vortices, it is $\pi(s+1)$. Thus the wavefunction changes sign at exchange of two particles when s is even and does not change the sign when s is odd.

[5] If we were able to distinguish two particles in a state described by a single Slater determinant, even such a state would also be entangled: consider a state $\Psi(1,2) = \psi_L(1)\psi_R(2) - \psi_R(1)\psi_L(2)$ and say the states L and R are localized on the left and on the right, respectively. There is an uncertainity in whether it is the particle 1 or the particle 2 which is on the right. If we measure one particle on the right, we automatically know that it is the *other* particle which is on the left. Owing to the indistinguishability of indentical particles, however, we cannot say whether it was the particle 1 or the particle 2 which we have just caught on the right. If the particles 1 and 2 have different spin, the indistinguishability requirement is lifted and the state Ψ is entangled. In that case, Ψ is the spin–singlet state.

[6] To show that a state is entangled we would have had to show that we must linearly combine more than one Slater determinant in *any* basis. In reality, however, we usually demonstrate that in the Slater determinant basis *of our choice* we need many terms in the linear combination in order to describe the many-particle state. A demonstrative example of how misleading conclusions drawn for one particular choice of basis can be is the state describing a $\nu = 1$ system: writing it as $\Pi_{i<j}(z_i - z_j)$, an ordinary physicist would have never guessed that it can be also written as a single Slater determinant (Vandermond determinant $\det A$, $A_{nm} = (z_n)^m$). Note: Question of how an ordinary physicist looks like is beyond the scope of this thesis.

[7] Several lowest of these polynomials are: $L_0^1(x) = 1$, $L_1^1(x) = 2 - x$, $L_2^1(x) = \frac{1}{2}(6 - 6x + x^2)$, $L_3^1(x) = \frac{1}{6}(24 - 36x + 12x^2 - x^3)$.

[8] In fact, there are *some* analytical results. Very appealing schemes how to evaluate energy and correlation functions were suggested by Girvin [30] Takano and Isihara [92]. Interesting extension of the former work was presented by Görbig (Subsec. 1.2.2. in [33]). All these schemes however present closed formulae neither for energy nor for correlation functions.

[9] If we completely fill the lowest Landau level with spin up electrons and with spin down electrons (imagine $\nu = 2$ and zero Zeeman energy), then spin up and spin down electrons are uncorrelated, $g_{\uparrow\downarrow}(r) = 1$. It is *not* a claim of composite fermion theories that the same is true if we do the same with CF Landau levels. The attachment of flux quanta introduces correlations between the originally uncorrelated $(n = 0, \uparrow)$ and $(n = 0, \downarrow)$ levels: spin up CFs do not feel the spin down CFs (owing to LL mixing neglect) but they do feel fluxes attached to the spin down CFs.

[10] Precise formulation in disc geometry: $\Psi_{CM}(Z) = N(Z - Z_1)(Z - Z_2)(Z - Z_3) = N(Z^3 + aZ^2 + bZ + c)$ with $c = -Z_1Z_2Z_3$, etc. The space of Ψ_{CM}'s is spanned by

functions Z^3, Z^2, Z and 1 and the true coefficients of the linear combination are a, b, c, not directly Z_1, Z_2, Z_3 (the last coefficient N is only a normalization factor which is fixed by the normalization of the relative part of the wavefunction). In torus geometry, this discussion is technically more difficult since powers of Z are replaced by powers of $\vartheta(Z|i)$.

[11] Consider the integral in Eq. 4.13 $n(z_1) = \int \mathrm{d}z_2 \ldots \mathrm{d}z_{N_e} \Psi_{CM}(z_1 + z_2 + \ldots + z_{N_e})\psi_r$ where all $N_e - 1$ integration variables go through the whole system, i.e. $[0; a] \times [0; a]$. We have just learned that variations of $n(z_1)$ stem from non–constant Ψ_{CM}. The integral in Eq. 4.13 is in principle a weighted average of Ψ_{CM} with weights ψ_r; when z_1 is fixed, this average is taken over the set $z_1 + \delta z$ with $\delta z \in [0, (N_e - 1)a] \times [0, (N_e - 1)a]$. If we had averaged over only a slightly larger area, $\delta z \in [0, N_e a] \times [0, N_e a]$, the average would have been constant (with respect to z_1) and equal to N_e (this would be just the norm of the whole wavefunction). The variations in $n(z_1)$ thus come from the omission of an area of $a^2[N_e^2 - (N_e - 1)^2]$ during the averaging. The omitted area is the smaller compared to the total area $a^2 N_e^2$ the larger N_e is, and thus variations in $n(z_1)$, i.e. the 'average' should vanish at least as $[N_e^2 - (N_e - 1)^2]/N_e^2 \to 0$ for $N_e \to \infty$. A quantitative discussion would have to take into account the form of the 'weighting function' ψ_r and it is was therefore beyond my capabilities.

[12] M. Allesch, E. Schwegler, F. Gygi, and G. Galli. *cond-mat*, page 0401267, 2004.

[13] V.M. Apalkov, T. Chakraborty, P. Pietiläinen, and K. Niemelä. *Phys. Rev. Lett.*, 86:1311, 2001.

[14] G. Bertotti. *Hysteresis in magnetism : for physicists, materials scientists and engineers.* Acad. Press, San Diego, California, 1998.

[15] L. Bonsall and A. Maradudin. *Phys. Rev. B.*, 15:1959, 1977.

[16] T. Chakraborty. *Adv. Phys.*, 49:959, 2000.

[17] T. Chakraborty and Pietiläinen, P. *The Quantum Hall Effects.* Springer, Berlin, second edition, 1995.

[18] T. Chakraborty and F.C. Zhang. *Phys. Rev. B.*, 29:7032, 1984.

[19] H. Cho, J.B. Young, W. Kang, K.L. Campman, A.C. Gossard, M. Bichler, and W. Wegscheider. *Phys. Rev. Lett.*, 81:2522, 1998.

[20] R.G. Clark, S.R. Haynes, A.M. Suckling, J.R. Mallett, P.A. Wright, J.J. Harris, and C.T. Foxon. *Phys. Rev. Lett.*, 62:1536, 1989.

[21] S. Das Sarma and A. Pinczuk. *Perspectives in Quantum Hall Effects.* Wiley, New York, 1997.

[22] E.P. de Poortere, E. Tutuc, S.J. Papadakis, and M. Shayegan. *Science*, 290:1546, 2000.

[23] W. Dietsche and S. Kronmüller. *Physica E*, 10:71, 2001.

[24] M. Dobers, K. von Klitzing, J. Scheider, G. Weimann, and K. Ploog. *Phys. Rev. Lett.*, 61:1650, 1988.

[25] R.B. Dunford, M.R. Gates, V.W. Rampton, C.J. Mellor, O. Stern, W. Dietsche, W. Wegscheider, and M. Bichler. Absence of the huge longitudinal resistance maxima in surface acoustic wave measurements of narrow quantum wells. In *Proceedings of the 26th International Conference on the Physics of Semiconductors*, page P143, Edinburgh, UK, July 2002. IOP.

[26] J.P. Eisenstein, H.L. Stormer, L. Pfeiffer, and K.W. West. *Phys. Rev. Lett.*, 62:1540, 1989.

[27] J. Eom, H. Cho, W. Kang, K.L. Campman, A.C. Gossard, M. Bichler, and W. Wegscheider. *Science*, 289:2320, 2000.

[28] G. Fano, F. Ortolani, and E. Colombo. *Phys. Rev. B.*, 34:2670, 1986.

[29] N. Freytag, Y. Tokunaga, M. Horvatić, C. Berthier, M. Shayegan, and L.P. Lévy. *Phys. Rev. Lett.*, 87:136801, 2001.

[30] S.M. Girvin. *Phys. Rev. B.*, 30:558, 1984.

[31] S.M. Girvin. *cond-mat*, page 9907002, 1999.

[32] S.M. Girvin, A.H. MacDonald, and P.M. Platzman. *Phys. Rev. Lett.*, 54(6):581, 1985.

[33] M.O. Goerbig. *Etude théorique des phases de densité inhomogeène dans les systeèmes à effet Hall quantique*. PhD thesis, Université de Fribourg, Switzerland, 2004.

[34] J. Goldstone. *Nuovo Cimento*, 19:154, 1961.

[35] I.S. Gradshteyn and I.M. Ryzhik. *Tables of Integrals, Series, and Products*. Academic Press, New York, any edition, 1980.

[36] F.D.M. Haldane. *Phys. Rev. Lett.*, 51:605, 1983.

[37] F.D.M. Haldane. *Phys. Rev. Lett.*, 55(20):2095, 1985.

[38] F.D.M. Haldane and E.H. Rezayi. *Phys. Rev. B.*, 31:2529R, 1985.

[39] F.D.M. Haldane and E.H. Rezayi. *Phys. Rev. Lett.*, 54:237, 1985.

[40] F.D.M. Haldane and E.H. Rezayi. *Phys. Rev. Lett.*, 60:956, 1988.

[41] B.I. Halperin. *Helv. Phys. Acta*, 56:75, 1983.

[42] K. Hashimoto, K. Muraki, T. Saku, and Y. Hirayama. *Phys. Rev. Lett.*, 88:176601, 2002.

[43] M. Helias. *Quasihole tunneling in the fractional quantum Hall regime*. PhD thesis, University of Hamburg, Germany, 2003.

[44] J.K. Jain. *Phys. Rev. Lett.*, 63:199, 1989.

[45] J.K. Jain. *Science*, 266:1199, 1994.

[46] T. Jungwirth and A.H. MacDonald. *Phys. Rev. B.*, 63:035305, 2000.

[47] T. Jungwirth and A.H. MacDonald. *Phys. Rev. Lett.*, 87:216801, 2001.

[48] T. Jungwirth, S.P. Shukla, L. Smrčka, M. Shayegan, and A.H. MacDonald. *Phys. Rev. Lett.*, 81:2328, 1998.

[49] R.K. Kamilla, J.K. Jain, and S.M. Girvin. *Phys. Rev. B.*, 56:12411, 1997.

[50] W. Kang, J.B. Young, S.T. Hannahs, E. Palm, K.L. Campman, and A.C. Gossard. *Phys. Rev. B.*, 56:12776R, 1997.

[51] K. von Klitzing, G. Dorda, and M. Pepper. *Phys. Rev. Lett.*, 45:494, 1980.

[52] S. Kraus, O. Stern, J.G.S. Lok, W. Dietsche, K. von Klitzing, M. Bichler, D. Schuh, and W. Wegscheider. *Phys. Rev. Lett.*, 89:266801, 2002.

[53] S. Kronmüller, W. Dietsche, K. von Klitzing, G. Denninger, W. Wegscheider, and M. Bichler. *Phys. Rev. Lett.*, 82:4070, 1999.

[54] S. Kronmüller, W. Dietsche, K. von Klitzing, W. Wegscheider, and M. Bichler. *Physica B*, 256:82, 1998.

[55] S. Kronmüller, W. Dietsche, J. Weis, K. von Klitzing, W. Wegscheider, and M. Bichler. *Phys. Rev. Lett.*, 81:2526, 1998.

[56] I.V. Kukushkin, K.v. Klitzing, and K. Eberl. *Phys. Rev. Lett.*, 82:3665, 1999.

[57] N. Kumada, D. Terasawa, Y. Shimoda, A. Sawada, Z.F. Ezawa, K. Muraki, T. Saku, and Y. Hirayama. *Phys. Rev. Lett.*, 89:116802, 2002.

[58] P.K. Lam and S.M. Girvin. *Phys. Rev. B.*, 30:473, 1984.

[59] R. Laughlin. *Phys. Rev. Lett.*, 50:1395, 1983.

[60] R. Laughlin. *Phys. Rev. B.*, 27:3383, 1983.

[61] D.R. Leadley, R.J. Nicholas, D.K. Maude, A.N. Utjuzh, J.C. Portal, J.J. Harris, and C.T. Foxon. *Phys. Rev. Lett.*, 79:4246, 1997.

[62] D. Levesque, J.J. Weis, and A.H. MacDonald. *Phys. Rev. B.*, 30:1056, 1984.

[63] C.A. Lewis. *Alice in Wonderland*.

[64] A.H. MacDonald and J.J. Palacios. *Phys. Rev. B.*, 58(16):R10171, 1998.

[65] E. Mariani, N. Magnoli, F. Napoli, M. Sassetti, and B. Kramer. *Phys. Rev. B.*, 66:241303, 2002.

[66] S. Mitra and A.H. MacDonald. *Phys. Rev. B.*, 48:2005, 1993.

[67] N.G. Morawicz, K.W.J. Barnham, C. Zammit, J.J. Harris, C.T. Foxon, and P. Kujawinski. *Phys. Rev. B.*, 41:12687, 1990.

[68] R.H. Morf, N. d'Ambrumenil, and S. Das Sarma. *Phys. Rev. B.*, 66:075408, 2002.

[69] Ch. Müller. *Disorder and vortex detachment in fractional quantum Hall liquids*. PhD thesis, University of Hamburg, Germany, 2005.

[70] G. Murthy. *Phys. Rev. Lett.*, 84:350, 2000.

[71] G. Murthy. *Phys. Rev. Lett.*, 87:179701, 2001. comment.

[72] G. Murthy and R. Shankar. *Rev. Mod. Phys.*, 75:1101, 2003.

[73] K. Niemelä, P. Pietiläinen, and T. Chakraborty. *Physica B*, 284:1717, 2000.

[74] W. Nolting. *Grundkurs: Theoretische Mechanik, Teil 5*. Verlag Zimmermann–Neufang, Ulmen, Germany, 2nd edition, 1994.

[75] K. Nomura. *Various broken symmetries in two–component quantum Hall systems*. PhD thesis, Department of Basic Science, University of Tokyo, Japan, 2003.

[76] M.A. Paalanen, D.C. Tsui, and A.C Gossard. *Phys. Rev. B.*, 25:5566, 1982.

[77] R. E. Prange and S. M. Girvin. *The Quantum Hall Effect*. Springer, Berlin, 1987.

[78] M. Rasolt and A.H. MacDonald. *Phys. Rev. B.*, 34(8):5530, 1986.

[79] S. Reimann and M. Manninen. *Rev. Mod. Phys.*, 74:1283, 2002.

[80] E.H. Rezayi and F.D.M. Haldane. *Phys. Rev. B.*, 32:6924, 1985.

[81] E.H. Rezayi and F.D.M. Haldane. *Phys. Rev. B.*, 50:17199, 1994.

[82] E.H. Rezayi, T. Jungwirth, A.H. MacDonald, and F.D.M. Haldane. *Phys. Rev. B.*, 67:201305(R), 2003.

[83] L. Šamaj. *cond-mat*, page 0402027, 2004.

[84] L. Šamaj, J. Wagner, and P. Kalinay. *cond-mat*, page 0407346, 2004.

[85] U. Schollwöck. *cond-mat*, page 0409292, 2004.

[86] N. Shibata and D. Yoshioka. *Phys. Rev. Lett.*, 86:5755, 2001.

[87] N. Shibata and D. Yoshioka. *J. Phys. Soc. Jpn.*, 72:664, 2003.

[88] N. Shibata and D. Yoshioka. *cond-mat*, page 0308122, 2003.

[89] N. Shibata and D. Yoshioka. *cond-mat*, page 0403493, 2004.

[90] J.H. Smet, R.A. Deutschmann, F. Ertl, W. Wegscheider, G. Abstreiter, and K. von Klitzing. *Nature*, 415:281, 2002.

[91] J.H. Smet, R.A. Deutschmann, W. Wegscheider, G. Abstreiter, and K. von Klitzing. *Phys. Rev. Lett.*, 86:2412, 2001.

[92] K. Takano and A. Isihara. *Phys. Rev. B.*, 34:1399, 1986.

[93] R. Tao and F.D.M. Haldane. *Phys. Rev. B.*, 33:3844, 1986.

[94] S.A. Trugman and S. Kivelson. *Phys. Rev. B.*, 31:5280, 1985.

[95] D.C. Tsui and A.C. Gossard. *Appl. Phys. Lett.*, 38:550, 1981.

[96] D.C. Tsui, H.L. Stormer, and A.C. Gossard. *Phys. Rev. Lett.*, 48:1559, 1982.

[97] R Willett, J.P. Eisenstein, H.L. Störmer, D.C. Tsui, A.C. Gossard, and J.H. English. *Phys. Rev. Lett.*, 59:1776, 1987.

[98] A. Wójs and J.J. Quinn. *Phys. Rev. B.*, 66:045323, 2002.

[99] X.G. Wu, G. Dev, and J.K. Jain. *Phys. Rev. B.*, 71:153, 1993.

[100] Jingbo Xia. *Commun. Math. Phys.*, 204:189, 1999.

[101] D. Yoshioka. *Phys. Rev. B.*, 29:6833, 1984.

[102] D. Yoshioka. *The Quantum Hall Effect*. Springer, Berlin, 2002.

[103] D. Yoshioka, B.I. Halperin, and P.A. Lee. *Phys. Rev. Lett.*, 50:1219, 1983.

[104] D. Yoshioka, B.I. Halperin, and P.A. Lee. *Surf. Sci.*, 142:155, 1984.

[105] D. Yoshioka and N. Shibata. *Physica E*, 12:43, 2002.

[106] J. Zak. *Phys. Rev.*, 134:A1602, 1964.

[107] J. Zak. *Phys. Rev.*, 134:A1607, 1964.

[108] F.C. Zhang and T. Chakraborty. *Phys. Rev. B.*, 30:7320, 1984.

[109] F.C. Zhang, V.Z. Vulovic, Y. Guo, and S. Das Sarma. *Phys. Rev. B.*, 32:6920, 1985.

At the very end. . .

. . . I would like to say thank you. I should mention many people at this place, but, unfortunately, I was told that this thesis should not exceed two hundred pages. At least at the last page, I shall therefore try to be brief. I hope I will not hurt anybody's feelings.

First of all, many thanks to Daniela Pfannkuche, my supervisor, for that the door of her office was always open to me, for her restless effort at reading the concept of this thesis and many very helpful comments. Instead of enumerating all the other good things I could enjoy while staying in her group, let me simply say: thank you for giving me good conditions to work on my thesis.

I appreciate the company of Bernhard Wunsch with whom I shared the office nearly three and half years. Bernhard and other members of our group — and also some members of other groups — they all contributed to a pleasant atmosphere where it was a joy to work. Thank you, Michael, Frank & Frank, Stefan, Christian, Moritz, Maxim, Eros, Riccardo, Andreas, Daniel, Alex, it was my pleasure.